CONSTRUCTION AND OPERATION OF AN IN-PILE LOOP FOR PWR DOSE REDUCTION EXPERIMENTS

by

Rene G. Sanchez
B.S. Nuclear Engineering, Columbia University
(May 1984)
B.A. Physics, Jacksonville University
(May 1984)
S. M. Nuclear Engineering, MIT
(January 1986)

SUBMITTED TO THE DEPARTMENT OF NUCLEAR ENGINEERING IN PARTIAL FULFILLMENT OF THE REQUIREMENTS FOR THE DEGREE OF

DOCTOR OF PHILOSOPHY

at the

MASSACHUSETTS INSTITUTE OF TECHNOLOGY

May 1990

Signature of Author_____
Department of Nuclear Engineering
May 4, 1990

Certified by_____
Michael J. Driscoll Thesis Advisor
Professor Emeritus, Nuclear Engineering

Certified by_____
Otto K. Harling Thesis Advisor
Professor, Nuclear Engineering

Accepted by_____
Allan F. Henry
Chairman, Departmental Graduate Committee

CONSTRUCTION AND OPERATION OF AN IN-PILE LOOP FOR PWR DOSE REDUCTION EXPERIMENTS

by

Rene G. Sanchez

Submitted to the Department of Nuclear Engineering on the 16th May 1990, in partial fulfillment of the requirements for the Degree of Doctor of Philosophy in Nuclear Engineering

ABSTRACT

One of the major problems facing Light Water Reactors (LWRs) is the radiation fields on out-of-core components from corrosion product transport back and forth between core and ex-core surfaces. To support the effort to understand the complex mechanisms that govern the release/transport/deposition of corrosion products so as to devise means to alleviate this problem, an in-pile loop has been designed, constructed, and operated in the MIT Research Reactor.

The PWR Coolant Chemistry Loop (PCCL) has been designed to closely simulate the thermohydraulic, as well as the chemical coolant environment of a representative full scale PWR. The present thesis describes in detail all subtasks involved in refinement of the conceptual design, construction of the loop and auxiliary facilities, shakedown tests and de-bugging of operational problems. Once successful operation was achieved, the PCCL was used to evaluate the effect of coolant pH on corrosion product release. Four one-month-long in-pile runs were completed; two of them at $pH_{300°C}$ = 7.0, one at low pH, $pH_{300°C}$=6.5, and one at high pH, $pH_{300°C}$=7.5. These chemistry conditions were chosen to ensure that precipitating or dissolving conditions existed on the core when operating at a low or high coolant pH, respectively.

At the completion of the runs, the simulated core and steam generator surfaces were assayed for radionuclide surface densities (nCi/cm^2 of Co-60, Co-58, Fe-59, Mn-54, Cr-51). The differences in deposition of activity on the Inconel steam generator tubes and core Zircaloy tube show the significant benefit of operating in the $pH_{300°C}$=7.0 to 7.5 range, as opposed to a lower pH. These results give strong support to the postulation of a solubility-driven mechanism as

the factor, which controls transition metal radionuclide transport in PWR primary coolant.

Thesis Supervisor: Michael J. Driscoll
Title: Professor Emeritus, Nuclear Engineering
Thesis Supervisor: Otto K. Harling
Title: Professor Nuclear Engineering

ACKNOWLEDGEMENTS

The author wishes to express the most sincere appreciation to the following persons who helped in the completion of this study.

To Profs. Michael Driscoll and Otto Harling for their invaluable advice and guidance throughout the course of this study.

To Dr. William T. Lindsay for his suggestions throughout the course of this study.

To Dr. Gordon Kohse and Mr. Michael Ames for their continued support, help, guidance, commitment, and long hours of work.

To his officemate and friend, Ernesto Cabello for his help and interesting discussions throughout the course of this study.

To Philip Borys, and Chan Bock Lee for their cooperation in running computer transport models.

To John Outwater III, Thomas Ippolito, Ricardo Medina, and Guido Solares for helping with some of the PCCL tasks.

To his friend Joseph Alfeo for his encouragement prior to the start of this study.

To Reactor Operations and Reactor Radiation Protection for their support and understanding of the importance of this project.

To the artisans of the MIT Nuclear Reactor Machine Shop who produced needed items essential for this project.

Finally, to his parents, grandmother and brothers for their continuous support.

I also acknowledge with appreciation the financial support provided in the form of a research assistantship under the EPRI/ ESEERCO contract, which has supported the MIT coolant loop project,

and the dedicated efforts of the sponsor's technical monitors, who included C. J. Wood, J. M. Burger, C. Spalaris, W. Yario, and H.Ocken.

TABLE OF CONTENTS

LIST OF FIGURES

LIST OF TABLES

1 INTRODUCTION

1.1 Foreword

One of the major problems facing Light Water Reactor (LWR) operators is the exposure of maintenance personnel to radiation fields. In Pressurized Water Reactors (PWRs), the primary source of radiation is associated with the primary reactor coolant loop: corrosion products are transported by the circulating coolant and made radioactive in the core; some of these radioactive corrosion products are then deposited on the ex-core surfaces, thus increasing radiation doses to maintenance personnel [H-1]. This prolongs expensive downtime for maintenance, and makes it more difficult to achieve the high quality needed to insure high plant reliability. The status of this situation, and the scientific basis for understanding the phenomena involved are reviewed and documented in detail in what are generally referred to as the Bournemouth Conferences [B-1], [B-2], [B-3], [B-4], [B-5].

While LWR maintenance doses worldwide have stabilized and even decreased in the past several years, there remains considerable room and incentive for continued research to improve the situation further. In the long term one has the competitive goal set by alternative reactor systems such as the Liquid Metal Reactor (LMR) and the High Temperature Gas Cooled Reactor (HTGR), prototypes of which have maintenance dose rates due to corrosion product activation an order of magnitude lower than that in LWRs. Motivated by these considerations, a research team proposed a program focused around small in-pile loops, for which a conceptual design was

developed [W-1] under MIT Electric Utility Program auspices. Support to construct and operate these loops was then provided by the Electric Power Research Institute (EPRI) and the Empire State Electric Energy Research Corporation (ESEERCO). The present thesis reports the results of the final design and construction phase of the PWR loops and their use in an initial campaign of runs to evaluate the efficacy of pH control (by $LiOH/H_3BO_3$ adjustment) in minimizing activity transport.

1.2 Background

In the past decade, occupational radiation exposure in the U.S. PWR nuclear power plants has levelled off, as shown in Fig. 1.1 [B-6]. Nonetheless, the occupational exposure remains higher in the United States plants compared to those in other countries. To reduce operator doses, the nuclear industry has concentrated its effort in several areas: reducing maintenance by corrosion prevention, minimizing the time spent by workers in radiation fields, and reducing the radiation fields in out of core components [W-2]. It is clear that a combination of all of these approaches is needed to further reduce exposure.

The present study focuses on one of these areas, namely; how to minimize the radiation fields in out of core components. Studies [W-3] have shown that the radiation from out of core components in PWRs is mainly due to the radioisotopes cobalt-60 and cobalt-58. Cobalt-60 has a half life of 5.27 years and is formed when cobalt-59, which is the only naturally occurring isotope, absorbs a neutron. On the other hand, cobalt-58 has a half life of 71.3 days and is formed

when nickel-58, which is 68% of the naturally occurring nickel, captures high energy neutrons. Cobalt and nickel ions associated with corrosion product films are released to the coolant from which they deposit on the core, where radioactivation takes place, followed once again by release/transport/deposition to create out-of-core radiation fields.

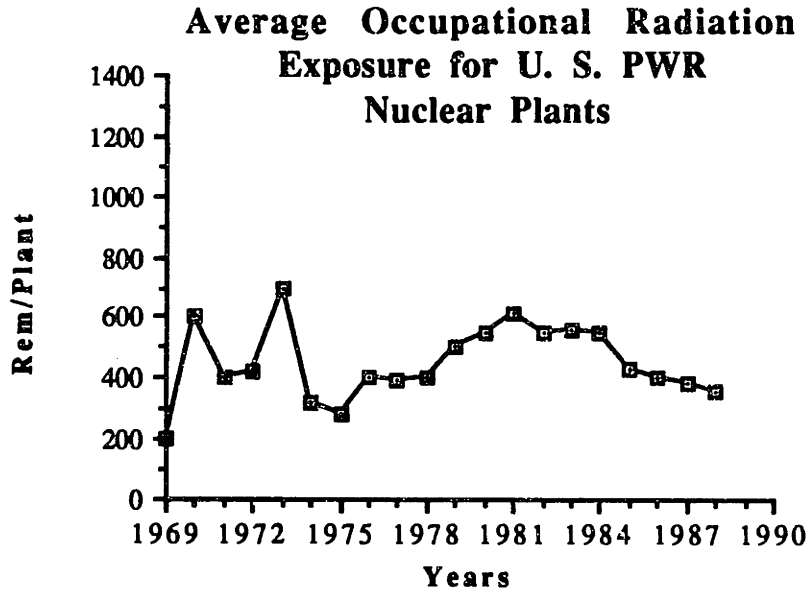

Figure 1.1 Average Occupational Radiation Exposure in U.S. PWRs [B-6].

The source of cobalt in a PWR primary circuit is mainly hard-facing materials, such as Stellite, which is the material used in valve seats, pump journals, and other components. Nickel, on the other hand, is found in great quantities in nickel base alloys, such as Inconel-600, which is the material used in PWR steam generator tubes. As shown in Table 1.1 [C-1], approximately 75% of the surface area in the primary circuit of a PWR is Inconel-600, which contains 75% (by weight) nickel. Cobalt, as an impurity, accounts for only 0.2%

of SS and Inconei-600; whereas, the cobalt content of Stellite is 50 to 60%.

The nuclear industry has pursued the reduction of radiation fields through a program which includes:

1. The reduction of cobalt in primary circuit components.

2. The reduction of corrosion release by pre-conditioning the primary circuit surfaces.

3. The control of water Chemistry to minimize the release of corrosion products to the coolant.

Table 1.1 Principal Alloys used in PWR water reactor coolant circuits [C-1].

	Surface area of coolant circuit (%)
Stainless Steel	5
Inconel-600	75
Zircaloy (fuel cladding)	20

As noted earlier, the major contributor of cobalt in PWR primary circuits is Stellite, which is found in components that require outstanding wear resistance such as valves. The cobalt input to the coolant can be reduced if Stellite is replaced by an alloy with lower cobalt content and better corrosion resistance, such as 440C SS. Another approach to reduce the cobalt input to the coolant is by reducing the cobalt impurities in SS and Inconel-600.

Pre-conditioning of surfaces prior to plant start-up reduces the subsequent release of corrosion products. It is well known that when

fresh surfaces are exposed to water, the initial corrosion release is quite high until an oxide film layer is formed. This film inhibits to some extent the release of corrosion products. Thus, Westinghouse PWR guidelines strongly recommend the pre-conditioning of surfaces for a period of four weeks at a temperature of 500° F for new plants prior to plant start-up [W-3]. Research is currently under way on other beneficial practices, such as post manufacture electropolishing.

Finally, the control of water chemistry is probably the easiest and most effective method to reduce the release, transport, activation, and deposition of corrosion products. Previous studies have suggested that this goal can be achieved when there is a strict control on the primary water chemistry to ensure operation near the minimum in transition metal solubility as a function of temperature and pH.

To permit evaluation of such stratagems, the subject PWR loop facility was designed, constructed, and operated. Figure 1.2 shows the final as-built design of the MIT-PCCL. The Pressurized Water Reactor Coolant Chemistry Loop (PCCL) simulates a PWR primary circuit (actually one unit flow cell: steam generator tube and fuel pin channel) by matching as close as possible coolant temperatures and temperatures differences, flow rates, heat fluxes, heat transfer coefficients, construction materials, surface area ratios, and neutron fluxes. Table 1.2 presents a comparison of the characteristic and operating parameters of the PCCL and a typical Westinghouse PWR nuclear plant.

As seen in table 1.2, average heat fluxes, bulk temperatures (inlet and outlet) and boundary layer temperature differences for a

Table 1.2 Parametric Comparison between a Representative PWR and the MIT PCCL.

Parameter	PWR	MIT PCCL
Core inlet T, °F (°C)	545 (285)	530 (277)
Core outlet T, °F (°C)	608 (320)	600 (316)
Hydraulic dia., in. (cm) Core Steam Gen.	 0.47 (1.2) 0.82 (2.1)	 0.256 (0.65) 0.242 (0.62)
Boundary layer ΔT, °F (°C) Core Steam Gen.	 32.4 (18) 10.26 (5.7)	 35.8 (19.9) 12.8 (7.1)
Coolant Velocity Core (m/sec) Steam Gen.(m/sec)	 4.8 5.9	 2.8 3.0
Core Average, neutron flux, n/cm^2-sec Thermal Fast(>1 Mev)	 2.3E13 9.4E13	 2.6E13 5.0E13
Average Heat flux, (kW/m^2) Core Steam Gen.	 614.6 178.2	 550.0 194.5
Material surface ratios: Total Inconel/Zircaloy Cooled Inconel/heated Zircaloy Total SS/Inconel	 2.73 3.44 0.15	 4.94 2.63 0.24

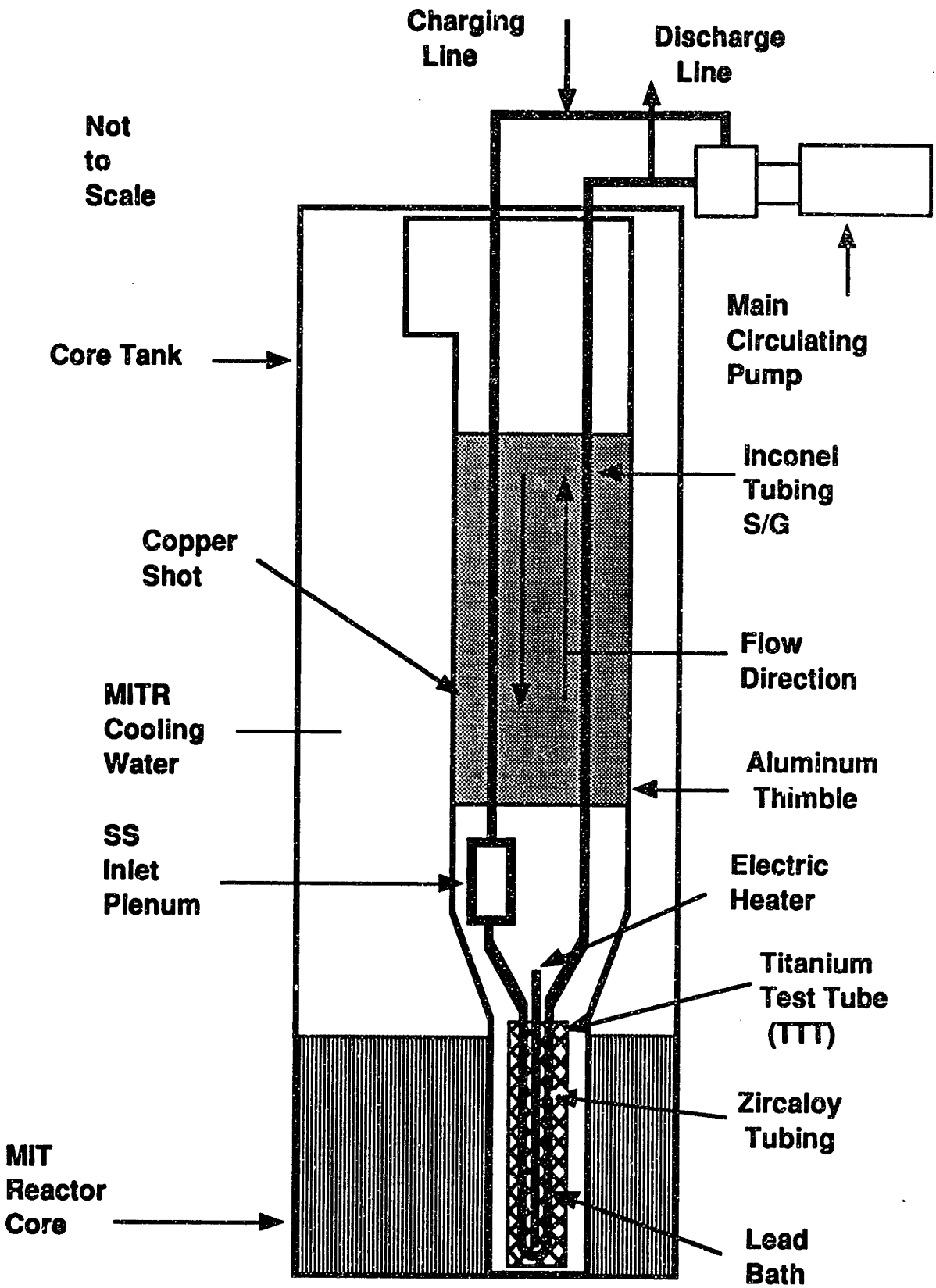

Figure 1.2 Schematic of the MIT PCCL.

typical PWR plant and the MIT PCCL are quite similar, which properly models the primary mechanism of solubility-difference-driven mass transfer.

As noted in this table, the major construction materials are the same for both systems. An effort was made to match as closely as possible the area ratios of the different materials. However, the constraints imposed by the MIT reactor core tank configuration and the need to employ an externally located circulating pump prevented a perfect match.

Another important parameter that needs to be considered is the neutron flux. The MIT reactor has approximately the same thermal neutron flux, and about half the fast neutron flux compared to a typical PWR. Thus, essentially real time simulation of activity buildup histories is possible.

The main objective of the initial series of PCCL in-pile runs is to determine the optimal coolant chemistry conditions which minimize the deposition of activity in out-of-core components.

Prior to irradiation, the loops are pre-filmed and pre-conditioned for a total of seven weeks to establish stable corrosion product coated surfaces, and also to simulate, to some extent, recommended plant start-up practice. Once the loops have been pre-filmed and pre-conditioned, they are installed in the MIT reactor (Fig. 1.2), one at a time, and irradiated for about a month. Parameters such as those presented in table 2.1 (core inlet and outlet temperatures, flow rates, film differential temperatures, heat fluxes) are monitored and controlled.

In summary, a concerted effort has been made to simulate as closely as possible the dominant mechanisms that govern the release, transport, deposition, and activation of corrosion products in a PWR primary circuit in the design and operation of the subject loops.

1.3 Outline of Present Work

The present report is divided into chapters and sections that describe the final as-built design, construction, and operation of an in-pile loop used for the study of release, transport, deposition, and activation of corrosion products in an environment similar to that of the primary coolant system of a PWR nuclear plant.

Chapter 2 discusses the construction and design of the in-pile loop and the auxiliary facilities used for handling and transporting the different loop components. Each section in this chapter includes a brief discussion of major loop components and how they are configured to form an overall system arrangement.

Chapter 3 describes the pre-filming and pre-conditioning techniques used to prepare the loops for an in-pile run. In addition, the out-of-pile and in-pile tests to determine the heat rejected and the gamma heating component, respectively, are also discussed.

Chapter 4 discusses the data obtained to date on the loop for the four runs which constitute the first campaign of studies. Emphasis is given to the results obtained from the Inconel S/G tubes, which are the major out-of-core components.

Chapter 5 summarizes the above material and suggests future improvements in loop design, operating procedures, and test program.

Appendix A describes the chemical analysis methods used to monitor loop water chemistry. Appendix B discusses a computer program used to calculate loop parameters such as heat fluxes, mass flow rates, surfaces area of materials, etc. Appendix C summarizes the procedures that must be followed when using the hot cell facility located inside the reactor containment building.

2 FINAL DESIGN OF LOOP AND AUXILIARY FACILITIES

2.1 Introduction

The following sections describe the final design of the MIT-Pressurized Water Reactor Coolant Chemistry Loop (PCCL). Emphasis is given to the description of major components and how they were configured to form an overall system arrangement. The final as-built version is described; for a historical perspective K. Burkholder's, A. Morillon's and J. Wicks' theses [B-7] [M-1] [W-1] should be referred to; these reports also summarize the philosophy and engineering principles behind the scale-down process adopted in designing the loop. The auxiliary facilities for handling the PCCL loop are also discussed in the present report. Figures 2.1 through 2.17 show in- and out-of-pile schematics of the loop and the associated handling facilities. In the sections which follow, each of the depicted features will be described in sufficient detail to enable the reader to appreciate their function in the achievement of design goals. Tables 2.1, 2.2 and 2.3 list the location of engineering drawings, as well as component manufacturer information and project reports which provide more detailed discussion of the different PCCL components.

2.2 Aluminum Thimble

The purpose of the aluminum thimble is to enclose the PCCL components and at the same time comply with MITR-II technical specifications, which define the materials that can be exposed to the MITR-II coolant water. The thimble is made of 6061-T6 aluminum. Figure 2.1 shows the major components of the MIT-PCCL loop. As

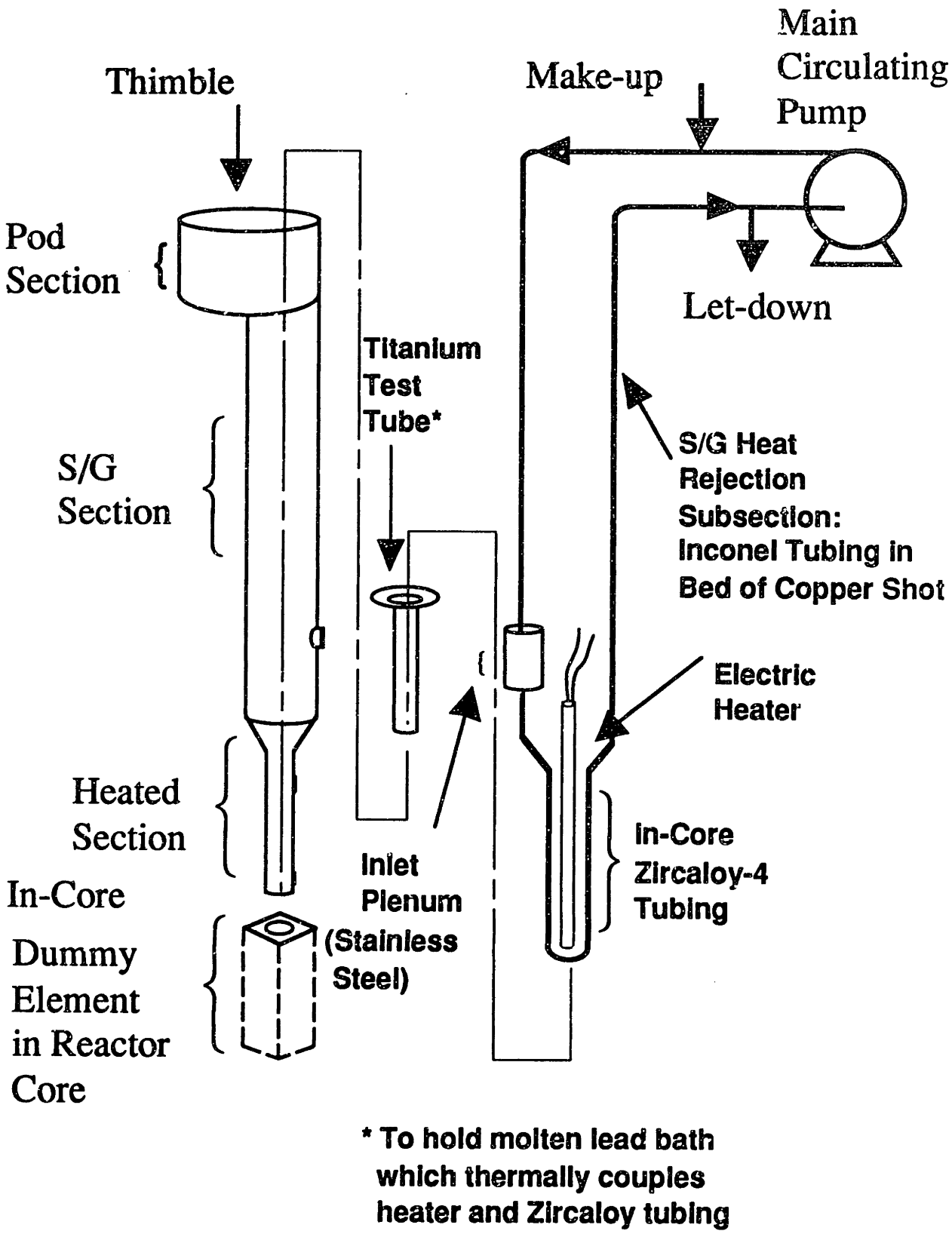

Figure 2.1 Major MIT-PCCL Components.

Table 2.1 Information on PCCL Fabricated components.

Component	File Drawing Number	Q/A File Number
1. Dummy Element	R3L-1	M-86-2
2. Thimble	R3L-2	M-86-2
3. Titanium Test Tube	R3L-3	PCCL Project File
4. S/G Support Assy.	R3L-4	PCCL Project File

Note: Engineering drawings and Q/A files are located in the MITR Operations Office, under the custody of the Nuclear Reactor Laboratory (NRL) Quality Assurance (QA) officer (617) 253-4211.

seen in this figure, the thimble is divided into three major sections, namely; the Pod Section, the Steam Generator (S/G) Section, and the Core Section.

The Pod Section is 12 inches (30.48 cm) in length and 8 inches (20.32 cm) in outside diameter with a 1/4 inch (6.35 mm) wall thickness. The Pod Section was originally designed to house the main circulating pump. However, the custom-built pump commissioned for this application was not completed by the manufacturer in time for the first series of out-of-pile experiments. A decision was made to use a more robust commercially available pump, located external to the MITR-II core tank [H-2]. Thus, the Pod Section presently contains the thermocouple and heater connectors and unions to allow connection of the S/G tubing to the tube sections which penetrate the thimble lid. The top of the pod is flanged for bolting and sealing the thimble lid. The status of the qualification test program on the

Table 2.2 Manufacturers Information on Purchased Components.

Component	Manufacturer	Model #or Specs*
Main Coolant Circulating Pump	Autoclave Engineers, Inc. 2930 W. 22nd St. Box 4007 Erie, PA 16512 USA (814) 838-2071	Model# MP2040 05 65 60
Heater	Delta M Corp. 525 Warehouse Rd. Oak Ridge, TN 37830 Mr. R McCullough (615) 483-1569	Custom LMFBR fuel pin simulator capable of delivering up to 20 kW.
Inconel Tubing	Teledyne-Scottdale Box 302 Scottdale PA 15683	Seamless type see section 2.4.1.2 for more details.
Stainless Steel Tubing	Salem Tube, Inc. P. O. Box 144 Greenville, PA 16125	Seamless type see section 2.4.1.2 for more details.
Aluminum Tubing	Edgcomb Metals C. S. 2015 Nashua, NH 03061-2015 (603) 883-7731	Seamless type
Aluminum Plate	Edgcomb Metals C. S. 2015 Nashua, NH 03061-2015 (603) 883-7731	
Charging Pump	American LEWA ARMAC Co. 1 Wakefield, MA 01880 Mr. R. MacDonald (617) 245-2600	Type EK16
Pulsation Dampener (used in the first two runs)	Liquid Dynamic Pulse Inc. SR 1563, Sloop Point P.O. Box 506 Hampstead, NC 28443-0506	
Back-Pressure Regulator	TESCOM Corporation Pressure Control Division 12616 Industrial Boulevard Elk River, Minnesota 55330	Rated up to 4000 psig

Fittings, Ultraseals	Parker Hannifin Corp. Instrumentation Connectors Division P.O. Box 4288 Huntsville, Alabama 35802-4288 (205) 881-4288	P/N; Unions: 2-2 HBZ-SS, 4-2 HBZ-SS, 4-4 HBZ-SS, 5-4 HBZ-SS, 5-5 HBZ-SS, Union Tee: 5-5-5 JBZ-SS, 4-4-4 JBZ-SS; Ultraseals, 6-4 Q1W, 6-4 QHW
Feedthroughs	Conax Co. 2300 Walden Ave. Buffalo, NY 14225 (716) 684-4500	P/N: PG4-312-A-L
Charging System Ball Valves	Parker Hannifin Corp. Instrumentation Connectors Division P.O. Box 4288 Huntsville, Alabama 35802-4288 (205) 881-4288	P/N: 4Z B6LJ-SS, 4Z, B6XJ2-SS
High Pressure Stop Valves	NUPRO Company 4800 East 345th Street Willoughby, OH 44094	P/N: SS-4UW-TW-(PH) with 17-7 PH stainless tip instead of Stellite.
Uninterruptible Power Supplies	Best Power Technology, Inc. P.O. Box 280 Necedah, WI 54646 (608)565-7200	Model# MD1.5KVA, and MD2KVA.
Heater Controller	PAYNE ENGINEERING Box 70 Scott Depot, W. Va. 25560 (304) 757-7353	Model# 18D
Pump Controller	MagneTek Drives & System 16555 W. Ryerson Road New Berlin, WI 53151	Lancer GPD 502
Computer/Data Logger	Martindale Distribution 212 Main Street North Reading, MA 01864	Equipped with 20 MB hard disk drive, 80286 CPU, 1.2 MB floppy drive, 512 KB RAM memory, DAS-8 A/D converter timer board, and EXP-16 multiplexor board.
Heater Process Controller	Taylor Instrument Combustion Engineering, Inc. P.O. Box 110 Rochester, NY 14692 (716) 235-5000	Model# 500R Model A

* The manuals for the components listed above are kept in the PCCL Project File.

Table 2.3 List of Progress Reports which Discuss PCCL Components.

Project Reports No. (Date)	Topic
Monthly #11 (Nov/87)	Heater Problem
Monthly #14 (Mar/88)	New Heater Design
Monthly #18-24 (Jul-Nov/88)	Main Circulating Pump
Safety Evaluation Report, MITNRL-020, (Feb/1987)	Safety Issues of PCCL
Pump Task Force Report, MITNRL-038 (Aug/1987)	Main Circulating Pump
An In-Pile Loop for Corrosion Transport Studies in a PWR by K. Burkholder, M.S. Thesis (May/1985)	Early PCCL Design
Modelling of Radionuclide Transport in Simulated PWR Environment by A. Morillon, M.S. Thesis (May/1986)	Modelling of Radionuclide Transport in PWRs.
Design, Construction and Testing of an In-Pile Loop for PWR Simulation by J. Wicks, M.S. Thesis (May/1986)	Description of PCCL in nearly final form

original pump is documented in a thesis by A. Esteves [E-1].

The Steam Generator Section is divided into two subsections; the Plenum Subsection and the Heat Rejection Subsection. The Plenum Subsection is 4 inches (10.16 cm) in outside diameter and has a 1/4 inch (6.35 mm) wall thickness. Its function, as indicated in reference [W-1], is to house the inlet plenum and to serve as a transition piece between the Heated Section and the Heat Rejection Subsection. The Heat Rejection Subsection is 75 inches (190.5 cm) in length and 4 inches (10.16 cm) in outside diameter. Its wall thickness is also 1/4 inch (6.35 mm) thick. The primary function of this section is to house the heat transfer medium (copper shot) (sec. 2.4.2.1) as well as the Inconel tubes.

Finally, the Heated Section (sec. 2.5) is 36 inches (90.72 cm) in length and has an elliptical cross section with a major diameter of 2-1/2 inches (6.35 cm), a minor diameter of 1-13/32 inches (3.57 cm) and a wall thickness of 1/8 inches (0.3175 cm). Its function is to house the Titanium Test Tube, the Zircaloy-4 U tube, and the Liquid Lead Heat Bath. The Heated Section is connected to the 4 inch (10.16 cm) S/G Section through a 1/4 inch (6.35 mm) thick transition piece. The function of the transition piece is to minimize the impact of the PCCL on MITR-II core cooling flow.

2.2.1 Thimble Penetrations

The aluminum thimble has several penetrations, namely; the copper shot drain port, which is located in the bottom of the S/G section, and six feedthrough penetrations in the thimble lid.

The copper shot drain port is designed so that the heat transfer medium (copper shot) can be easily drained out, but with a highly reliable seal to prevent escape of the shot from the thimble into the MITR core tank. A circular stainless steel plate 1/8 inch (0.3175 cm) thick with six 8-32 Allen head screws is used to cover the port. The heads of the bolts are wired to prevent inadvertent loosening sufficient to permit escape of the shot. The port is sealed against thimble fill gas (12 psig) leakage or water ingress using a lead coated Inconel C-ring. To prevent hang up of the thimble shot port on obstacles during thimble handling, trapezoidal aluminum pieces were welded at either side of the shot port. Figure 2.2 shows a side view of the thimble and the welded pieces around the shot port area.

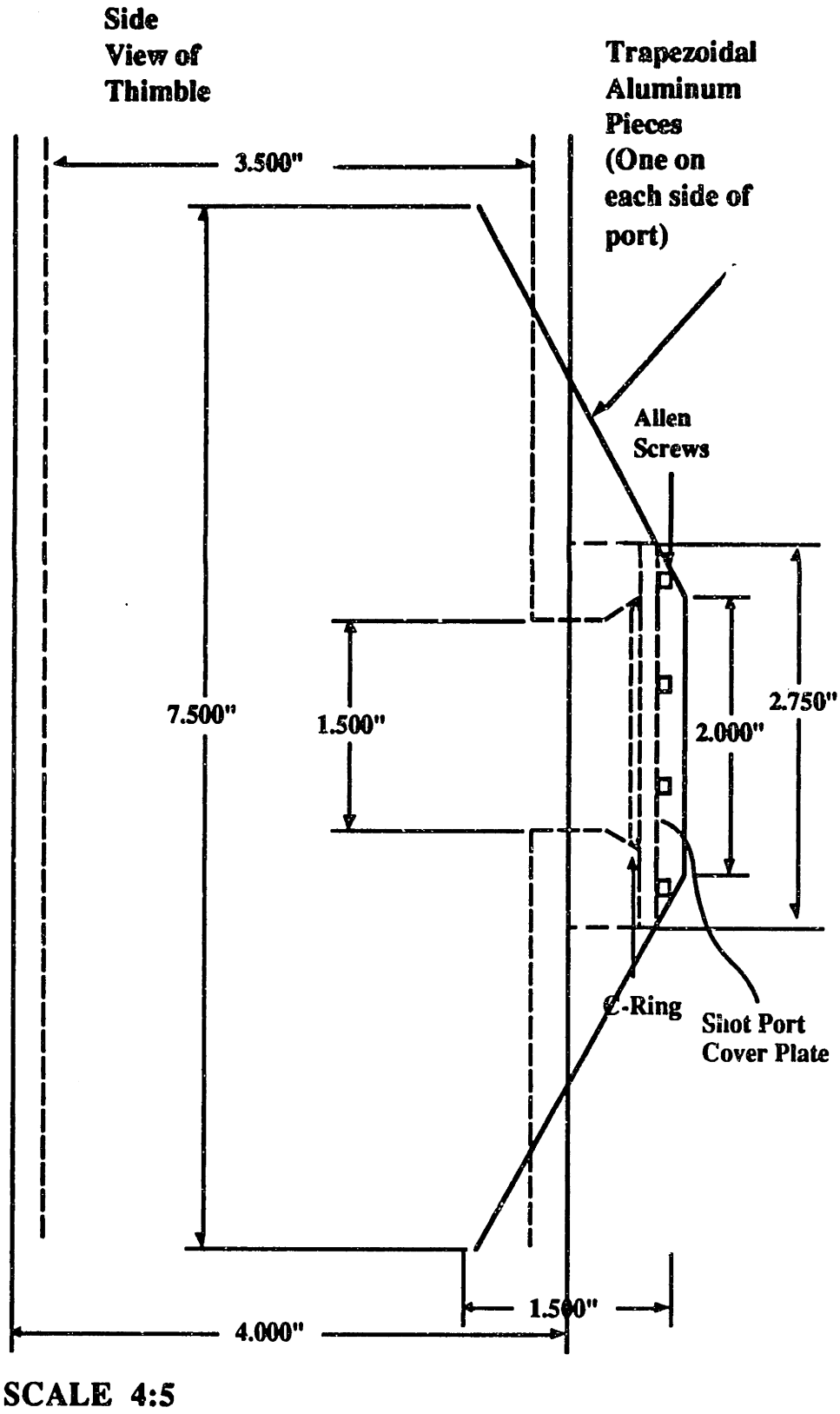

Figure 2.2 Side View of Thimble (Shot Port Region).

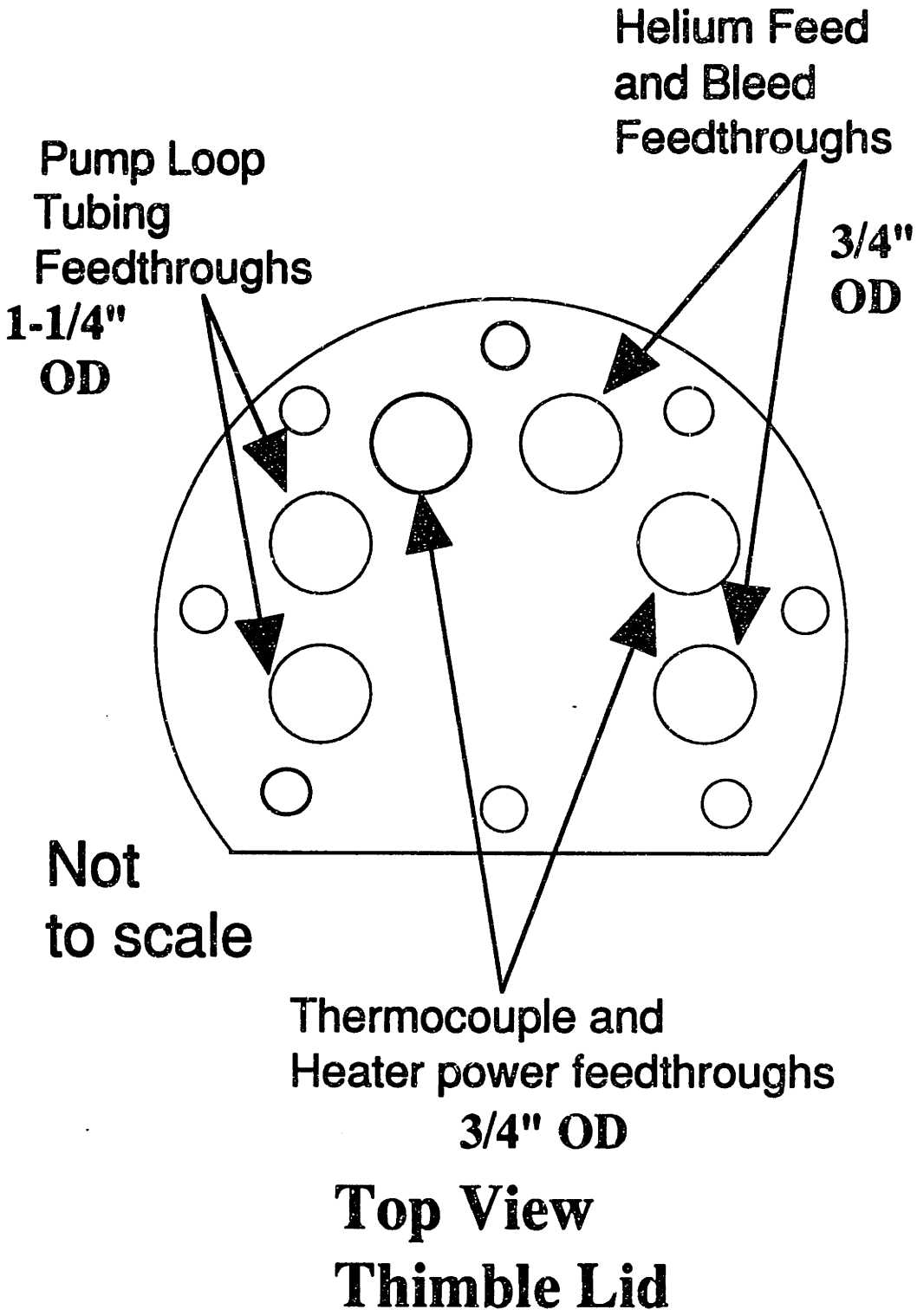

Figure 2.3 Schematic of Thimble Lid.

Feedthroughs in the thimble lid are provided for the high temperature and pressure loop circulating lines (main circulating inlet and outlet), the helium inlet and outlet lines, the heater power leads and thermocouple wires. Two of the penetrations are 1-1/4 inches (3.175 cm) in diameter with welded Cajon fittings. The other four penetration are 3/4 inches (1.90 cm) in diameter and have welded pipe couplings. Figure 2.3 shows a top view of the thimble lid and the locations of the feedthrough penetrations.

2.2.2 Thimble Helium Purge and Overpressure Protection System

During thimble construction and pre-irradiation testing, a helium leak detector was used to verify the integrity of the thimble welds. The thimble is also pressure tested at 150 psig (1.03 MPa) using helium to simulate the pressure buildup in the event of a loss of coolant accident (tube break) inside the thimble. During normal operation, the thimble is pressurized to 12 psig (0.082 MPa) with helium. For the first two in-pile runs the thimble was evacuated with a vacuum pump first and then back filled with dry helium. However, when the loops experienced fitting and plenum leaks, the high humidity caused condensation on the heater connectors, particularly when a vacuum was pulled in the thimble (cloud chamber effect), thus causing electrical shorts. Therefore, for subsequent runs a purge system was installed (other measures are also described later). Figure 2.4 shows the locations where these leaks and electrical shorts occurred.

To supply helium into the thimble, there is a helium supply

line 3/4 inches (1.9 cm) in diameter. In addition, there is also a 1/4 inch (0.635 cm) helium bleed line connected to a humidity detector and ventilation system (Fig 2.8). This line extends through the shot bed into the plenum region. If a water leak develops in the interior of the thimble, feed and bleed of helium removes the moisture from the interior and the humidity detector indicates the efficacy of the purge and the magnitude of the leakage. The normal purge rate is on the order of 0.4 ft^3(STP)/hr.

The helium supply line has a safety relief valve set at 19 psig (0.131 MPa) so that the thimble pressure can be relieved in case of pressurization due to a loop leak. In addition, the helium bleed line has a rupture disk that will protect the thimble against any sudden pressure transient. The disk will rupture at 65 psig (0.44 MPa).

2.2.3 Core Tank Support Bridge

The core tank support bridge is designed to align the thimble with respect to the core and support its total weight and that of other in-pile facilities. The support bridge is made of Aluminum 6061-T6 and is capable of supporting approximately three times the weight of the thimble. Figure 2.5 shows the arrangement of the support bridge in the core tank.

2.3 Pod Section

2.3.1 Main Cooling Pump

The main coolant pump, as noted before, is not housed in the Pod section of the aluminum thimble because the original pump

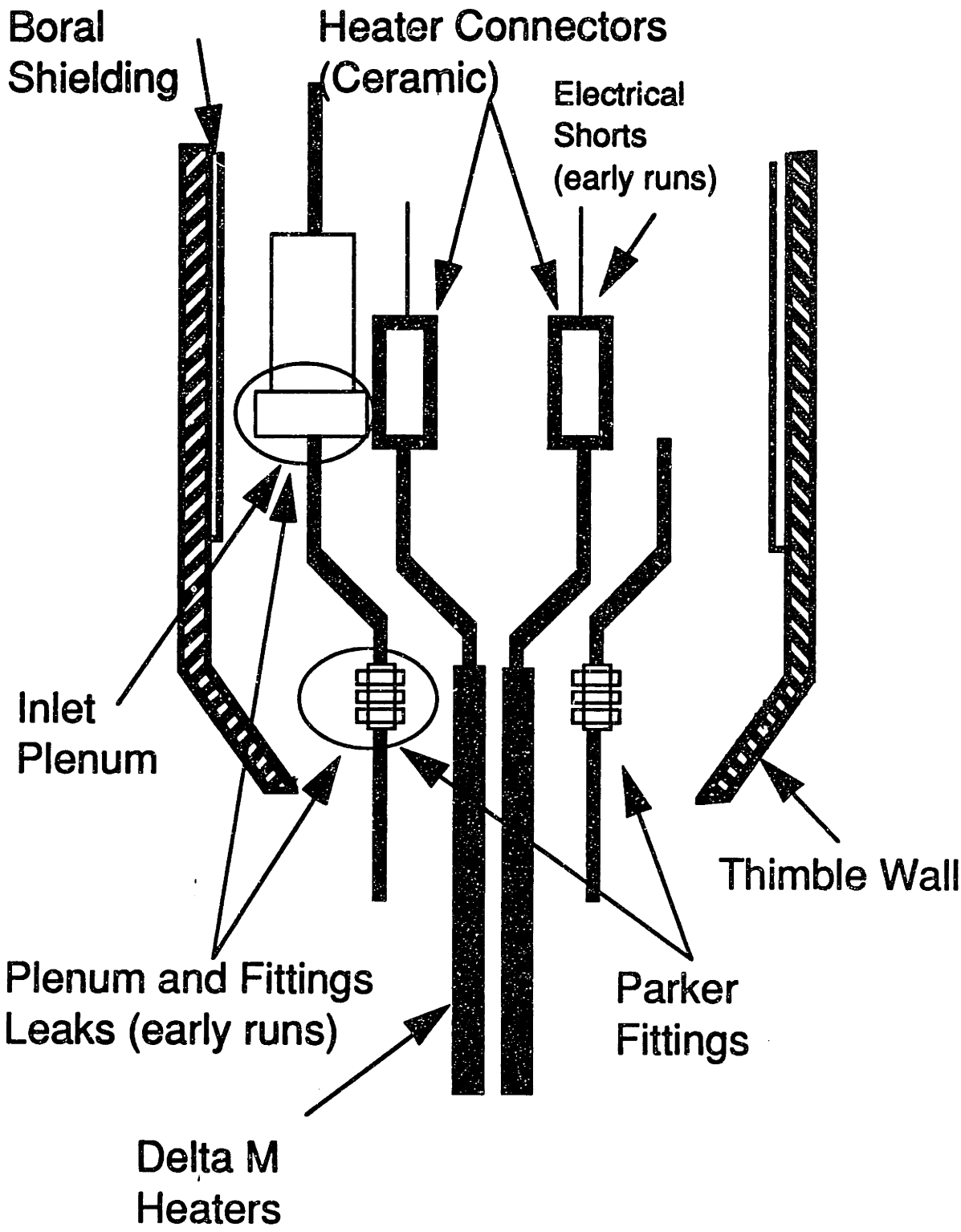

Figure 2.4 Schematic of PCCL Internals.

manufactured by Northern Research and Engineering Corporation (NREC) was not ready in time for use. The NREC pump has since been tested and evaluated in detail by A. Esteves (E-1); this reference also describes its physical characteristics in greater detail. An extensive search for a new pump was conducted and an Autoclave Engineering

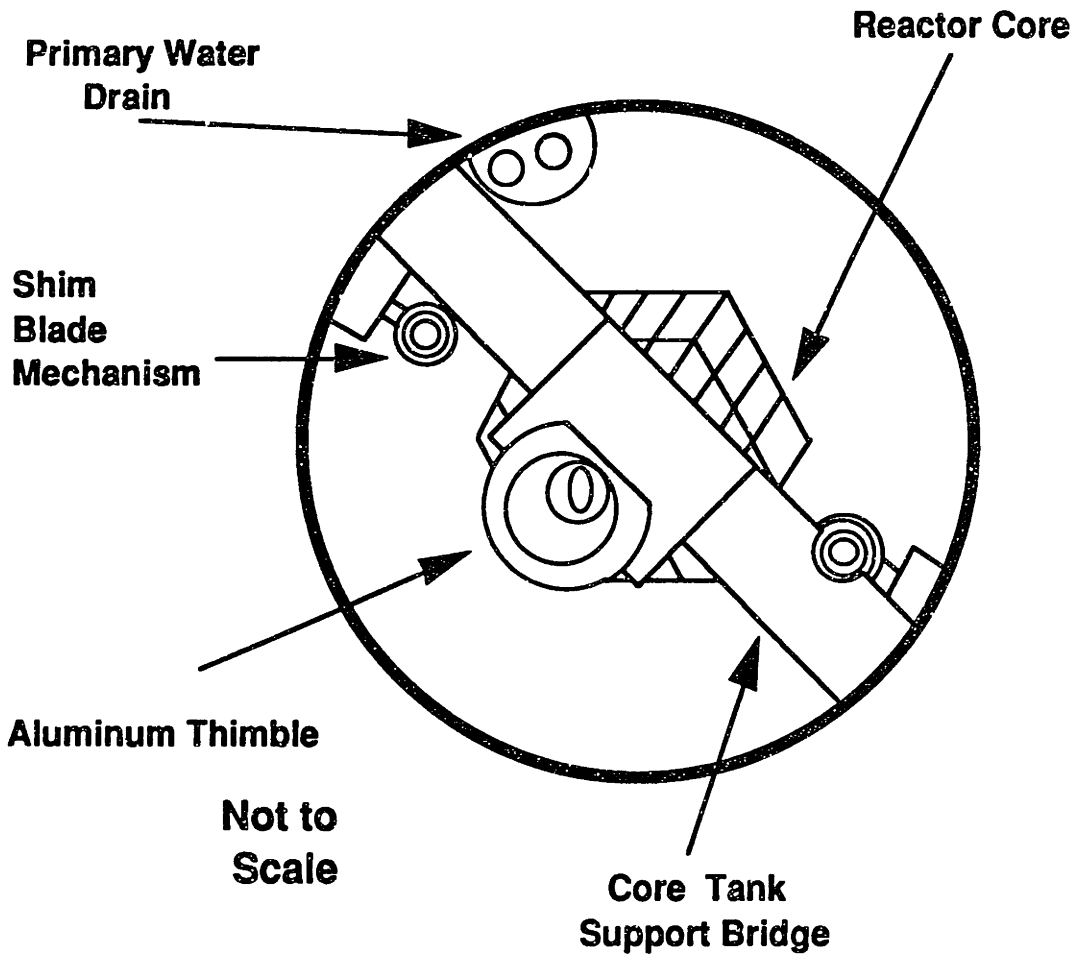

Figure 2.5 Support Bridge in Reactor Core Tank.

(AE) pump was chosen as the one that best met the requirements [H-2]; it is interesting to note that this is the same pump recommended by K. Burkholder in his initial conceptual design. Table 2.4 shows

some of the most important parameters for the AE pump. The AE pump is larger and much heavier than the specially designed NREC canned rotor pump, hence it had to be mounted outside the MIT reactor tank.

Table 2.4 AE Pump Parameters.

Design Conditions	Maximum System Pressure	5000 psi (34.475 MPa)
	Maximum Temperature	650 °F (343 °C)
	Operating Speed	4000 RPM max
	Magnet Cooling	Water cooling must be used
Pump Construction	Part	Material
	Pump Head	316 SS
	Impeller	316 SS
	Shaft	316 SS
	Fasteners	300 series SS
	Bearings	Graphite
	Seals C-Ring	Inconel
Port Size	Inlet	1.0" tubing, I.D. 0.688"
	Outlet	1.0" tubing, I.D. 0.688"
Motor Rating	variable frequency Up to 70 Hz	Voltage 115/230 VAC, 60 Hz single phase
	3/4 HP	Three Phase
General Information	Mounting Position	Horizontal
	Weight	170 lbs
	Maximum Flow	19 GPM
	Maximum Head	17 psi
	Completely metal sealed construction, no rotating seals, magnetic drive, cooled permanent magnet rotor system	

The AE pump is a centrifugal type which operates under the following conditions in the present application.

*	Operating fluid temperature	565° F (315° C)
*	Operating pressure	2250 psig
*	Flow rate	1.5 GPM
*	Rotor can temperature	200-250° F
*	Pump differential pressure	15 psig

* Pump instrumentation consists of a thermocouple on the rotor can in the vicinity of the cooling jacket
* Continuous operation for a month at a time

The AE pump head water volume is 130 cc and its internal wetted surface area is approximately 225 cm^2. Because the AE pump is mounted outside the reactor core tank, the area and volume ratios among the various PCCL materials have changed from those cited in earlier design descriptions; for instance, the total length of quarter inch Inconel tubing was increased from 16.36 to 33.09 ft. A summary of the as-built area and volume ratios will be presented in the next section.

During the first in-pile run, the AE pump experienced two trips because its Variable Frequency Power Supply (VFPS) was unduly sensitive to line voltage dips. A more versatile and forgiving VFPS was purchased, which permits the AE pump to run through or restart after voltage dips or outages of up to 2 seconds in duration. In addition, two uninterruptible power supplies (UPS) were also purchased; one provides emergency power for a period of 45

minutes to the AE pump in the event of a total electric power failure, and the other supports the PCCL control and instrumentation circuits.

2.4 Steam Generator Section

2.4.1 Plenum Subsection

2.4.1.1 Function

The main purpose of the plenum subsection is to house the inlet plenum and to provide room for the inlet and outlet thermocouple and heater connectors. This subsection also houses a cylindrical boral shell that encloses the inlet plenum and the multiple connectors so that the neutron activation of these items can be reduced as much as possible.

2.4.1.2 Loop Plenum

The inlet plenum is 9.625 inches (24.44 cm) in length and has a one inch (2.54 cm) ID. It is made of 316 stainless steel (SS) and its purpose is to match the area and volume ratios between SS, Zircaloy, and Inconel as closely as possible to those in a real PWR plant. During the pre-filming and pre-conditioning stages of the loops (see sections 3.2 and 3.3), the inlet plenum contains coupons of actual plenum material which provide information about the composition and thickness of the oxide layer formed.

The size of the inlet plenum was based on matching the SS :Zircaloy:Inconel ratios using the NREC pump and inlet plenum as a source of SS. Since the AE pump is used in the final configuration, the area and volume ratios have changed from those calculated by J. Wicks [W-1].

The PCCL consists primarily of three type of materials: 316 SS, Inconel-600, and Zircaloy-4. The 316 SS components are: the AE pump head whose area and volume are 34.9 in^2 (225 cm^2) and 7.93 in^3 (130 cm^3), respectively; the inlet plenum with an area of 31.71 in^2 (204.6 cm^2) and a volume of 7.56 in^3 (123.9 cm^3); and SS tubing whose area and contained volume are 5.71 in^2 (36.83 cm^2) and 0.35 in^3 (5.68 cm^3), respectively. The Inconel-600 components are the steam generator tubes which extend throughout the S/G section, and their uncooled extensions through the thimble lid, in and out of the core tank, ending in the inlet and outlet ports of the AE pump; the total area is 296.82 in^2 (1915.0 cm^2) of which 107.9 in^2 (696.1 cm^2) are in the S/G cooled region. The total Inconel-contained volume is 18 in^3 (295 cm^3) of which 6.54 in^3 (107.2 cm^3) are also in the S/G cooled region. The Zircaloy-4 component is the Zircaloy U tube, which is located in-core and immediately above. The Zircaloy tubing has a surface area of 60.03 in^2 (387.31 cm^2) of which 40.7 in^2 (262.5 cm^2) are in-core and 41.1 in^2 (265.1 cm^2) are heated in the lead bath. The total Zircaloy volume is 3.84 in^3 (63 cm^3) of which 2.61 in^3 (42.7 cm^3) are in-core and 2.63 in^3 (43.2 cm^3) are in the lead bath. Hence the MIT-PCCL area and volume ratios are as follows:

Area Ratios

Inconel/Zircaloy-4(total)	=	4.94
Inconel/Zircaloy-4(in core)	=	7.29
SS/Zircaloy-4(total)	=	1.20
SS/Zircaloy-4 (in core)	=	1.78
SS/Inconel-600	=	0.24

Volume Ratios

Inconel/Zircaloy-4(total) = 4.68

Inconel/Zircaloy-4(in core) = 6.90

SS/Zircaloy-4(total) = 4.11

SS/Zircaloy-4 (in core) = 6.07

SS/Inconel-600 = 0.88

Table 2.5 summarizes these ratios and compares them with the corresponding values for a representative Westinghouse PWR plant

Table 2.5 Comparison of PCCL Using AE Pump and PWR area and volume ratios.

	PWR (Westinghouse)		PCCL	
Material	Area Ratios	Volume Ratios	Area Ratios	Volume Ratios
Inc-600/Zr-4 (Total)	2.73	NA	4.94	4.68
Inc-600/Zr-4 (in core)	2.73	NA	7.29	6.90
Inc-600 (Cooled) /Zr-4(Heated)	3.44	NA	2.63	2.48
SS/Zr-4 (Total)	0.39	NA	1.20	4.11
SS/Zr-4 (in core)	0.39	NA	1.78	6.07
SS/Inc-600	0.15	NA	0.24	0.88
SS (no AE Pump) /Inc-600 (S/G)	-	-	0.26	1.65
In-Core/Ex-Core	0.33	0.055	0.11	0.074
In-Core/Ex-Core (S/G)(No AE Pump)	-	-	0.19	0.05

[W-1]. Note that the added Inconel lines to and from the AE pump and the SS in the pump account for most of the differences in the PCCL vs PWR comparison.

2.4.1.3 Boral Shielding

To reduce the neutron activation of the inlet plenum and thermocouple connectors, a cylindrical Boral shell 1/8 inch (0.32 cm) thick surrounds these components. The Boral shell is made of 30 to 50 weight percent boron carbide in aluminum.

2.4.2 Heat Rejection Subsection

As noted before, the Heat Rejection Subsection is approximately 75 inches (190.5 cm) in length with a 4 inch (10.16 cm) outside diameter and a 1/4 inch (0.635 cm) wall thickness. It contains the copper shot heat transfer medium, the steam generator tube support assembly, the shot drain port, the Inconel S/G tubes and the heater and thermocouple wires.

2.4.2.1 Copper Shot Heat Transfer Bed

The purpose of the copper shot and the helium gas in the Heat Rejection Subsection is to provide a reliable, reproducible and passive heat flow path in which the heat flux through PCCL S/G tubes is similar to that in a standard PWR plant. Copper shot and helium gas were chosen as the heat transfer medium because calculations and experiments performed by Wicks [W-1] and Burkholder [B-7] showed that this combination provided a larger effective thermal conductivity compared to other shot-gas combinations and one in the

range which permitted a convenient internal configuration. It was also found in out-of-pile experiments (sec. 3.4) that the effective thermal conductivity was essentially independent of the helium pressure in the thimble. However, a thimble pressure of 12 psig is maintained at all times to prevent any reactor primary water from entering the thimble if a thimble leak develops.

The copper shot is screened to a particle size between 0.1 inch (0.254 cm) and 0.14 inch (0.3556 cm). This size prevents the shot from passing through the fuel plates (spacing 0.078 in. (0.198 cm)) in the MIT reactor core and assures that several of them can fit between the S/G tubes and the thimble wall to assure good heat transfer.

In addition to the properties that have been discussed before, it is worth mentioning that the copper shot/helium gas combination exhibits a low neutron activation cross section, which results in a relative low induced activity. This is important whenever the loop is disassembled since the loop operators will be subjected to less exposure.

2.4.2.2 Steam Generator Tube Support

The S/G Tube Support, as shown in Figs. 2.6 and 2.7, consists of top and bottom support plates, and a 1-1/4 inch (3.175 cm) OD spinal tube with welded 90° angle pieces.

The 1/4 inch (0.635 cm) top support plate is made of aluminum and has several penetrations. One of these penetrations (shot-fill-port) allows the shot to be loaded into the S/G section. It is important to point out that the shot is always loaded with the

thimble in a vertical position. In addition, while the loading of the shot is taking place, the thimble is gently tapped with a rubber mallet to help the shot settle into a more compact geometry. The other two penetrations in the top support plate serve as a passthrough for the S/G Inconel tubes. The top support plate is welded to an aluminum tube to form a spine. In addition, the top support plate is bolted to the bottom of the Pod Section. The spinal aluminum tube is approximately 1-1/4 inch (3.175 cm) in OD and houses the power leads for the electric heaters and the inlet and outlet thermocouple leads. As mentioned before, it has two 90° angle pieces welded along its length. The purpose of the angle pieces is to increase the effective thermal conductivity of the shot bed. The location of these angles and the S/G tubes relative to one another and to the thimble wall are crucial determinants of the overall thermal conductivity of the heat rejection system and hence the total PCCL input/output power balance.

Finally, the bottom support plate is made of stainless steel and is split to allow installation after make-up of the loop tubing. The clearance between this plate and the tubing is minimized to prevent leakage of the copper shot into the plenum and in-core regions. The bottom plate is inclined at a 45° angle to facilitate draining of the copper shot.

2.5 Core Section

2.5.1 Zircaloy-4 Fuel Rod Simulator

The fuel rod simulator is located at the bottom of the thimble. It consists of a Zircaloy-4 seamless U tube which is the same material

used as cladding in PWR fuel elements. It was provided by EXXON Nuclear. Table 2.6 shows the composition of the Zircaloy-4 tubing used in the PCCL. Neutron activation analysis was used to determine

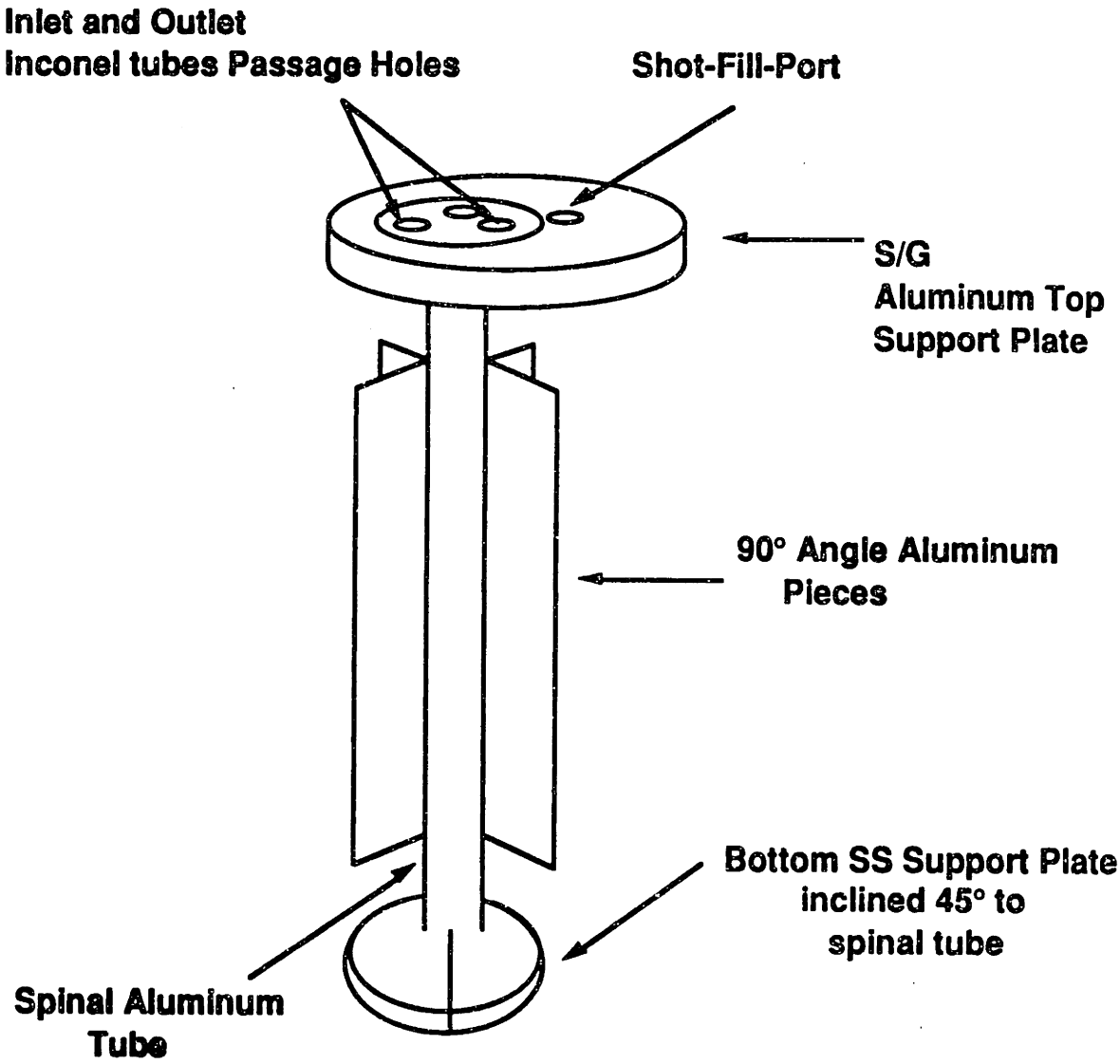

Figure 2.6 S/G Tube Support Assembly.

the Zircaloy-4 composition. Table 2.6 also shows the ASTM material composition specs.

The Zircaloy tube is 6 ft (182.9 cm) in length and has a 5/16

inch (7.94 mm) outside diameter and a wall thickness of 0.028 inches (0.71 mm) hence an ID of 0.2565 inches (0.65 cm). The Zircaloy U

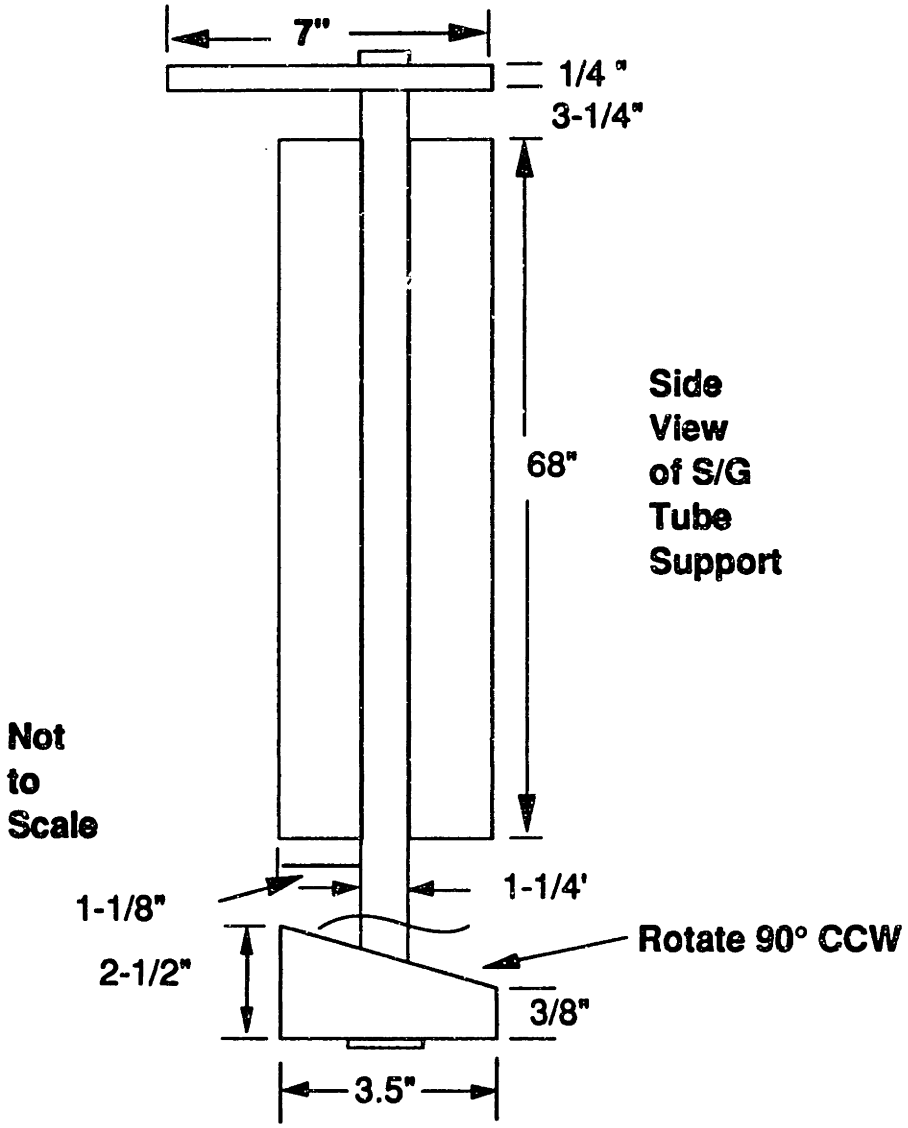

Figure 2.7 Side View of S/G Tube Support.

tube is imbedded in a lead bath which is contained in a titanium test tube. It is estimated that approximately 50.5 inches (128.27 cm) of this tubing are within the MIT reactor core, and 56 inches (142.25 cm) are submerged in the bath (and therefore subjected to heat flux).

Table 2.6 Composition of Zircaloy-4 Tubing.

Zircaloy-4				
Element	MIT NRL*	MIT NRL*	MHI	ASTM (Spec) [F-1]
	1990	1989	1989	1988
Sn (%)	-	-	1.47	1.2 to 1.7
Cr (%)	0.1 ± 2%	0.1 ± 2%	0.1	0.07 to 0.13
Fe (%)	0.22 ± 5%	0.21 ± 5%	0.21	0.18 to 0.24
Ni (%)	-	-	-	<0.007
Co (ppm)	0.72 ± 8%	0.72 ± 8%	10	<20
Sb (ppm)	-	0.93 ± 10%	-	-
W (ppm)	-	-	-	<100
Hf (ppm)	52 ± 7%	-	-	-

* By Neutron Activation Analysis

2.5.2 Titanium Test Tube

The earlier Titanium Test Tube (TTT) design consisted of a Titanium tube bent into an elliptical shape with a welded plate at the bottom. The major problem of this TTT design was the bulging of the tube at high temperatures. To mitigate the bulging, a weld bead was welded along its length. Nonetheless, high temperature tests showed that the bulging of the tube still existed. Thus, a new TTT design was implemented.

The new TTT is machined to shape from solid bar stock and seam welded to form a container. The TTT contains the electric

heaters, the Zircaloy U tube, and the lead bath. A titanium flange is welded to the top of the can to support the TTT at the bottom of transition section. Underneath this flange, there is a 1/8 inch thick boral shield to reduce, to some extent, the streaming of neutrons into the S/G section.

Titanium was selected as the material for the TTT because of its high strength and corrosion resistance at elevated temperatures as well as the low neutron activation cross section of titanium. The TTT cross section is shown in Fig. 2.8. Its length is approximately 36 inches (91.44 cm). The average clearance between the TTT and the thimble wall is 0.15 inches (0.38 cm). This space was kept at a minimum so that in the event of thimble leakage or a loop loss of coolant accident (LOCA) the water-floodable volume will not insert more than 20 mβ of reactivity. This gap also determines the heat loss by conduction in the in-core segment of the loop, which has been shown to provide sufficient passive heat rejection to maintain maximum temperatures below the 2200° F Zircaloy-steam exothermic reaction during LOCA without reactor shutdown [H-3].

2.5.3 Electric Heater

The electric heater used in the heated section performs two main tasks:

a). While operating in-pile, the heater provides the energy necessary to match prototypic core (and steam generator) heat fluxes (hence film temperature gradients) while maintaining the loop water bulk temperature at 300° C.

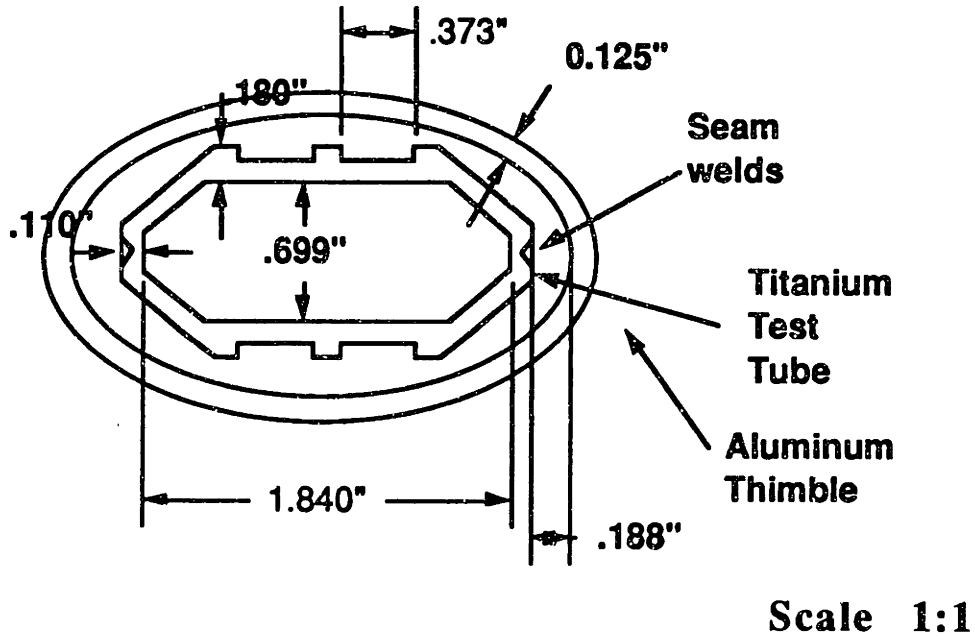

Figure 2.8 TTT Cross Section

b). It provides sufficient heat to conduct out of pile experiments that determine, for instance, the effective thermal conductivity of the copper shot bed or the heat rejected in the S/G section.

The most confining constraint on heater design was the requirement (because the heater and thimble are grounded to the reactor structures) not to employ a common grounded sheath type design. An initial prototype using a multipass axial filament proved failure prone. The successful final design is shown in Fig 2.9. It is based upon use of proven Liquid Metal Fast Breeder Reactor (LMFBR) fuel simulator technology.

The heater consists of two legs, side by side, and joined at the bottom end in a junction box. Each leg contains a helical filament, as shown in Fig 2.9. This arrangement has a reduced linear heat flux (hence internal ΔT values) because the heated length in a U configuration is approximately twice that of a rod design. The heater

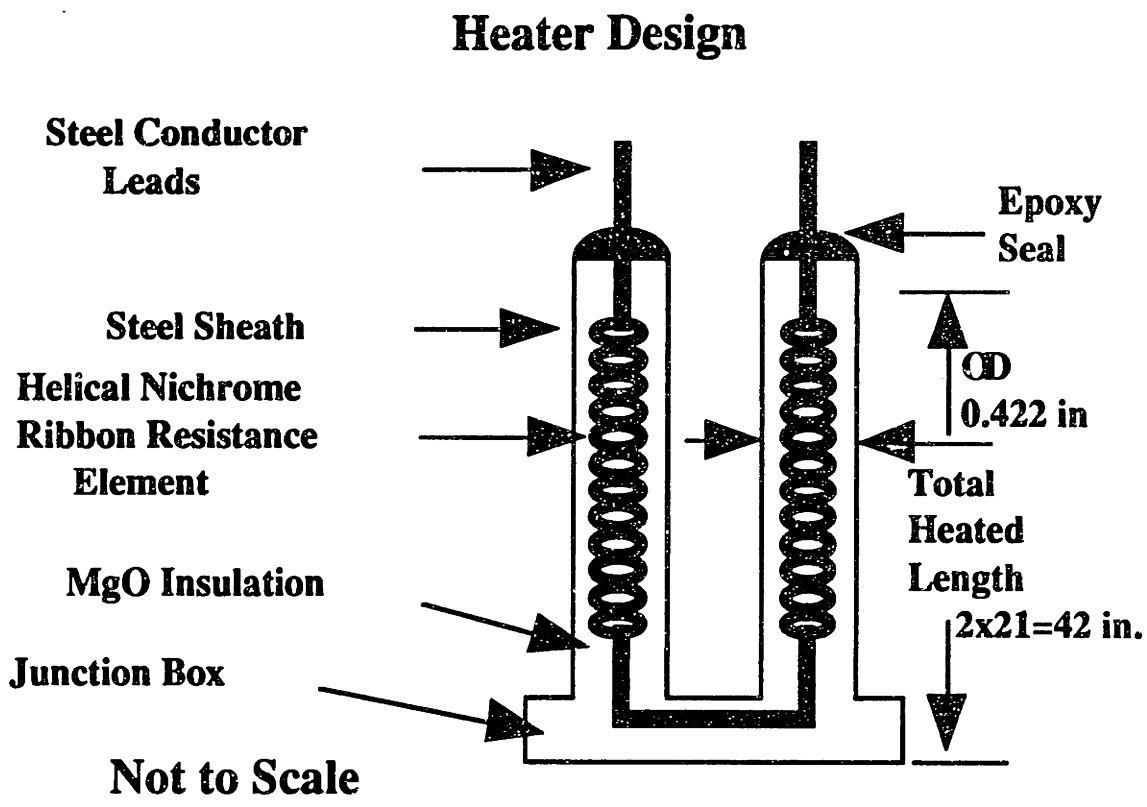

Figure 2.9 Schematic of Heater.

is capable of delivering approximately 20 kW at a constant heat flux of 5.7 kW/ft over a length of 42 inches (106.7 cm), however, the heater normally operates at 12 kW when the reactor is at full power, due to the contribution of 7 kW of reactor gamma heating. When the reactor is shut down, it is necessary to reduce the outlet temperature from 600° F to 570° F to avoid operating the heater at excessive power. The heater is insulated with Magnesium Oxide (MgO) which gives a 10 Megohm resistance between the heater element and the outside steel sheath. The heater sheath is fabricated of low cobalt 1018 low carbon steel with an outside diameter of 0.422 inches (1.12 cm). There are two thermocouples attached to the surface of the

heater sheath to monitor the lead bath temperature.

The principal shortcoming of this design is its susceptibility to moisture pickup through the epoxy end seal (which degrades at high temperatures and gamma doses). This can lead to heater failure by filament to sheath electrical shorts. Hence periods of post-incident bake out of the heaters are routinely required.

2.5.4 Liquid Lead Heat Bath

The purpose of the liquid lead bath in the heated section is to uniformly distribute the energy generated by the heaters to the Zircaloy tubing. When the MIT Reactor is at power approximately 7 kW of thermal energy is also deposited in the lead bath, due primarily to gamma ray interactions. Thus, the heater power is decreased by this amount, since the heater is operated in a mode which keeps a constant loop water outlet temperature. The amount of lead in the heated section must be limited such that passive rejection of the gamma heating can be achieved during loss of flow incidents, without excessive lead bath, hence Zircaloy, temperatures. Since gamma heating is also lost following a reactor shutdown, a high value in this component would lead to excessive power demands on the electric heaters to replace the lost energy input. Also, if the reactor scrams, the resulting rapid ramp-up of the heater power can cause excessive thermal stress in the heater. The need to limit nuclear heating is the principal reason why the liquid lead is contained in an elliptical TTT instead of a circular one.

According to the Safety Evaluation Report (SER) for the PCCL [H-3], the in core gamma dose rate produces an average of 1 watt of

energy per gram of material in the core. The total weight of the TTT (lead, heaters, and Zircaloy tubing) accounts for 5.68 kg, hence approximately 5.68 kW of gamma heating. The actual gamma heating determined by heat balance during in-pile experiments is 7 kW.

2.5.5 Instrumentation of the Heated and S/G Sections

The instrumentation of the heated and S/G sections consists of six thermocouples (TCs), two of which are attached to the sheath of the heaters. They measure the lead bath temperature at two different locations. One is located 16 inches (40.64 cm) from the top of the TTT and the other is 6 inches (15.24 cm) from the bottom of the TTT. Their outputs are connected to an Omega controller and to a thermocouple readout located in the MIT Reactor control room, respectively.

The other four thermocouples (2 TCs per inlet and outlet) are located at the junction of the Inconel or Stainless Steel (SS) and Zircaloy tubing in Swagelok connectors. They measure the water inlet and outlet temperatures. The output of the outlet thermocouple is connected to the heater controller, which automatically shuts the heaters off if the outlet temperature exceeds 650° F. The output of the inlet thermocouple is connected to an Omega controller for monitoring purposes, except that one can switch to inlet T control should the water outlet thermocouple fail.

2.6 Control Instrumentation

As mentioned in sec. 2.5.3, there are two thermocouples attached to the surface of the heater sheath, and they both monitor

the lead bath temperature. One of the thermocouple outputs is connected to an Omega controller which will cut off the electrical power to the heater if the lead bath temperature exceeds the normal operating range of 950 to 1100 °F by more than 150° F. This value was selected to insure that the maximum heater element temperature does not exceed 1600° F, the value specified by the manufacturer (Delta M Corp. of Oak Ridge Tenn). The other thermocouple output is connected to a thermocouple readout in the MIT reactor control room so that the reactor operator can monitor the lead bath temperature.

The heater power supply is a phase firing silicon control rectifier (SCR) type. The heater power is controlled with a proportional power controller which tries to maintain an outlet temperature of 600° F. If for any reason, the outlet temperature exceeds the 650° F alarm set point; the controller will automatically shut the heater off.

2.7 Safety and Data Logging Systems

The most important safety features of the PCCL are summarized in Fig 2.10. An alarm system has been incorporated in the final PCCL design to warn reactor or loop operators about any abnormal condition existing while the PCCL is running. There are nine alarms that can be activated if an abnormal condition exists. In addition, once the alarm has been activated, an audible sound is emitted and a light corresponding to the particular alarm condition in the front mezzanine and reactor control room alarm panels is lit. The nine alarms are:

Alarm	Condition
1. High Temperature #1 (HT#1)	When lead bath temperature exceeds the normal operating range by 150° F, this alarm is activated. The heater power will be automatically cut off.
2. High Temperature #2 (HT#2)	This alarm is activated whenever the outlet water temperature exceeds 650° F. As soon as this alarm is activated the electric power to the heater is automatically cut off.
3. Low Pressure (LP)	This alarm is activated when the system pressure drops below 1800 psig.
4. Pressure Relief Valve Lifted (PRVL)	This alarm is activated if the system pressure exceeds the PRV set point of 2500 psig or, in the event of PRV failure, the burst disk set point of 2850 psig.
5. Low Level Charging Tank (LLCT)	This alarm is activated whenever the charging tank#1 level drops below 17 inches.
6. High Thimble Humidity (HTH)	This alarm is activated when the humidity in the purge line exceeds the expected value (which can vary from run to run, typically 10%).
7. Low Thimble Pressure (LTP)	This alarm is activated any time the thimble pressure drops below 10 psig.

8. Low Heater Current (LHC)	This alarm is activated when the PCCL heater current is below 10% of its normal maximum operating current.
9. Low Level Test Tank (LLTT)	This alarm is activated either because a low water level exists in the test tank or because the main circulating pump magnet region temperature exceeds 285° F. The test tank water is used to cool the main circulating pump.

A summary list of different accident scenarios, alarm conditions, and action taken is next presented. Some of these scenarios have actually occurred and will be discussed in more detail in Chapter 4. The Safety Evaluation Report (SER) for the PCCL [H-3] and Abnormal Operating Procedures for the PCCL should be referred to for additional detail.

Scenario	Alarm	Action Taken
Loss of Coolant Accident (LOCA) caused by rupture of piping or safety relief valve stuck in the open position.	PRVL, LP, HTH, HT#1	Turn off main circulating pump, charging pump, and heated autoclave heaters. Reactor must shut down.
Failure of Main Circulating Pump	HT#1, HT#2	Reactor must shut down. Shut down main circulating and charging pumps and isolate loop for long outage.
Failure of Charging Pump	LP	Cool down in-pile loop, turn off main circulating pump and heated autoclave heaters. Reactor must shut down.

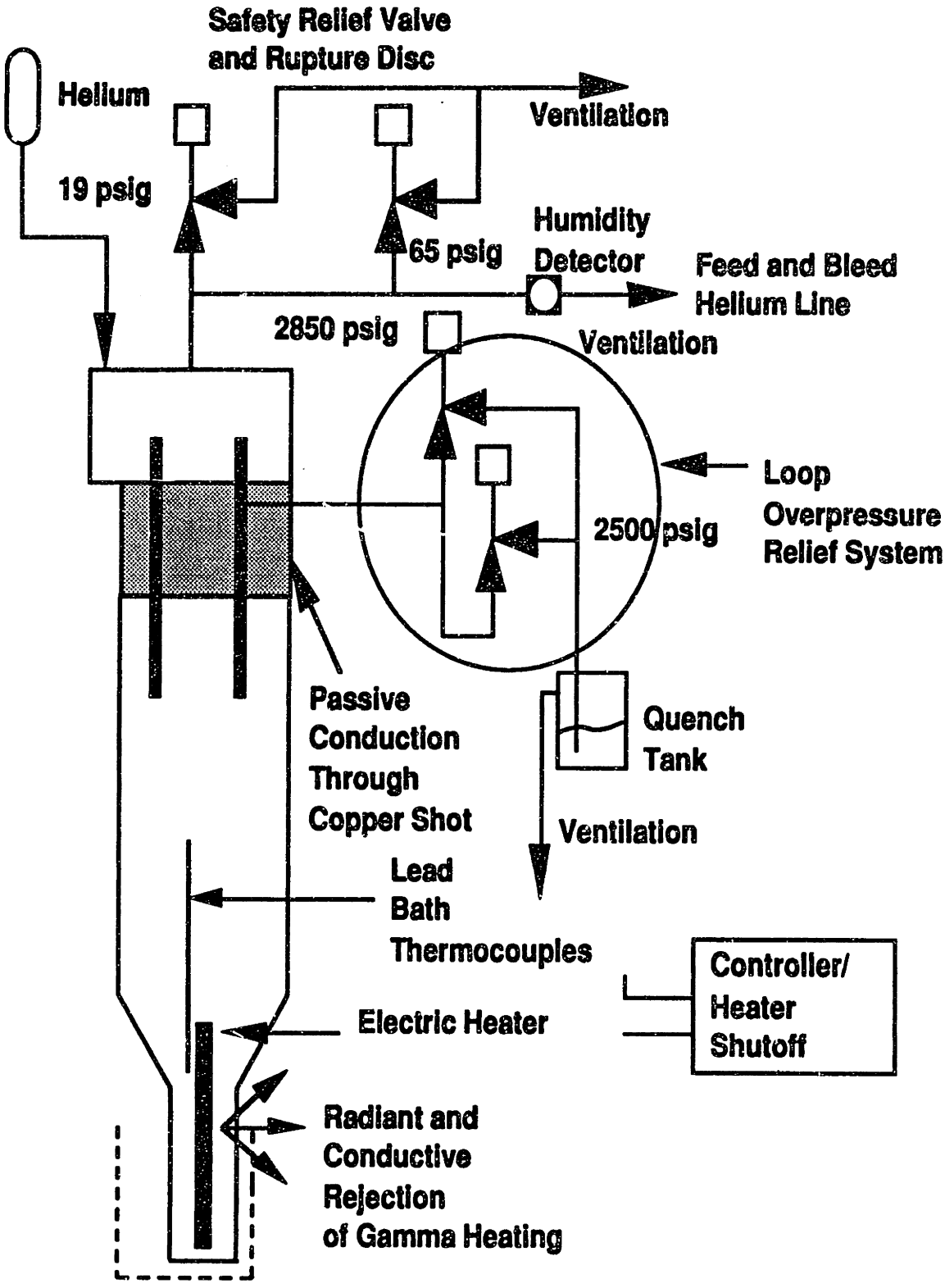

Figure 2.10 Safety Features of the PCCL.

Heater Failure	LHC	Turn off main coolant and charging pumps and heated autoclave heater. Reactor must shut down.
Loss of Electrical Power	LHC	The UPSs will automatically provide electrical power to instruments and main circulating pump for a period up to 45 minutes. However, heater power will be cut off . Boiling in the loop will be prevented by the heated autoclave pressurizer. No action is required by PCCL operators.
Failure of Heater Controller	HT#1	Turn off main coolant and charging pumps. If heater controller is not repairable in a short period of time, reactor must shut down.

The data logging system consists of a personal computer with data acquisition capability that displays and records inlet and outlet temperature, heater power and system pressure. In the event of a rapid transient, the data logging system retains the previous variables over a five second interval so that the loop personnel can evaluate and diagnose the transient scenario. When the loop is operating in steady-state mode, the above mentioned variables are recorded at five minute intervals, thus, reducing the computer memory requirements.

2.8 Charging System

The charging system, shown in Fig 2.11, consists of two main components; the charging pump and the make up water subsystem.

The charging pump in combination with the let-down line back pressure regulator maintains the loop pressure at its normal operating point (2200 psig) and supplies the make up water at a constant flow rate. This pump (LEWA type EK16) is a positive displacement type capable of delivering a flow rate from 0 to 2420 cc/hr at a maximum operating pressure of 4600 psia (31.72 MPa). The loop pressure is controlled with a TESCOM back pressure regulator located in the letdown line. The normal letdown flow rate is 300 cc/hr. A pulse dampener was originally installed at the outlet of the charging pump to reduce pressure pulsations. This device was found not to be essential and was removed following the first two in-pile runs after it developed a leak.

The make up water subsystem provides make up water for the loop. It consists of two 50 liter storage tanks made of Pyrex glass and capable of withstanding up to two atmospheres of hydrogen overpressure. It is normally operated at 5 psig. This subsystem has two major auxiliary circuits; the hydrogen sparging circuit and the chemistry analysis loop.

The hydrogen sparging circuit consists of a valveless metering pump capable of delivering up to 450 ml/min of hydrogen gas and a platinum-carbon-teflon wet catalyst, used at the outlet of the valveless pump, to recombine oxygen and hydrogen so that the water chemistry in the storage tanks can be maintained at less than one ppb oxygen content.

The chemistry analysis loop is designed for the purpose of monitoring the oxygen (usual) or hydrogen (occasional) concentration in the charging tank water. The oxygen and hydrogen electrodes

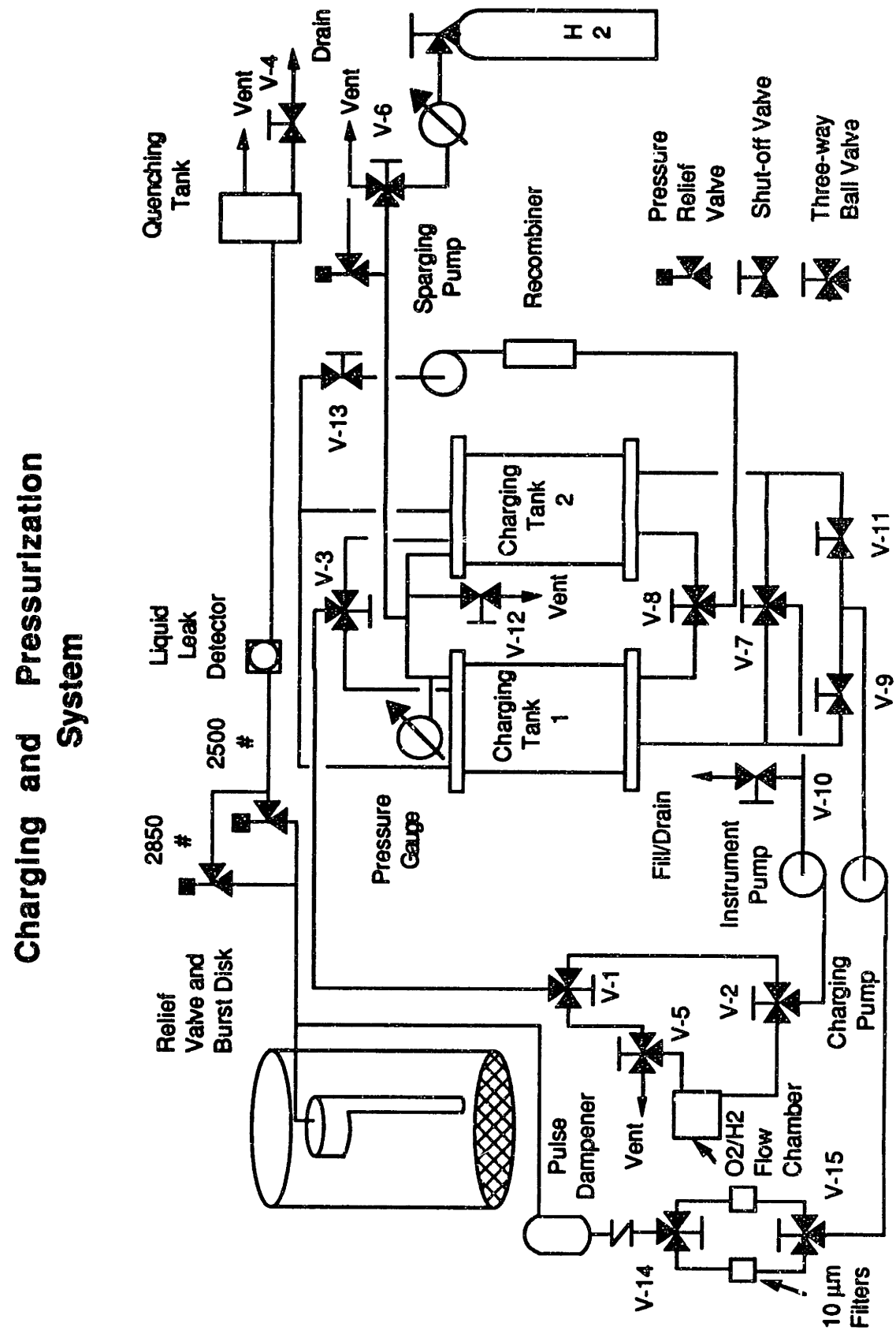

Figure 2.11 Charging System.

(ORBISPHERE Models 2713 and 2730) are swapped periodically to check that the hydrogen and oxygen are within PWR specifications. The chemistry loop employs a Teflon gear pump to circulate the water from the charging storage tank through the detector chamber and back into the tanks. This pump is also capable of charging new batches of water chemistry into one of the storage tanks, where the water is deoxygenated prior to its transfer to the adjacent charging storage tank. At a makeup/letdown flow rate of 300 cc/hr a single charge lasts approximately 165 hrs (7 days). As shown in Fig 2.11, the PCCL contains an overpressure protection system (OPS) which will protect the PCCL loop and the charging system in the event of an overpressurization incident. The OPS consists of a Parker pressure relief valve and a burst disk which are set at pressures of 2500 (17.24 MPa) and 2850 psig (19.71 MPa), respectively. Both of these relief mechanisms relieve to a quenching tank, where steam is condensed, and a leak detector activated if an overpressure condition exists.

2.9 Coolant Sampling and Let-Down System

The Coolant Sampling and Let-down System (Figure 2.12) consists of a discharge tank, an ion exchange column, a Stainless Steel (SS) deposition monitor filter, a TESCOM back-pressure regulator, and a recirculating ion exchange pump loop.

The discharge tank is made of acrylic plastic and is capable of holding up to 70 liters of discharged liquid. It has a 5-1/4 inch (13.33 cm) OD with 1/4 inch (0.635 cm) wall thickness. The discharge tank has a helium cover gas to avoid accumulation of a hydrogen-

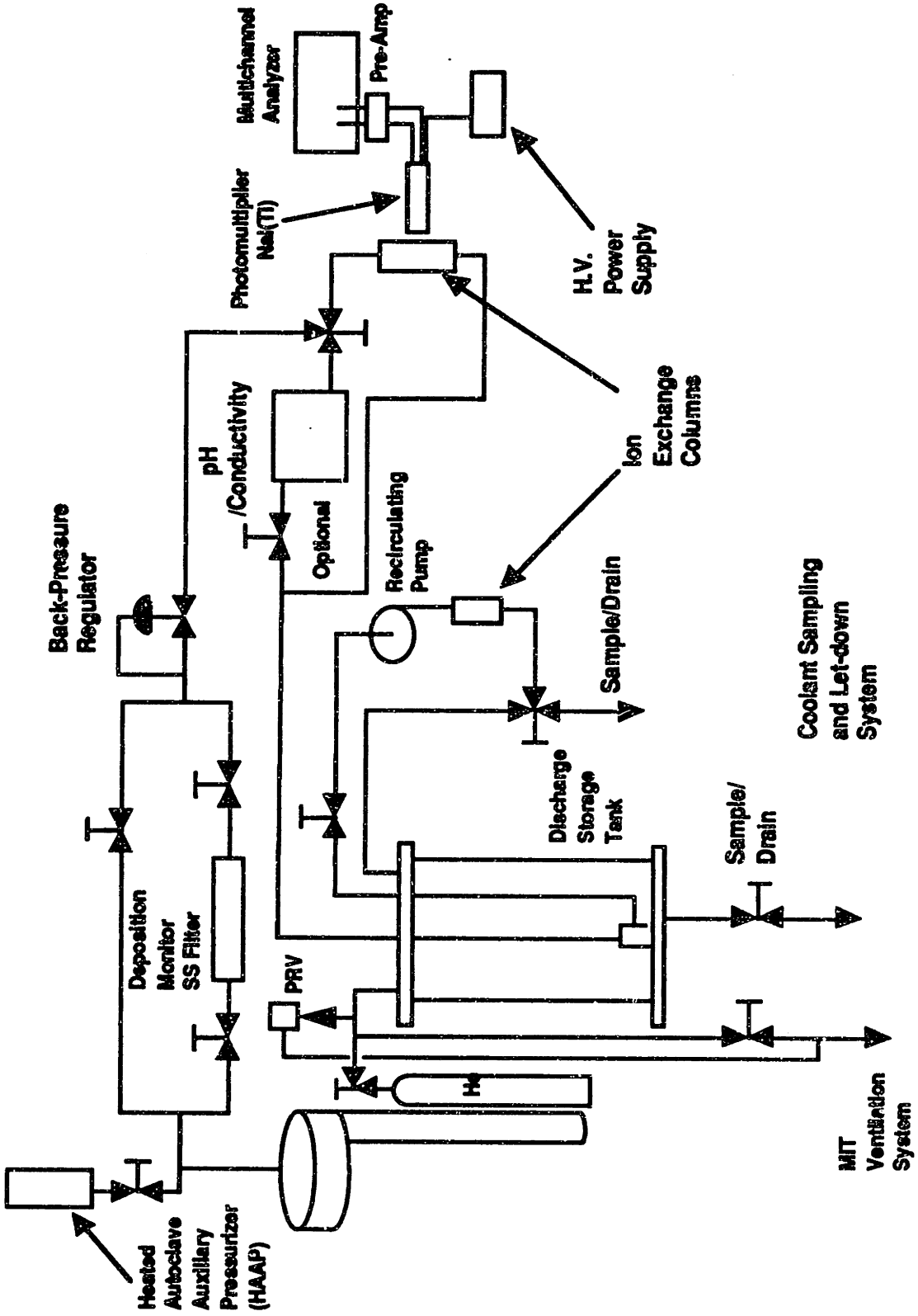

Figure 2.12 Coolant Sampling and Let-down System.

oxygen explosive mixture. In addition, the helium cover gas and hydrogen can be vented out through the MITR ventilation system, or if the pressure exceeds 19 psig, through a safety relief valve whose outlet is connected to the same ventilation system.

The Ion Exchange Column is also made of acrylic plastic. Its dimensions are 7/8 inches (2.22 cm) OD with a 1/8 inch (0.3175 cm) wall thickness and 6-1/4 inch (15.87 cm) length. It contains a mixed bed resin to remove radioactive corrosion products from the coolant water. The long tubing run and low flow rate ensure that the letdown water has reached room temperature before it reaches the IX column inlet. The Ion Exchange Column is used as a monitor during each in-pile run. A NaI(Tl) photomultiplier detector connected to a Canberra Series 20 Multichannel Analyzer is placed in front of this column so that proper identification of radioactive corrosion products being deposited in the mixed bed resin can be determined. The Ion Exchange (IX) Column is discussed in more detail in sec. 2.9.

The SS deposition monitor filter, as shown in Fig. 2.13, consists of a SS housing in which the SS sintered filter and spring element are placed (Parker CPI/ MI-106). The sintered filter has a 10 μm pore size and is replaced, on the average, every third day during each in-pile run. To determine the radioisotopes deposited on the sintered filter, a high purity Germanium detection system is used outside the containment building where the background is considerably lower than inside the containment building. The SS filter normally operates at approximately 195 °F [90° C] (about 370 °F [188° C] lower than the loop operating temperature due to considerable heat losses).

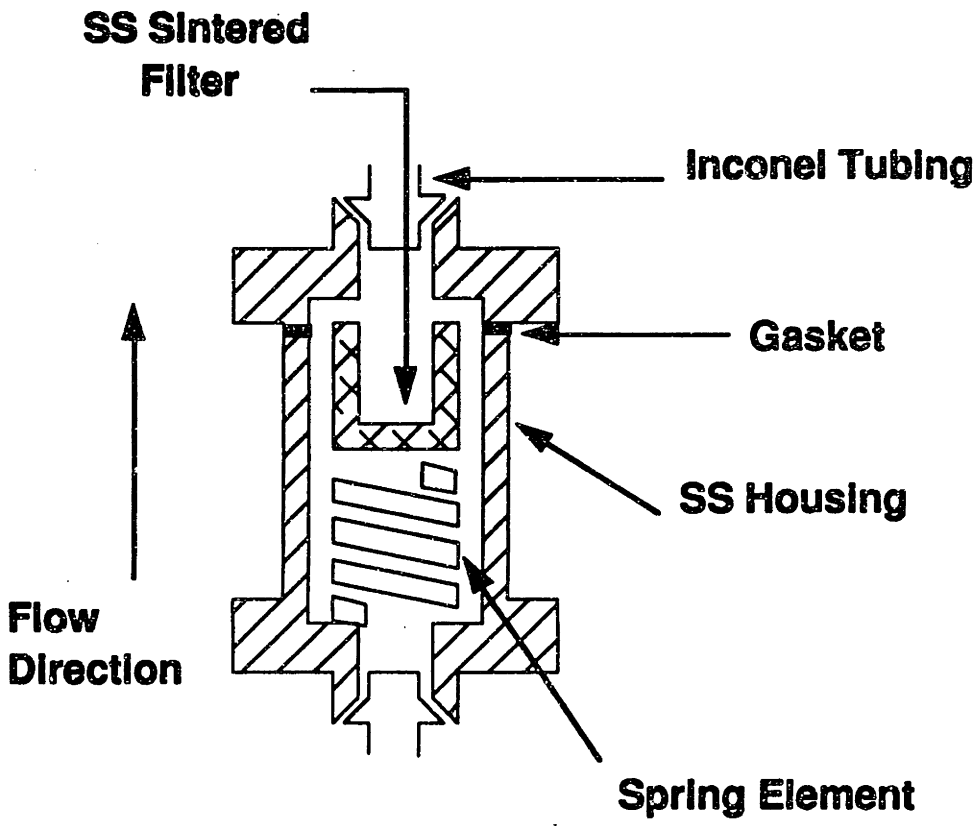

Figure 2.13 SS Deposition Monitor Filter.

The TESCOM back-pressure regulator is designed to maintain the system pressure of 2200 psig. The back-pressure regulator is made of 316-SS and is rated up to a maximum inlet pressure of 4000 psig.

Finally, the Recirculating Ion Exchange Loop is designed to remove any of the residual activity still left in the discharged liquid prior to its disposal. It consists of a Ryton gear pump capable of delivering up to one liter per minute. This gear pump is used to recirculate the water contained in the discharge tank through an ion exchange column (not to be confused with the one in the let-down line (see Fig 2.12)) and back into the discharge tank. After two or

three hours of continuous operation, a water sample is taken to the MITR Radiation Protection Office for a radioisotope analysis. The Radiation Protection Officer determines whether or not the sample is below the maximum permissible concentration (MPC) so that the discharged liquid can be disposed of properly.

2.9.1 Heated Autoclave Auxiliary Pressurizer (HAAP)

The HAAP is designed to prevent boiling in the PCCL due to rapid cooldown because of a loss of an electric heater. A reliability and prototype component test study was performed by T. Achorn [A-1] to show that in the event of a heater loss, the heated pressurizer would be able to supply the water volume needed to compensate for the loss of volume due to the rapid cooldown. Thus, the saturation temperature in the HAAP at its (and the loop's) final system pressure will be above the system temperature. In this way, boiling in the PCCL is prevented.

The final HAAP design is shown in Fig. 2.14. It consists of a pipe made of 304-SS closed by welded plugs at top and bottom, a K-type thermocouple, two Chromalox heaters, an Omega Controller, and fiber glass pipe insulation.

The pressurizer's 304-SS is approximately 2-7/8 inches (7.30 cm) in outside diameter with a 0.203 inch (0.515 cm) wall thickness. Its total volume is 54.92 in^3 (900 cm^3). In addition, the pressurizer has a venting fitting at the top, a tube with an open top and sealed bottom for K-type thermocouple access, and a fitting at the bottom of the pressurizer for connecting it to the let-down sampling line.

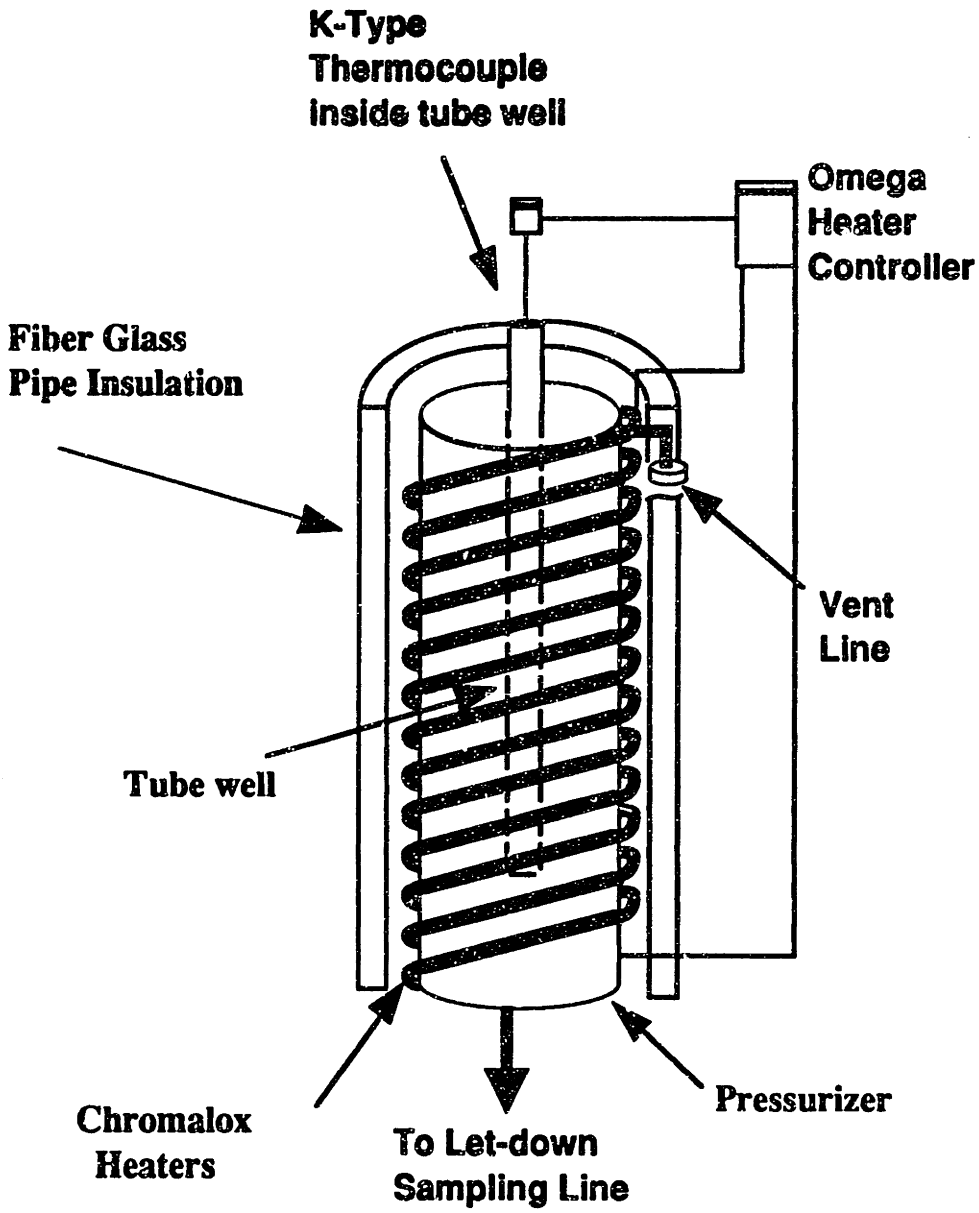

Figure 2.14 Heated Autoclave Auxiliary Pressurizer.

Two Chromalox Heaters connected in series are wrapped around the pressurizer. These heaters provide the necessary heat to maintain the average temperature in the pressurizer at 630 °F (332.2° C), to ensure that the pressurizer is the hottest point in the

system.

The Omega Controller is responsible for maintaining the pressurizer temperature at 630° F by turning the heaters on and off.

The entire pressurizer is wrapped with fiber glass pipe insulation to reduce unnecessary heat losses and to ensure that the pressurizer always remains the hottest (hence first to boil) point in the system.

2.10 Ion Exchange/Let-Down Line Detection System

As described in sec. 2.8, the Ion Exchange/Let-down Line Detection System provides information about the radioactive corrosion products transported in the coolant. As seen in Fig. 2.12, a detection system composed of a 2x2 inch Canberra Model 802-3 NaI(Tl) crystal and photomultiplier tube, a 2000 Volt Power Supply, and a Canberra Series 20 Multichannel Analyzer is used to record gamma spectrums of the different radioisotopes deposited on the Ion exchange Column. The NaI crystal and photomultiplier are enclosed in a lead pig to reduce the background when the reactor is at full power. The decay time in the let-down line (3000 sec) is sufficient for the decay of short lived species such as N-16. A small window in the lead pig facing the Ion Exchange Column is used to reduce the count rate and dead time of the detector. Figure 2.15 shows the arrangement of the different components.

The mixed bed resin is Amberlite IRN-150 nuclear grade type capable of removing anions and cations from the water. The resin consists of 0.025 inch diameter spherical beads which are in a hydrogen/hydroxide form. This resin is designed specifically for use

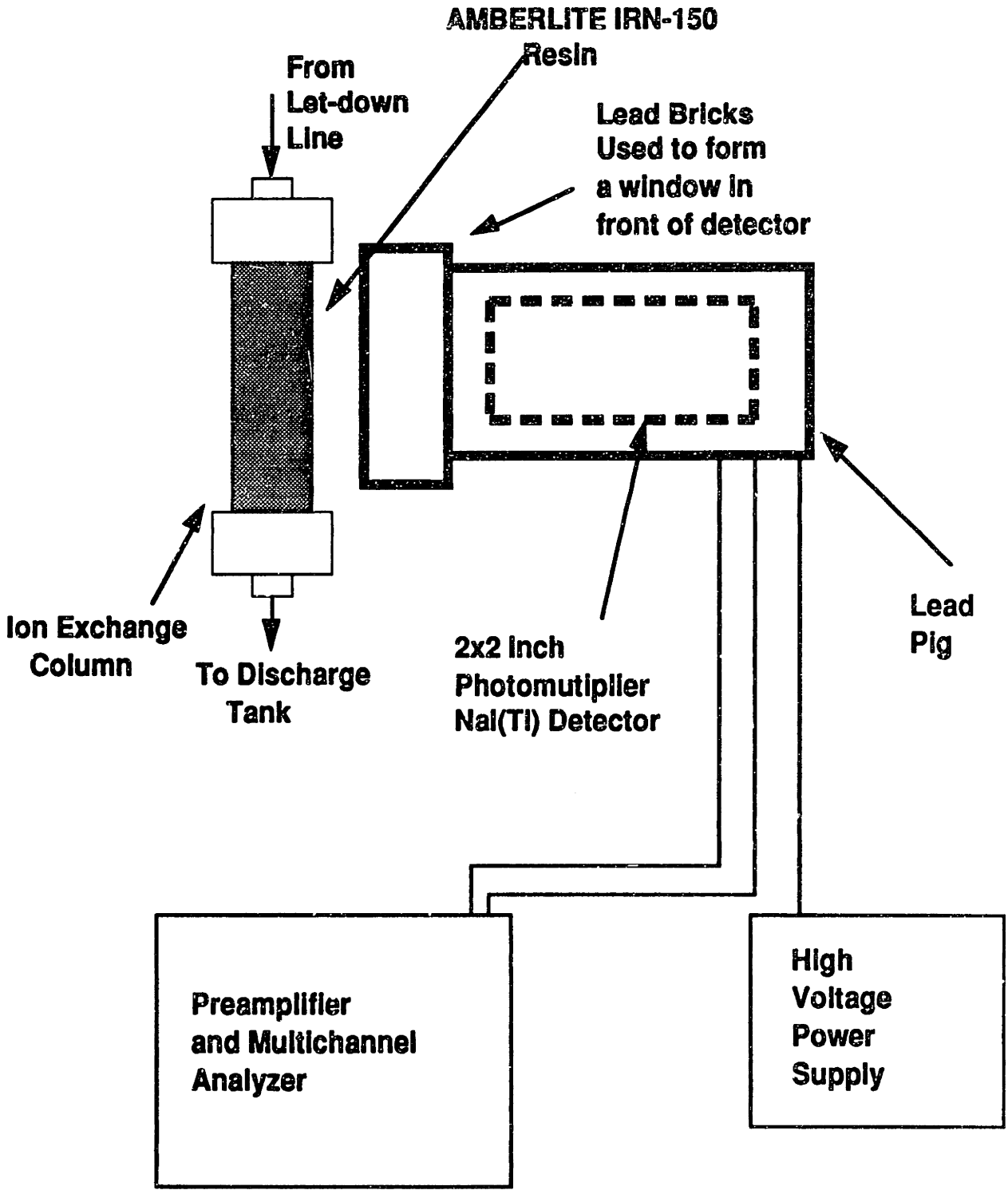

Figure 2.15 Schematic of the IX Detection System.

in water treatment applications, particularly in once through applications such as primary water chemistry control in nuclear power plants.

Daily spectrums are taken when the loops are in-pile and running. Once the run has ended, the resin is poured out of the IX column into a standard sample container and counted outside the containment building with a high resolution semiconductor detector.

2.11 Post Irradiation Data Acquisition System

To determine the specific activity of loop water samples, and S/G Inconel tubes, a data acquisition system was assembled as shown in Fig. 2.16. This system consists of a High purity Germanium (HpGe) detector, a Series 35 multichannel analyzer, a stepping motor programmable motion controller (MITAS), a stepping motor, and a printer (EX-1000). The arrangement and integration of the components mentioned above is described in detail by G. Solares [S-1].

Once the loop has been disassembled, the Inconel S/G tubes are cut with a tube cutter approximately 15 cm above and one cm below the shot bed region. The S/G tubes are then placed one at a time in a horizontal tube support channel and a stepping motor driver chain is attached to both ends. The stepping motor is used to pull the S/G tube in front of a shielded High purity Germanium detector in 4 cm increments every 1000 seconds. A gamma spectrum is then taken and recorded for approximately 50 positions of each S/G Inconel tube.

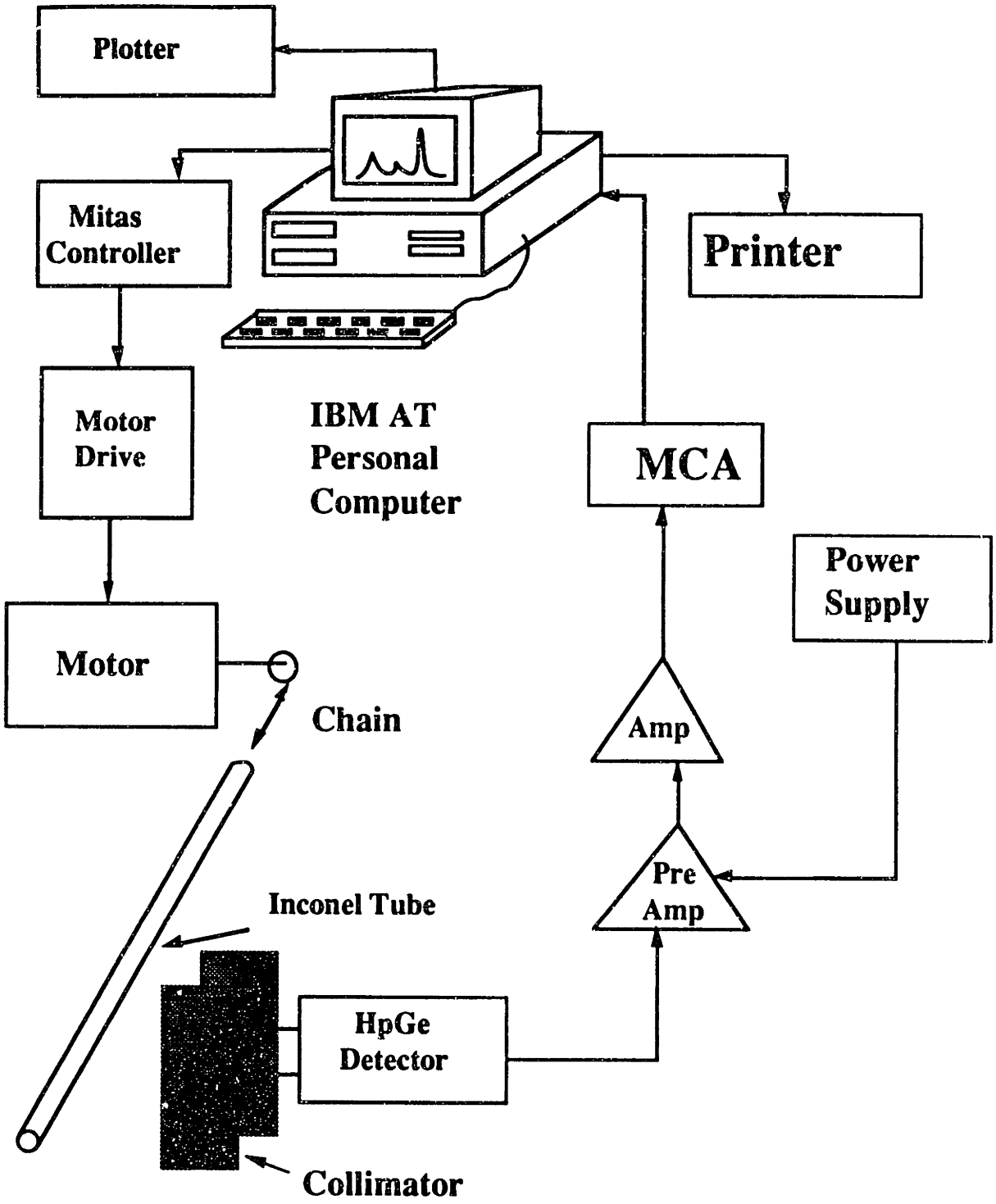

Figure 2.16 Post Irradiation Data Acquisition System.

2.12 Loop Handling System

The loop handling operation is best described as a two step

operation:

1. When the thimble (Loop) is being installed in the reactor core.
2. When the thimble (Loop) is being removed from the reactor core.

The loop handling system (Fig. 2.17) consists of a 3-ton polar reactor crane hoist, a shielding cask, a manual hoist, a cask support plate, and a boom hoist.

The 3-ton polar reactor crane hoist is capable of lifting and transporting the thimble and shielding cask anywhere along the reactor floor or reactor top. The reactor crane can only be operated by an authorized crane operator.

The shielding cask is made of lead and has a 4-1/2 inch (11.43 cm) diameter central hole. It is constructed in a hinged clamshell configuration to permit it to pass the large diameter pod atop the thimble. The thickness of the shielding cask is approximately 3-1/2 inches (8.89 cm) which is enough to reduce the exposure dose rate to 300 mR/hr at contact with the cask while the loop is being removed from the reactor core. (Because the same TTT and lead bath were used in the last two runs, the exposure dose rates were a bit higher than previous runs.) Since personnel are normally more than five meters from the cask during handling, their absorbed doses are quite small. A wedge is used to hold the thimble in place in the shielding cask. In addition, the shielding cask has a shutter at its bottom that can be opened to allow the thimble to be lowered into the reactor core.

Once the thimble is set in place on the top of the shielding

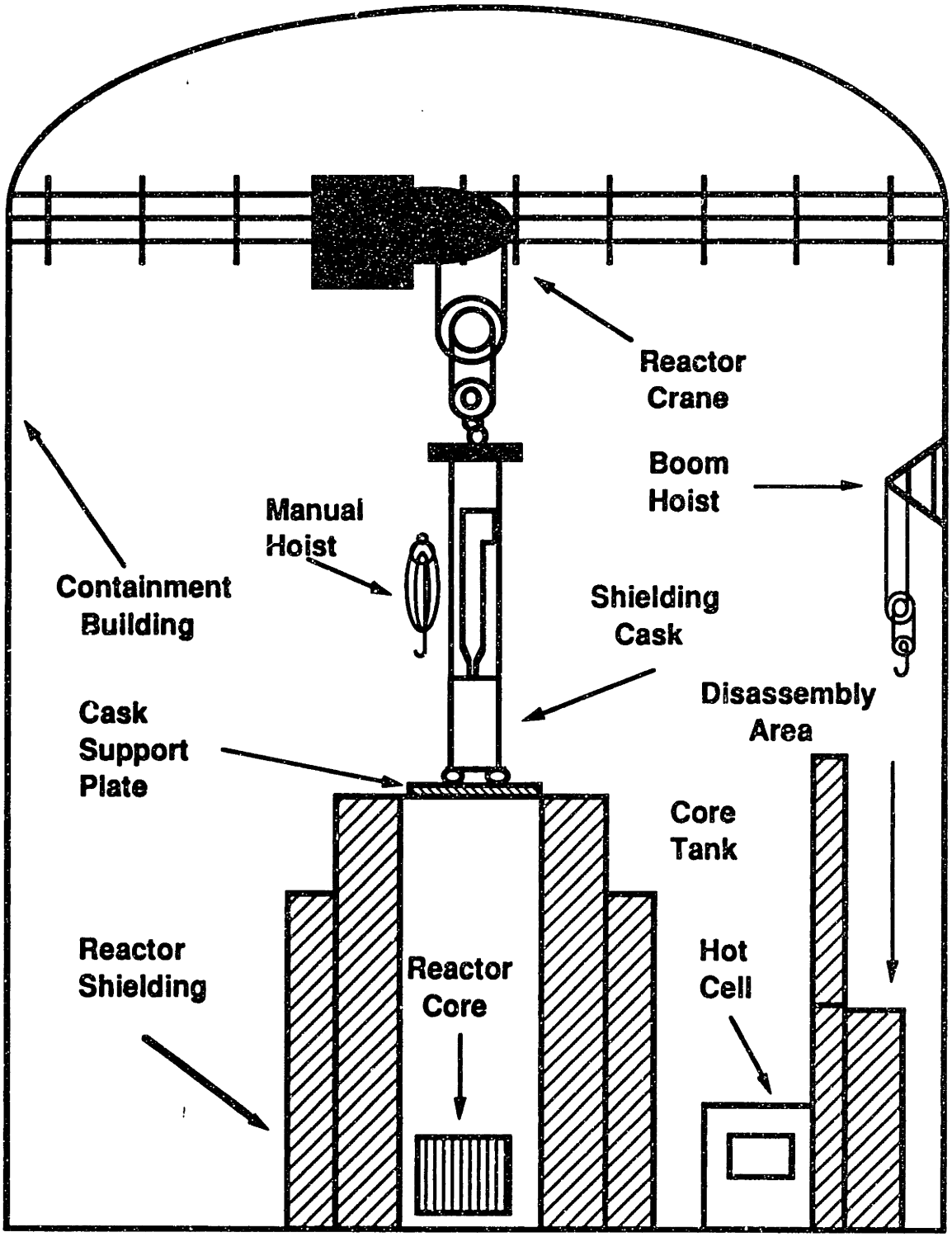

Figure 2.17 Schematic of the Loop Handling System.

support plate, the manual hoist is used to lower the thimble into the reactor core. The hoist line has a spring in series whose tension indicates the degree of free motion when the thimble is lowered into the dummy element and provides a flexible lifting system to prevent a sudden high load due to a hang-up of the thimble.

The cask support plate is made of Carbon Steel and its purpose is to provide support and a limited amount of shielding when the thimble is being lowered into or removed from the core. The support plate is approximately one inch (2.54 cm) thick and covers the top of the reactor core tank.

The boom hoist is used to remove/install the loop internals from/in the thimble. The boom hoist is attached to the containment wall and can be swung out of the way to provide room for the reactor crane to rotate a full (360°).

The following steps are taken when installing the thimble in the reactor core:

1. The cask support plate is placed on the top of the reactor core tank.

2. The secured thimble and shielding cask are transported with the 3-ton crane hoist to one of the top holes in the hot cell.

3. The cask shutter is opened and the thimble is lowered into the hot cell to reduce the exposure dose from the thimble heated section.

4. The clamshell shielding cask is opened and cleaned with a vacuum cleaner.

5. The clamshell shielding cask is closed and the thimble pulled out of the hot cell.

6. The cask shutter is closed.

7. The clamshell shielding cask and thimble are then transported to the cask support plate on the reactor top.

8. The cask shutter is opened.

9. The thimble is lowered until the thimble pod rests on the top of a securing wedge.

10. The manual (hand) hoist is rigged to the thimble.

11. The clamshell shielding cask is opened and the thimble lowered with the 3-ton hoist until the pod is level with the cask support plate.

12. The thimble is lowered with the manual hoist into the dummy element. The spring tension is monitored to verify free motion while lowering the thimble into the dummy element.

13. The thimble is secured to the bridge using pull-down bolts.

14. The loop umbilicals are made up between the thimble and penetration shield block.

For removing the thimble from the core tank, the following steps are taken:

1. The loop umbilicals are disconnected.

2. Using the 3-ton hoist, the cask support plate is placed on top of the reactor core tank.

3. Using the 3-ton hoist, the shielding cask is positioned on the top of the cask support plate.

4. The clamshell shielding cask is opened.

5. The manual hoist is rigged to the top of the thimble and to the 3-ton reactor crane hoist.

6. Using the manual hoist, the thimble is lifted, observing the

spring tension to verify that free motion exists until the thimble heated section clears the dummy element.

7. The thimble is lifted with the 3-ton hoist until the pod section clears the top of the cask.

8. The clamshell shielding cask is closed.

9. The manual hoist is detached while the thimble pod rests on the top of a securing wedge.

10. The 3-ton hoist is reattached to the thimble.

11. The reactor top is cleared and the thimble lifted to its fully withdrawn position.

12. The cask shutter is closed and the thimble and cask transported to the disassembly area.

Table 2.7 lists the loop handling (sec 2.12), and abnormal operating (sec. 2.7) procedures which discuss in more detail the installation/removal of the PCCL and abnormal loop conditions. Loop operating procedures with the reactor at power or in shutdown mode are also listed in this table and will be discussed in the next chapter.

2.13 Hot Cell and Disassembly Area

The hot cell (inside the containment building) is used to melt the radioactive lead (once the heated section of the loop has been disconnected from the rest of the loop) and to chop up the activated Zircaloy tubing. The internal dimensions of the hot cell are 57 inches (144.78 cm) by 80 inches (203.20 cm); it has three 6 inch (15.24 cm) diameter holes on its top. A large lead glass window (22 inch by 34 inch) is located at the front of the cell. In addition, two hand controlled manipulators are available to handle activated tubing.

Table 2.7 List of PWR Loop Procedures.

Procedure	Procedure or QA Number
Maintenance of Schematic Diagrams	PCCL-1
General Safety Requirements	PCCL-2
Loop In-Core Installation	PCCL-3
Loop Removal From In-Core	PCCL-4
PCCL Hydrogen Inventory	PCCL-5
PCCL Charging Tank	PCCL-6
PCCL Rigging Checklist	PCCL-C1
PCCL Cask Cleanliness Checklist	PCCL-C2
PCCL Hydrogen Checklist	PCCL-C3
PCCL Charging Tank Checklist	PCCL-C4
Abnormal Operating Procedure for PCCL	Q/A M-86-2 (SR#-0-89-2)
Pre-operational Testing of the PCCL	Q/A M-86-2 (SR#-0-88-14)
Special Procedure for Initial PCCL Startup and Operational Testing In-core with Reactor Shutdown	Q/A M-86-2 (SR#-0-89-3)
Special Procedure for Initial PCCL Operation with Reactor at Power	Q/A M-86-2 (SR#-0-89-6)

Q/A files are located in the MITR Operations Office, under the custody of the Nuclear Reactor Laboratory (NRL) Quality Assurance (QA) officer (617) 253-4211. PCCL files are located in the project scientist's office, NW13-260.

The hot cell contains a 800 watt furnace, a scale, and a tube chopper.

The 800 watt furnace is used, as mentioned above, to melt the

radioactive lead so that the Zircaloy tubing can be removed from the lead bath.

The 20 kg scale is used to weigh the Titanium Test Tube (TTT) with the tubing and lead in it. If there is a discrepancy in the total weight, more lead is added to the TTT.

Finally, the tube chopper is designed to cut the activated Zircaloy tubing into pieces of desired length. The chopper is a commercial rod shear (Bench model #5), motor driven, that can cut the Zircaloy tubing in a single stroke with minor distortion of the metal. The Zircaloy pieces are placed into labeled test tubes and taken in a lead pig to the decontamination laboratory for further treatment and analysis (see thesis report by E. Cabello [C-1]).

It is important to point out that the hot cell cannot be operated if proper ventilation does not exist. Procedures (Appendix C) for proper utilization of the hot cell must be followed at all times.

The disassembly area (Fig 2.17) is located next to the hot cells and is surrounded by concrete walls to reduce radiation exposure from the loop to reactor and PCCL personnel. The loop is assembled or disassembled in this area.

When the loop is being assembled, the internals are lifted with the boom hoist and transported into the thimble. The shot port is properly sealed and the copper shot loaded into the Steam Generator (S/G) section. The heater and thermocouple connectors are checked and connected at the bottom of the thimble pod. The thimble lid is bolted down to the pod section and the screws are secured with SS lock wire.

When the loop is being disassembled, the steps are reversed.

For instance, the copper shot is poured out, and so on.

2.14 Chapter Summary

In this chapter, the final design of the as-built PCCL has been presented. Each PCCL component has been described, together with its function in the loop. Operating procedures have been described at a level of detail appropriate to the appreciation of how the loop is employed for experiments: the subject of the chapter which follows.

3 PREPARATIONS AND PRE-OPERATIONAL TESTS

3.1 Introduction

In this chapter, the pre-filming and pre-conditioning techniques used to prepare the loops for an in-pile run are discussed. A description of the out-of-pile tests to determine the actual heat rejection through different heat transfer modes is presented. Finally, a series of tests to determine the gamma heating component, to characterize the weekend mode of operation, and to measure the deposited activity in the deposition monitor are described.

3.2 Pre-filming of Loops

It is a well known phenomenon that when a fresh metal surface is exposed to water, the initial rate of corrosion decreases due to the formation of a protective oxide film [W-2], [L-1], [M-2]. These passive films protect against sustained high dissolution rates by separating the base metal from an aggressive coolant environment. The simplest method to develop this passive film is to expose the surfaces of the new pipes and S/G tubes of the primary reactor coolant system to high temperature water for a period of two to four weeks before reactor start-up. For instance, Westinghouse recommends a pre-filming period of four weeks at 500 °F for new nuclear plants.

Following this philosophy, in the present program ten loops composed of the S/G Inconel tubing and SS plena were pre-filmed simultaneously for 1000 hrs (41.7 days) inside a large oven built expressly for this purpose, under the following conditions:

Pre-cleaning	-	Degrease with acetone and rinse with deionized water
Li (Lithium)	-	1.41 ppm
B (Boron)	-	600 ppm
pH(300°C)	-	7.0
Conductivity(μmhos/cm)	-	15.2
Temperature (isothermal oven)	-	600 °F (315° C)
H_2 (Hydrogen)	-	24 cc-H_2/kg-H_2O
O_2 (Oxygen)	-	less than 10 ppb
Let-down Flow Rate	-	300 cc/hr
Duration of hot exposure	-	1000 hrs

To develop a smooth interior surface, the SS plena were honed using silicon carbide stones. Three specimens (coupons) were placed in each plenum for documentation of the pre-filmed and pre-conditioned (sec 3.3) surfaces. The specimens (1 by 1/3 inch) consisted of sections cut from plena replicates with interior surfaces honed in exactly the same way as the plena used in the test loops, and with exterior surfaces polished. Of the three specimens provided per plenum: one was removed after the pre-filming and the other two after the pre-conditioning. After the 1000 hr run, the loops were disassembled, rinsed with deionized water, and filled and stored with nitrogen prior to their re-insertion in the oven for individual loop pre-conditioning.

Because the let-down flow rate is small and the loops are in a isothermal field, local differences in soluble transition metal species

should be small. Thus, transport of corrosion products during the pre-filming stage is kept to a minimum.

Water samples were taken to check pH, conductivity, and boron and lithium concentrations during the pre-filming operation. Figures 3.1 to 3.4 show the trend of the above variables versus time. Also shown are the "acceptable" parameter ranges according to current PWR chemistry guidelines [W-5]. The pH and conductivity of the discharged water samples were measured with properly calibrated pH and conductivity meters at room (25°C) temperature. Boron concentrations in water samples were determined by a B-10 prompt gamma neutron activation analysis technique [W-4]. The amount of lithium in the water samples was determined by a standard atomic absorption technique. In addition, impurities in water samples (Table 3.1) were determined by Ion Chromatography (IC). These techniques are described in more detail in Appendix A. The IC samples were analyzed after more than one year of storage, hence the values quoted represent upper limits on actual amounts present.

3.3 Pre-conditioning of Loops

One to two months prior to a scheduled in-pile run, a prefilmed set of Inconel tubes and a SS plenum were connected to a (cleaned but previously untreated) Zircaloy U-tube and pre-conditioned inside the same large oven used during the pre-filming stage under the following conditions:

Lithium	-	Same as subsequent in-pile run
Boron	-	Same as subsequent in-pile run

Table 3.1 Impurities in Pre-filming Water Samples.

	PCCL	PWR (EPRI PWR Guidelines [S-2])
Chloride (ppb)	2	<50
Nitrite (ppb)	<8	-
Nitrate (ppb)	<1	-
Sulfate (ppb)	93	<50
Bromide (ppb)	86	-

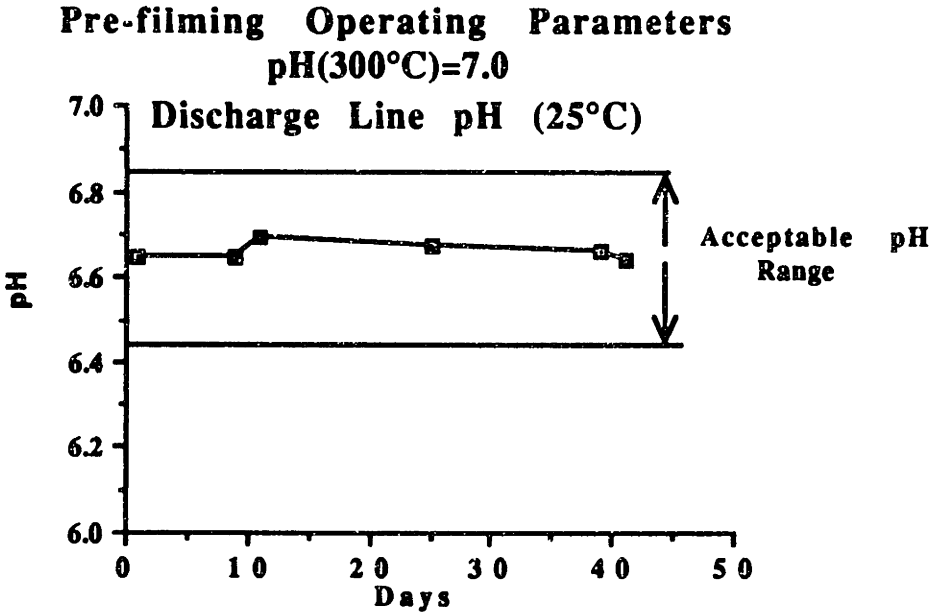

Figure 3.1 Discharge pH vs time during pre-filming.

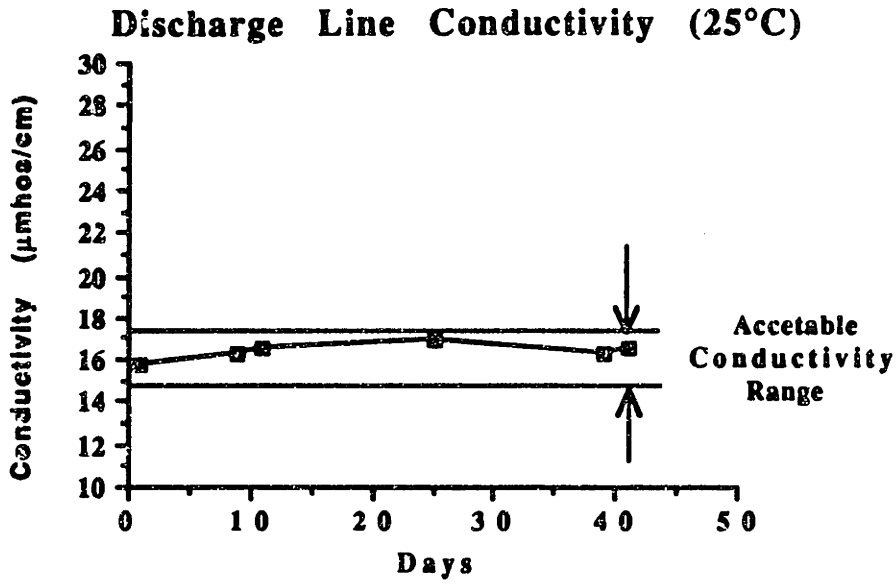

Figure 3.2 Discharge Conductivity vs time during pre-filming.

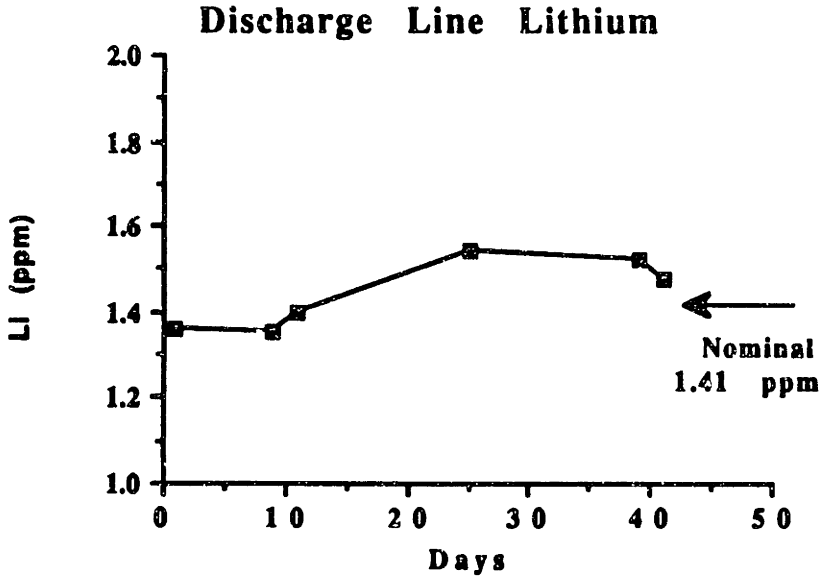

Figure 3.3 Discharge Lithium vs time during pre-filming.

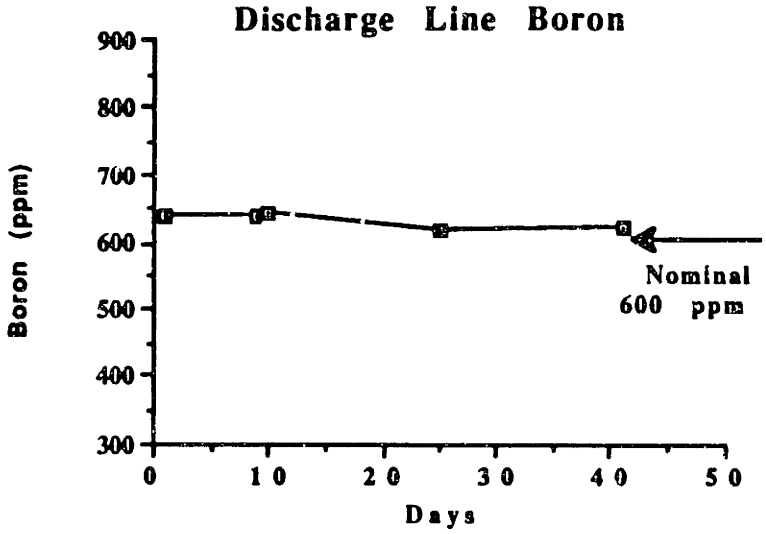

Figure 3.4 Discharge Boron vs time during pre-filming

pH(300°C)	-	Same as in subsequent in-pile run
Conductivity (μmhos/cm)	-	Same as in subsequent in-pile run
Temperature (Isothermal oven)	-	600°F (315°C)
H_2 (Hydrogen)	-	17 cc-H_2/kg-H_2O
O_2 (Oxygen)	-	< 5 ppb
Let-down Flow Rate	-	100 cc/hr
Duration of hot exposure	-	3 to 4 weeks

Each loop was pre-conditioned for a period of three to four weeks under the same water chemistry as the subsequent in-pile run. A different charging system (Fig. 3.5), operating in a recirculating mode, was used during the pre-conditioning stage.

Water samples were also taken periodically to check pH, conductivity, lithium, and boron as described in the previous section. The function of the pre-conditioning is to reach an equilibrium

condition between surfaces and bulk coolant prior to the start-up of the in-pile run. Again low flow/low heat flux conditions are employed to avoid corrosion product transport. C. B. Lee [L-2] has shown that short in-pile runs best predict long-term behavior if initial core region crud inventories are small.

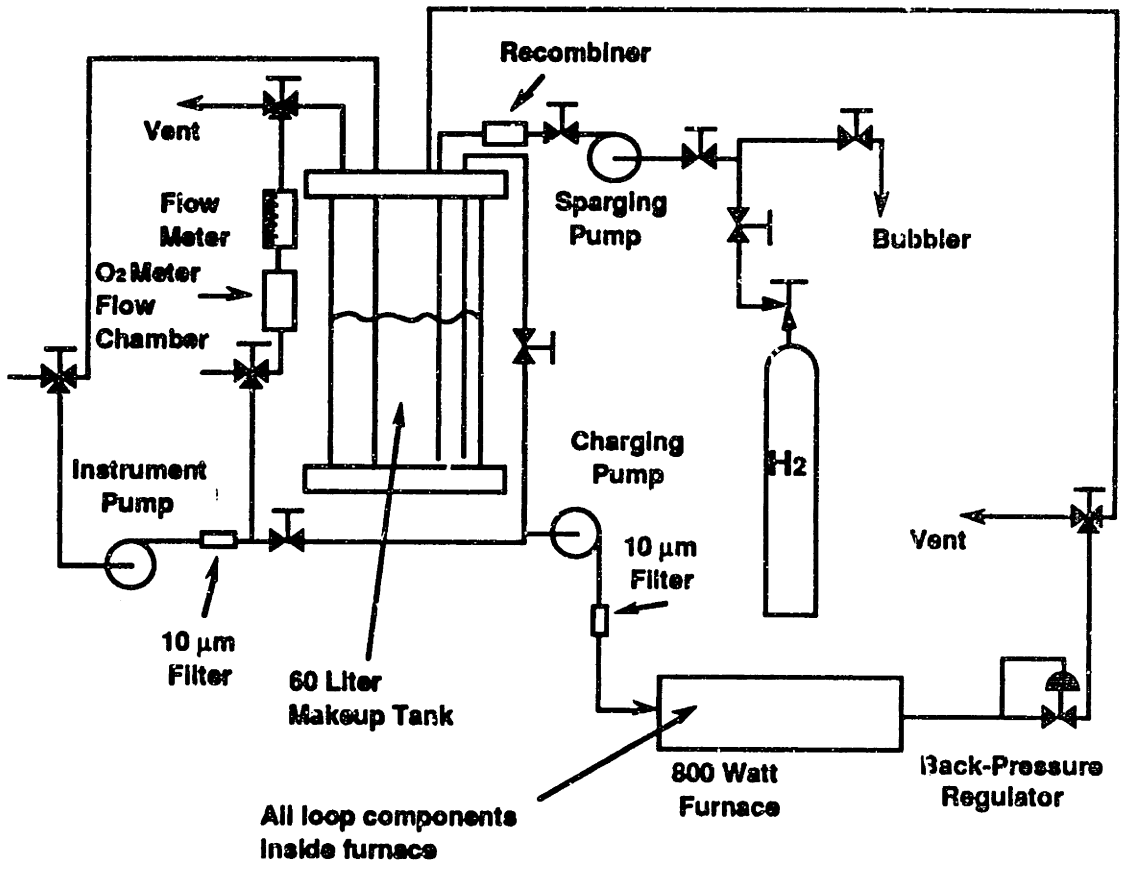

Figure 3.5 Schematic of Charging System used in Pre-conditioning.

3.4 Out-of-Pile Tests

3.4.1 Heat Rejection Measurements

A series of out-of-pile tests were carried out to determine the optimal spacing of the Inconel tubes in the Steam Generator subsection with the intention of matching film differential

temperatures believed to be important factors in the release/transport/deposition of corrosion products. Hot and wet heat rejection tests were also carried out to demonstrate that in the event of a main circulating pump trip or a loss of coolant accident (LOCA), the heated section was capable of rejecting the 7 kW of gamma heating without exceeding the 2200 °F (1204 °C) temperature limit above which the rate of Zircaloy oxidation is excessive.

3.4.1.1 Effective Copper Shot Bed Thermal Conductivity

To match as closely as possible the core inlet and outlet temperatures, flow rates, and film differential temperatures in the PCCL with those in a representative PWR, the spacing between the PCCL Inconel tubes (Fig 3.6) was adjusted. Based on a spacing between Inconel tubes of 2.6 inches, the effective thermal conductivity of the PCCL shot bed was calculated using the following expression (Eq. 3.1) which treats each tube as an isolated off center heat source

$$Q' = 2q' = k_{eff} S_2 \Delta T \qquad (3.1)$$

where

Q' = Energy removed per unit length of thimble

q' = Energy loss per unit length of tube

k_{eff} = Effective Thermal Conductivity of shot bed

S_2 = Shape Factor

ΔT = Temperature difference between tube and thimble walls.

The shape factor is given by the following expression:

$$S_2 \leq \frac{4\pi}{\ln(u + \sqrt{u^2 - 1})} \qquad (3.2)$$

with

$$u = \frac{1 - \left(\frac{\delta}{D}\right)^2 + \left(\frac{d}{D}\right)^2}{2\left(\frac{d}{D}\right)} \qquad (3.3)$$

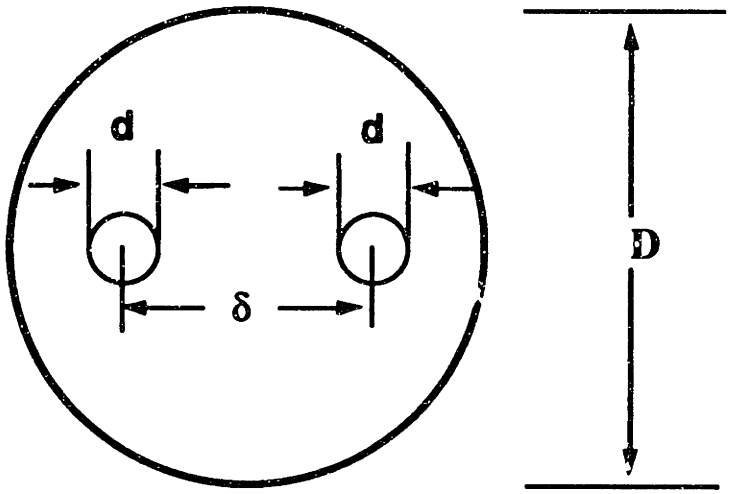

Figure 3.6 Cross Section of the Steam Generator Subsection

where

δ = Distance between Inconel tubes (2.6 inches)

D = thimble diameter (3.5 inches)

d = Inconel tubing diameter (5/16 inches)

J. H. Van Sant [S-2], J. C. Rowley and J. B. Payne [R-1] have shown that the above expression for the shape factor is a good approximation for the two tube case. For measured values of Q' and ΔT, this expression yields a value of 1.03 BTU/hr-ft-°F (1.8 W/m-°C) for the effective thermal conductivity of the shot bed, which is in

good agreement with the experimental value obtained by J. Wicks [W-1] using a centrally positioned heat source. Another approach to calculate the effective thermal conductivity of the shot bed is to use the following correlation developed in reference [B-8].

$$k_{eff} = (4.0 \ln\alpha - 11)k_{He} \quad (3.4)$$

where

keff = is the effective thermal conductivity (BTU/hr-ft-°F)

α = k(Cu shot)/k(He gas)

k(Cu shot) = thermal conductivity of copper shot (215 BTU/hr-ft-°F)

k(He gas) = thermal conductivity of helium (0.11 BTU/hr-ft-°F)

According to reference [B-8], when the results of the above expression are compared to experimental data for the case of steel shot in various gases, the fit given by this expression is within ± 50%. Thus, for the copper shot and helium case, Eq. 3.4 yields a value of 2.12 BTU/hr-ft-°F ± 50% which is in rough agreement with the value predicted by Eq. 3.1. As discussed in section 2.4.2.2, the final adjustment in the effective k was achieved by inserting 90° angle aluminum pieces in the bed.

3.4.1.2 Hot Heat Rejection Test

As noted earlier, this test was designed to show that under any loss of coolant accident scenario such as a tube break, the heated section would be capable of rejecting the 7 kW of gamma heating

generated by the MIT-reactor when operated at full power without exceeding the 2200 ° F (1204 °C) Zircaloy-water reaction limit.

A complete loop was assembled and inserted into the thimble. Thermocouples were connected to the inlet and outlet of the Zircaloy tubing and to the lead bath. The Steam Generator subsection of the thimble was filled with copper shot. The entire system (thimble and internals) was placed in the test tank to simulate the same heat transfer conditions as encountered in the core tank.

With the Inconel loop tubing open to the atmosphere, the thimble was filled with helium (2 psig). Figure 3.7 shows the trend of the heater power (heat rejected) versus the lead bath temperature. As seen in this figure, for a heater power of 7 kW the lead bath temperature never exceeds the temperature of 2200 °F (1204 °C) which is the conventional limit for avoiding an autocatalytic Zircaloy-water reaction. Thus, the heated section was judged capable of rejecting gamma heating by purely passive means (conduction and radiation between the lead bath can and thimble wall) in the event of a loss of coolant accident.

3.4.1.3 Wet Heat Rejection Test

This test was designed to show that the heated section could reject the 7 kW of gamma heating produced by the MIT reactor without exceeding the 2200 °F Zircaloy reaction limit in the event of a main circulating pump trip. The loop was assembled in the same fashion as for the hot heat rejection test. To simulate the pump loop section, the loop tubes were connected together above the thimble

lid. The loop tubing was filled with water and pressurized to 1000 psig. These conditions were similar to those which would

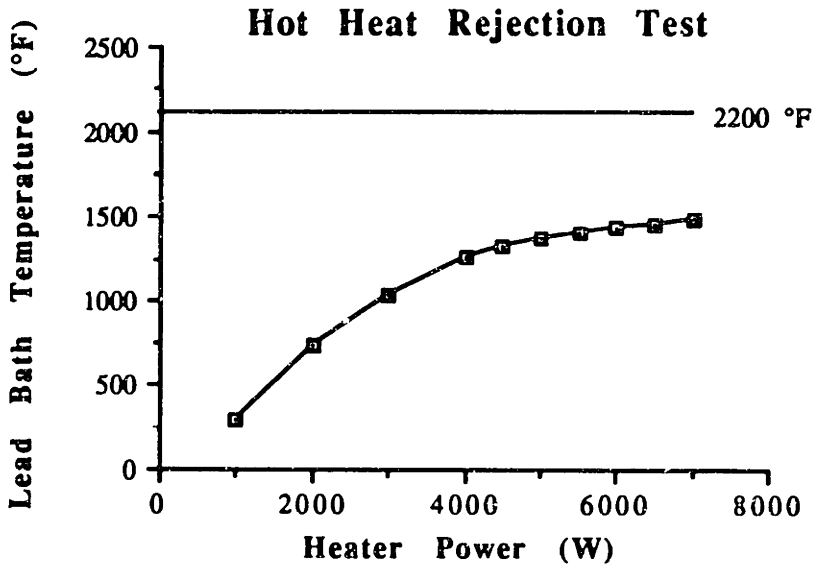

Figure 3.7 Heater Power vs. Lead Bath Temperature During Passive Heat Rejection Test.

occur after a main circulating pump trip. Table 3.2 shows the inlet and outlet temperatures as well as the heater power and lead bath temperature. As seen in this table, a maximum heater power of 6.5 kW was observed before reaching the 545 °F saturation temperature at a 1150 °F lead bath temperature. From this observation, it is assumed that the water in the loop would boil during a main circulating pump trip scenario, which would limit, to some extent a further increase in temperature, since heat would be transported to, and rejected by condensation in the shot bed section. Thus, it was concluded that the heated section would reject the heat necessary to maintain the temperature of the Zircaloy tubing well below the 2200

°F limit (assuming of course, that the electric heater power is interrupted and only nuclear heat need be rejected). Note that the heated autoclave (auxiliary pressurizer) would suppress boiling until the loop temperature exceeds roughly 630 °F.

It is interesting to point out that table 3.2 shows a higher core inlet than core outlet temperature. An explanation for this behavior is that the combined effect of natural convection and the small charging flow lead to a net flow in the direction opposite to normal flow (see Fig. 3.8).

Table 3.2 Relevant Variables for the Wet Heat Rejection Test.

Heater Power (Watts)	Core Inlet °F (°C)	Core Outlet °F (°C)	Lead Bath Tem. °F (°C)
2000	503 (262)	490 (254)	575 (302)
2250	535 (279)	492 (256)	-
2500	543 (284)	525 (274)	-
3500	545 (285)	538 (281)	621 (327)
5000	545 (285)	541 (283)	850 (454)
6000	545 (285)	542 (283)	1075 (579)
6500	545 (285)	542 (283)	1150 (621)

3.5 In-Pile Tests

These tests were conducted with the complete loop system assembled and installed in the MIT reactor. The purpose of the in-pile tests was to show that the overall loop system configuration

was operational and to determine the contribution of gamma heating, evaluate the deposition of corrosion products in the deposition monitor, and assess the weekend mode of operation.

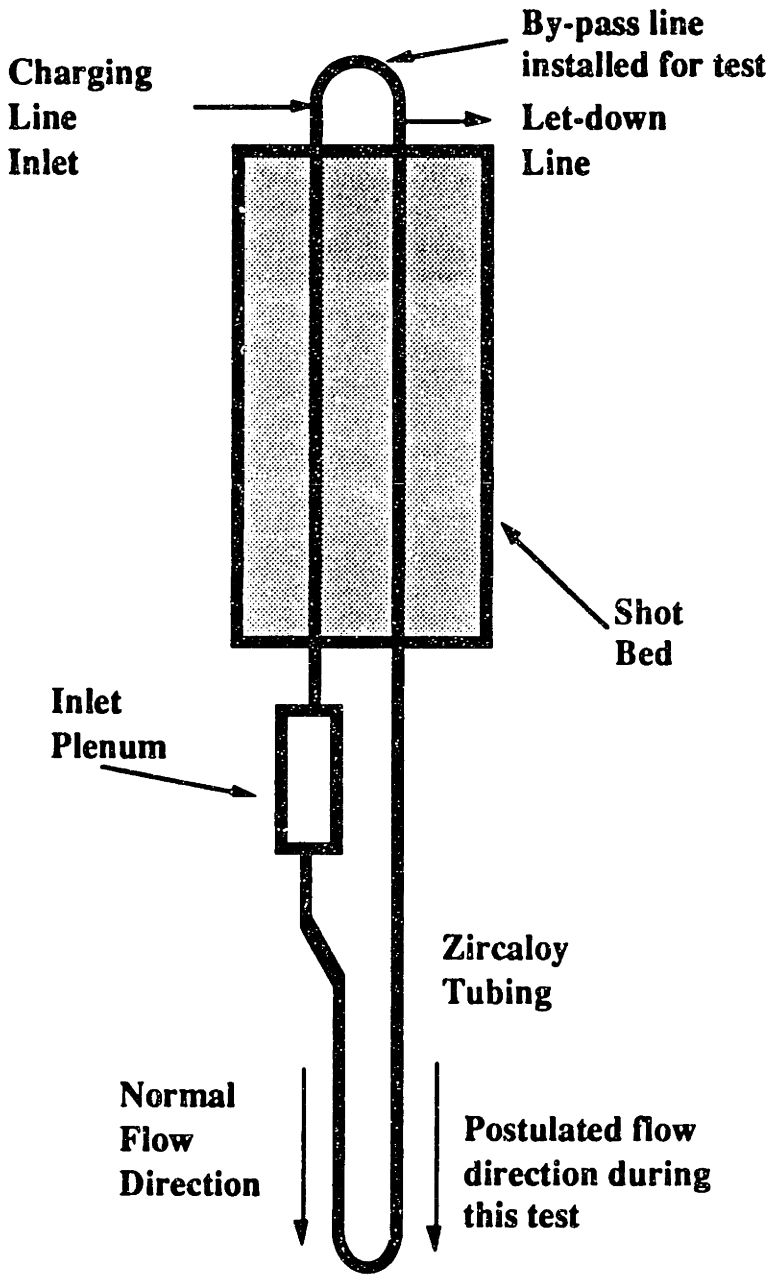

Figure 3.8 Schematic of the Loop Used for the Wet Heat Rejection Test.

3.5.1 Shakedown Run

As noted before, the purpose of the one week long shakedown run was to demonstrate that the loop components, alarm systems and instrumentation were operational. Prior to the start of this run, a series of pre-operational tests and measurements were performed. These tests were divided into six groups as follow:

A. Hydrostatic Testing. These tests verified that the thimble and loop component welds were acceptable. In addition, the PCCL thimble and a prototype in-core heated section were also hydrostatically tested to 150 and 1000 psig, respectively. Once the thimble was installed in the core tank, cold and hot leak checks of the high pressure lines were conducted to verify their integrity.

B. Reactivity Measurements. These measurements were performed to insure that under any circumstances, the insertion of reactivity due to the void-reflood of the Zircaloy tubing or the reflood of the space between the Titanium Test Tube (TTT) and the aluminum thimble would not exceed the 0.2% $\Delta k/k$ limit for movable experiments or 0.5% $\Delta k/k$ for nonsecured experiments. The results showed a maximum reactivity change of 0.042% $\Delta k/k$ and 0.14% $\Delta k/k$ for the PCCL in-core tube flooding (154 cc) and the in-core free volume flooding (1600 cc), respectively. These results are within the limits for movable and non-secured experiments.

C. Instrumentation. The nine PCCL alarms that register in the control room were verified operable. The instrumentation components, such as thermocouple and pressure readouts were properly calibrated. Finally, pressure relief valves, pushbutton

"emergency and heater off" switches were checked to confirm that they were operable.

D. Installation/removal of PCCL. The installation and removal of the PCCL was done according to procedures listed in table 2.7. The removal or installation of the PCCL is always performed with the reactor shutdown.

The last two test groups were related to the unattended and attended operation of the PCCL loop. Before initiating any of these modes of operation, PCCL personnel had to verify that all instrumentation was operational. In addition, abnormal operating procedures in their final form were made available in the control room, together with the procedures for the loop's installation/removal in/from the core tank and its transfer to/from the assembly/disassembly area. For long term unattended operation, PCCL personnel had to verify that in the event of reactor shutdown, the reactor cooling system was able to remove the decay heat from the reactor plus the heat generated by the PCCL.

Once the preoperational tests had been completed, the PCCL was taken to a hot standby mode prior to reactor startup. The following steps were (are) taken to achieve a hot standby mode for this and all subsequent runs:

1. The PCCL is pressurized to 2250 psig using the LEWA charging pump. A letdown flow rate between 200 and 400 cc/hr is established.

2. The main circulating pump is turned on, making certain that a ΔP of 20 psig in the loop is achieved, which corresponds to a volumetric flow rate of 1.15 GPM at room temperature.

3. The heaters for the heated autoclave (auxiliary pressurizer) are turned on. The temperature set point controller is raised approximately 5 °F/min to avoid overshooting the final pressurizer temperature of 630 °F.

4. The in-pile heater is turned on and power ramped up slowly until a core outlet temperature of 570 °F is achieved. The heatup rate is 5 °F/min. At this step, the experimenters verify that $T_{lead\ bath} > T_{core\ outlet} > T_{core\ inlet}$ and that the AE pump's drive magnet temperature is less than 300 °F.

5. If the above conditions are met, the in-pile heater controller is switched to automatic control of core outlet temperature. The PCCL remains in this condition for at least 30 minutes prior to reactor startup. Personnel in the control room are informed of PCCL readiness for reactor operation.

Once the loop is in a hot standby mode, the following steps were (are) taken to bring the reactor to full power.

7. With the PCCL operating under automatic in-pile heater control, $T_{core\ outlet}$ = 570 °F, the reactor power is raised to 1 MW and maintained at this level for at least 5 minutes or until all temperatures are stable. A radiation survey of the main circulating pump is conducted to determine the dose rate from N-16.

8. The reactor power continues to be raised in one MW steps, verifying at each step that all temperatures remain stable and that the heater controller produces less than 10 °F of overshoot during each step.

9. Once the reactor is at full power, the in-pile heater controller is switched to manual and the core outlet temperature is raised to

600 °F at a rate of 5 °F/min. After raising the core outlet temperature, the heater controller is returned to its automatic mode and kept in this mode until the loop or reactor are ready to be shut down.

When the reactor is ready for shutdown (weekend mode), similar steps are taken; for instance

10. The in-pile heater controller is switched to manual mode and the core outlet temperature is reduced to 570 °F in a 5 °F/min ramp down rate.

11. At 570 °F, the in-pile heater controller is switched to automatic to allow temperatures to stabilize.

12. The reactor power is lowered in 1 MW steps allowing 5 to 10 minutes between steps for all temperatures to stabilize. If the loop's core outlet temperature overshoots by more than 20 °F, the in-pile heater controller is switched to manual.

After a month long run, the loop is shut down by first shutting the reactor down as described above and by decreasing the heater power as described in the following steps:

13. Once the reactor is shut down, the in-pile heater controller is switched back to manual and the heater power is reduced to lower the core outlet temperature at a ramp rate of 5 °F/min until this temperature is below the 212 °F boiling point at 1 atm.

14. The heated autoclave (pressurizer) heaters are turned off while assuring that the system pressure remains above 2000 psig.

15. The main circulating pump is turned off.

16. Finally, the charging pump is also turned off and the loop depressurized.

It is important to point out that steps 3 and 14 were omitted during the shakedown and first two runs because the heated autoclave was not then part of the system.

Another scenario that is important to mention is the one that occurs when the reactor scrams while the loop is operating at its nominal 600 °F core outlet temperature. Because the gamma heating source is lost when the reactor scrams, the electric in-pile heater which is operated in an automatic mode to maintain a core outlet temperature of 600 °F, has to compensate for this loss in a matter of seconds. Thus, the electric heater power increases from 12 to 19 kW, which is near its maximum rated power. Once this reactor condition has been established, PCCL personnel must reduce the core outlet temperature to 570 °F in order to avoid a premature heater failure due to the operation of the in-pile electric heater at excessively high power levels.

Finally, the last scenario to consider is the one that occurs when the in-pile electric heater or main cooling pump trip while the reactor is operating at full power. PCCL personnel must evaluate the nature of the trips and determined if is necessary to shut down the reactor. Table 3.3 summarizes the reactor and loop operation modes and the operating procedures or section in this chapter that are relevant to each condition.

3.5.1.1 Gamma Heating

As noted earlier, the contribution of gamma (nuclear) heating in the Titanium Test Tube (TTT) and its constituents is an important factor in the event of a loss of coolant accident or a main

Table 3.3 Summary of Reactor and Loop Modes of Operation.

Reactor	Loop	Procedure/Section
At Full Power	At Full Power	(SR#-0-89-3) (SR#-0-89-6) Sections 3.51 and 3.5.1.1
	Shut Down (γ Heat only)	
Shut Down	At Full Power	(SR#-0-89-3)
	Shut Down	(SR#-0-89-3) (SR#-0-89-6)

circulating pump trip. Sections 3.1.1.2 and 3.1.1.3 showed that the heated section was capable of rejecting the total amount of gamma heating without exceeding the 2200 °F Zircaloy-water reaction limit.

The actual amount of gamma heating was determined by

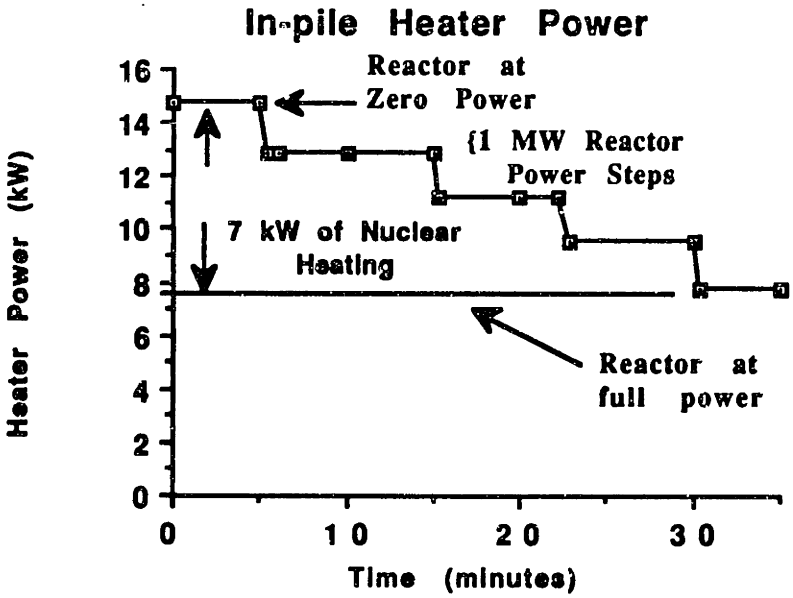

Figure 3.9 Heater Power vs time while reactor is coming on-line.

changing reactor power with the PCCL in a hot standby mode with a constant core outlet temperature of 550 °F. Figure 3.9 shows the trend of heater power vs. time with the in-pile heater in automatic mode, as reactor power is increased in 1MW steps. As seen in this figure, the heater power decreased as the reactor increased in power. The total contribution of nuclear heating is the reduction in the in-pile electric heater power; namely, 7 kW when the reactor is brought from zero to full power.

3.5.1.2 Deposition Monitor

As mentioned before, one of the purposes of the shakedown run was to evaluate the deposition of activated corrosion products on the deposition monitor. The original design for an on-line deposition monitor consisted of a NaI(Tl) photomultiplier detector enclosed in a lead cylinder (Fig 3.10) with approximately 30 ft of 316 SS (1/16 inch OD) tubing wrapped around it. The outlet of the loop letdown line was connected to the inlet side of this tubing. The outlet side of this small diameter tubing was in turn connected to the discharge line so that coolant from the loop could flow through this tubing. Activated corrosion products in the coolant are then deposited on this capillary tube.

A NaI(Tl) photomultiplier detector was connected to a Canberra Series 20 Multichannel Analyzer. Spectrums were taken when the reactor was at zero and full power to determine the background and the incremental deposition of activated corrosion products on the small capillary.

It was determined that because of the poor energy resolution

of the NaI(Tl) detector and the high background when the reactor

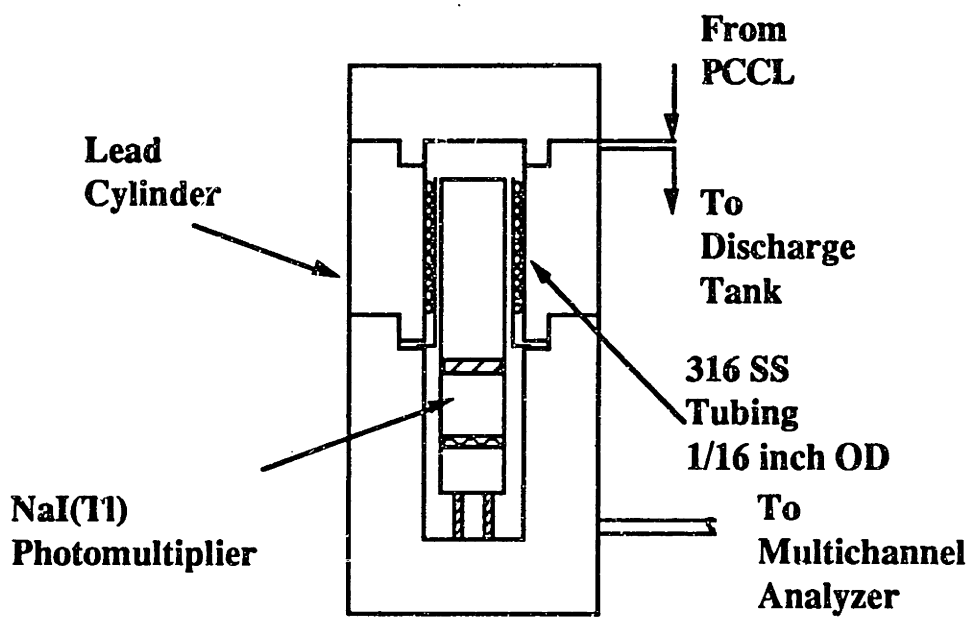

Figure 3.10 Schematic of Original Deposition Monitor Design.

operated at full power, this design was not suitable for determining the different elements deposited on the capillary tube. Hence, a new deposition monitor was installed in the letdown line.

As noted in section 2.9, this new device consists of a SS 10 μm pore size filter as shown in Fig. 3.11. This filter is replaced every three days and counted with a high energy resolution High Purity Germanium detector outside the containment building where the background is insignificant. The filter is counted 40 to 50 minutes after removal from the let-down line so that the short lived isotopes can be accounted for.

The deposition monitor filter is placed in a configuration as shown in Fig 3.12 and replaced every three days according to the

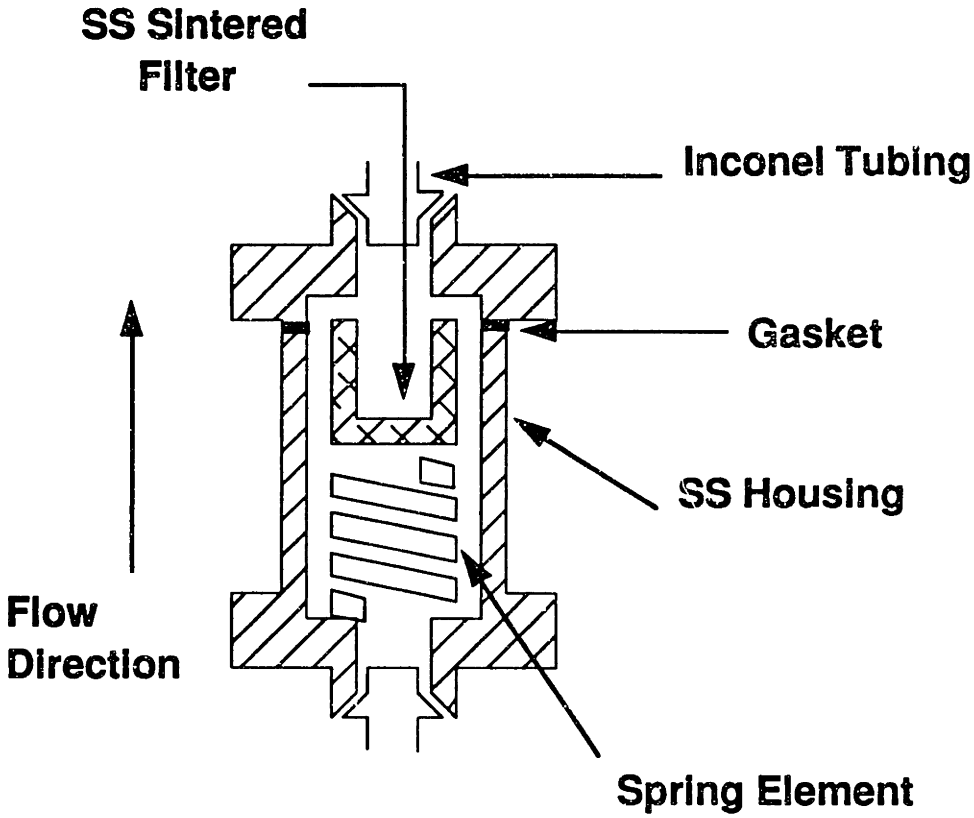

Figure 3.11 Schematic of Present Deposition Monitor.

following procedure:

1. The experimenter must wear appropriate clothing such as gloves, goggles, and coveralls.

2. Valve #3, which is normally closed (NC), is opened.

3. Valves #1 and #2 are closed, thus completely bypassing the filter.

4. At this point, the filter is replaced.

5. Valves #1 and 2# are opened.

6. Finally, the bypass valve #3 is closed.

It is important that the above steps are followed in the order given; otherwise, the loop will overpressurize if all valves are closed

at the same time, or a steam leak leak will develop if valves #1 and 2# are not properly closed when replacing the filter.

3.5.1.3 Weekend Mode of Operation

This test was carried out in the last two days of the shakedown run. The purpose of this test was to simulate weekend conditions such as no reactor power, and small rate of decay heat removal, while the PCCL in-pile heater operates at an average power of 18 kW, to show that the primary water temperature limit of 60 °C in MITR-II Technical Specifications [M-3] is not exceeded for a period of two days.

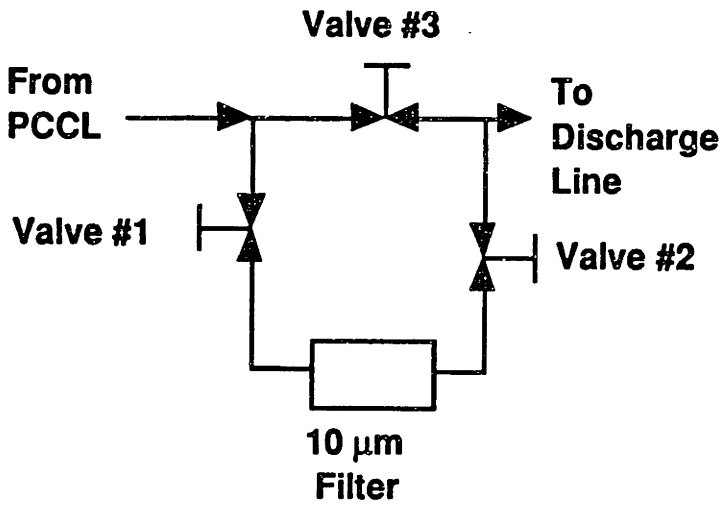

Figure 3.12 Schematic of the On-line Filter and Bypass Line.

Prior to reactor shutdown, the PCCL core outlet temperature was reduced to 550 °F to prevent the in-pile heater (which was operated in automatic mode) from exceeding its maximum rated power after the loss of gamma heating due to reactor shutdown. For

two or three hours prior to the start of this test, the reactor primary (flow rate 2080 gpm) and secondary (flow rate 1770 gpm) pumps were left on to achieve a minimum primary water temperature of 22 °C.

During this test, the reactor primary and D_2O pumps were turned off and the auxiliary primary and secondary pumps were left on at a flow rate of 4 and 30 gpm, respectively. After 45 hours, the maximum primary water temperature was 54.2 °C. Three hours before the end of this test, the flow rate of the auxiliary primary pumps was increased from 4 to 7 gpm. A drop of 3 °C was observed over the following three hours. Thus, it was confirmed that the primary water temperature never exceeded the 60 °C limit.

3.5.2 Boiling Test

The in-pile boiling test was carried out to evaluate the insertion of core reactivity in the event of a void/reflood scenario in the Zircaloy tubing. This experiment was performed using the PCCL loop with the main circulating pump bypassed. Since the in-pile PCCL Zircaloy tubing has the same dimensions as the one used in the Boiling Water Reactor Coolant Chemistry Loop (BCCL), the results of this experiment are also applicable to the BCCL.

Two reactor criticalities were conducted at low power. One of these was established with a solid system and became the baseline reactivity measurement. The other one was established with boiling in the loop. It was calculated that an exit quality of approximately 57% existed during the second criticality.

The results of this experiment showed no measurable or observable reactivity noise due to in-core boiling at reactor power levels up to 10 kW. From these results, it is concluded that the steady state boiling in the BCCL will not adversely interact with MITR-II control, nor will transient boiling in the PCCL, should it occur in severe transients.

3.6 Chapter Summary

In this chapter, the preparation and evaluation of the loops prior to in-pile irradiation have been described. A brief discussion of the pre-filming and pre-conditioning techniques has also been presented.

Major out-of-pile tests to match film differential temperatures with those in a representative PWR have been discussed. Out-of-pile heat rejection tests simulating accident scenarios have also been evaluated and their results documented.

Finally, in-pile pre-operational tests and operational procedures have been described. The in-pile gamma heating source has been determined and an appropriate weekend mode of operation established. In addition, an in-pile boiling experiment was conducted with no apparent reactivity noise attributable to the PCCL in evidence.

4 MEASURED DATA

4.1 Introduction

The PWR Coolant Chemistry Loop (PCCL), described in chapter 2, has been designed to investigate the effect of coolant pH on the release/transport/deposition of corrosion products in a PWR environment. In the past, studies of plant data have suggested that a correlation exists between crud buildup in the PWR primary circuit and the coolant pH. Since solubility differences between bulk coolant and coolant in contact with in-core and out-of-core surfaces constitute an important factor for the transport of corrosion products, experiments have been conducted in a number of laboratories to determine the solubility of iron, nickel, and cobalt under PWR conditions.

At one time, it was believed that the crud layer in PWR primary circuits was mainly composed of magnetite (Fe_3O_4). Hence, Sweeton and Baes [S-2] conducted measurements to determine iron solubility using magnetite in an aqueous solution saturated with H_2 at 1 atm. These solubility measurements were performed as a function of temperature and hydroxyl ion concentration. The results showed (Fig. 4.1 [L-3]) that the iron solubility decreases as the hydroxide concentration increases until a minimum is reached. Further increase of hydroxide concentration increases the iron solubility. It should be noted that the hydroxide concentration is related to the pH of the solution; an increase in the hydroxide concentration corresponds to an increase in solution pH. Figure 4.1 also shows the existence of a minimum at which the solubility temperature coefficient

changes sign; the minimum shifts towards lower hydroxyl concentration with increasing temperature, which means that the solubility temperature coefficient will change sign at a lower solution pH as solution temperature increases.

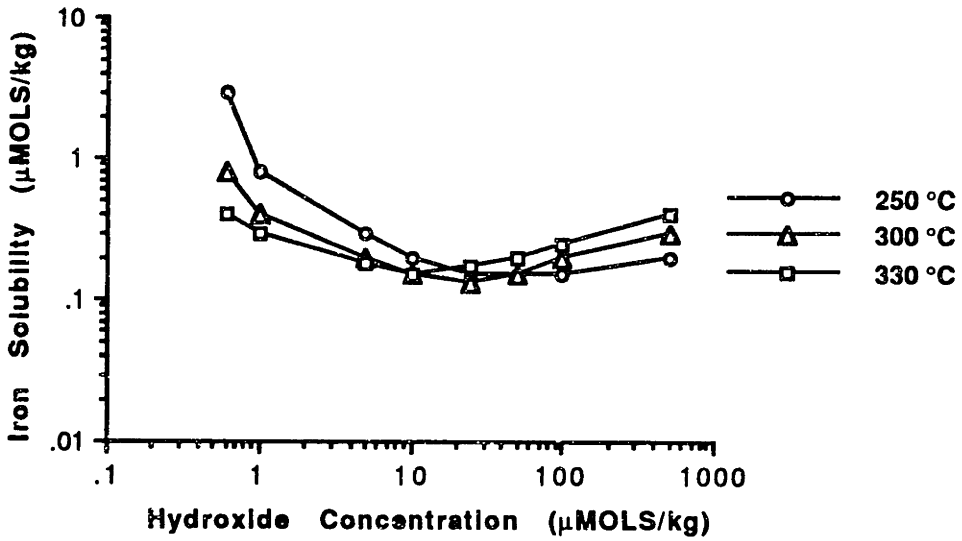

Figure 4.1 Iron Solubility from Magnetite as a Function of Temperature and Hydroxide Concentration [L-3].

Sweeton and Baes [L-3] also calculated the minimum iron solubility at temperatures between 25 °C and 300 °C for different lithium and boron concentrations for magnetite at a 1 atm partial pressure of hydrogen. Figure 4.2 shows the combinations of lithium and boron for which the iron solubility at 285 °C and 1 atm hydrogen partial pressure is at its minimum (i.e., zero solubility temperature coefficient). It should be noted that the upper right corner of Fig. 4.2 represents the region where the solubility temperature coefficient is positive, and non-precipitating coolant conditions exist on hot-core-

surfaces. On the other hand, the lower left corner of Fig. 4.2 represents the region where the solubility temperature coefficient is negative and precipitating coolant conditions exist.

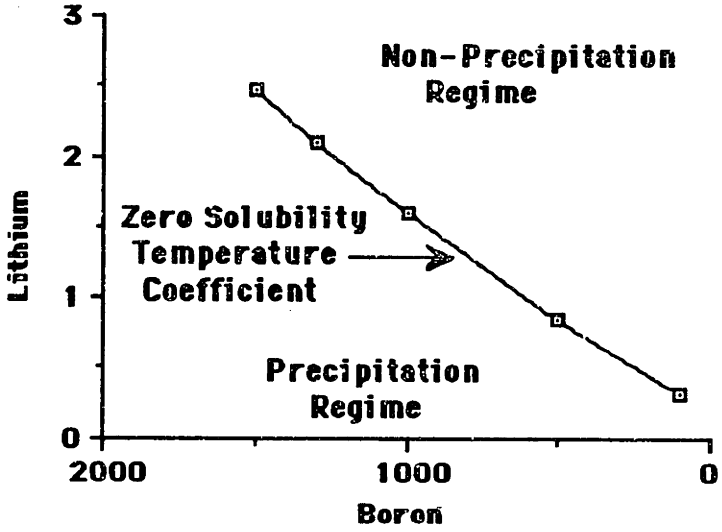

Figure 4.2 Boron and Lithium Concentration for a Zero Solubility Temperature Coefficient at 285 °C [L-3].

From these initial experiments, it was found that a pH_{300} of 6.9 would yield a zero temperature coefficient. Therefore, it was postulated that the transport and deposition of corrosion products on core surfaces (and hence the production and subsequent deposition of radionuclides on ex-core surfaces) could be minimized if a primary coolant pH_{300} of 6.9 could be maintained throughout the entire reactor cycle.

Present studies have shown that the crud composition on discharged fuel elements is a nickel ferrite structure of varying stoichiometry rather than the magnetite structure assumed in the studies described above. Sandler and Kunig [S-3] performed similar

experiments to measure the iron solubility, this time from nickel ferrite instead of magnetite, under simulated PWR reactor coolant conditions. In addition, experiments were also conducted to determine the solubility of nickel and cobalt from a cobalt-nickel ferrite compound of varying stoichiometry. Figure 4.3 shows the solubilities of iron, nickel, and cobalt as a function of temperature and pH. Note that the solubility of nickel appears to be virtually temperature independent between 280 °C and 320 °C. On the other hand, iron and cobalt solubilities behave very similarly in the

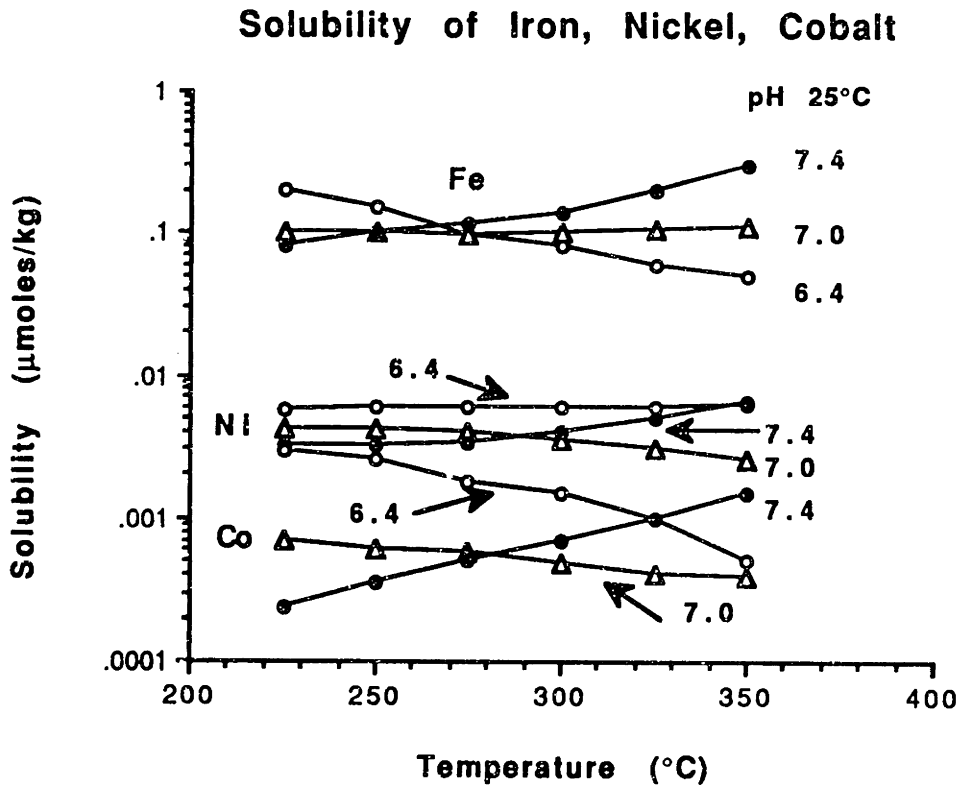

Figure 4.3 Solubility of Iron, Nickel, and Cobalt as a Function of Temperature and pH [L-3].

same temperature range. Another important factor is that at pH 7.4, all three elements showed the same trend and a positive solubility

temperature coefficient. Thus, these studies showed that the minimum solubility occurs at a higher pH (7.0-7.5) than the one indicated by the magnetite studies.

To help resolve the issue of solubility-driven transport, a series of one month runs were carried out as part of the present research effort to measure the effect of coolant pH on the build-up of radiation fields on out-of-core components, using the loop design described in chapter 2. A total of four runs were conducted in this first campaign. These runs were:

1. Reference Run #1, pH_{300}=7.0 (800 ppm B, 1.84 ppm Li)
2. Reference Run #2, pH_{300}=7.0 (800 ppm B, 1.84 ppm Li)
3. Low pH Run #1, pH_{300}=6.5 (800 ppm B, 0.56 ppm Li)
4. High pH Run #1, pH_{300}=7.5 (800 ppm B, 6.26 ppm Li)

A constant coolant pH was maintained during each run. Reference run #2 was conducted under the same chemistry conditions as reference run #1 to establish the degree to which results were reproducible. The pH of 7.0 for reference runs #1 and #2 was chosen to reflect a representative operating point for existing PWR plants. The high and low pH points were chosen to provide dissolving and precipitating coolant conditions, respectively, based on nickel ferrite solubility. Figure 4.4 shows the coordinated pairs of boron and lithium concentrations at which the solubility of $Ni_{0.5}Fe_{2.5}O_4$ exhibits a zero solubility temperature coefficient at a temperature of 293 °C. The pH points selected for the four runs are also indicated in this figure.

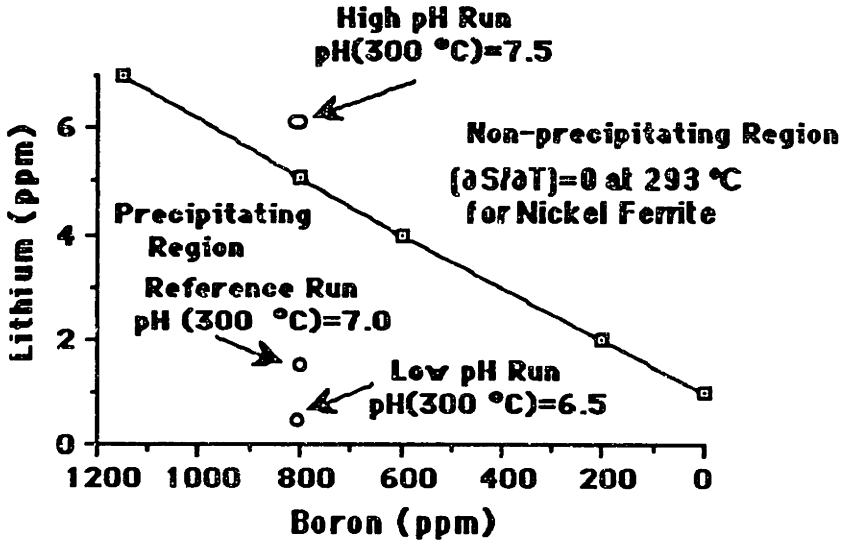

Figure 4.4 Coordinated Pairs of Lithium and Boron Concentrations that Yield a Zero Solubility Temperature Coefficient for Nickel Ferrite at 293 °C [L-3].

Because the same main circulating pump and pump tubing were used for the second reference, low pH, and high pH runs, a decontamination step was performed on these components prior to the start of each new run. The decontamination step consisted of injecting through the charging pump an oxidizing agent such as alkaline permanganate (AP) (1% $KMnO_4$, 1% NaOH in deionized water, pH_{25}=12.2) to oxidize the chromium oxide layer. The oxidizing step lasted 2 hours at a charging flow rate of 1 liter/hr. Once the oxidizing step was completed, a deionized flush water solution was injected for a period of half an hour at a flow rate of 2 liters/hr followed by a two hour addition of an acidic/reductive agent such as citrox (1% oxalic acid, 1% citric acid in deionized water, pH_{25}=2.3) to dissolve the iron, cobalt, and manganese found in the crud layer [W-7].

In this chapter, the radionuclide deposition data obtained for PCCL components is presented. In addition, the methods used to obtained the data are briefly described.

4.2 Reference Run #1

4.2.1 Introduction

Reference run #1 was operated for a total of 43 days. Out of these 43 days, 20 were with the reactor at "full" power, which yielded a total of 2328.3 MW-hrs. Throughout the run, a pH_{300} of 7.0 (800 ppm B, 1.84 Li) was maintained. A brief run history is presented in the next section, which discusses the transients that occurred during this run. The data from the Inconel steam generator tubes, in-core Zircaloy tubes, 10 μm deposition monitor filters, daily outlet water samples, and the let-down line ion exchange column are also presented.

4.2.2 Run History

The first run, PR1, experienced two types of transients during its 43 day run history. The first of these transients occurred approximately 21 hours after start up of this run. As seen in Fig. 4.5, the in-pile heater power (operating under automatic coolant outlet temperature control) was constantly increasing, without reaching the steady-state mode. After three days of operating the loop under these conditions, it was decided to stop the run and transfer the thimble and internals to the disassembly area for a routine inspection. Once the internals were pulled out, it was found that a white

powder had been deposited at the bottom of the TTT.

Neutron Activation Analysis (NAA) performed on this powder showed that its main constituent was aluminum oxide. This result indicated a possible steam leak in one or both internal fittings or the plenum cap (Fig. 2.4). Because the interior thimble walls were at temperatures between 50 to 60 °C, steam condensation was occurring on these walls and water was collecting at the bottom of the heated section between the TTT and thimble wall. Hence, the effective thermal conductivity of the heated section gap was constantly increasing as more water vapor from the Zircaloy-Inconel fittings or the region around the SS plenum was condensed and collected at the bottom of the heated section, where it boiled. Thus, the total amount of heater power necessary to maintain a core outlet temperature of 600 °F was also increasing as seen in Fig. 4.5.

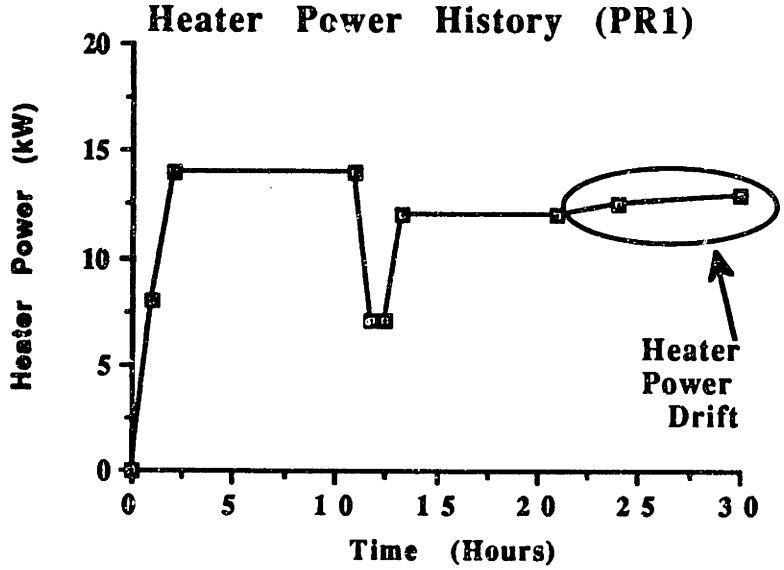

Figure 4.5 Heater Power vs Time During the First 30 Hours of PCCL Run #1.

It should be noted that during this slow heater power transient, the humidity detector was not effective because it was installed on a stagnant line. A helium bleed line was subsequently added to the original thimble design to allow flow of helium through the on-line humidity detector and in this way, make it possible to detect a leak in the interior of the thimble. This change also made removal of moisture by helium feed and bleed more effective.

The second type of transient occurred twice, approximately 22 and 37 days (Fig. 4.6), respectively, after startup of the run. The first of these transients occurred with the reactor at full power while the second one occurred with the reactor in a shutdown mode. Both transients were caused by a Cambridge Electric power dip in the main power line, which tripped the main circulating pump.

The paragraphs and figures that follow describe the first of these transients. After the in-pile heater trip (on core outlet or lead bath overtemperature), a series of events, as listed in table 4.1, occurred which ended up in releasing a small amount of radioactive steam through the main circulating pump head flange.

The scenario proceeded as follows: once the main coolant pump was tripped, the heat removal from the core was practically nonexistent; hence, the core outlet temperature reached the 650 °F (saturation temperature at 2200 psi) heater controller set point which tripped the in-pile heater and, because of rapid loop cooldown/water shrinkage/depressurization, produced steam in the loop. Figure 4.7 shows the core outlet temperature as a function of time during the pump trip. Note that it took only 1 to 3 seconds

before the core outlet temperature reached the 650 °F heater controller set point. Thus, experimenters had only a short period of time to react and turn the main circulating pump back on to avoid this transient.

Figures 4.8 and 4.9 show the system pressure and heater power observed during this transient. As seen in Fig. 4.8, the system pressure dropped rapidly due to contraction of the coolant caused by the cooldown of the loop after the heater power trip. For a time, the coolant temperature was above the saturation temperature at the existing pressure, which caused the coolant water to flash into steam. It is interesting to note that no reactivity noise due to the boiling (or other events) was observed by reactor operators during this loss of coolant flow transient.

The second transient of this type (loss of coolant flow) occurred, as mentioned above, 37 days after the startup of this run. Similar events to the ones described above occurred during this transient. However, the reactor was in a weekend shutdown mode of operation with a loop core outlet temperature of 550 °F. These transients, as will be seen in the next sections, had a direct impact on the coolant inventory of radioactive corrosion products, as indicated by the filter data. Nonetheless, the total activated corrosion product inventory was not affected appreciably by these transients.

As noted in section 2.9.1, chapter 2, a heated autoclave auxiliary pressurizer to prevent boiling transients of the type described above (and others as well) was added to the loop prior to the low pH run.

Table 4.1 Series of Events After Main Circulating Pump Trip.

ACCIDENT SCENARIO

	EVENT	TIME (SEC)
1.	CIRCULATING PUMP POWER SUPPLY TRIPS DUE TO LINE TRANSIENTS	0
2.	CIRCULATING PUMP STOPS	0
3.	HIGH OUTLET TEMPERATURE TRIP SET POINT REACHED	1 - 3
4.	HEATER TRIPS	1 - 3
5.	CHARGING PUMP FLOW RATE INCREASED	3 - 4
6.	LOOP PRESSURE DROPS (APPROX. 210 PSI)	5 - 1 0
7.	STEAM RELEASE FROM PUMP FLANGE	1 0 - 2 0
8.	CIRCULATING PUMP TURNED ON	3 0 - 4 0
9.	LOOP PRESSURE BACK TO 2200 PSI	1 8 0 - 2 0 0

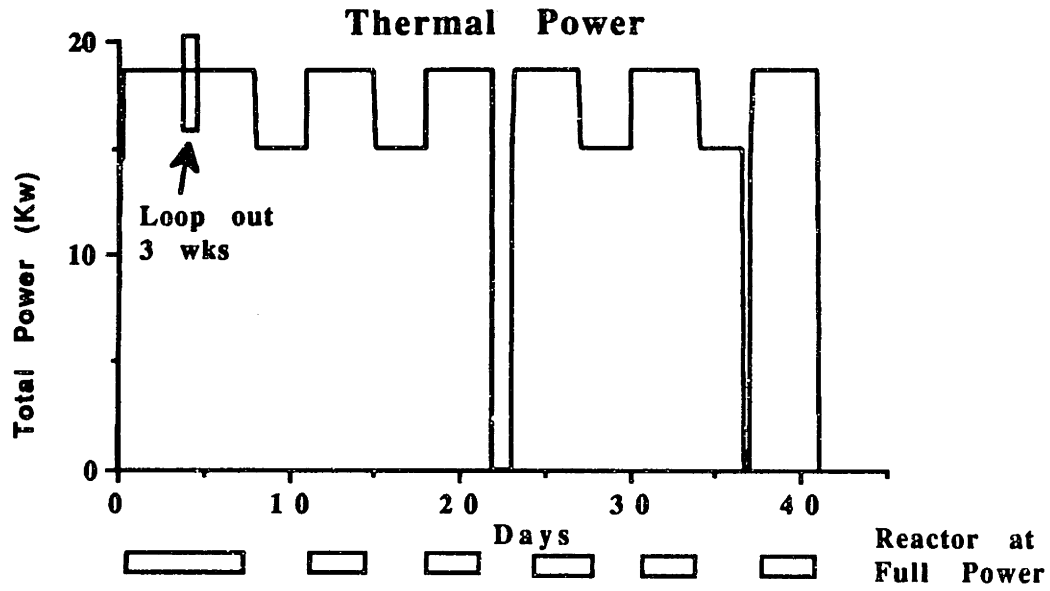

Figure 4.6 Total (Heater + Gamma) Power History of Reference Run #1 (PR1).

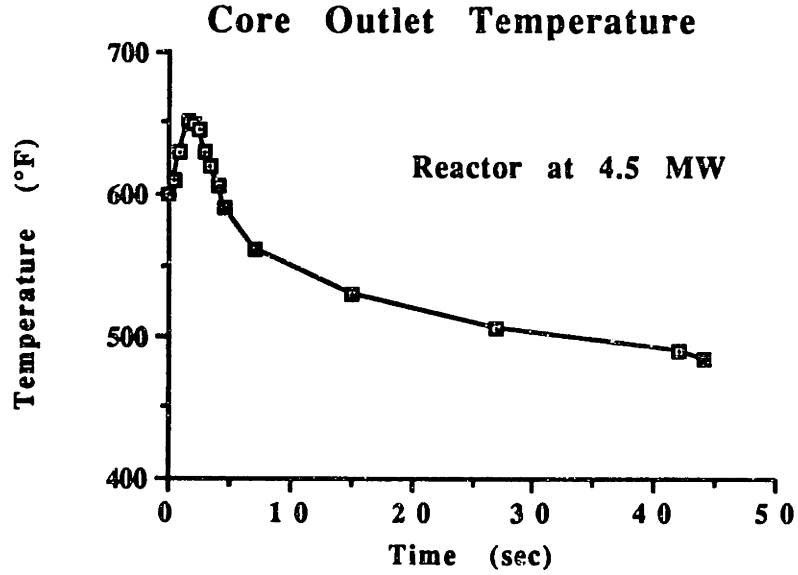

Figure 4.7 Core Outlet Temperature as a Function of Time Following Main Circulating Pump Trip.

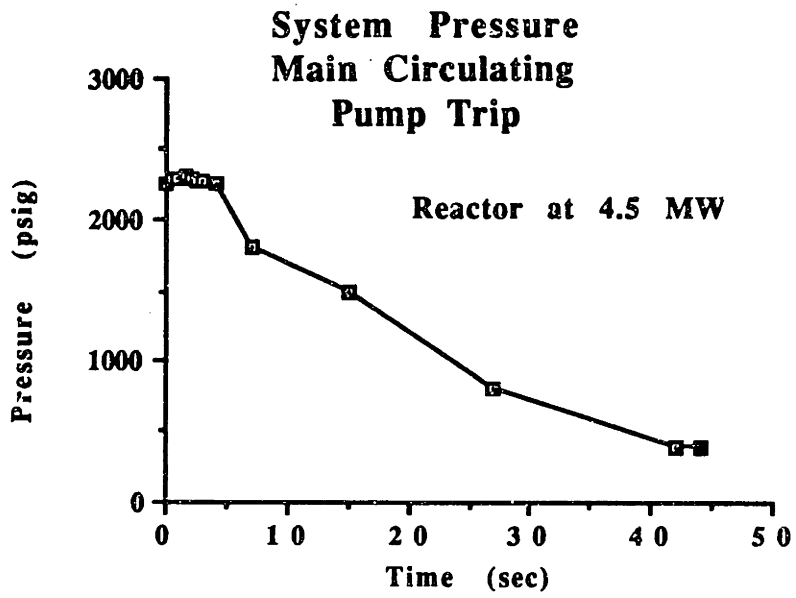

Figure 4.8 Pressure as a Function of Time Following Main Circulating Pump Trip.

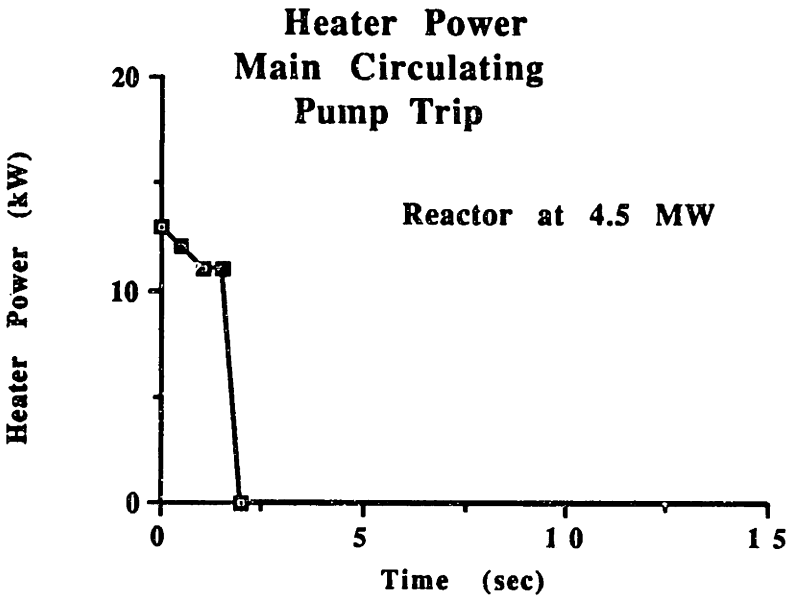

Figure 4.9 Heater Power as a Function of Time Following Main Circulating Pump Trip.

4.2.3 Inconel Tubes

The Inconel tubes in the copper shot region constitute the most important part of the loop from the point of view of the deposition of radioactive corrosion products; namely Co-58 and Co-60. After the one month long run, the loop was transferred to the disassembly area, where the Inconel tubes were disconnected from the Zircaloy tubing. Each Inconel tube (inlet and outlet) was then cut one cm below and approximately 15 cm above the copper shot bed, respectively. The Inconel tubes were placed inside polyethylene tubes which were properly labeled and capped. Once this operation was completed, the tubes were then taken to the automated counting facility described in section 2.11, chapter 2, and counted for a period of 1000 seconds every 4 cm. The Inconel tubes in the shot bed region are approximately 180 cm long, as seen in Fig 4.10.

Figures 4.11 and 4.12 show the Co-58 activity (nCi/cm^2) of the steam generator tubes versus distance from the steam generator inlet. Note the dimensions of the Inconel tubes in Fig. 4.10. The inlet Inconel tube to the shot bed region (hot leg) showed an average of 12.8 nCi/cm^2, and a total activity of 4.6 μCi. On the other hand, the outlet Inconel tube of the shot bed region (cold leg) showed an average activity of 10.4 nCi/cm^2 for a total of 3.7 μCi. It is interesting to note the effect of heat flux at the top end of the shot bed region where the deposition of Co-58 increases slightly.

Figures 4.13 and 4.14 show the Co-60 activity of the hot and cold steam generator tubes, where the average deposited activity was 1.76 and 1.73 nCi/cm^2, respectively. Thus, the total Co-60 activ-

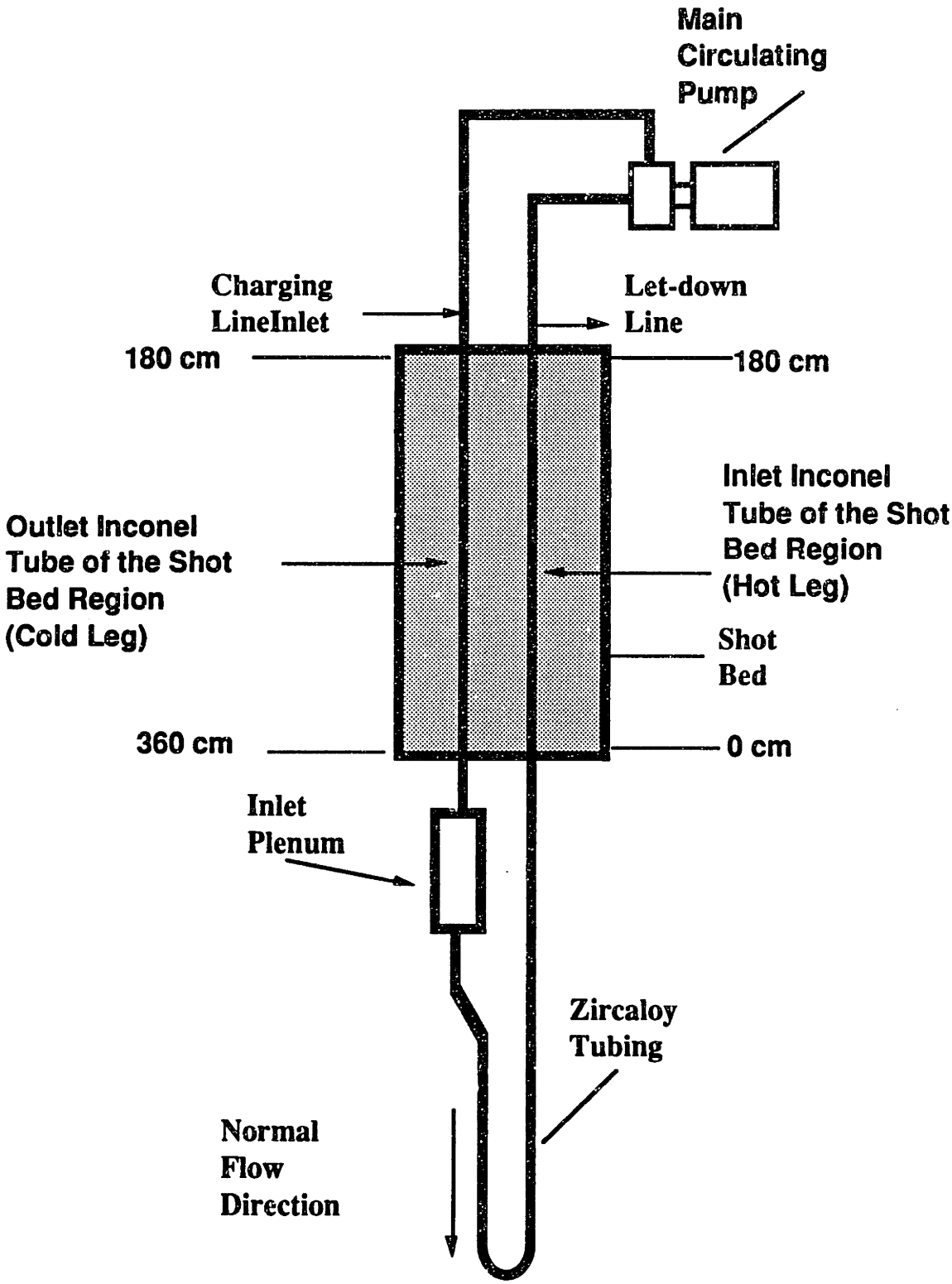

Figure 4.10 Schematic of PCCL Internal Components.

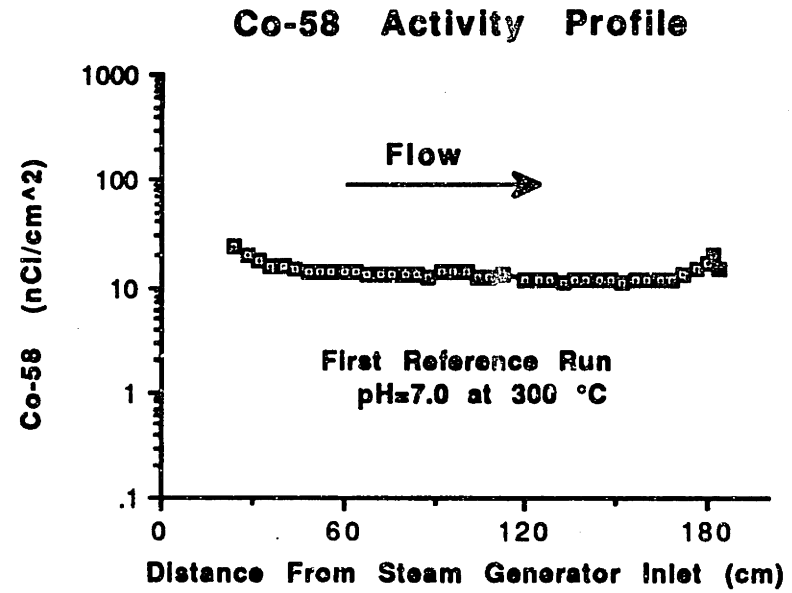

Figure 4.11 Co-58 Activity Profile (Hot Leg), First Reference Run.

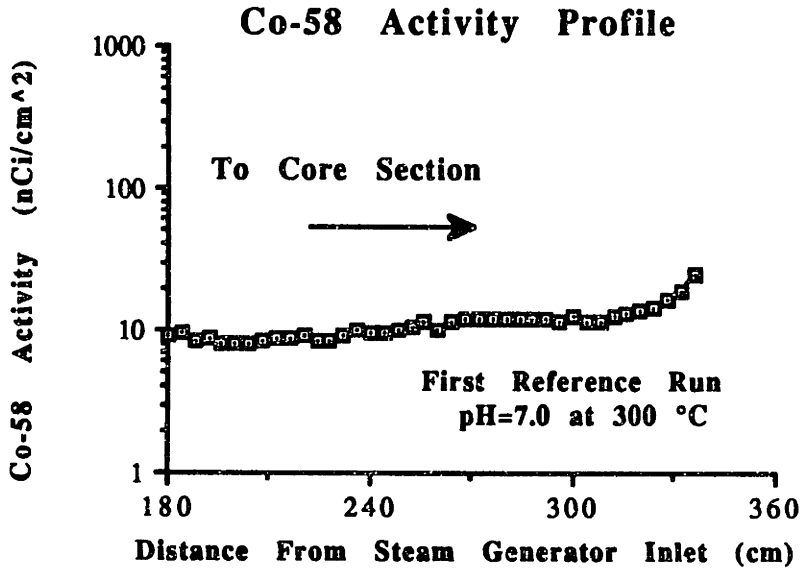

Figure 4.12 Co-58 Activity Profile (Cold Leg), First Reference Run.

ity in the steam generator (hot and cold) tubes was 1.25 μCi. It should be noted that activity deposition studies [R-2] performed in German reactors have shown a higher Co-60 activity at the (hotter) inlet to the steam generators than at the (colder) outlet . This trend is also observed in this reference run; however, this effect is more pronounced for the low pH run (see sec. 4.4, chapter 4).

Figures 4.15 and 4.16 show an average of 7.8 and 6.8 for Co-58/Co-60 ratios for the hot and cold legs, respectively. Plant data published in reference [L-3] reported a Co-58/Co-60 ratio between 12 to 14 for the steam generator tubes. In part the difference between the ratios obtained from the PCCL loop and those from plant data is due to the fact that the MIT reactor core has only half the fast neutron flux compared to a representative PWR plant. Thus, the Co-58 produced by activation in the MIT reactor core is a factor of two lower, since Ni-58(n,p)Co-58 is a fast neutron reaction. On the other hand, since the MIT reactor core has the same thermal flux as a representative PWR plant, the production of Co-60 is in the same proportion as for a PWR. Other factors contributing to these differences are differences in crud composition (cobalt/nickel ratio) and the short time history of the PCCL runs.

The Cr-51, and Fe-59 activities are shown in Fig. 4.17. The average activities are 14 and 2.3 nCi/cm^2, respectively. The total Cr-51 and Fe-59 activities deposited on the steam generator tube (hot leg) are 5 and 0.82 μCi, respectively. Because the solubility of chromium and iron decrease at higher temperatures until a minimum is reached, the higher temperatures in the hot leg of the steam

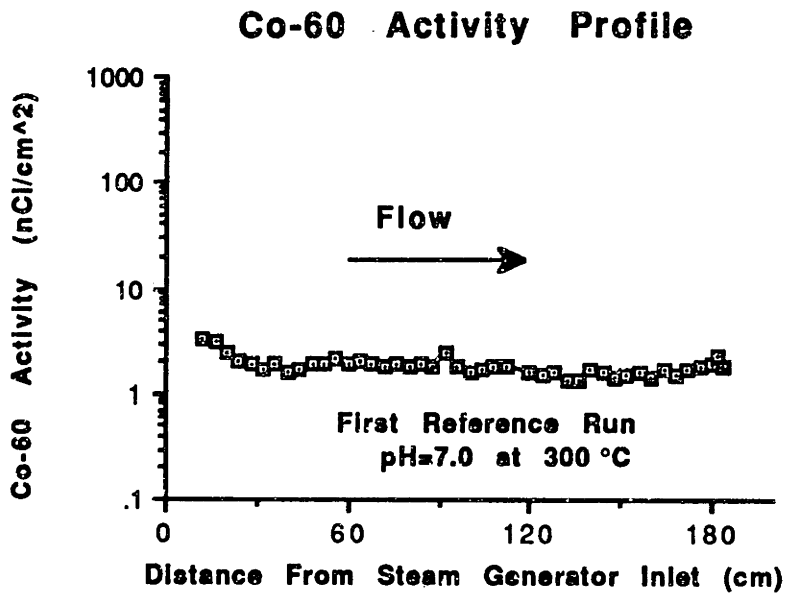

Figure 4.13 Co-60 Activity Profile (Hot Leg) First Reference Run.

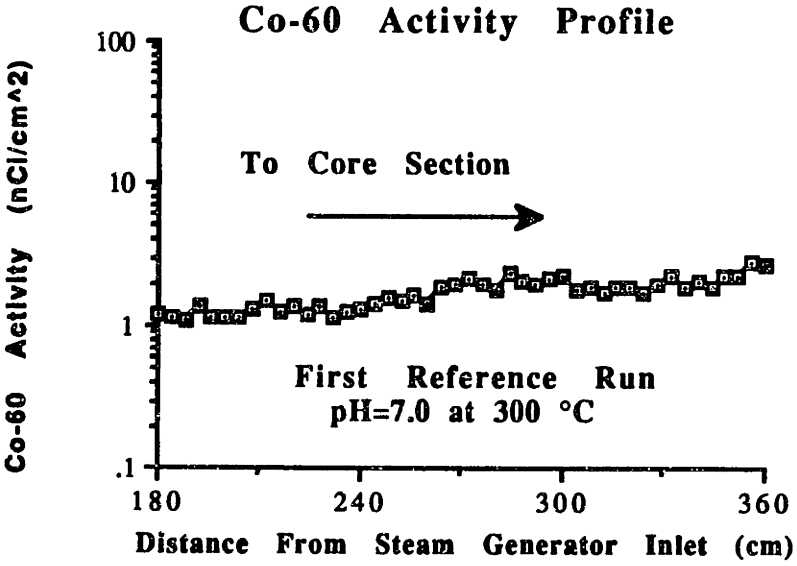

Figure 4.14 Co-60 Activity Profile (Cold Leg) First Reference Run.

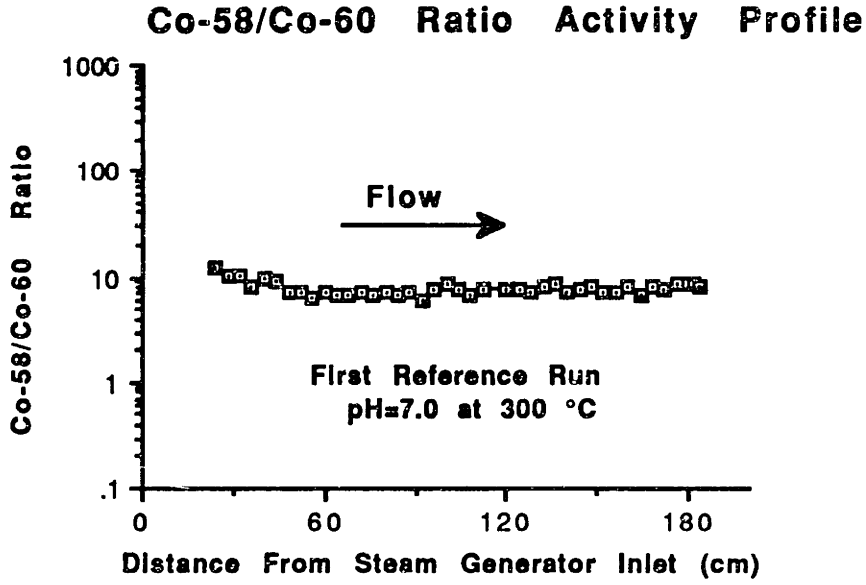

Figure 4.15 Co-58/Co-60 Ratios (Hot Leg) First Reference Run.

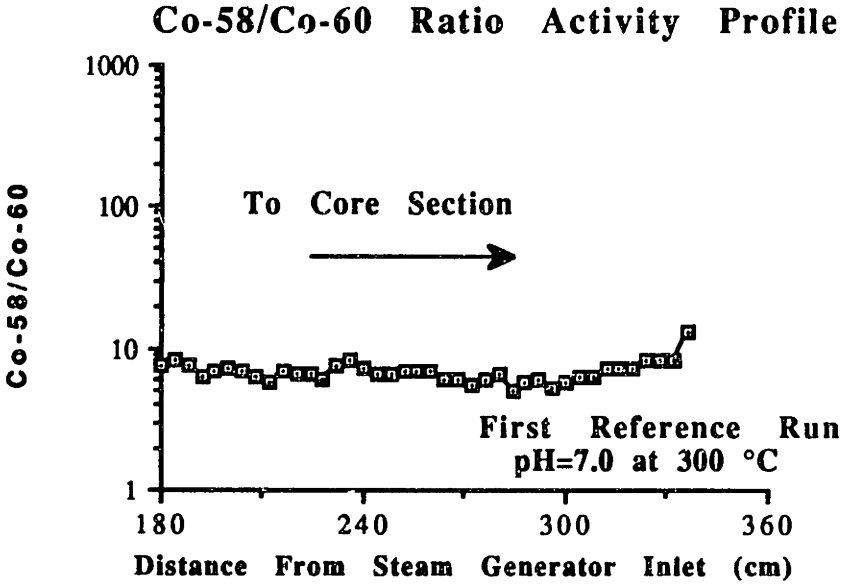

Figure 4.16 Co-58/Co-60 Ratios (Cold Leg) First Reference Run.

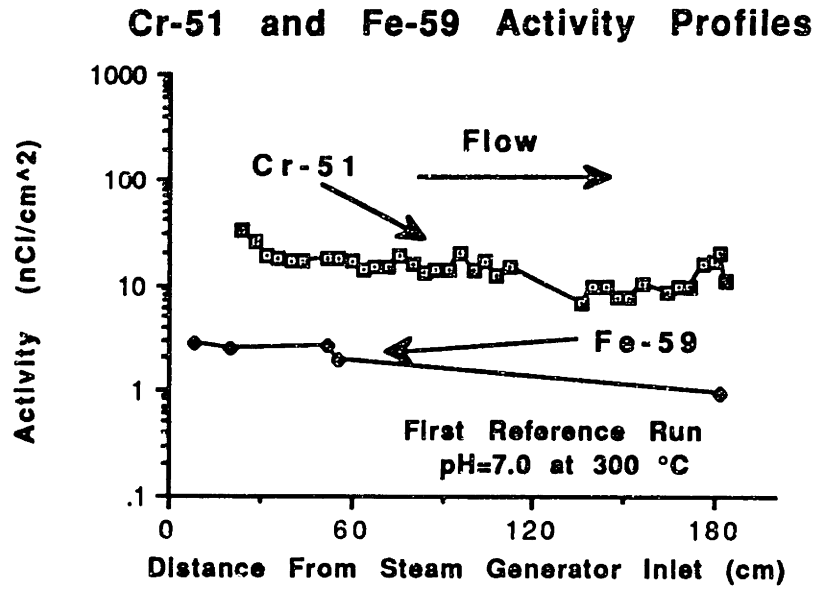

Figure 4.17 Cr-51 and Fe-59 Activity Profiles (Hot Leg) First Reference Run.

generator (compared to the lower temperatures in the cold leg) suggest that precipitating conditions existed only in the hot leg. Thus, the hot leg of the PCCL steam generator showed only the deposition of chromium and iron whereas the cold leg, where dissolving conditions existed, showed a much lower detectable deposition of these elements.

4.2.4 Zircaloy Tube

The Zircaloy tube constitutes an important element in the loop because the crud activity on its interior surfaces is approximately 10 times higher than the crud activity on the steam generator tubes. However, the bulk metal is highly activated, which poses serious problems for the handling and determination of the radionuclide composition of its crud layer. Chemical methods, which are described in reference [C-2], were used to decontaminate the segments of the

Zircaloy in-pile tubing. Figure 4.18 shows the schematic of the Zircaloy segmentation. According to this schematic, the Zircaloy tubing is typically cut into 27 segments of alternating 3 and 10 cm sections; thus, a total of fourteen 3 cm and thirteen 10 cm segments resulted from the segmentation procedure. Once this operation is completed, the 3 cm segments, which are labeled Z1 through Z14 in Fig. 4.18, are decontaminated by soaking them in aqua regia (one part concentrated nitric acid, three parts hydrochloric acid, and two parts deionized water) for a period of 9 to 12 hours. The aqua regia solutions are usually too radioactive for gamma spectroscopy analysis because the Zr-95 content is very high. Hence, a zirconium chemical separation method was devised from procedures given in reference [A-2] and applied to the aqua regia solutions to separate the zirconium from iron, cobalt, chromium, and manganese.

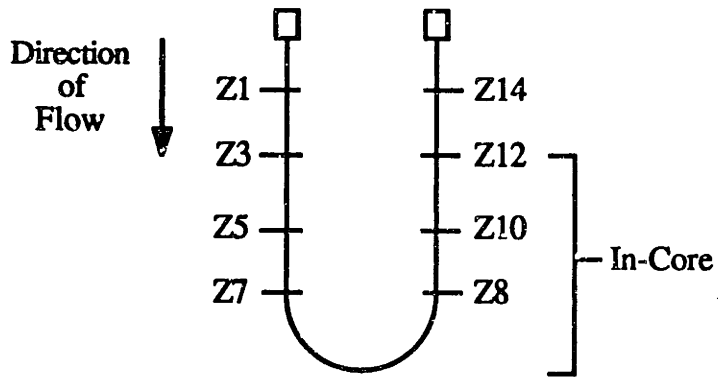

Figure 4.18 Schematic of Zircaloy Tubing Segmentation.

The chemical zirconium separation method, which is described in more detail in reference [C-2], consisted of adding 2 ml each of $ZrOCl_2 \cdot H_2O$ and sodium arsenate solutions to a 50 ml centrifuge tube

containing 20 ml of the aqua regia soak solution, followed by a 30 minute wait period. The tube was then placed in a centrifuge and spun at 3000 rpm for 15 minutes. The centrifuged solution was then filtered. To ensure that the precipitate in the centrifuge tube does not contain any residual cobalt or iron, a 5 ml wash solution (1 ml of the sodium arsenate solution plus 99 ml of 2.4 N hydrochloric acid) was added to the precipitate and agitated. The wash solution was then centrifuged at 3000 rpm for 5 minutes. Once again, the 5 ml solution was filtered, and then added to the original filtered liquid. The wash solution step was repeated twice. The filtered solution was then diluted to 110 ml and counted on the gamma counting system to determine the radionuclide concentrations.

Table 4.2 shows the Co-58, Co-60, Fe-59, and Mn-54 activities found in the in-pile Zircaloy tubing for the positions shown in Fig. 4.18. Note that positions Z3 through Z12 are located in the core. In addition, the thermal and fast neutron peak fluxes in the MIT reactor core occur 61 and 24 cm from the bottom of the core, respectively, according to measurements published in reference [B-10], and recently confirmed by R. Medina [M-3].

According to this table, the Co-60 activity was more predominant in the top of the core than the Co-58 activity because Co-60 is produced by a thermal neutron reaction, whereas Co-58 is produced by a fast neutron reaction. On the other hand, table 4.2 shows that the Co-58 activity was more predominant near the middle of the core where the fast neutron flux peaked. The axial thermal and fast neutron flux profiles are shown in Fig. 4.19 [B-10].

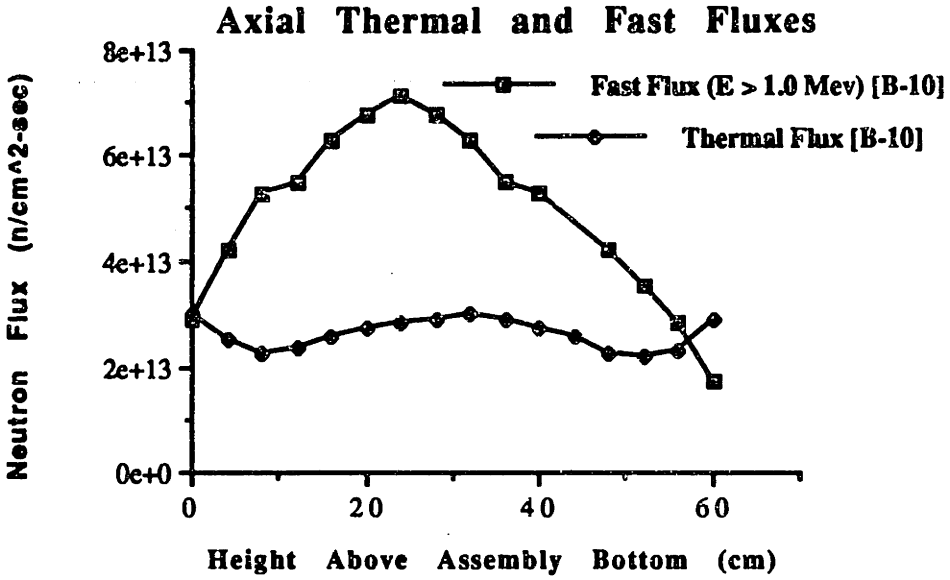

Figure 4.19 Axial Thermal and Fast Neutron Fluxes in the MIT Reactor [B-10].

It was found that the in-core average Co-58 and Co-60 activities were 68 and 31 nCi/cm^2, respectively. The in-core Zircaloy area is roughly 250 cm^2, which yields a total of 17 μCi of Co-58 and 7.8 μCi of Co-60 in-core. The total Fe-59 and Mn-54 activities were 7.8 μCi and 1.5 μCi, respectively.

4.2.6 Stainless Steel Filter

As mentioned in section 2.9, chapter 2, a SS filter is used in the let-down line as a deposition monitor. Its function is to retain some of the most important corrosion products such as Co-58, Co-60, Mn-54, and Fe-59 in order to understand their behavior during the one month long run. Since the temperature of the filter was lower than the bulk coolant temperature in the loop, the radionuclide activities deposited on the deposition monitor filters are not necessarily repre-

sentative of actual activities in the coolant, because their solubilities depend on temperature. Flow conditions also differ; hence the deposition monitor data is only of qualitative significance.

Table 4.2 Results of Core Activity Deposition Measurements, First Reference Run.

Position	Co-58 (nCi/cm^2)	Co-60 (nCi/cm^2)	Fe-59 (nCi/cm^2)	Mn-54 (nCi/cm^2)
Z3(61 cm)*	65 ± 3.9	80 ± 0.08	-	-
Z5(35 cm)*	190 ± 3.3	44 ± 0.72	-	15 ± 0.32
Z7(9 cm)*	45 ± 1.9	16 ± 0.35	31 ± 9.5	5.1 ± 0.21
Z8(9 cm)*	56 ± 2.1	20 ± 0.38	51. ± 17	5.6 ± 0.22
Z10(35 cm)*	48 ± 1.8	14 ± 0.30	12 ± 14	3.0 ± 0.17
Z12(61 cm)*	9.3 ± 2.5	11 ± 0.30	<17	0.5 ± 0.1
Z14(87 cm)*	5.5 ± 2.7	0.7 ± 0.1	<14	0.5 ± 0.1

* Distance measured from the bottom of the core.

The SS filters were replaced every third day and counted outside the containment area, where the radiation background was much lower. Figure 4.20 illustrates the Co-58 activity deposited on the let-down filters. Two peaks are observed, which correspond to the two pump trips experienced during this run. Figure 4.21 shows the previous plot amplified ten times so that the activity trend is more easily determined. Excluding the pump trip transients, an average activity of approximately 1E-04 nCi/cm^3 is indicated. The cumulative Co-58 and Co-60 activities deposited on the filters are

shown in Figs. 4.22 and 4.23, respectively. Excluding again the transients, it can be calculated that the total Co-58 and Co-60 activities deposited on the filters are 0.05 and 0.01 μCi, respectively, which yield a Co-58/Co-60 ratio of 5.

Finally, the Co-58/Co-60 ratios of each filter are shown in Fig. 4.24. An average Co-58/Co-60 ratio of 4.37 was found in these filters, which is comparable to the deposition ratio in the steam generator tubes.

4.2.7 Water Samples

Water samples were taken on a daily basis and counted outside the containment building. The pH and conductivity of randomly se-

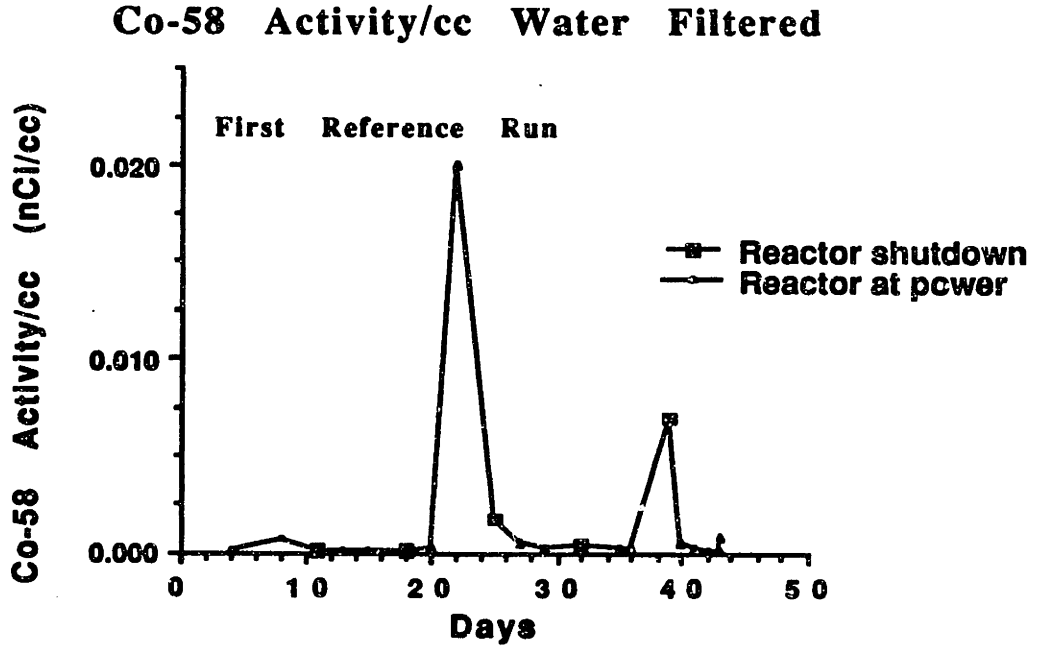

Figure 4.20 Co-58 Activity on Let-down Filters, First Reference Run.

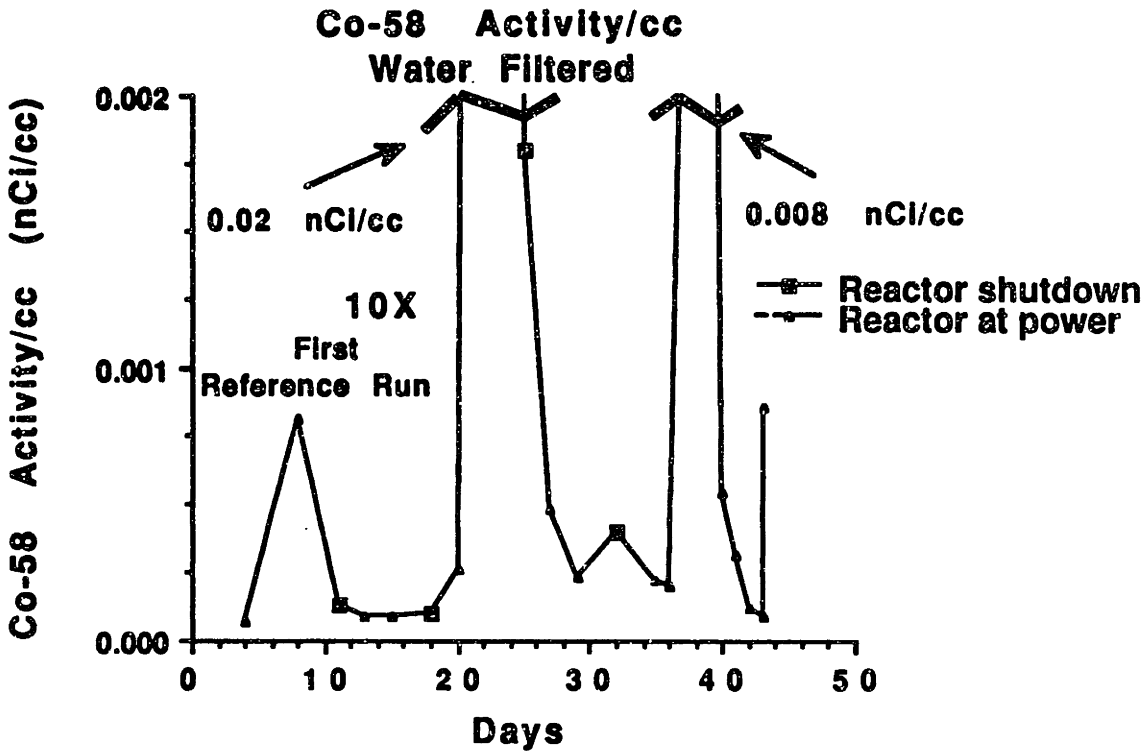

Figure 4.21 Amplified Plot of Co-58 Specific Activity on Let-down Filters, First Reference Run.

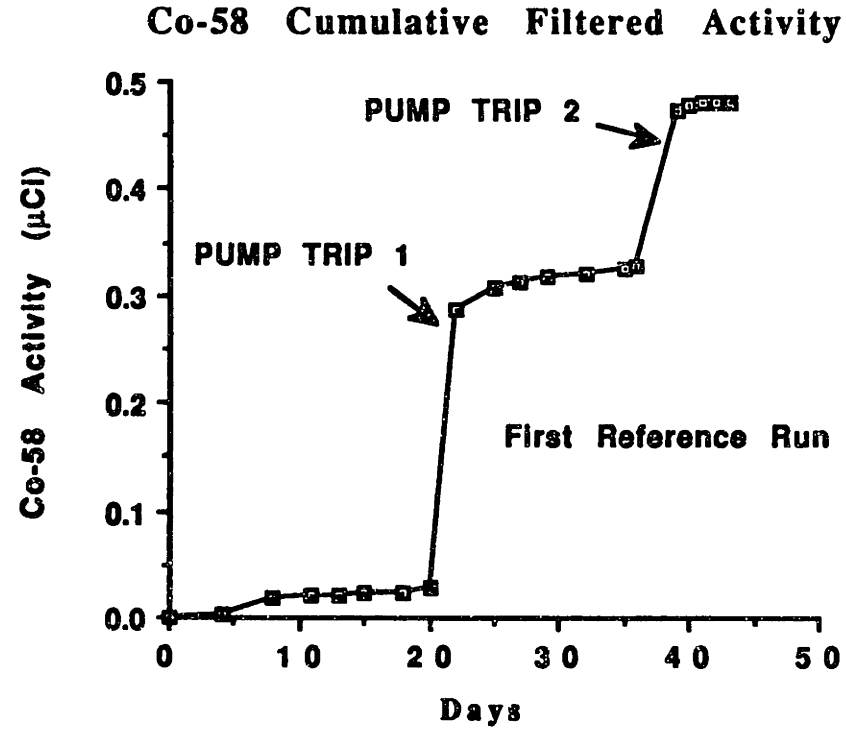

Figure 4.22 Cumulative Co-58 Activity Deposited on Filters, First Reference Run.

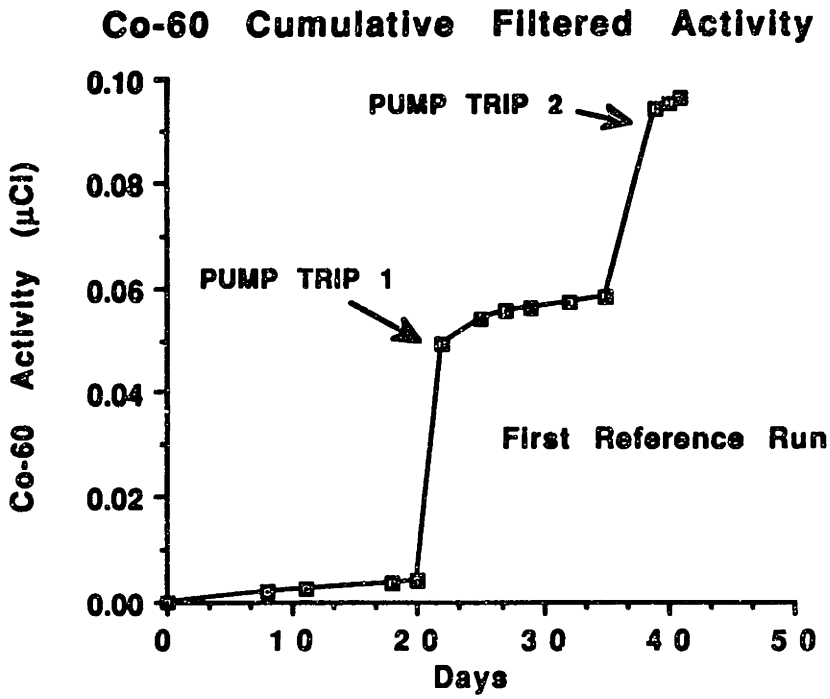

Figure 4.23 Cumulative Co-60 Activity Deposited on Filters, First Reference Run.

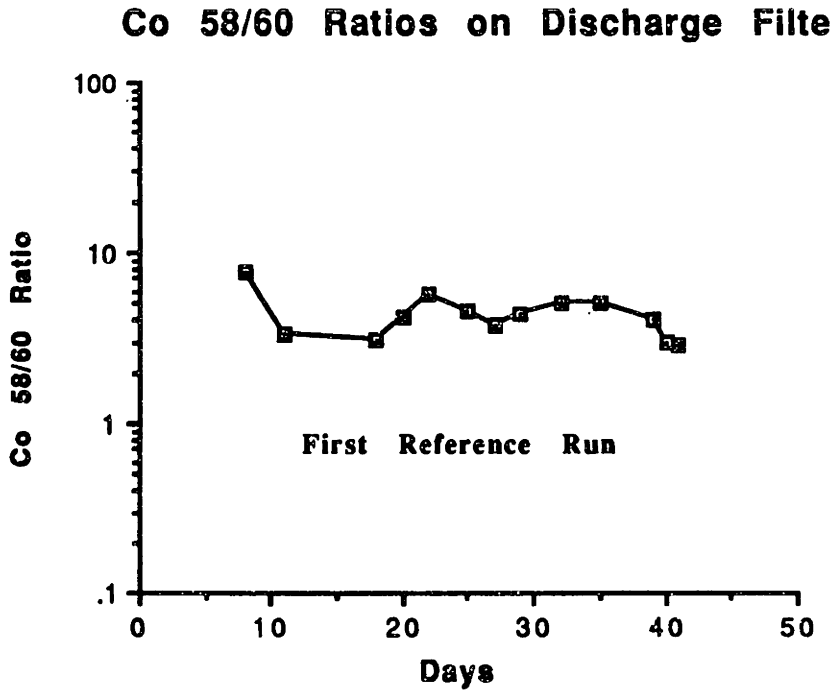

Figure 4.24 Co-58/Co-60 Ratios on Filters, First Reference Run.

lected water samples were measured as shown in Figs. 4.25 and 4.26. Boron and lithium concentrations were also checked by atomic absorption and colorimetric techniques, respectively (see Appendix A). The results of these analyses are plotted in Figs. 4.27 and 4.28. The pH of these samples never deviated by more than ± 0.1 pH units which is within the acceptable range (PWR Primary Water Chemistry Guidelines, Ref. [W-5]). In addition, the samples' conductivity never exceeded a deviation greater than ±10%, which is also within the acceptable range.

A colorimetric technique [H-4] was used to determine the boron concentration of these samples (subsequently validated by a prompt gamma method, which was adopted as a standard for later runs). Because the colorimetric boron determination technique was only effective in the range between 0 and 14 ppm, the samples had to be diluted by a factor of 100. Thus, a small error was introduced in the measurement. The typical boron values obtained were within ± 10% of the nominal 800 ppm value. A conventional mannitol titration was also carried out to check the accuracy of this method.

As mentioned above, the lithium in these samples was checked using atomic absorption. The lithium values obtained with this technique were within ± 5% of the nominal 1.84 ppm value.

The analysis of water samples using gamma spectroscopy yielded the activities and radionuclides listed in table 4.3 near the end of this run [D-1].

Ce-144 and I-132 are produced as a result of fission of the small amount of uranium contamination in the water and/or loop

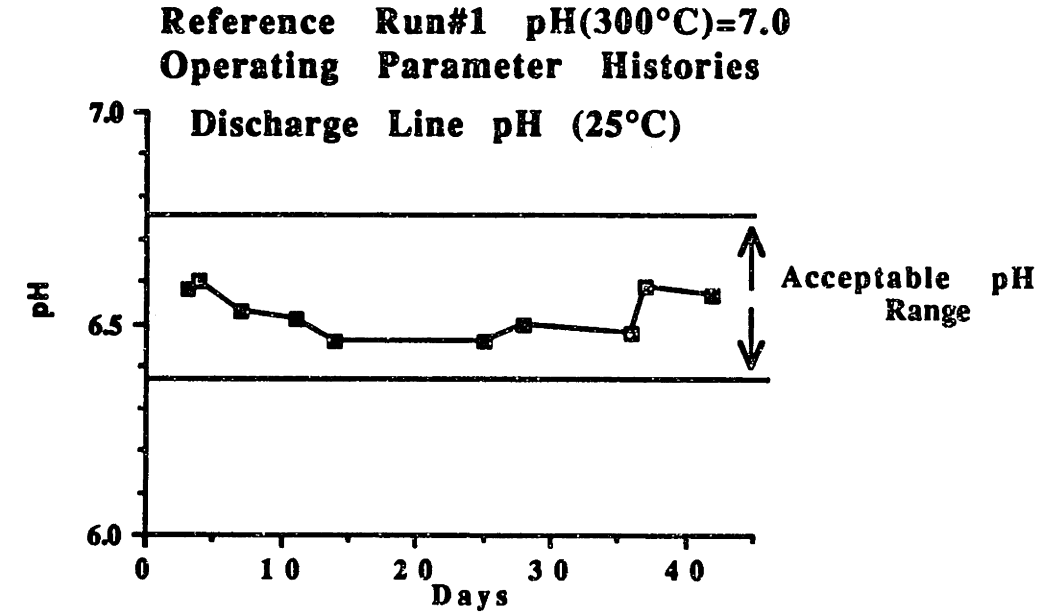

Figure 4.25 Discharge Line pH (25°C), First Reference Run.

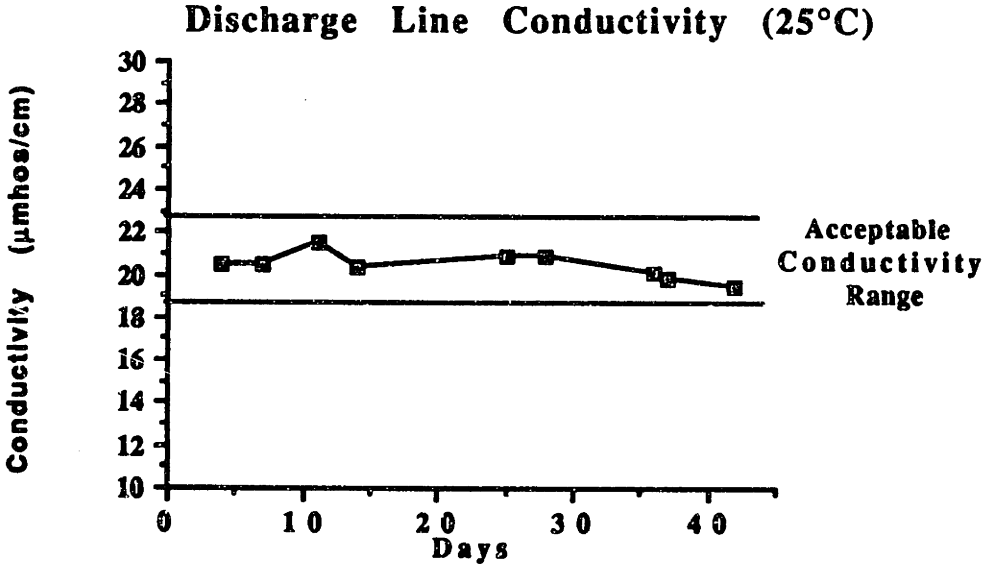

Figure 4.26 Discharge Line Conductivity (25°C), First Reference Run.

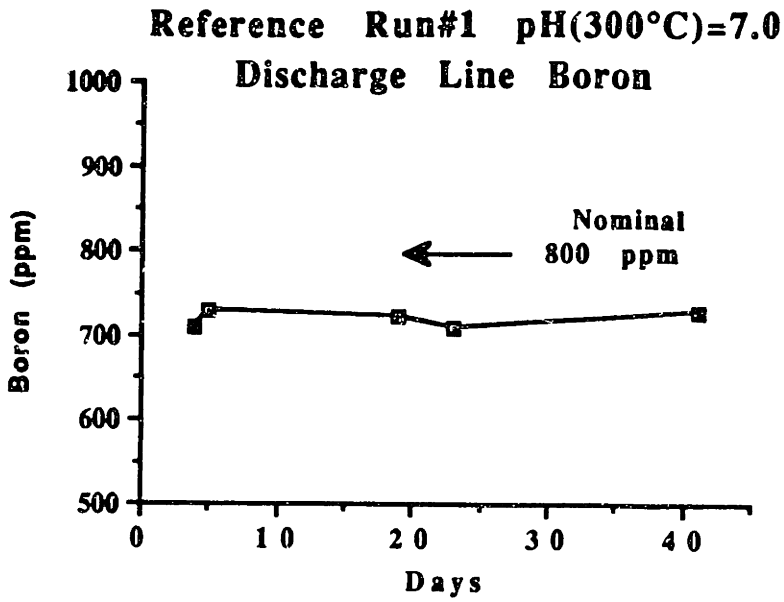

Figure 4.27 Discharge Line Boron, First Reference Run.

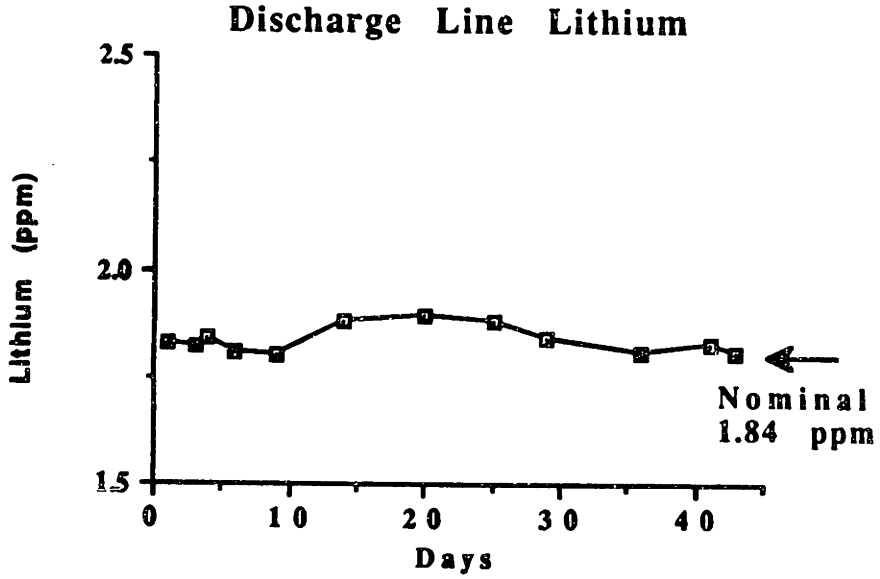

Figure 4.28 Discharge Line Lithium, First Reference Run.

materials prior to irradiation.

Ar-41 is produced by the following nuclear reaction: Ar-40(n,γ)Ar-41. The source of Ar-40 is the air saturated water which is charged into one of the charging tanks and subsequently stripped with hydrogen and catalytically deoxygenated (< 1 ppb O_2) prior to its injection into the loop.

Na-24 activity is detected in almost every water sample (see Fig. 4.29). Its activity corresponds to approximately 20 ppb of dissolved sodium. The sources of sodium include the pyrex glass which the charging makeup water tanks are made of, and the deionized water which is used to prepare the water chemistry.

The activity of W-187 corresponds to roughly 20 ppb of dissolved tungsten. As shown in Fig. 4.30, the tungsten activity also appears in every outlet water sample. The potential sources of this contaminant are believed to be the Hastalloy pump check valve balls which contain approximately 120 ppm of W, and the inlet plenum steel which contains 350 ppm of W. A test was conducted using an

Table 4.3 Radionuclides in Water Samples, First Reference Run.

Radionuclide	Activity/cc (μCi/cc)
Ce-144	1.0E-06 ± 100%
I-132	3.61E-04 ± 8%
Ar-41	1.8E-04 ± 13%
Na-24	1.5E-03 ± 3%
W-187	1.2E-02 ± 1%

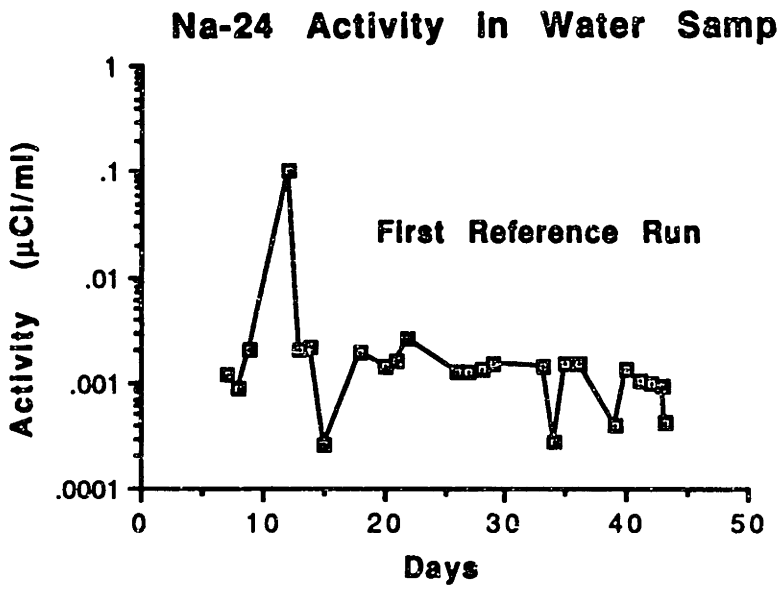

Figure 4.29 Na-24 Activity in Water Samples, First Reference Run.

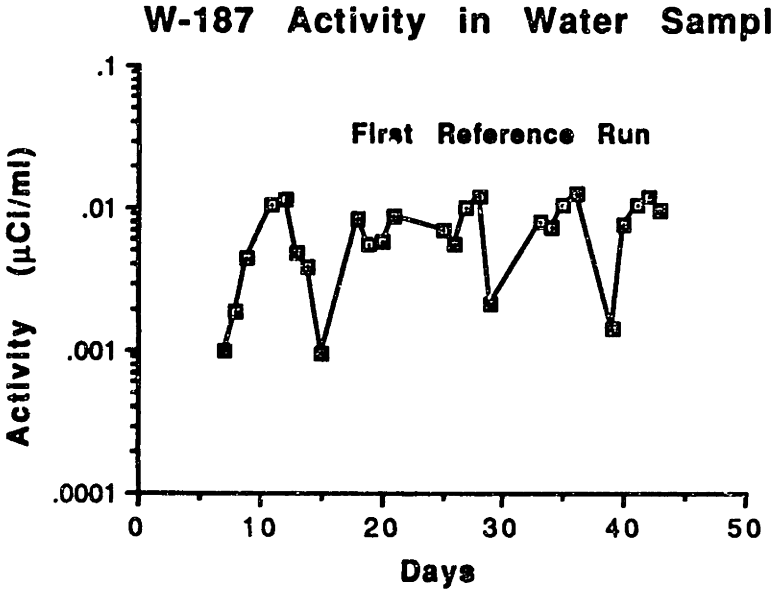

Figure 4.30 W-187 Activity in Water Samples, First Reference Run.

anion resin to determine the chemical form of the tungsten. This test indicated tungsten is present as a soluble anion, probably $WO_3^=$.

Water samples from the charging system were analyzed using ion chromatograph techniques [B-9] to determine input concentrations of transition metals into the loop. Table 4.4 presents these results. Since the make water is injected at approximately 1E-03 of the main coolant flow rate, the increase in metal ion inventory per pass is much less than its presumed saturated value (≅ 5 ppb total transition metal ions).

Table 4.4 Ion Chromatograph Measurements of Make-up Water Trace Elements, First Reference Run.

Element	Concentration (ppb)
Zinc	13 (12)
Nickel	106 (54)
Cobalt	4 (<4)
Iron (II)	116 (54)
Manganese	23 (<4)

Note: Values in parenthesis were measured on an aliquot of the same sample in December 1989, 4 months earlier.

4.2.8 Ion Exchange Column

The ion exchange column (see sec. 2.10, chapter 2) was designed to recover all radioactive and non-radioactive contaminants which were dissolved or suspended in the let-down water flow. Once the run ended, the mixed bed resin was analyzed using gamma

spectroscopy to determine the radioactive corrosion products that had been removed. The results showed a total deposition of Co-58 and Co-60 of 7.82 and 0.95 μCi, respectively with a Co-58/Co-60 ratio of 8.2. Table 4.5 summarizes the total activities of transition metals and other species (e.g. fission products) deposited on the IX resin, and their inferred activities per cm^3 of coolant that passed through the resin.

Table 4.5 Summary of Activities Deposited on IX Column, First Reference Run.

Radionuclide	Activity (μCi)	Activity* (μCi/cc)
Co-58	7.82 ±1%	3.0E-05
Co-60	0.95 ±2%	3.1E-06
Cr-51	0.16 ±100%	5.2E-07
Fe-59	0.15 ±19%	4.8E-07
Mn-54	0.97 ± 0.84%	3.1E-06
Nb-95	0.11 ±28%	3.2E-07
Sb-124	0.48 ±9%	1.6E-06
Zn-65	0.16 ± 4%	5.2E-07

* Total cc passed through resin = 3.09E05 cc

4.3 Reference Run #2

4.3.1 Introduction

Reference run #2 was operated for a total of 22 days. Out of these 22 days, 20 were with the reactor at full power, which yielded a total of 1871 MW-hrs. To simulate the same conditions as reference run #1, a pH of 7.0 at 300 °C was maintained throughout the entire

run. Thus, the purpose of this run was to established to what extent this run could reproduce the results obtained under similar conditions to reference run #1.

The following sections will present a brief run history followed by the data obtained from Inconel and Zircaloy tubes, deposition monitor filter, water samples, and ion exchange column resin.

4.3.2 Run History

The second reference run experienced a series of fitting and plenum leaks that caused a high interior thimble humidity throughout the entire run. During the first two days after the startup of this run (Toutlet=600 °F), the thimble humidity alarm was activated on several occasions, indicating a possible plenum/fittings leak in the interior of the thimble. A decision was made to remove the thimble and internals from the core tank and transport them to the disassembly area for proper inspection. Once there, the internals were pulled out, inspected, and pressure tested. Traces of coolant chemicals were found on the plenum threads, indicating a leaky plenum O-ring seal. After several unsuccessful attempts to reseal the plenum, it was decided to install another preconditioned steam generator (cold) leg and pressure test the entire loop at 2400 psig with deionized water for a period of 3 hours. During this pressure test, no visible leaks were observed.

Once the test was completed, the internals were placed back in the thimble and thimble/internals reinstalled in the core tank. After two days of operation at an outlet temperature of 550 °F, the electric

heater tripped off. Resistance measurements indicated a low resistance (750 Ω) existed between a heater lead and ground. At this point, Delta M (heater manufacture) was consulted for advice. Since the electric heater had been operated in a very humid environment, there was a possibility that the heater ceramic insulation had absorbed moisture, which eventually caused a low resistance between ground and a heater lead. Hence, it was recommended to bake the electric heater for a period of 6 to 7 hours at a temperature of 300 to 400 °F to dry some of the moisture.

Following the above recommendations, the electric heater contained in the highly radioactive Titanium Test Tube (TTT) was lowered into a furnace located inside the hot cell and heated up to an average temperature of 350 °F for a period of 17 hours. During this operation, the Zircaloy and Inconel tubing were filled with helium to avoid any oxidation.

Once this operation was completed, the internals were placed back into the thimble, which then was evacuated to remove any existing moisture in its interior. A 230 volt VARIAC was then connected to the electric heater and a constant temperature of 300 °F maintained for a period of 12 hours.

The thimble and internals were reinstalled in the core tank. After reaching an outlet temperature of 500 °F, the thimble was evacuated one more time to remove the existing moisture in its interior. While the thimble evacuation was taking place, the electric heater tripped due to sudden water vapor condensation in the interior of the thimble. This "cloud chamber effect" explains why a

sudden depressurization in a humid environment can easily lead to extensive water vapor condensation, especially on heater lead connectors. A thorough inspection of the loop internals revealed that water condensation on heater lead connectors led to a short circuit, thus tripping the electric heater.

The loop was placed back in the core tank and operated for a total of 22 days in a humid environment until thermocouple failures combined with a heater short terminated this run. Based upon this experience, it was decided that for future runs the plenum cap would be welded shut and the Zircaloy fittings be made up only once. In addition, the Inconel Parker ferrules would be cut and replaced by new ones, to minimize as much as possible the likelihood of a water leak.

It is important to note that steam was produced during some of the heater transients, which undoubtedly affected the deposition of corrosion products on the steam generator tubes. Figure 4.31 shows the total power history for this run, indicating the time that the loop was out of service.

4.3.3 Inconel Tubes

Once the second reference run ended, the Inconel tubes were prepared for analysis in the same manner as for reference run #1. The Inconel tubes (cold and hot leg) were then scanned with a High purity Germanium detector.

Figures 4.32 and 4.33 show the Co-58 activity profile of the hot and cold S/G leg as a function of distance from the S/G inlet (Fig.

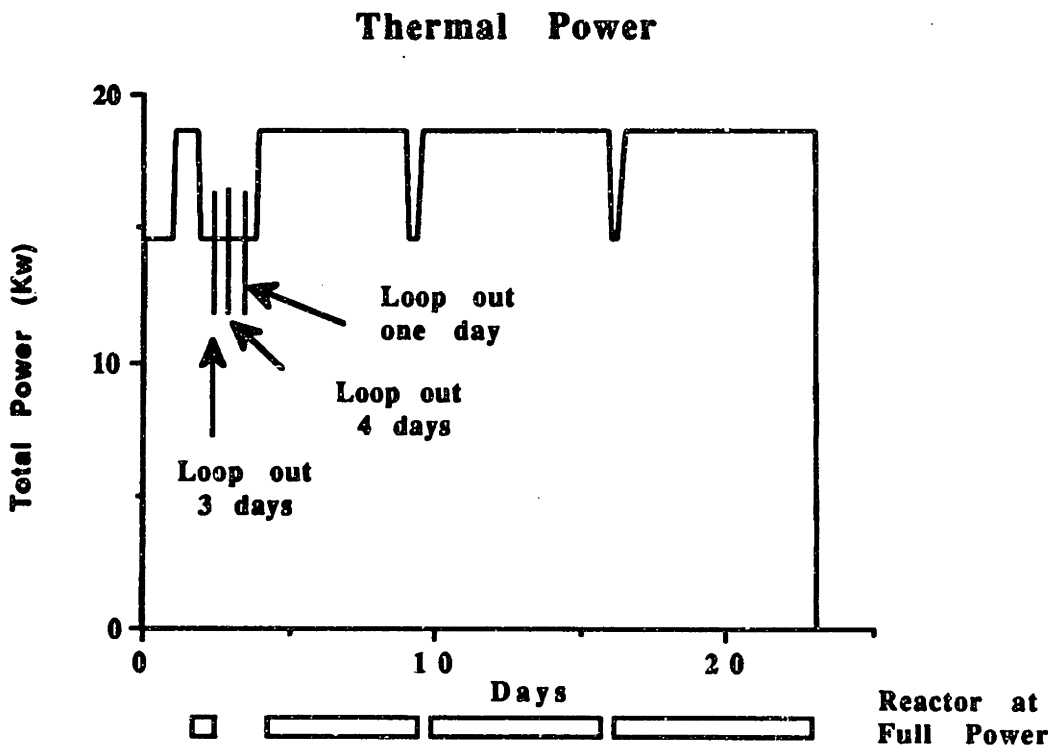

Figure 4.31 Total (Heater + Gamma) Power History of Reference Run #2 (PR2).

4.10), respectively. The hot leg showed an average activity of 20.5 nCi/cm^2, and a total activity of 7.4 μCi. It should be noted that the deposition of Co-58 activity was not uniform, as shown in Fig.4.32. It appears that the two phase flow conditions that existed during the heater trip at the end of this run, transported crud from the top of the in-pile Zircaloy tubing to approximately 60 cm into the S/G hot leg. As seen in Figs. 4.32 and 4.34, the composition of the transported crud is slightly enriched in Co-60 activity and depleted in Co-58 activity. This evidence suggests that the crud probably came from the top of the Zircaloy tubing, where the activation of Co-59 is the greatest, due primarily to the thermal neutron flux peak in this re

gion.

The average Co-58 activity in the S/G cold leg was 18.2 nCi/cm^2, which yielded a total activity of 6.5 μCi. Therefore, the total Co-58 activity deposited on the S/G tubes (hot and cold) was 13.9 μCi.

Figures 4.34 and 4.35 present the steam generator tubes' Co-60 activity profile as a function of the distance from the inlet of the steam generator section. The S/G hot and cold leg average activities were 0.94 nCi/cm^2 and 1.0 nCi/cm^2, respectively. As mention above, the hot leg Co-60 activity profile also exhibited the deposition irregularities already discussed. The total Co-60 inventory deposited on both legs was 0.7 μCi. It should be noted that the hot leg Co-58 and Co-60 activities both increased slightly when the Inconel tube was no longer in the upper shot bed region, ie. where isothermal conditions are experienced (bulk and tube wall temperatures are essentially the same).

The Co-58/Co-60 ratios are presented in Figs. 4.36 and 4.37. The average ratio was 18.6 for both legs, which resulted from a 67% increase in the Co-58 activity and a 44% decrease in the Co-60 activity compared to the deposition of these radionuclides on the steam generator tubes of the previous reference run. Note that Co-60 activity increased in the 60 to 90 cm region of the hot leg, whereas the Co-58 activity decreased in the same region.

The Fe-59 and Mn-54 activities for the hot and cold legs are plotted in Figs 4.38 and 4.39, respectively. The same type of deposition behavior is observed in the hot leg of the steam generator tube.

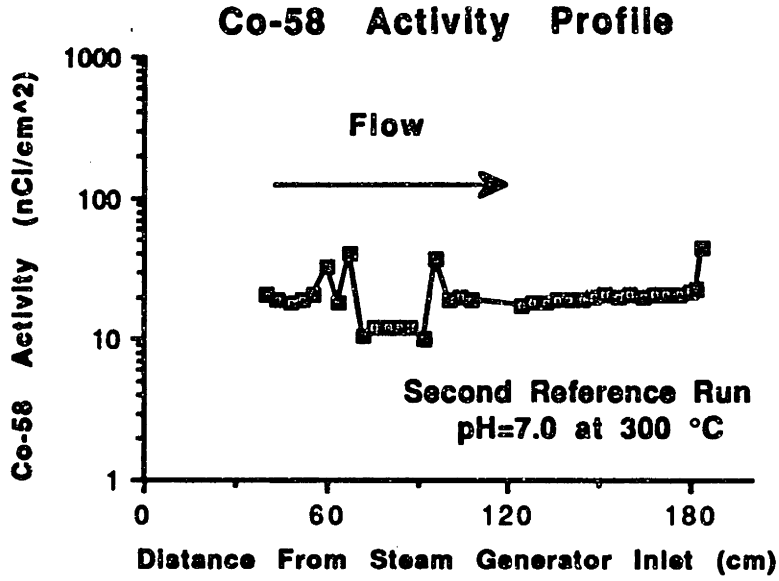

Figure 4.32 Co-58 Activity Profile (Hot Leg), Second Reference Run.

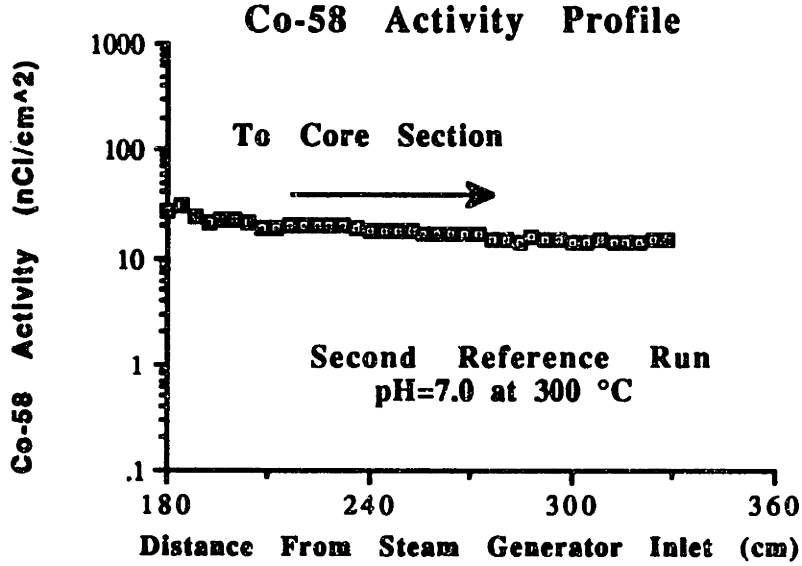

Figure 4.33 Co-58 Activity Profile (Cold Leg), Second Reference Run.

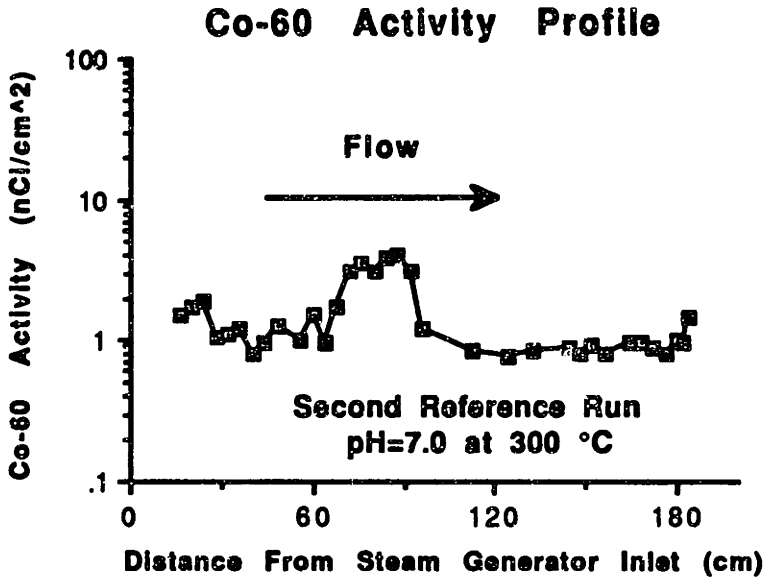

Figure 4.34 Co-60 Activity Profile (Hot Leg), Second Reference Run.

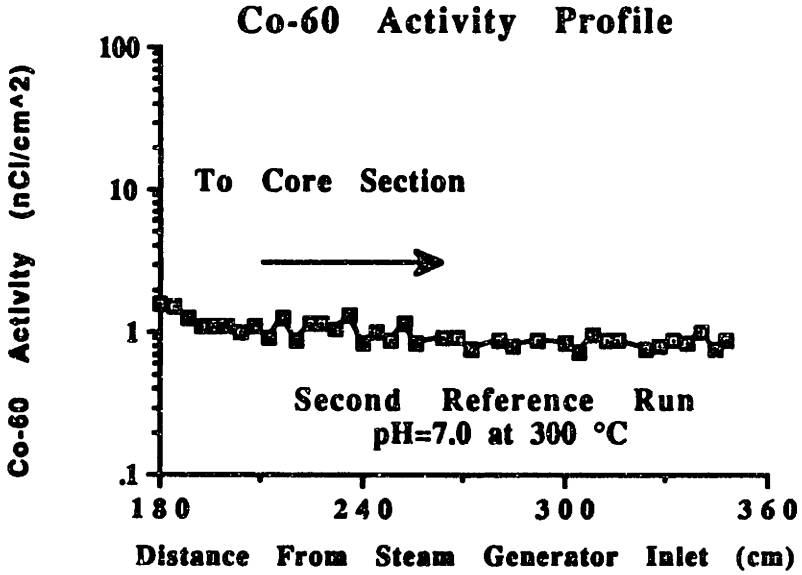

Figure 4.35 Co-60 Activity Profile (Cold Leg), Second Reference Run.

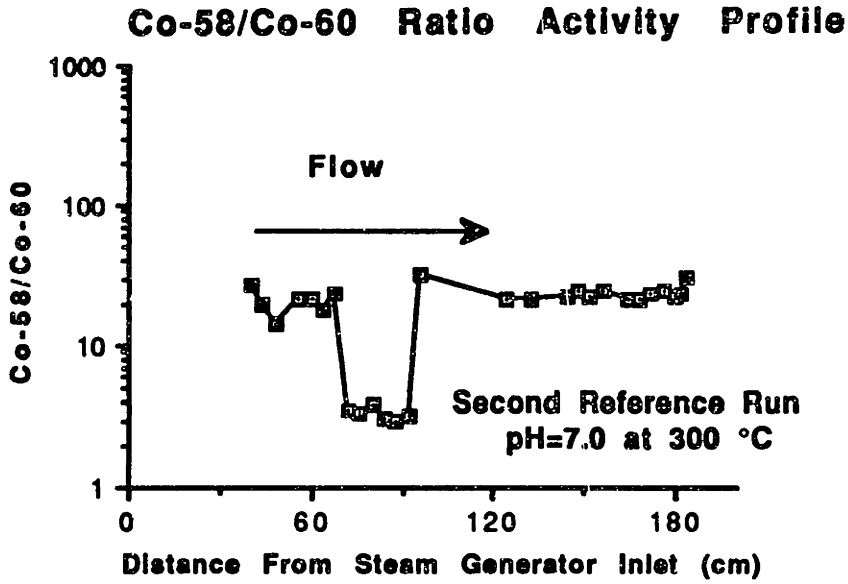

Figure 4.36 Co-58/Co-60 Ratios (Hot Leg), Second Reference Run.

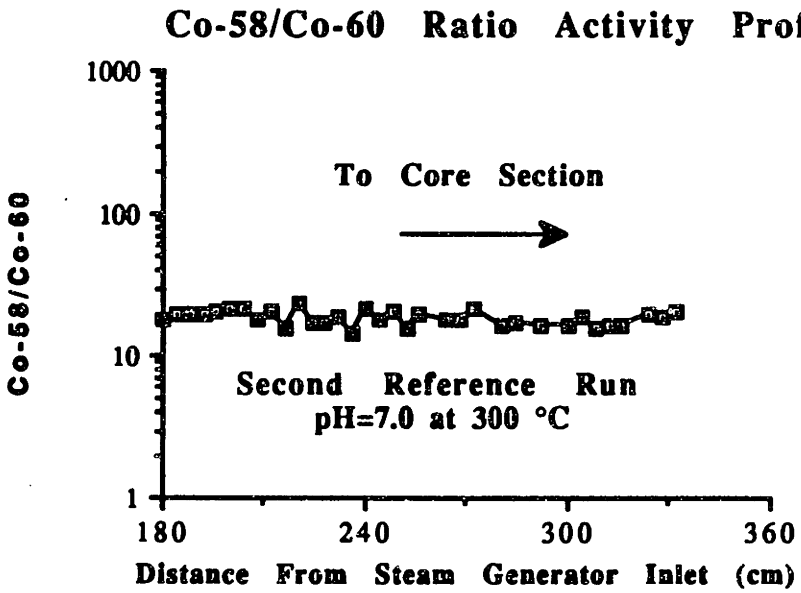

Figure 4.37 Co-58/Co-60 Ratios (Cold Leg), Second Reference Run.

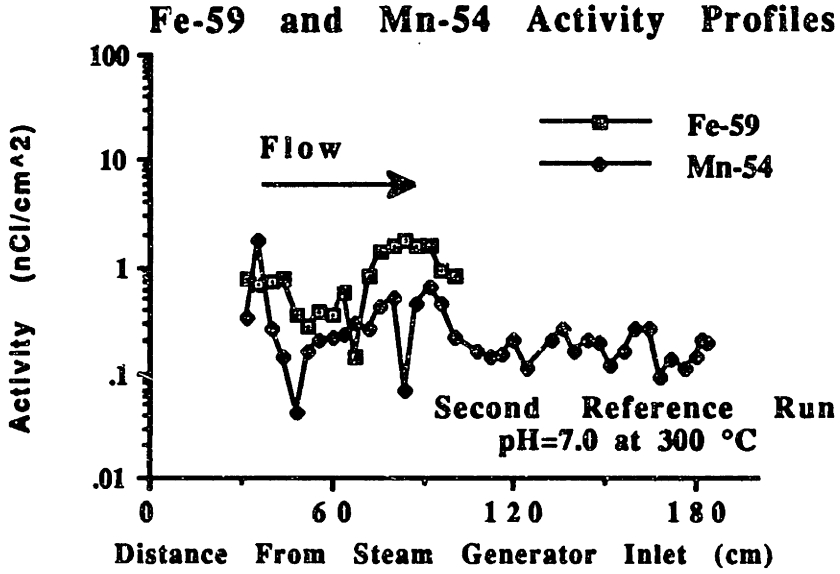

Figure 4.38 Fe-59 and Mn-54 Activity Profiles (Hot Leg), Second Reference Run.

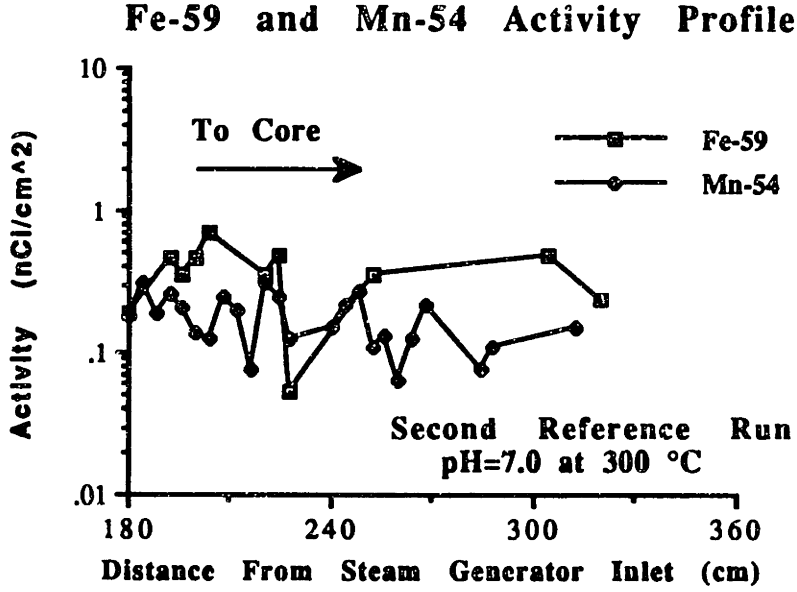

Figure 4.39 Fe-59 and Mn-54 Activity Profiles (Cold Leg), Second Reference Run.

In this case, the Fe-59 activity, which is produced primarily by thermal neutrons, increases slightly whereas the Mn-54 activity (fast neutron reaction) decreases in the same 60 to 90 cm region. In addition, the average Fe-59 and Mn-54 activities are higher in the hot leg than in the cold leg. The total Fe-59 and Mn-54 activities were 0.43 μCi and 0.160 μCi, respectively.

4.3.4 Zircaloy Tube

To determine the composition of corrosion products deposited on the in-pile Zircaloy tubing, a similar method to the one described in sec. 4.1.4, chapter 4 and reference [C-2] was followed. Table 4.6 presents the corrected radionuclide activities deposited on the in-pile Zircaloy tubing for the positions shown in Fig. 4.18. It should be noted that position Z1, which is located outside the heat flux zone, showed very little activity deposition. This trend agreed with the results obtained in the previous run.

The Co-58/Co-60 ratios are smaller at the top of the core compared to any other position. This result indicates a higher Co-60 production rate due to the thermal neutron flux, which peaks at the top of the reactor core. On the other hand, Co-58 is predominant in positions Z5 and Z10 which are near where the fast neutron flux peaks.

The average Co-58 and Co-60 activities deposited on the in-core section of the Zircaloy tubing are 212 and 18 nCi/cm^2, which yields a total activity of 53 and 4.5 μCi, respectively. In addition, the total Fe-59 and Mn-54 activity inventories are 31 and 8 μCi, respectively.

Table 4.6 Results of Core Activity Deposition Measurements, Second Reference Run.

Position	Co-58 (nCi/cm^2)	Co-60 (nCi/cm^2)	Fe-59 (nCi/cm^2)	Mn-54 (nCi/cm^2)
Z1(87 cm)*	1.4 ± 0.4	0.42 ± 0.1	-	0.14 ± 0.08
Z3(61 cm)*	7.1 ± 0.74	3.4 ± 0.17	8.3 ± 3.9	0.9 ± 0.13
Z5(35 cm)*	380 ± 5.5	21 ± 7.1	440 ± 15	110 ± 16
Z7(9 cm)*	200 ± 2.3	18. ± 0.44	31 ± 5.3	6 ± 0.36
Z8(9 cm)*	160 ± 2.0	19 ± 0.37	26 ± 4.2	4.9 ± 0.17
Z10(35 cm)*	510 ± 31	44 ± 2.9	240 ± 18	63 ± 6.2
Z12(61 cm)*	15 ±0.74	5.2 ±0.17	16 ±3.7	1.1 ±0.13
Z14(87 cm)*	1.0 ±0.39	0.44 ±0.09		0.28 ±0.12

* Distance measured from the bottom of the core.

According to the above data, it appears that the total Co-58 in-core activity inventory of this run is a bit higher than reference run #1, whereas the Co-60 total in-core activity inventory is lower. These results confirm the steam generator findings, which also show an increase in Co-58 total activity and a decrease in Co-60 compared with reference run #1.

4.3.6 Stainless Steel Filter

The SS filter has the same pore size as the one used in reference run #1. It is located in the same position as the filter used in the previous run, and its temperature is also lower than the temperature of the coolant.

Figure 4.40 presents the Co-58 specific activity deposited on the filters. A peak is observed, which represents the effect of the heater trip experienced at the end of the run. Figure 4.41 shows the above plot amplified ten times. According to this figure, and excluding the heater trip, the average specific activity deposited on the filters is 1.5E-04 nCi/cc, which is comparable to the filter activity found in the previous run. The cumulative Co-58 and Co-60 activities deposited on the filters are presented in Figs. 4.42 and 4.43, respectively. The total Co-58 and Co-60 activities deposited on the filters are 0.15 μCi and 0.015 μCi, respectively, which gives a Co-58/Co-60 ratio of 10. The Co-58/Co-60 ratio for each filter is plotted in Fig. 4.44. An average ratio of 8.8 was determined, which is a bit lower than the ratio found in the steam generator tubes. This result indicates a higher Co-60 concentration (vs Co-58) in the coolant compared to the steam generator tubes.

4.3.7 Water Samples

Water samples were also taken on a daily basis during the entire run. The pH and conductivity of these samples are plotted in Figs. 4.45 and 4.46, respectively. As seen in Fig. 4.45, the pH never deviated by more than ± 0.1 pH units from its nominal value of 6.56 at room temperature (25 °C), which is within the acceptable range given in reference [W-5]. The conductivity of the water samples never deviated by more than ± 10% from its nominal value.of 19.3 μmhos/cm at room temperature (25 °C).

Prompt gamma analysis was used to determine the boron con-

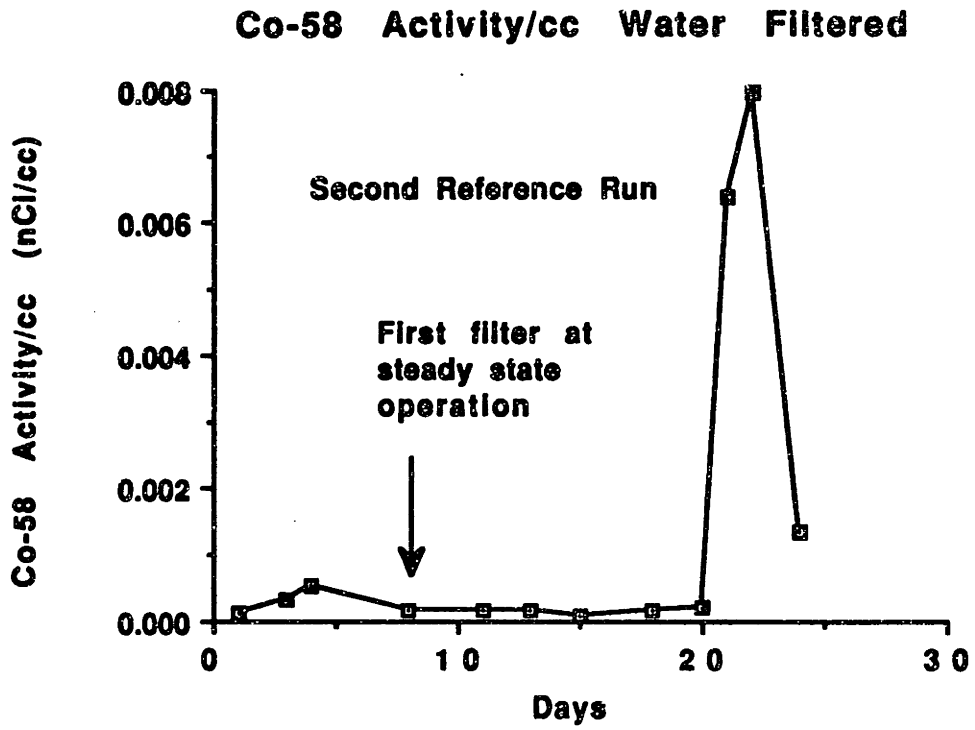

Figure 4.40 Co-58 Activity on Let-down Filters, Second Reference Run.

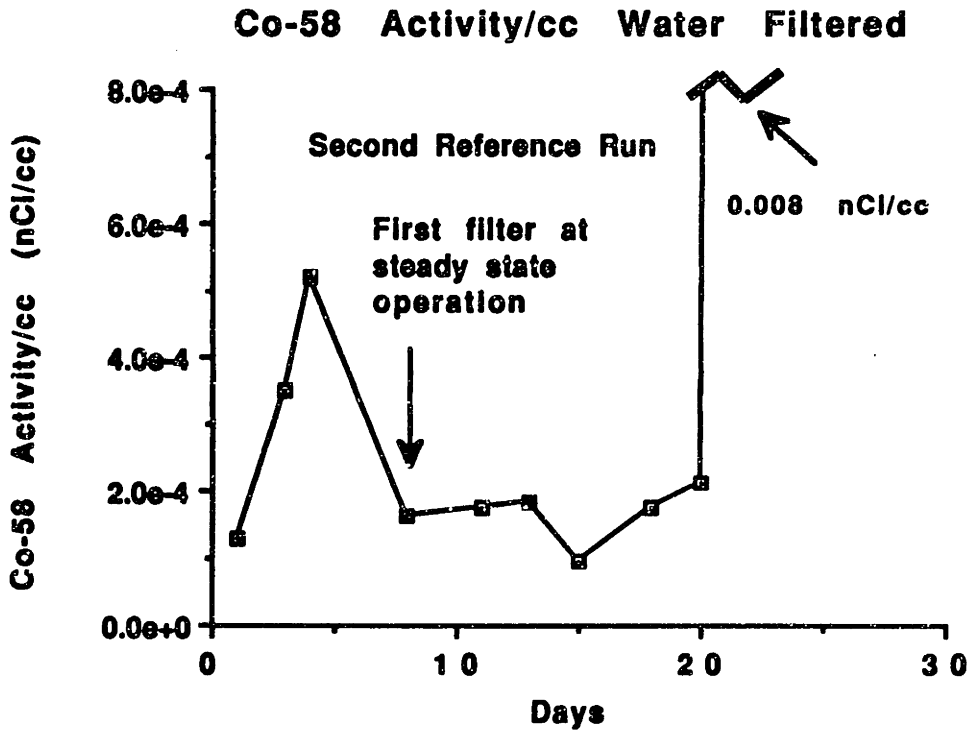

Figure 4.41 Amplified Plot of Co-58 Specific Activity on Let-down Filters, Second Reference Run.

centration in the outlet water samples. The results of these analyses are plotted in Fig. 4.47. Typical boron concentration values were within ± 10% of the nominal 800 ppm value.

To determine the lithium concentration, the technique used was once again atomic absorption (AA). The lithium values (Fig. 4.48) obtained using the AA technique were within ± 7% of the nominal 1.84 ppm value.

Typical radionuclides and activities found in water samples at the end of the this run are listed in table 4.7. As in reference run #1, Ce-144, and I-132, produced as a result of fission of uranium contamination in the water and loop materials, were detected in small amounts. Other fission products such as I-133, Tc-99, Xe-135, and Cs-137 were also detected.

Ar-41, Na-24, and W-187, produced as described in sec. 4.2.7, were found in almost every water sample. The activities from these radionuclides (Figs. 4.49 and 4.50) were comparable to those measured in reference run #1 water samples.

Mn-54 and Co-58, produced as a result of fast neutron interactions, were found in few water samples in very small quantities. The major sources of Fe-54 and Ni-58 are the the SS surfaces, Inconel steam generator tubes, and the input of transition metals from the charging system. To determine the input of transition metals into the loop, water samples were once again taken from the charging system and analyzed using ion chromatography techniques [B-9]. Table 4.8 shows the results obtained from the analysis of make-up water samples. The concentration of transition metals in

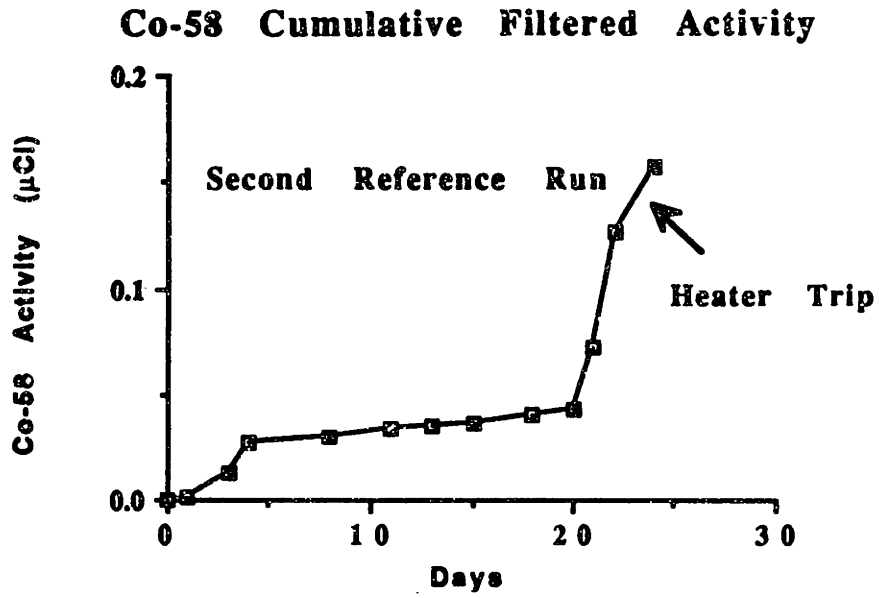

Figure 4.42 Cumulative Co-58 Activity Deposited on Filters, Second Reference Run.

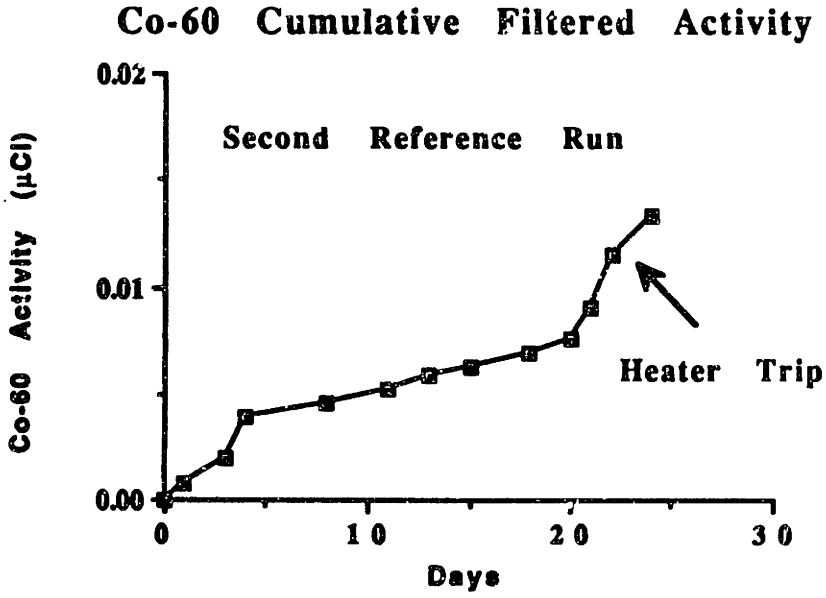

Figure 4.43 Cumulative Co-60 Activity Deposited on Filters, Second Reference Run.

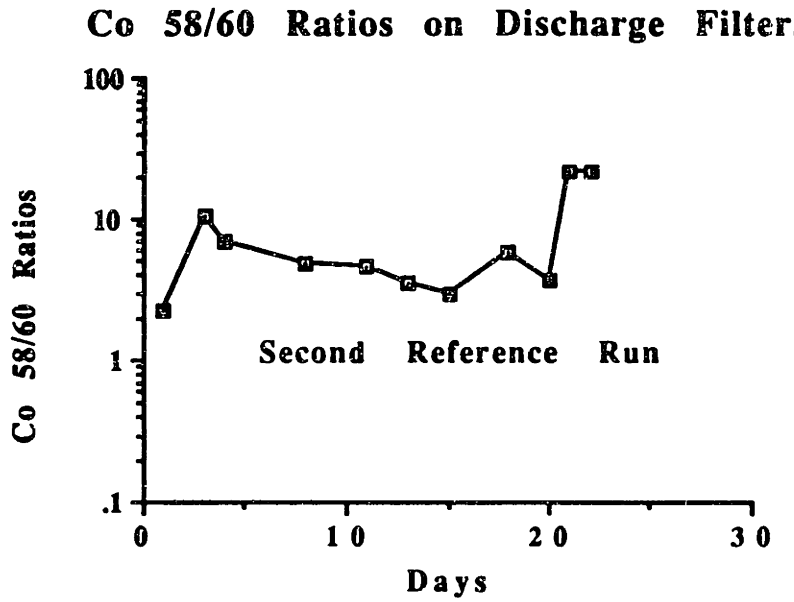

Figure 4.44 Co-58/Co-60 Ratios on Filters, Second Reference Run.

these water samples is comparable to the concentration of trace elements found in reference run #1.

4.3.8 Ion Exchange Column

Once the run ended, the ion exchange column resin was collected and analyzed using gamma spectroscopy, so that the total activities of transition metals and other species could be determined. Table 4.9 summarizes the total activities of trace elements and fission products deposited on the IX resin and their inferred activities per cm^3 of coolant that passed through the resin. These results showed a total Co-58 and Co-60 deposition of 7.97 and 0.2 μCi, respectively, with a Co-58/Co-60 ratio of 39.9.

4.4 Low pH Run #1

4.4.1 Introduction

The purpose of this run was to simulate highly dissolving

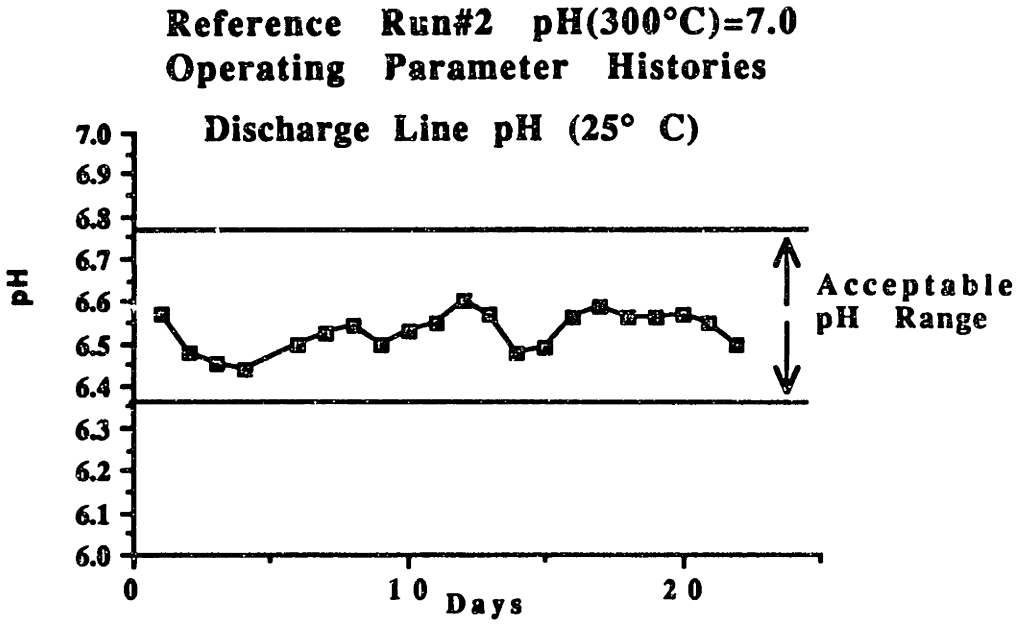

Figure 4.45 Discharge Line pH (25 °C), Second Reference Run.

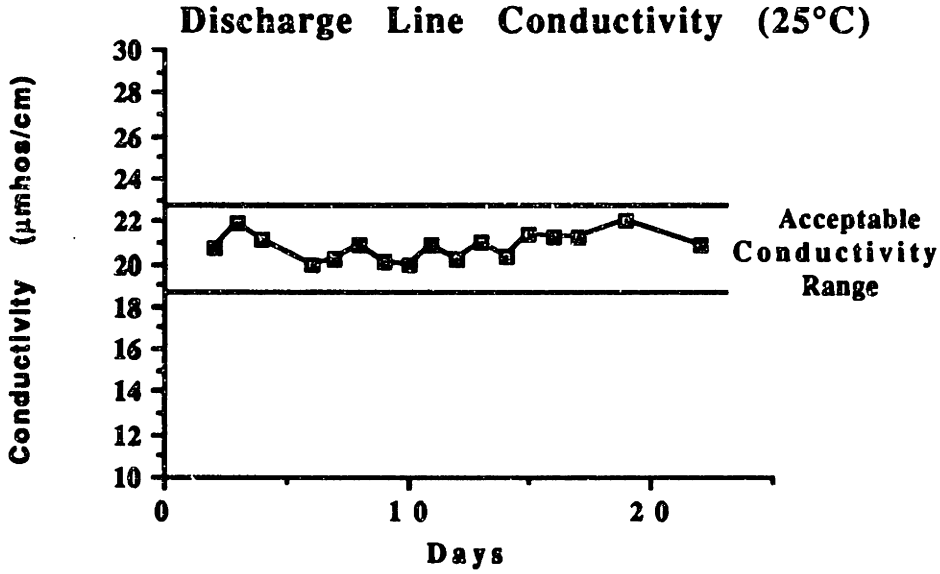

Figure 4.46 Discharge Line Conductivity (25 °C), Second Reference Run.

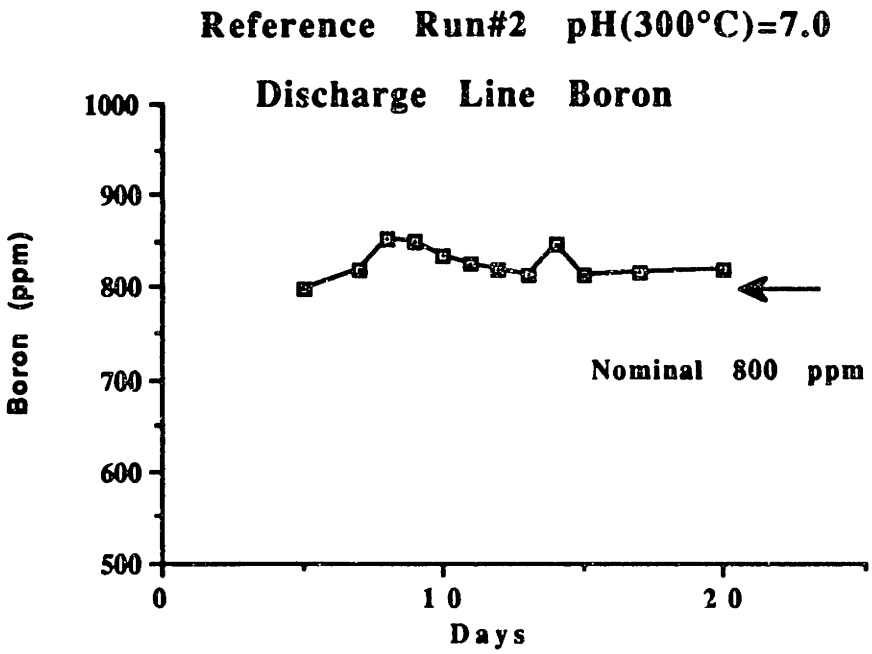

Figure 4.47 Discharge Line Boron, Second Reference Run.

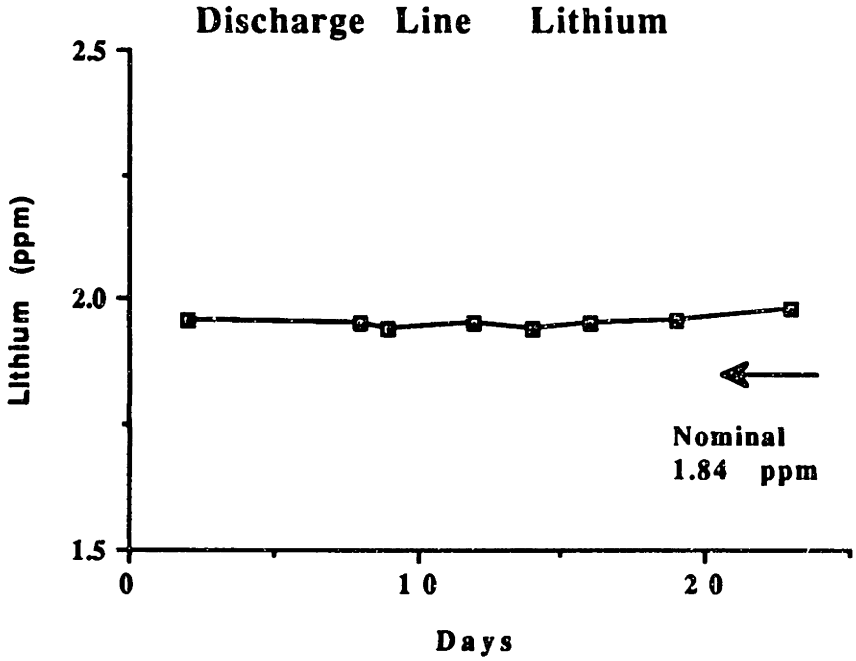

Figure 4.48 Discharge Line Lithium, Second Reference Run.

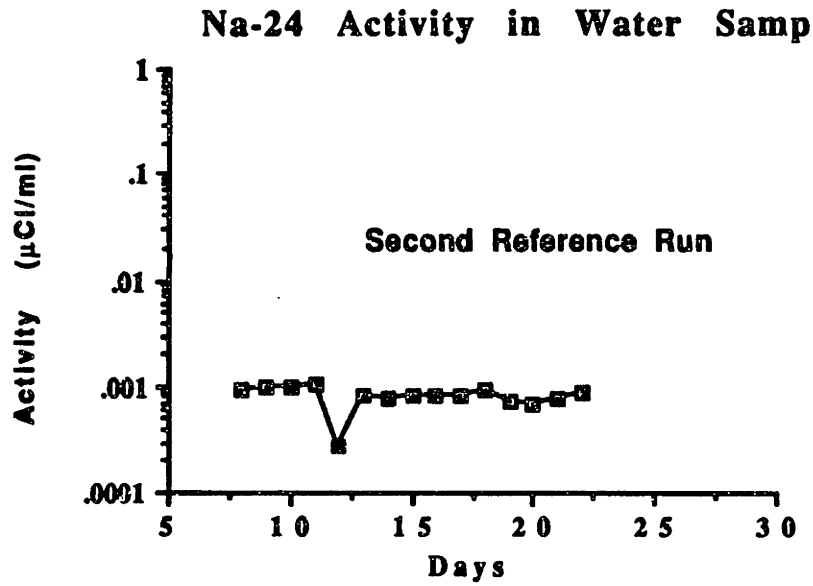

Figure 4.49 Na-24 Activity in Water Samples, Second Reference Run.

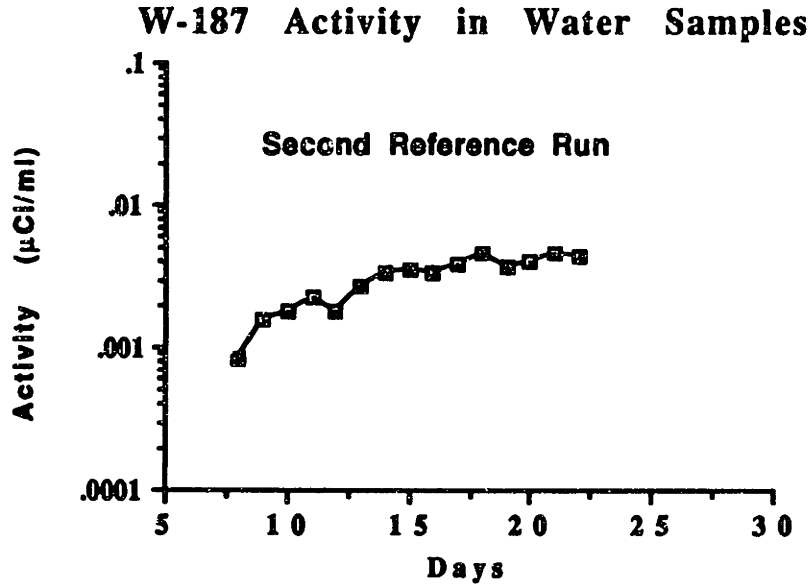

Figure 4.50 W-187 Activity in Water Samples, Second Reference Run.

Table 4.7 Radionuclides in Water Samples, Second Reference Run.

Radionuclide	Activity/cc (μCi/cc)
Ar-41	7.2E-04 ±3%
Ce-144	1.7E-06 ±77%
Co-58	5.2E-06 ±30%
Cs-137	5.5E-06 ±84%
I-132	3.7E-05 ±24%
I-133	1.2E-05 ±62%
Mn-54	2.5E-06 ±67%
Na-24	8.0E-04 ±2%
Tc-99	8.6E-08 ±72%
W-187	3.7E-03 ±1%
Xe-135	1.7E-06 ±64%
Zr-97	1.1E-05 ±13%

Table 4.8 Ion Chromatograph Measurements of Make-up Water Trace Elements, Second Reference Run.

Element	Concentration (ppb)
Zinc	52 (47)
Nickel	68 (41)
Cobalt	9
Iron (II)	83 (57)
Manganese	20 (8)

Note: Values in parenthesis were measured in an aliquot on December 1989, 4 months earlier.

Table 4.9 Summary of Activities Deposited on IX Column, Second Reference Run.

Radionuclide	Activity (μCi)	Activity/cc* (μCi/cc)
Co-58	7.97 ±3%	5.0E-05
Co-60	0.2 ±3%	1.3E-06
Cr-51	0.4 ±7%	2.5E-06
Fe-59	0.02 ±22%	1.3E-07
Mn-54	0.47 ± 0.3%	3.0E-06
Nb-95	0.02 ±16%	1.3E-07
Sb-124	0.32 ±7%	2.0E-06
Zn-65	0.02 ±10%	1.3E-07

* Total cc passed through resin = 1.6E05 cc

conditions in the steam generator tubes, particularly in the cold leg, and precipitating conditions in the core section (highly negative solubility temperature coefficient). To simulate these conditions a constant pH_{300} of 6.5 (800 ppm B, 0.56 ppm Li) was maintained throughout the entire run. This run accumulated approximately 2115.0 MW-hrs, equivalent to 20 full power reactor days.

Several changes were made prior to the startup of this run, compared to the two previous runs; for instance, the inlet SS plenum was seal-welded (after removing the pre-conditioning specimens) to prevent the leaks which occurred in the previous O-ring seal plenum design. In addition, the Zircaloy fittings were made only once and never broken during the final loop assembly. A static pressure test was carried out during the pre-conditioning stage at a temperature of 550 °F to ensure that the loop was leak free. Other changes

included the addition of two uninterruptible power supplies (UPSs) which provide electrical power to the (AE) main circulating pump and the alarm and instrumentation panel in the event of power outages. Finally, a Heated Auxiliary Autoclave Pressurizer (HAAP) was added to the final loop configuration to maintain system pressure and prevent boiling of the coolant during heater or main circulating pump trips.

The sections that follow will present a brief run history, as well as the radionuclide deposition data obtained from Inconel and in-pile Zircaloy tubes, deposition monitor filters and IX resin. The radionuclide composition and activities in daily water samples is also presented.

4.4.2 Run History

Ten days after startup, the low pH run experienced a small leak in one of the T connectors outside the thimble, between the steam generator outlet and the inlet to the main circulating pump. Once the leak was identified, the loop was cooled down, the old ferrule cut off, and a new ferrule installed. The loop was then pressure tested with a loss of 30 psig system pressure in 10 minutes. During this test, no water was observed at the T connector.

The loop was then heated up followed by full power reactor operation. This controlled transient lasted a total of approximately 8 hours. After this controlled transient, the loop operated stably for 8 more days until a scheduled two day reactor electrical power outage forced the loop to shut down for two days. It is important to note

that no uncontrolled transients occurred during this run. Figure 4.51 shows the power history of this run. Notice the two controlled transients occurring 10 and 18 days, respectively after startup of the run.

4.4.3 Inconel Tubes

Once this run ended, the Inconel tubes were cut and scanned with a high purity germanium detector in the same fashion as the two previous runs. Gamma spectroscopy analysis of the Inconel tubes showed an average Co-58 activity of 110 nCi/cm^2 (Fig. 4.52) deposited on the hot leg of the S/G and 13.9 nCi/cm^2 (Fig. 4.53) deposited on the cold leg. The total Co-58 activity deposited on the Inconel tubes was 44.6 μCi.

The relative high Co-58 activity observed in the hot leg of the S/G compared to the cold leg can be explained by the transition

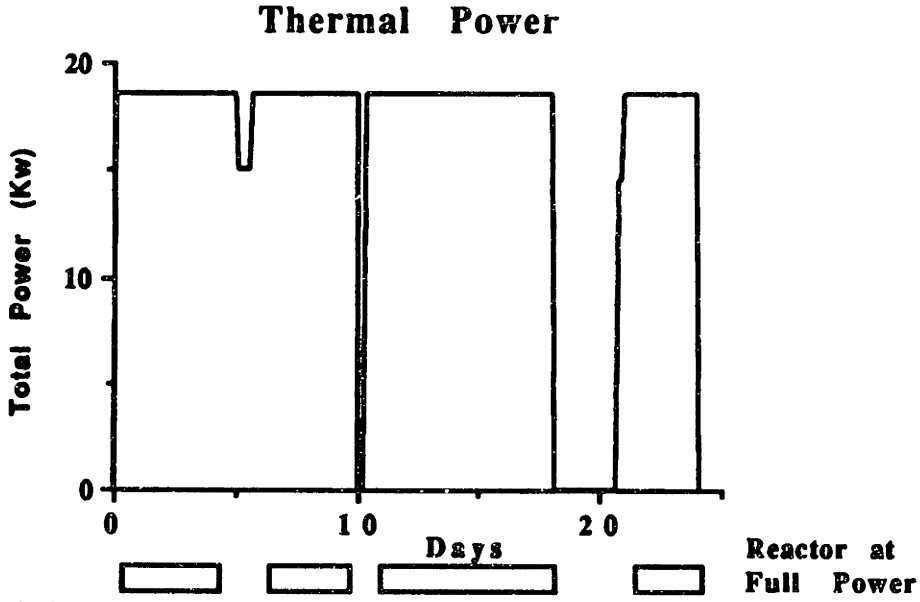

Figure 4.51 Total (Heater + Gamma) Power History of Low pH Run (PL1).

metal solubility curves. According to these curves (Fig 4.3), at low coolant pH, precipitating conditions exist on hot surfaces; namely the core and the hot leg of the steam generator. On the other hand, at low coolant pH, dissolving conditions exist on cold surfaces such as the cold leg of the S/G. Thus, there is a net transport of corrosion products from the cold to the hot surfaces. Therefore, a higher deposition of activated corrosion products is expected at the S/G hot leg compared to the S/G cold leg. (This evidence is also supported by measurements taken at the inlet (hot leg) and outlet (cold leg) of steam generators in German nuclear power plants [R-2]). The results showed a factor of 10 more activity on the inlet (hot leg) than on the outlet (cold leg).

Another interesting observation is the drop in activity (hot leg) in the isothermal region above the copper shot where there is no temperature boundary layer. An explanation for this phenomenon is that low pH water chemistry may develop an oxide layer which enhances isotopic exchange where a film temperature difference creates a solubility gradient tending to remove material from the oxide layer.

Figures 4.54 and 4.55 show the Co-60 activity profile for the hot and cold S/G tubes, where the average deposited activity was 7.4 and 1.14 nCi/cm^2, respectively. Thus, the total Co-60 activity (hot and cold legs) deposited on the S/G tubes was 3.1 μCi. It is evident that the Co-60 deposition activity undergoes the same deposition behavior as Co-58, which already has been described.

Figure 4.56 and 4.57 show the Co-58/Co-60 ratio profile.for the

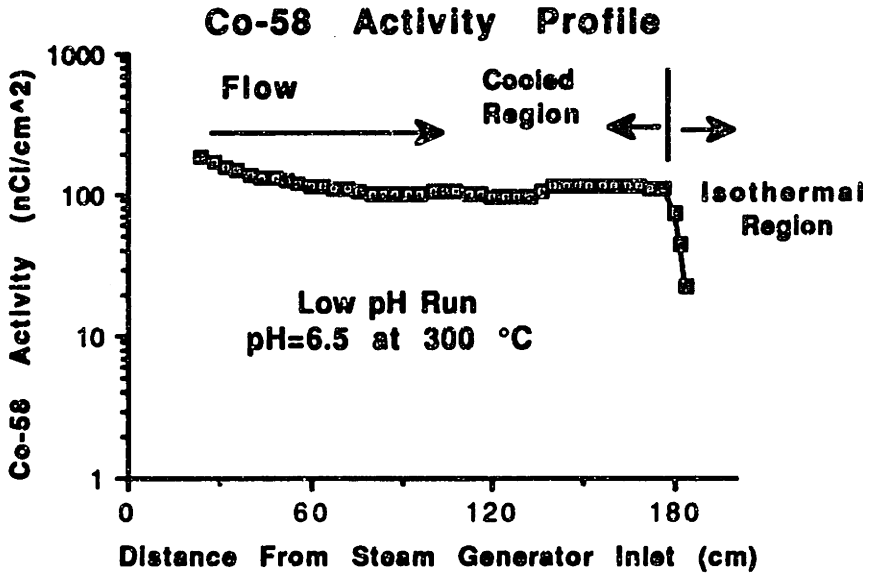

Figure 4.52 Co-58 Activity Profile (Hot Leg), Low pH Run.

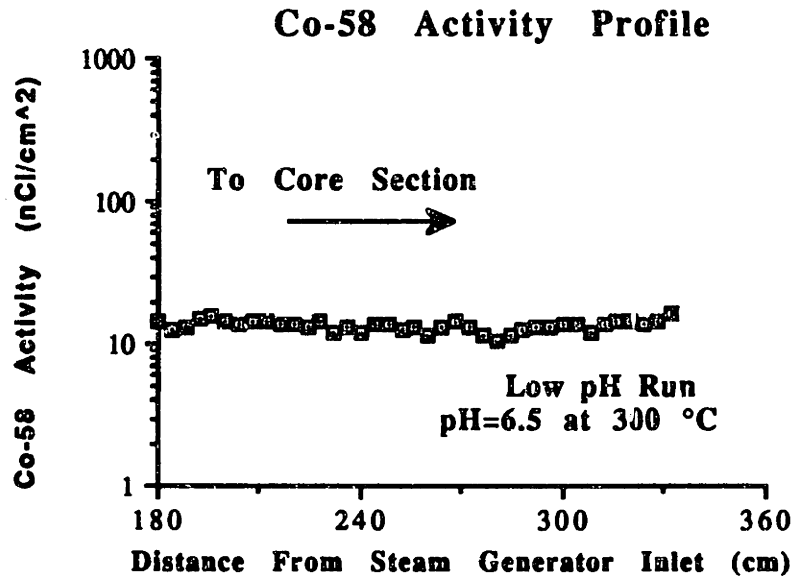

Figure 4.53 Co-58 Activity Profile (Cold Leg), Low pH Run.

hot and cold legs of the S/G. Average ratios of 15.8 and 12.6 were determined, which are higher than those in reference run #1.

Finally, Cr-51, Fe-59, and Mn-56 activity profiles are presented in Figs. 4.58 and 4.59. The total Cr-51, Fe-59, and Mn-56 activities deposited on the steam generator tubes were 2.6, 7.8, and 1 μCi, respectively.

The above radionuclide inventories are a factor of 10 higher than reference run #1, and a factor of 5 higher than reference run #2.

4.4.4 Zircaloy Tube

The in-pile Zircaloy tube was prepared, cut, and decontaminated following the same procedures used in reference runs #1 and #2. Table 4.10 presents the core activity deposition measurements for this run. Similar to reference run #1 and #2, the Co-58/Co-60 ratio is lower at the top of the core than at any other position, which is clear indication of a higher production of Co-60 due to the thermal neutron flux peak at the top of the core.

It is interesting to note that the deposition of activated corrosion products on the Zircaloy tubing in the absence of a film ΔT (no heat flux) yields a lower value compared to the deposition of corrosion products on the Inconel tubing in the isothermal region. A possible explanation for this phenomenon is that the Zircaloy tubing oxide layer contains less transition metals, which limits the exchange of radioactive species for non-radioactive atoms compared to the Inconel tubing.

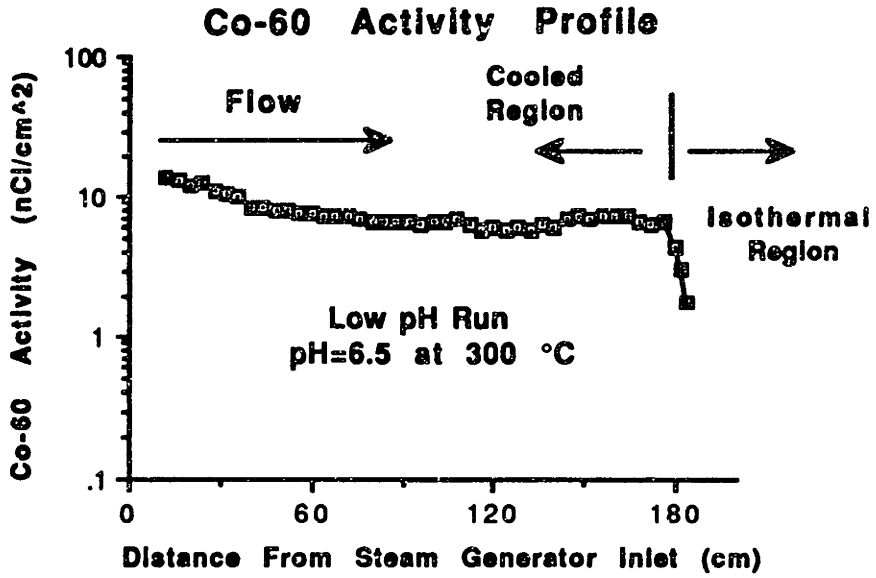

Figure 4.54 Co-60 Activity Profile (Hot leg), Low pH Run.

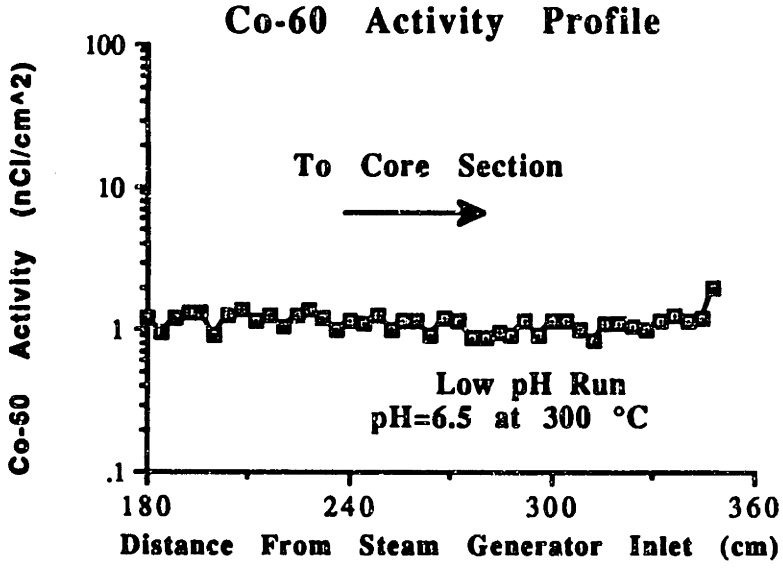

Figure 4.55 Co-60 Activity Profile (Cold Leg), Low pH run.

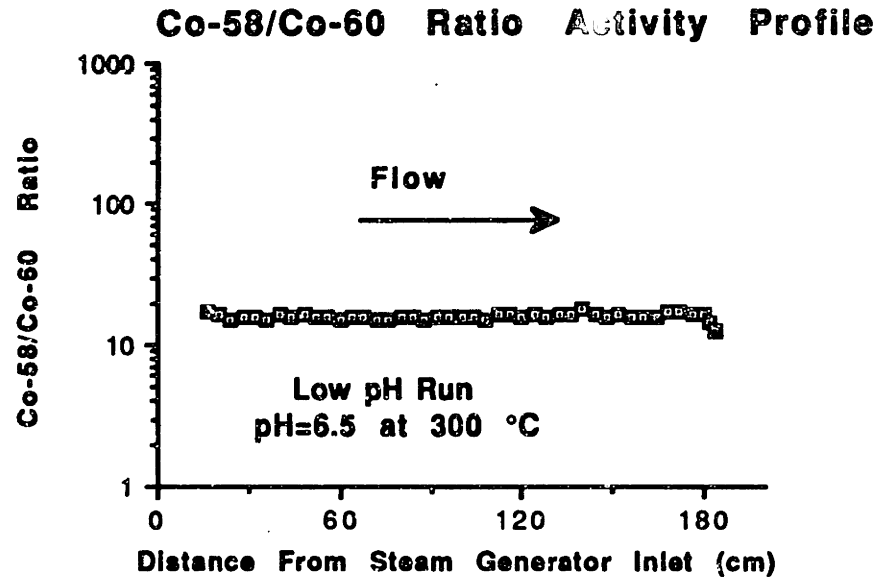

Figure 4.56 Co-58/Co-60 Ratios (Hot Leg), Low pH Run.

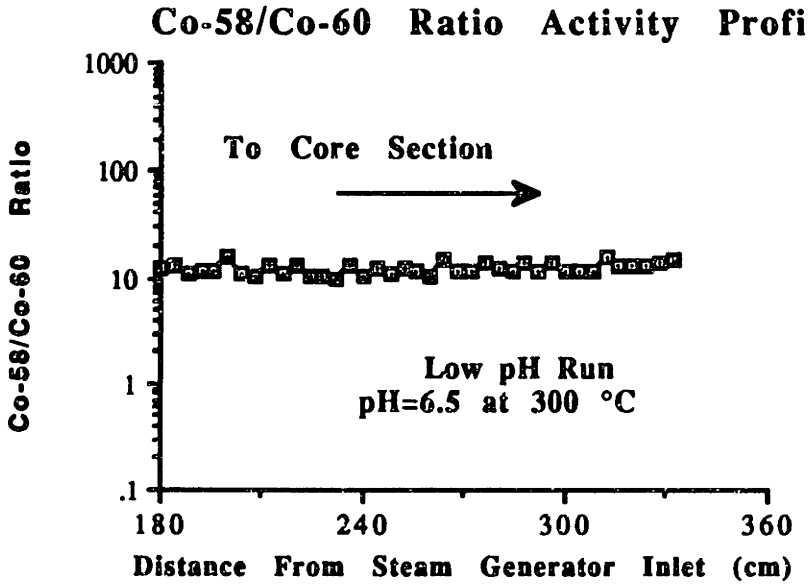

Figure 4.57 Co-58/Co-60 Ratio (Cold Leg), Low pH Run.

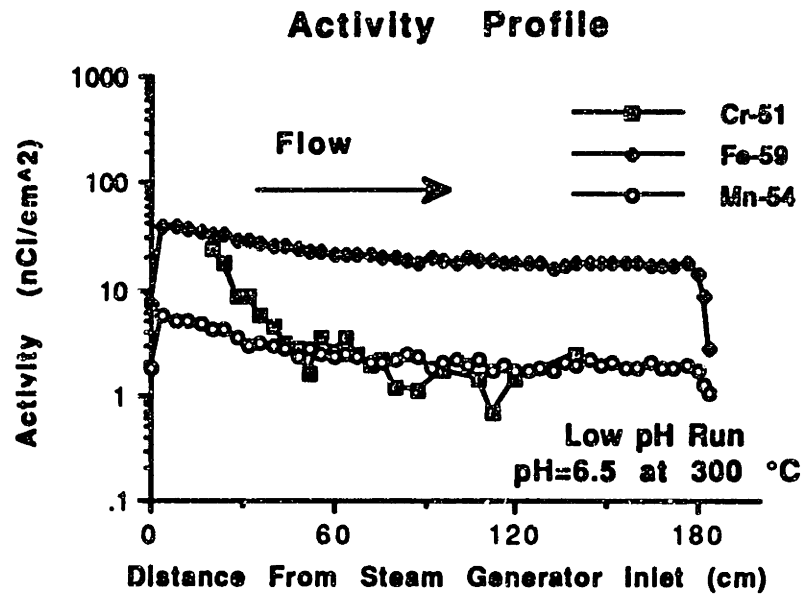

Figure 4.58 Cr-51, Fe-59, and Mn-54 Activity Profiles (Hot Leg), Low pH Run.

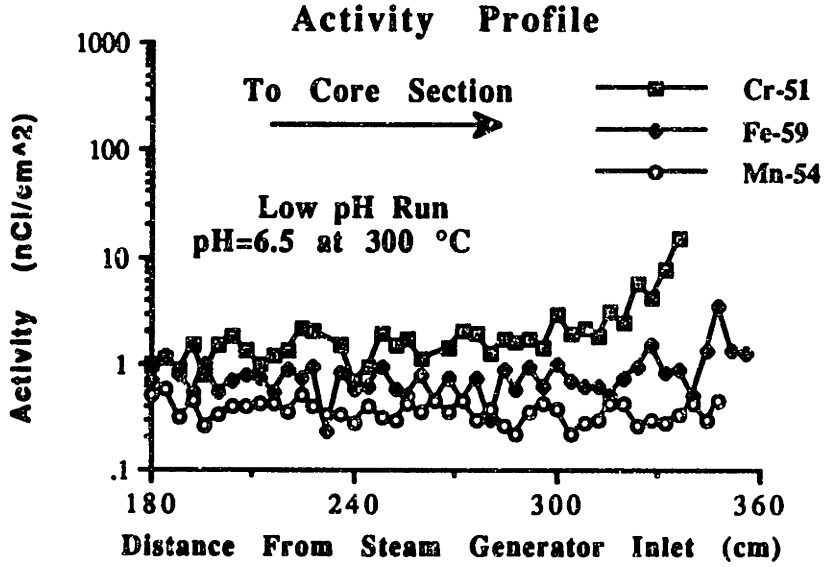

Figure 4.59 Cr-51, Fe-59, and Mn-54 Activity Profiles (Cold Leg), Low pH Run.

From table 4.10, the average Co-58 and Co-60 activities deposited on the in-pile Zircaloy tubing were 653 and 91 nCi/cm^2, which yielded a total deposited activity of 163 and 22.8 μCi, respectively. The total Fe-59 and Mn-54 deposited on the Zircaloy tubing were 57.1 and 19.3 μCi, respectively.

Table 4.10 Results of Core Activity Deposition Measurements, Low pH Run.

Position	Co-58 (nCi/cm^2)	Co-60 (nCi/cm^2)	Fe-59 (nCi/cm^2)	Mn-54 (nCi/cm^2)
Z1(87 cm)*	3.3 ± 0.28	0.6 ± 0.1	-	0.27 ± 0.07
Z3(61 cm)*	11 ± 0.66	8.0 ± 0.25	11 ± 2.2	0.8 ± 0.12
Z5(35 cm)*	1300 ± 14	200 ± 4.0	930 ± 23	310 ± 2.9
Z7(9 cm)*	1100 ± 12	110. ± 2.5	150 ± 19	45 ± 1.5
Z8(9 cm)*	920 ± 8.8	87 ± 2.0	31 ± 15	49 ± 13
Z10(35 cm)*	530 ± 6.8	100 ± 2.7	160 ± 10	53 ± 1.6
Z12(61 cm)*	57 ± 0.94	41 ± 0.67	88 ± 3.6	4.9 ± 0.2
Z14(87 cm)*	6.7 ± 0.34	0.86 ± 0.1		0.4 ± 0.08

* Distance measured from the bottom of the core.

It is evident that the low pH coolant created precipitating conditions in the core which resulted in higher deposition of corrosion products in the core compared to the previous two runs. Another effect shown in table 4.10 is that the activity (and hence, presumably the deposition of corrosion products) was higher at the inlet side than at the outlet. An explanation for this behavior is that

the coolant entering the inlet of the Zircaloy is in a supersaturated condition. Therefore, a higher deposition of corrosion products would occur at the entrance of the Zircaloy tubing. Note that no uncontrolled transients occurred during the entire run.

4.4.6 Stainless Steel Filter

The let-down deposition monitor filter was replaced every three days and counted in a low background room with a gamma detection system. The average Co-58 activity (Fig.4.60) deposited on the filters was 5E-04 nCi/cc, which is approximately a factor of 5 more activity than deposited on the filters in reference runs #1 and #2, if the uncontrolled transients are excluded. The cumulative Co-58 and Co-60 filter activities (Figs. 4.61 and 4.62) during the entire run were 0.055 and 0.015 μCi, respectively. It is understandable that the cumulative filter activities for this run were lower than in reference run #1 and #2, since both reference runs experienced trips that caused boiling in the loops. An average Co-58/Co-60 ratio (Fig. 4.63) of 4.2 was calculated, which is representative of the deposition of Co-58 and Co-60 on the Inconel tube in the isothermal region.

Finally, the Fe-59 and Mn-56 activities deposited on filters for the entire run are plotted in Figs. 4.64 and 4.65. The total Fe-59 and Mn-56 activities on the filters were 0.01 and 1.7 μCi, respectively. It should be noted that the Co-58 and Mn-56 activities (Figs. 4.60 and 4.65) increased a decade approximately 18 days into the run due to a controlled loop cooldown already discussed in sec. 4.3.2, chapter 4. This increase in activity is understandable since the cobalt and man

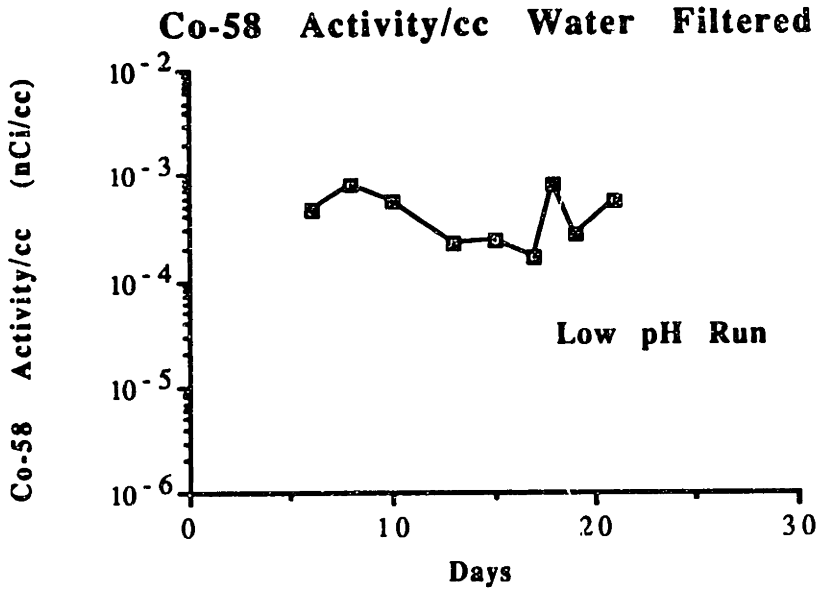

Figure 4.60 Co-58 Activity on Let-down Filters, Low pH Run.

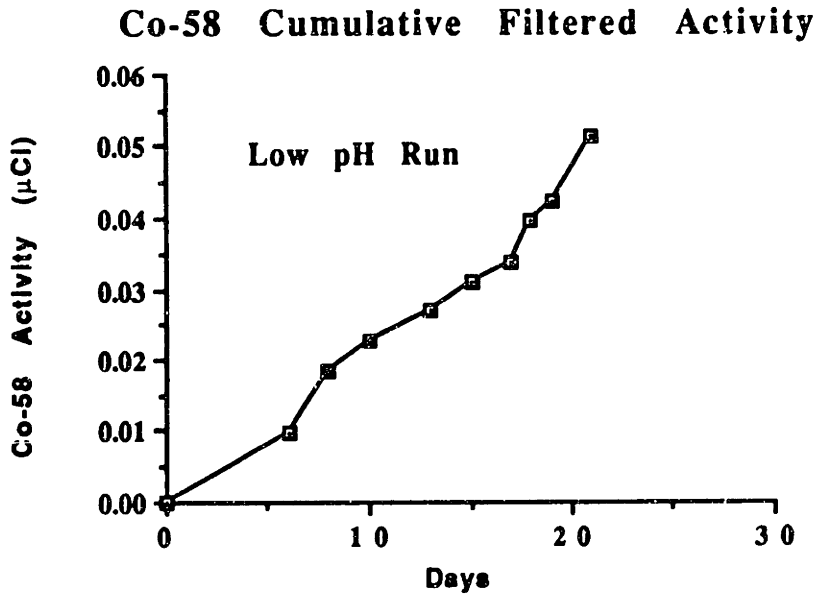

Figure 4.61 Cumulative Co-58 Activity Deposited on Filters, Low pH Run.

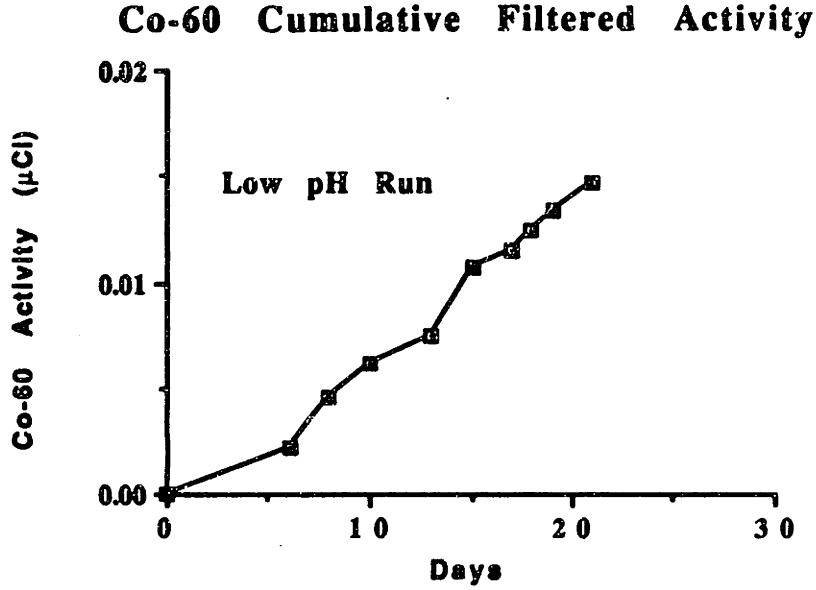

Figure 4.62 Cumulative Co-60 Activity Deposited on Filters, Low pH Run.

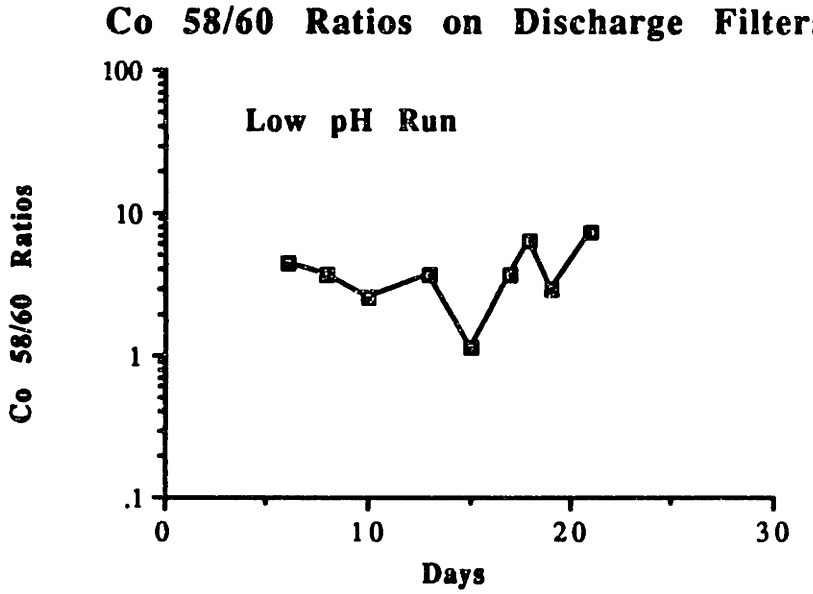

Figure 4.63 Co-58/Co-60 Ratios on Filters, Low pH Run.

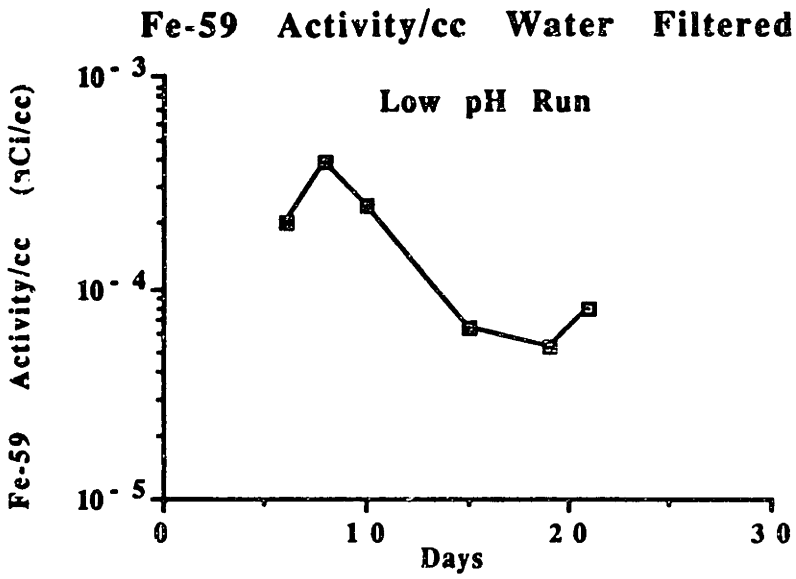

Figure 4.64 Fe-59 Activity on Let-down Filters, Low pH Run.

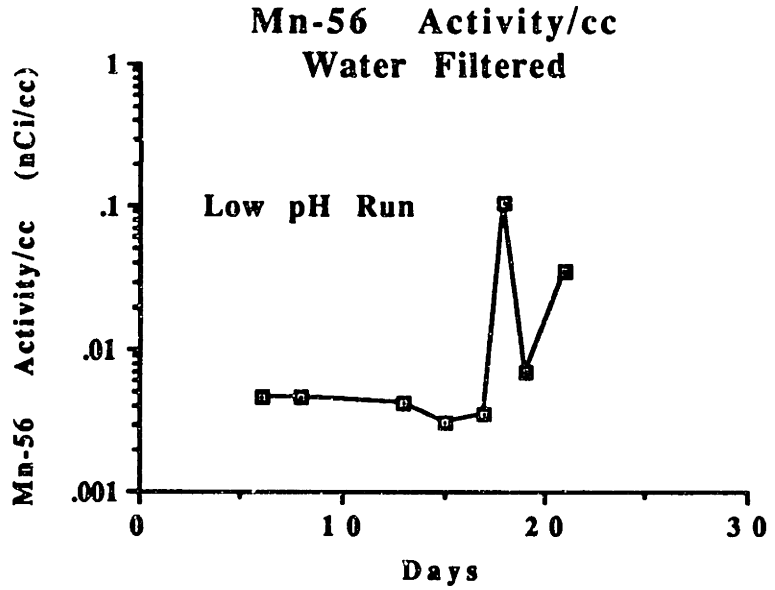

Figure 4.65 Mn-56 Activity on Let-down Filters, Low pH Run.

ganese solubilities increase by several orders of magnitude as the coolant temperature decreases from 300 °C to near room temperature.

4.4.7 Water Samples

As in reference runs #1 and #2, outlet water samples were taken on a daily basis. Each sample was then taken to a low background area and counted using a gamma detection system. The pH and conductivity of randomly selected water samples were measured; the results are shown in Figs. 4.66 and 4.67. The pH of the outlet radioactive water samples never deviated by more than ± 0.1 pH units from its nominal pH value of 6.04 at room temperature (25 °C); and the conductivity of these samples never deviated by more than ± 10% from its nominal value of 6.2 μmhos/cm.

The boron concentration in these samples was also checked using the colorimetric method described in appendix A. Figure 4.68 shows the boron concentration for the randomly selected water samples. The typical boron values were within ± 10% of the nominal 800 ppm value.

Finally, the lithium concentration in selected water samples was checked (Fig. 4.69) using atomic absorption. Typical lithium concentration values obtained with AA were within ± 8% of the nominal 0.56 ppm value.

Table 4.11 lists typical radionuclides and their activities found in outlet water samples taken near the end of the run. As seen in this table, fission products such as Ce-144, Cs-137, I-133, I-135, Tc-99,

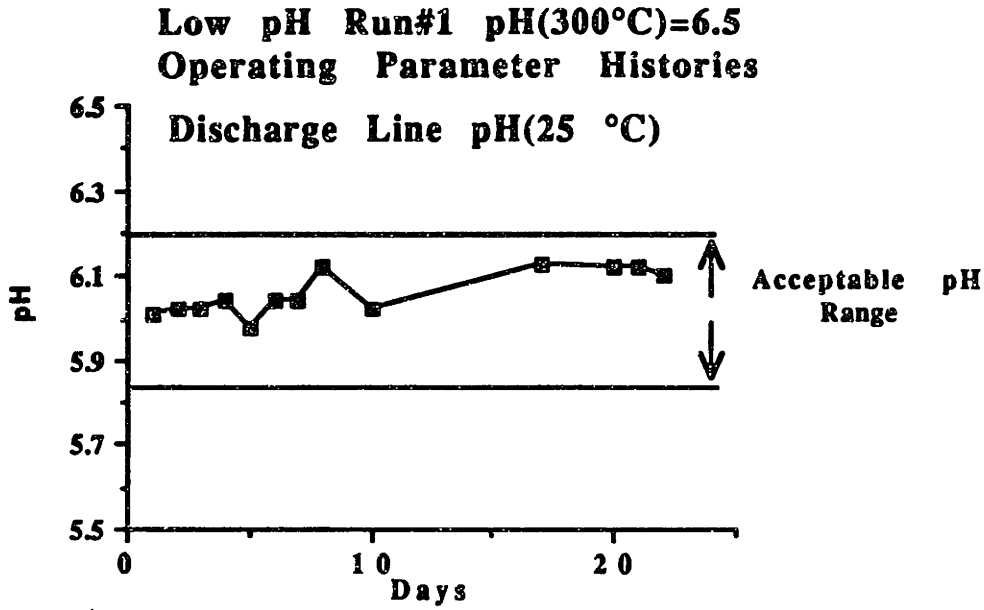

Figure 4.66 Discharge Line pH (25 °C), Low pH Run.

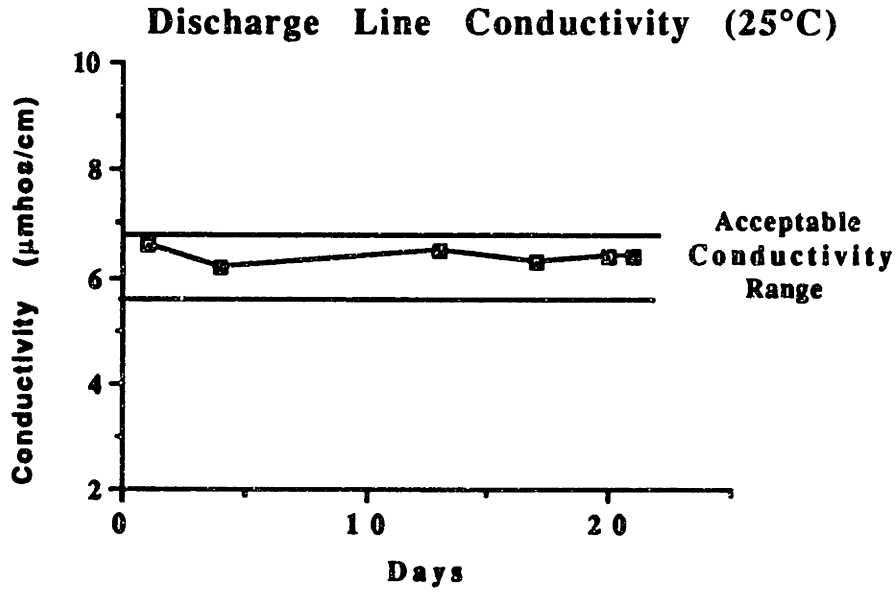

Figure 4.67 Discharge Line Conductivity (25 °C), Low pH Run.

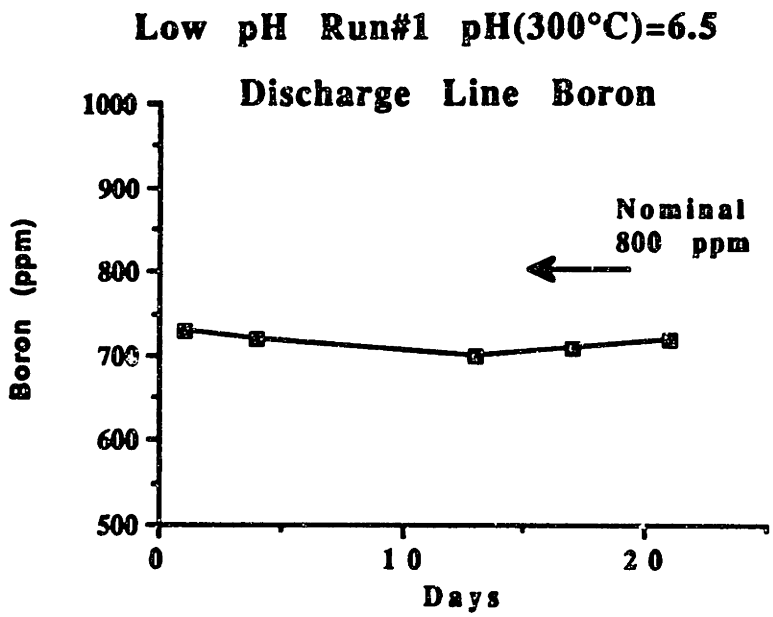

Figure 4.68 Discharge Line Boron, Low pH Run.

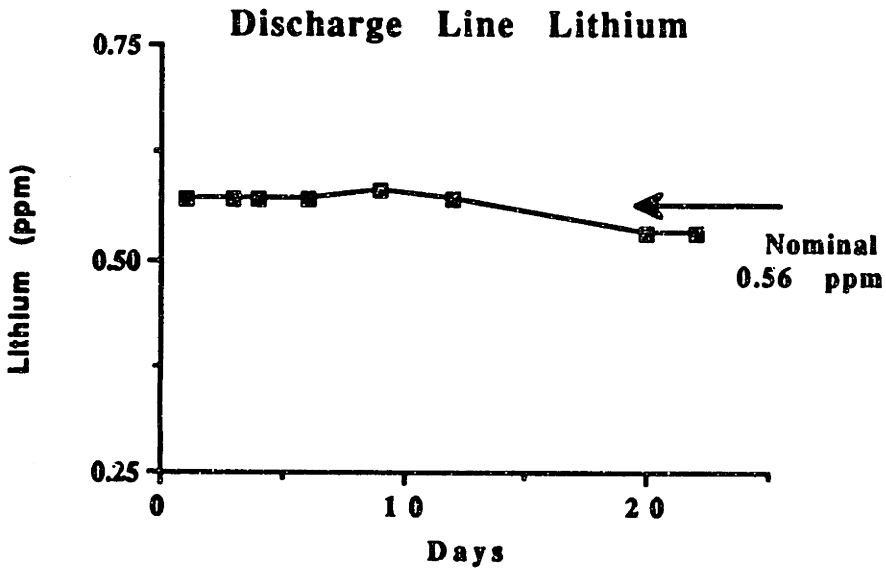

Figure 4.69 Discharge Line Lithium, Low pH Run.

and Xe-135 were detected in small amounts.

Once again, Ar-41, Na-24, and W-187 were found in almost every outlet water sample. Figures 4.70 and 4.71 show the Na-24 and W-187 activities found in the daily water samples. These activities are comparable with the ones from reference runs #1 and #2.

Mn-54 and Co-58, produced as described in sec. 4.2.7, were detected in a small number of samples and in very small quantities. Co-60, produced as a result of thermal neutron interactions, was also found in a limited number of samples.

Finally, Mn-56 (Fig. 4.72) was found in a large number of samples, throughout the run. Mn-56 is produced by the interaction of thermal neutrons with Mn-55. The average detected activity was 1.2E-02 μCi/cc. Since Mn-56 is a short lived radioisotope (half life 2.6 hrs.), this radioisotope was not detected in reference runs #1 and #2 because the waiting period prior to their gamma spectroscopy analysis was a relatively long, which allowed this element to decay

Ion chromatography analysis was also performed on make-up water samples to determine the input of transition metals into the loop for this run. Table 4.12 lists typical trace metals found and their concentration. It is evident that the nickel, iron, and cobalt concentrations found in the make-up water samples are of the same magnitude as in reference runs #1, and #2.

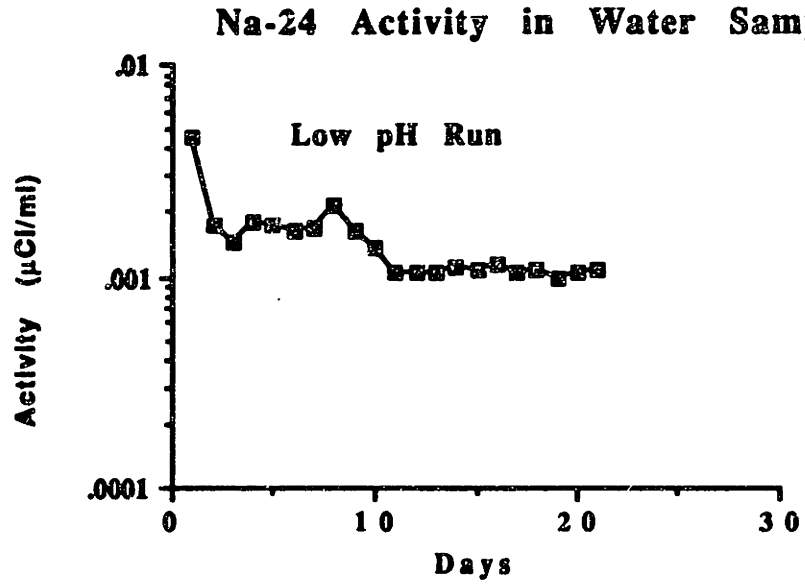

Figure 4.70 Na-24 Activity in Water Samples, Low pH Run.

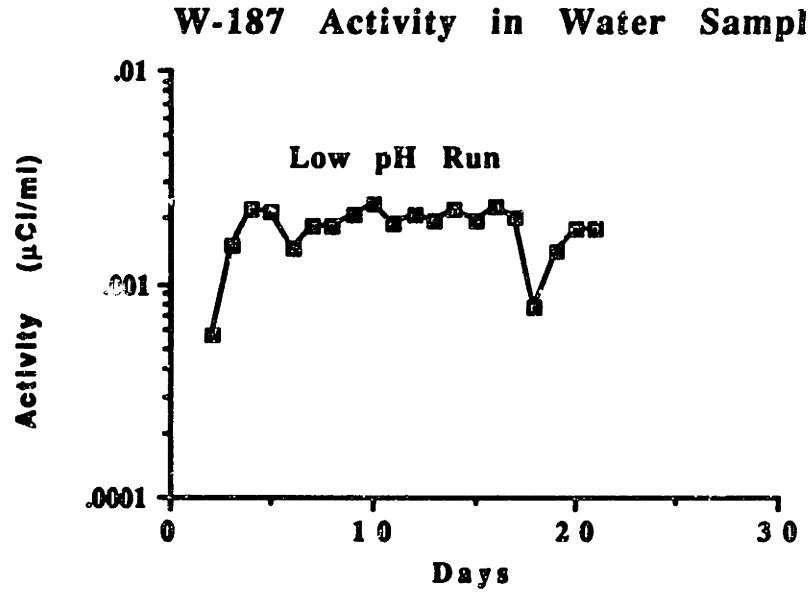

Figure 4.71 W-187 Activity in Water Samples, Low pH Run.

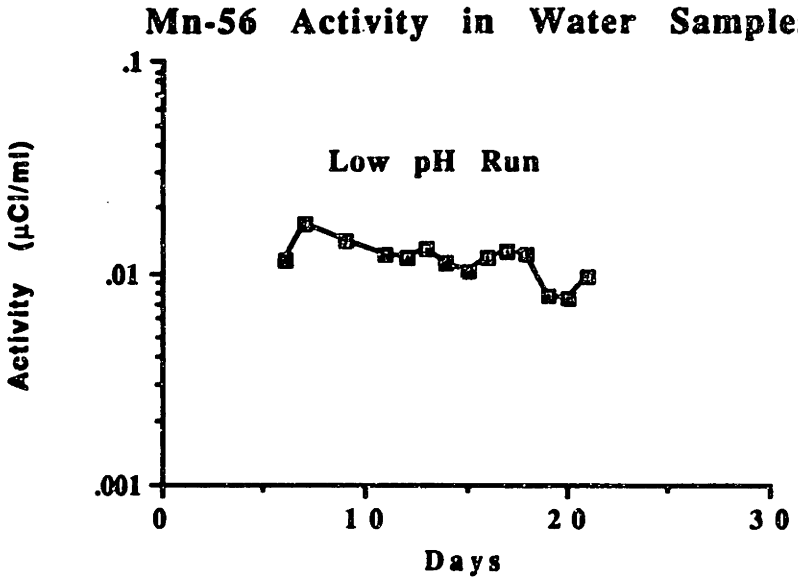

Figure 4.72 Mn-56 Activity in Water Samples, Low pH Run.

4.4.8 Ion Exchange Column

The ion exchange column resin was prepared for analysis in the same fashion as those in past runs. The gamma spectroscopy analysis yielded a total Co-58 activity of 6.6 µCi and a Co-60 activity of 0.4 µCi, with a Co-58/Co-60 ratio of 16.5. Table 4.13 summarizes, once again, the total activities of trace elements deposited on the IX resin as well as the activity per cm^3 of coolant that passed through the resin during the run.

4.5 High pH Run #1

4.5.1 Introduction

The purpose of this run was to simulate conditions opposite to the low pH run; that is to operate with a positive solubility temperature coefficient, where dissolving conditions occur in the core section and precipitating conditions in the steam generator tubes (cold leg in

Table 4.11 Radionuclides in Water Samples, Low pH Run.

Radionuclide	Activity/cc (μCi/cc)
Ar-41	4.8E-04 ±10%
Ce-144	7.1E-07 ±77%
Co-58	2.2E-06 ±55%
Co-60	3.8E-06 ±64%
Cs-137	2.2E-06 ±83%
I-133	3.0E-05 ±30%
I-135	3.1E-05 ±46%
Mn-54	6.4E-06 ±21%
Mn-56	9.5E-03 ±22%
Na-24	1.0E-03 ±3%
Tc-99	4.7E-07 ±72%
W-187	1.8E-03 ±1%
Xe-135	4.2E-06 ±25%

Table 4.12 Ion Chromatograph Measurements of Make-up Water Trace Elements, Low pH Run.

Element	Concentration (ppb)
Zinc	26 (15)
Nickel	142 (68)
Cobalt	10 (8)
Iron (II)	210 (83)
Manganese	29 (14)

Note: Values in parenthesis were measured on an aliquot on December 1989, 4 months earlier.

Table 4.13 Summary of Activities Deposited on IX Column, Low pH Run.

Radionuclide	Activity (μCi)	Activity/cc* (μCi/cc)
Co-58	6.6 ± 1%	4.0E-05
Co-60	0.4 ± 3%	2.6E-06
Cr-51	0.13 ± 12%	8.6E-07
Fe-59	0.2 ± 3%	1.3E-06
Mn-54	1.8 ± 1%	1.0E-05
Nb-95	0.005 ± 30%	3.3E-08
Sb-124	0.6 ± 3%	4.0E-06
Zn-65	0.03 ± 13%	2.0E-07

* Total cc passed through resin = 1.5E05 cc

particular). A high pH_{300} of 7.5 (800 ppm B, 6.26 ppm Li) was maintained throughout the entire run. The high pH run operated a total of 22 days, out of which 21 were at full reactor power, thus, accumulating a total of 2288 MW-hrs. In the same fashion as the low pH run, the inlet SS plenum was seal-welded and the Zircaloy fittings were made up only once to prevent leaks during in-pile operation.

The sections that follow present the history of the run and the radionuclide deposition data collected on the various components of the loop.

4.5.2 Run History

The high pH run experienced a small leak in one of the Inconel tube ultraseal fitting welds that connected the outlet Inconel tube in

the thimble to the pump loop tubing outside the core tank while operating at an outlet temperature of 570 °F prior to reactor startup. Once the leak was identified, the loop was cooled down and the ultra-seal fitting rewelded in situ and carefully inspected. A loop pressure test was then carried out at a system pressure of 2300 psig yielding no pressure loss in a 10 minute period, which indicated a leak free system. Figure 4.73 shows the power history of this run. Note that the controlled transient described above occurred one day into the run with the reactor at zero power. No other unexpected transients occurred throughout the rest of this run.

4.5.3 Inconel Tubes

To determine the radioactive corrosion products deposited on the Inconel tubes, the automated gamma detection system (sec. 2.11, chapter 2) was used. The Inconel tubes were prepared in the same manner as described in sec. 4.1.3.

The Co-58 activity profiles for the hot and cold steam generator tubes are presented in Figs. 4.74 and 4.75. Their average Co-58 deposited activities were 7.1 and 10.8 nCi/cm^2, respectively, which yielded a total Co-58 activity (hot leg + cold leg) of 6.5 μCi.

Since this run operated with a positive solubility temperature coefficient, dissolving conditions exist on the in-pile Zircaloy tubing and S/G hot leg. On the other hand, the cold leg of the S/G exhibits precipitating conditions. This would explain why higher deposition is observed on the cold leg as opposed to the hot leg. It should also be noted that the loop makeup water is introduced upstream of the cold

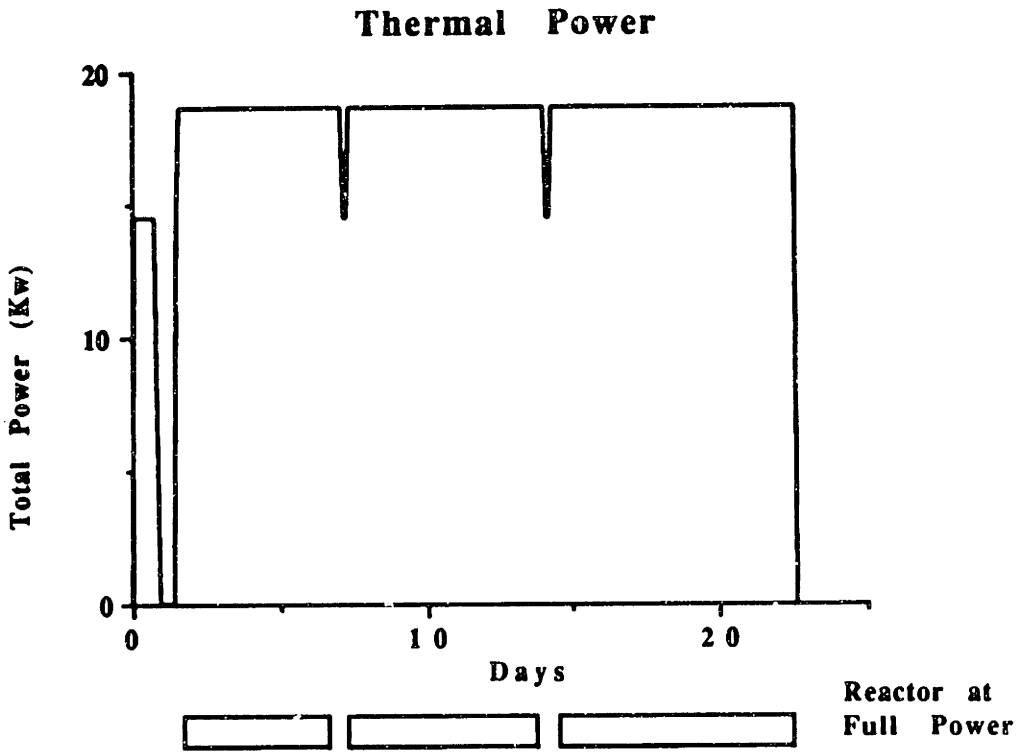

Figure 4.73 Total (Heater + Gamma) Power History of High pH Run (PH1).

leg; this water is in a supersaturated condition with respect to the bulk coolant. This would enhance particle nucleation and growth followed by deposition of radioactive and non-radioactive species on the cold leg. Finally, an increase of Co-58 activity (outlet of the S/G hot leg) is also observed in the region above the copper shot where isothermal conditions exist. This deposition behavior on the isothermal region is contrary to what solubility differences would predict. Thus, it is clear that at high coolant pH, the capability for isotopic exchange decreases in the cooled region of the hot leg relative to the isothermal region. This result indicates the possibility of a different oxide microstructure on the cooled and isothermal zones.

The Co-60 activity profiles (hot leg and cold leg) are shown in

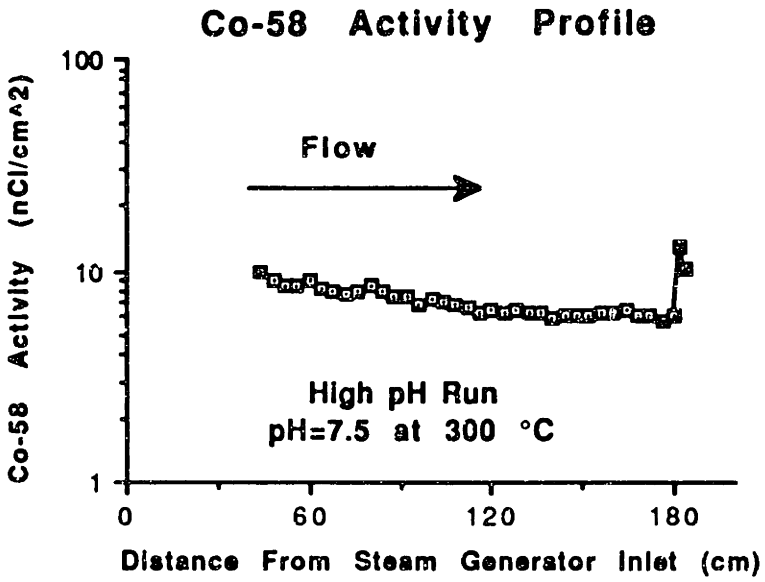

Figure 4.74 Co-58 Activity Profile (Hot Leg), High pH Run.

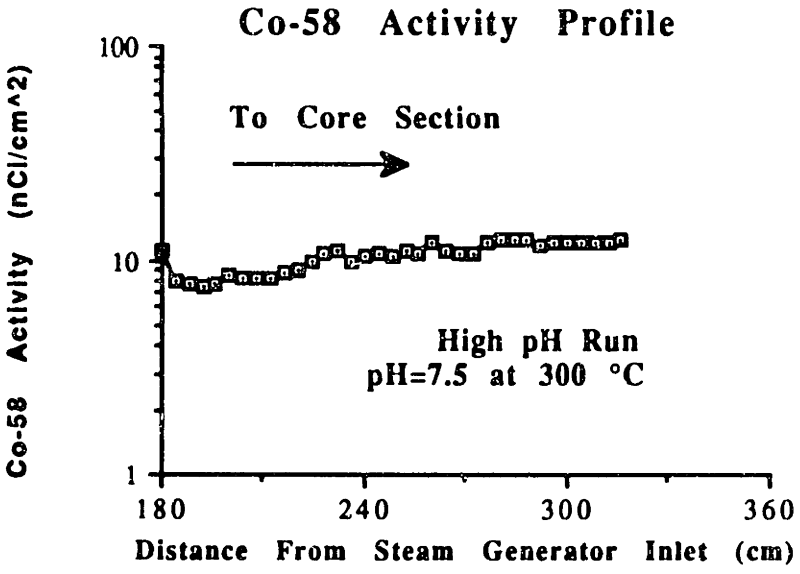

Figure 4.75 Co-58 Activity Profile (Cold Leg), High pH Run.

Figs. 4.76 and 4.77. The average deposited Co-60 on the hot and cold leg was 0.28 and 0.4 nCi/cm^2, respectively. The total Co-60 activity deposited on both tubes was 0.24 μCi. Once again, the Co-58 deposition pattern, already described above, was also observed for Co-60.

The average Co-58/Co-60 ratios (Figs. 4.78 and 4.79) for the hot leg and cold leg were 32 and 30.2, respectively. Other important corrosion products deposited on the Inconel tubes are plotted in Figs. 4.80 and 4.81. Their total deposited activity contributions were as follows:

Cr-51 yielded a total activity of 2.7 μCi. The Co-58 and Co-60 type deposition pattern was also observed for this radioisotope. On the other hand, Fe-59 and Mn-54 yielded a total activity of 0.44 and 0.17 μCi, respectively. However, the average deposited activity was higher in the cold leg than in the hot leg.

4.5.4 Zircaloy Tube

The in-pile Zircaloy tube was decontaminated following the same procedures used in reference runs #1 and #2 and the low pH run. Table 4.14 presents the results obtained from the decontamination of the different segments shown in Fig. 4.18. As seen in this table, more activity is present on the inlet side of the in-pile Zircaloy tubing than on the outlet.

The in-core Co-58 and Co-60 average deposited activities were 119 and 9.6 nCi/cm^2, respectively. The Co-58 average deposited activity is a bit higher in reference run#1 However, the Co-60

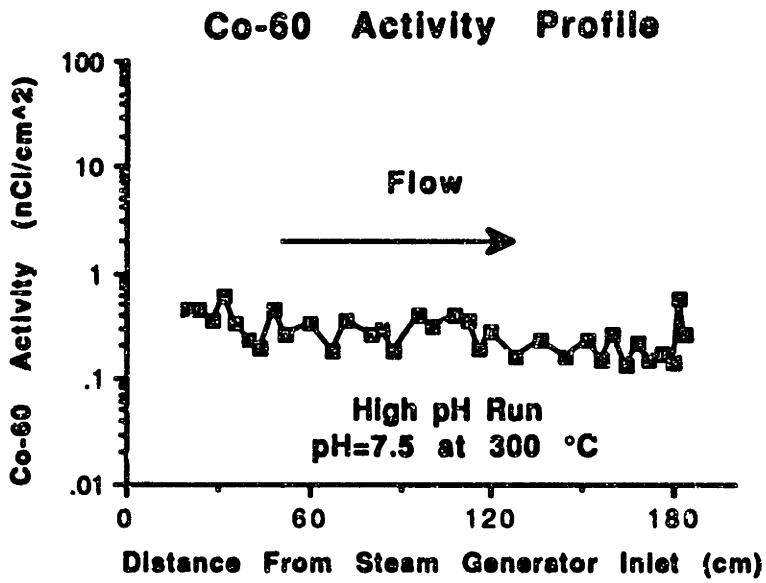

Figure 4.76 Co-60 Activity Profile (Hot Leg), High pH Run.

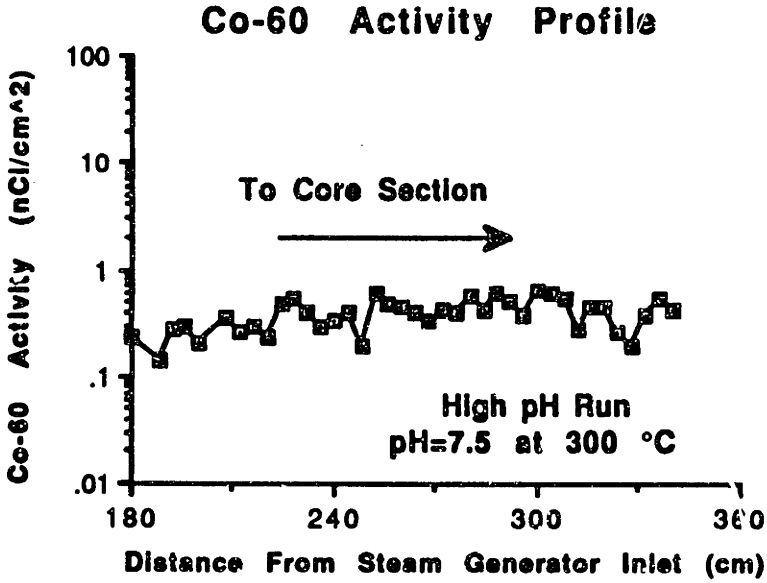

Figure 4.77 Co-60 Activity Profile (Cold Leg), High pH Run.

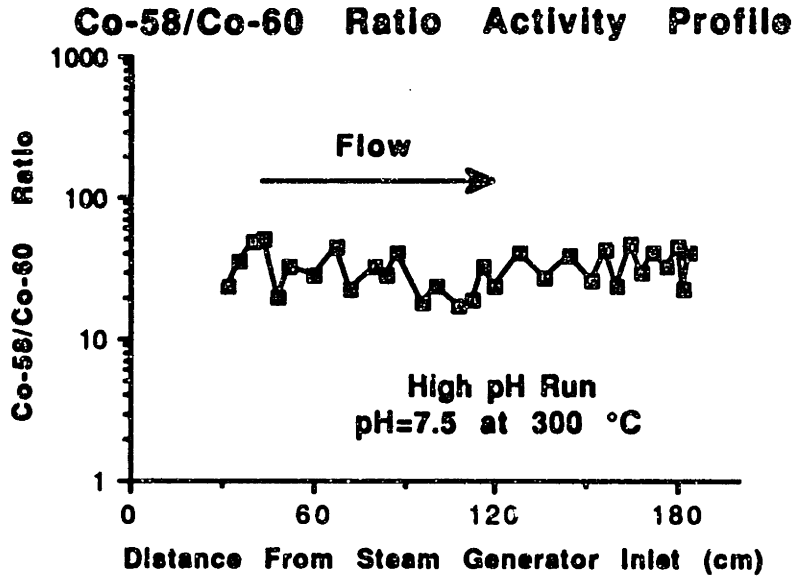

Figure 4.78 Co-58/Co-60 Ratios (Hot Leg), High pH Run.

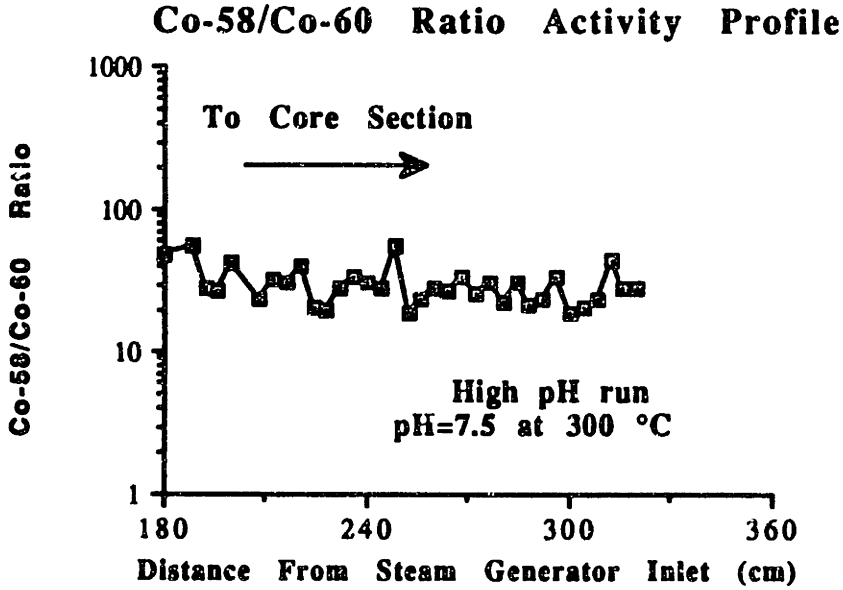

Figure 4.79 Co-58/Co-60 Ratios (Cold Leg), High pH Run.

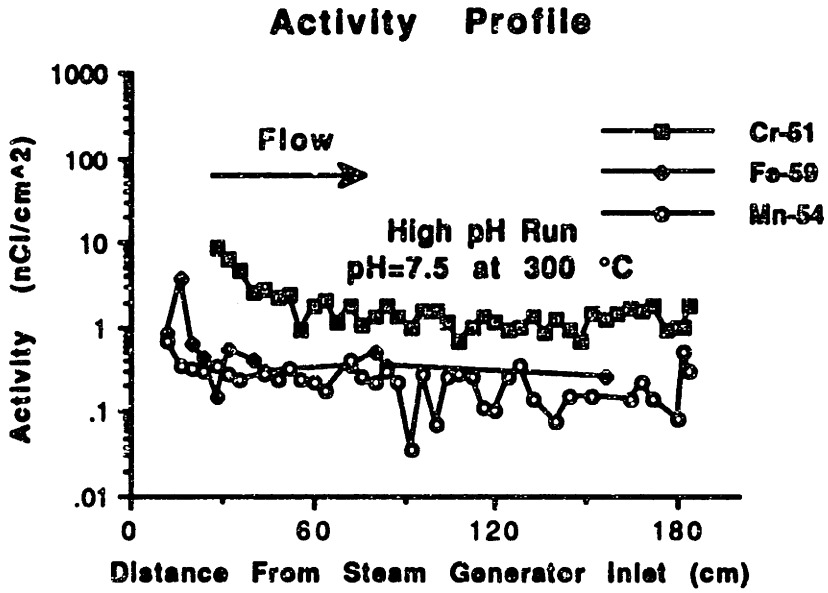

Figure 4.80 Cr-51, Fe-59, and Mn-54 Activity Profiles (Hot Leg), High pH Run.

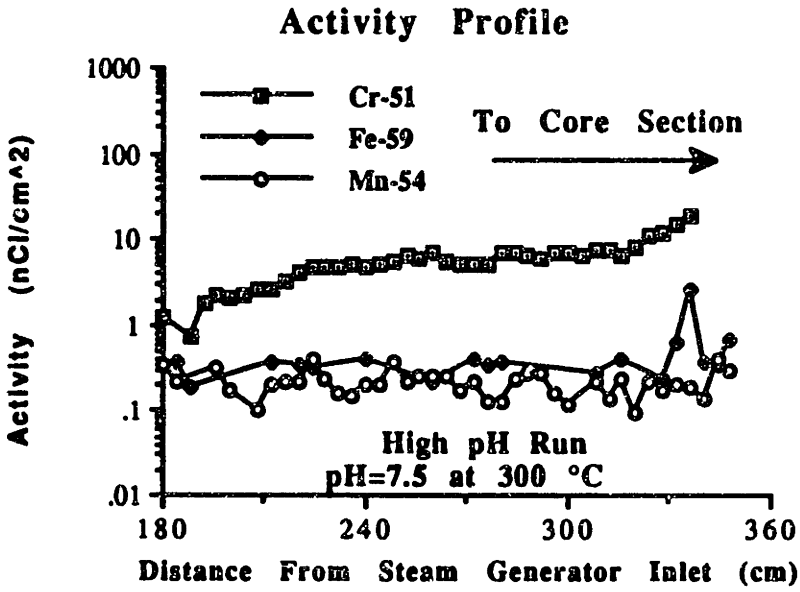

Figure 4.81 Cr-51, Fe-59, and Mn-54 Activity Profiles (Cold Leg), High pH Run.

average deposited activity is lower than for any other run. The total Co-58 and Co-60 deposited activities on the in-core Zircaloy tubing are 29.8 and 2.4 μCi, respectively.

In addition, the total Fe-59 and Mn-54 deposited activities were 77.2 and 5.9 μCi, respectively. These results suggest that the in-core deposition activities (with the exception of Co-60) are a bit higher than those in reference run #1. Nonetheless, it is important to point out that reference run #1 suffered two uncontrolled boiling transients that undoubtedly redistributed some of the deposited in-core activities into ex-core loop components.

Table 4.14 Results of Core Activity Deposition Measurements, High pH Run.

Position	Co-58 (nCi/cm^2)	Co-60 (nCi/cm^2)	Fe-59 (nCi/cm^2)	Mn-54 (nCi/cm^2)
Z1(87 cm)*	2.2 ± 0.46	0.16 ± 0.09	<0.85	0.31 ± 0.06
Z3(61 cm)*	<17	9.4 ± 2.9	700 ± 78	<5
Z5(35 cm)*	390 ± 28	37 ± 3.4	890 ± 69	110 ± 11
Z7(9 cm)*	144 ± 1.7	0.75. ± 0.17	6.8 ± 1.4	0.80 ±0.16
Z8(9 cm)*	130 ±2.2	7.9 ±0.36	200 ±7.0	24 ±0.45
Z10(35 cm)*	32 ±0.91	0.56 ±0.17	16 ±2.6	1.5 ±0.21
Z12(61 cm)*	2.2 ±0.27	1.8 ±0.12	40 ±8.4	1.4 ±0.1
Z14(87 cm)*	0.92 ±0.32	0.3 ±0.1	<0.85	0.17 ±0.07

* Distance measured from the bottom of the core.

4.5.6 Stainless Steel Filter

The SS filter, as in the three previous runs, was replaced every three days and counted immediately in a low background environment. As evident in Fig. 4.82, the Co-58 average deposited activity was on the order of 1E-04 nCi/cc, which is comparable to the average activities found for reference runs #1 and #2.

The cumulative Co-58 and Co-60 activities are shown in Figs 4.83 and 4.84. The total Co-58 and Co-60 activities deposited on the filters were 0.025 and 4E-03 μCi, respectively. These values are quite comparable with those for reference runs #1 and #2, if the uncontrolled transients are excluded. However, these activities are lower than for the low pH run. In addition, the average Co-58/Co-60 ratio (Fig. 4.85) was 7.6.

Finally, the Mn-56 filter activity (Fig. 4.86) decreased as a function of time. This result suggests that the release of corrosion products into the coolant decreases gradually due to the effect of operating with a positive solubility temperature coefficient, which would tend to inhibit release of transition metals from the cooled S/G tube walls.

4.5.7 Water Samples

Outlet water samples were taken, once again, on a daily basis during the entire run. To determine the amount and type of radionuclides released into the coolant, the outlet water samples were counted in a low background area with a gamma detection system.

The pH, conductivity, boron, and lithium of randomly selected

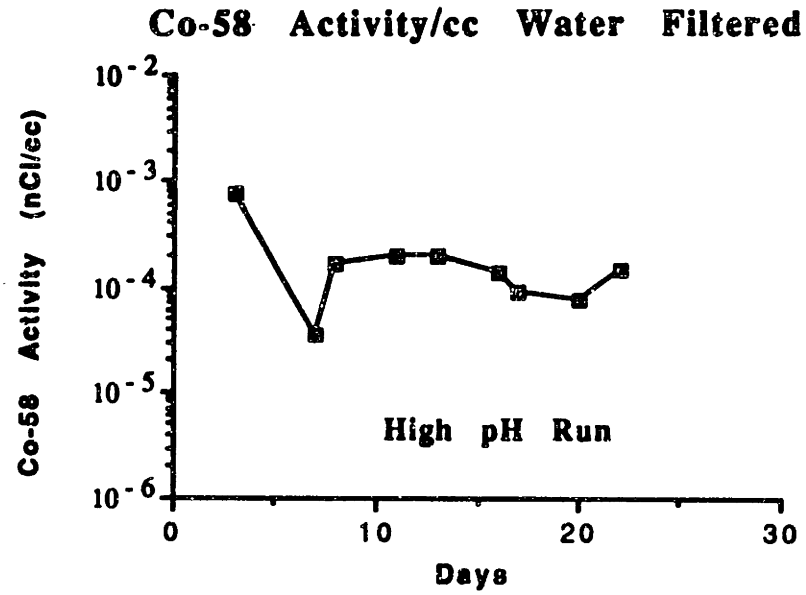

Figure 4.82 Co-58 Activity on Let-down Filters, High pH Run.

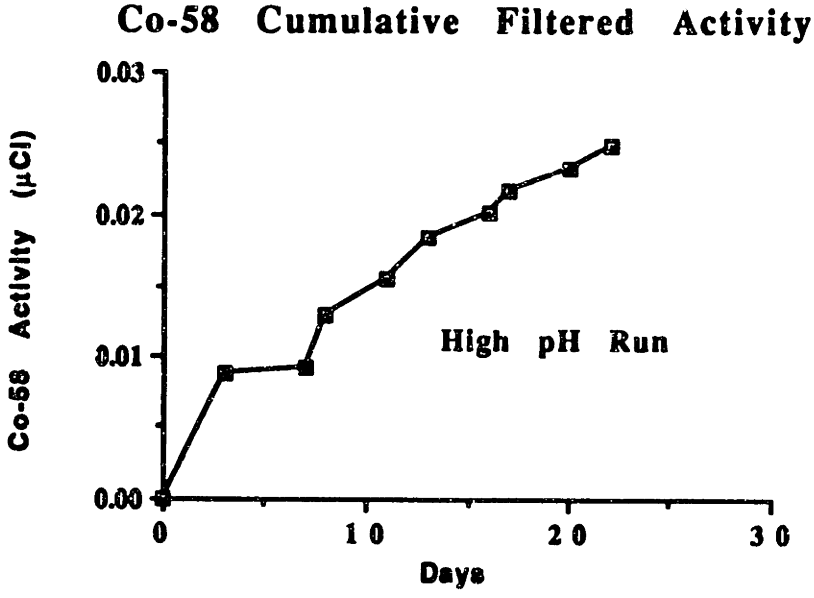

Figure 4.83 Cumulative Co-58 Activity Deposited on Filters, High pH Run.

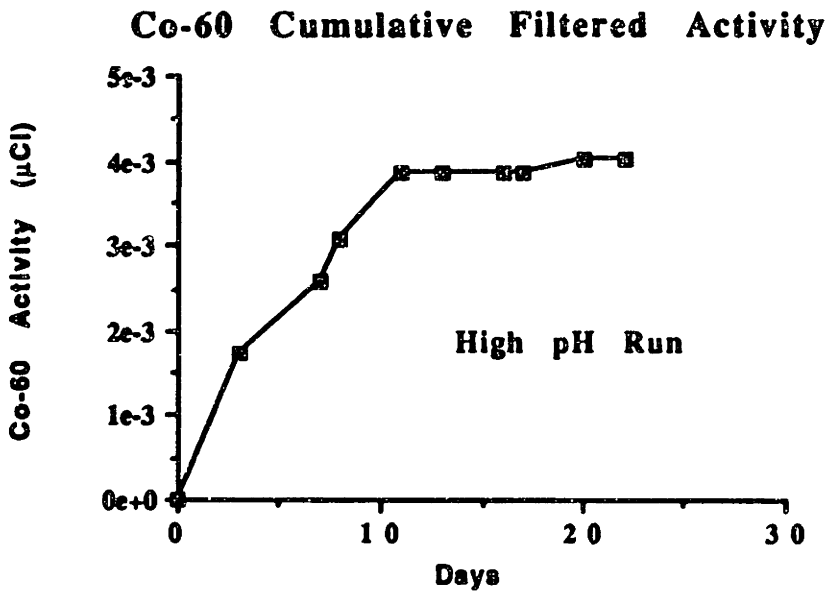

Figure 4.84 Cumulative Co-60 Activity Deposited on Filters, High pH Run.

samples were measured using the appropriate instrumentation already described. The results of the above variables are plotted in Figs. 4.87, 4.88, 4.89, and 4.90.

The pH of these samples never deviated by more than ± 0.1 pH units from the nominal pH value of 7.04 at room temperature (25 °C); and, the conductivity of the samples never deviated by more than ± 1% from the nominal conductivity value of 61 µmhos/cm.

The boron concentration was again measured by colorimetric techniques, which yielded values within ± 10% of the 800 ppm nominal value. The lithium concentration was determined by AA, which gave values within ± 7% of the 6.26 ppm nominal concentration.

Table 4.15 lists typical radionuclides and their activities found in outlet water samples near the end of the run. As in the past runs, fission products such as Ce-144, I-132, I-135, Kr-85, Tc-99, Xe-135,

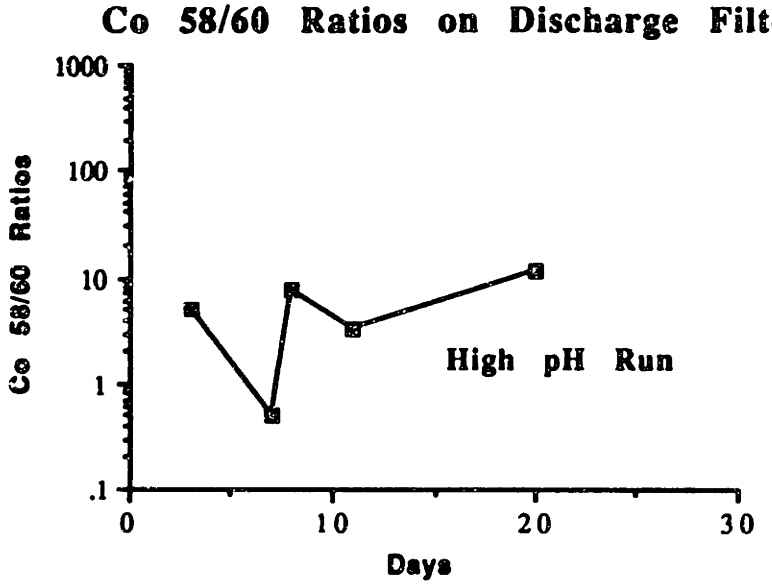

Figure 4.85 Co-58/Co-60 Ratios on Filters, High pH Run.

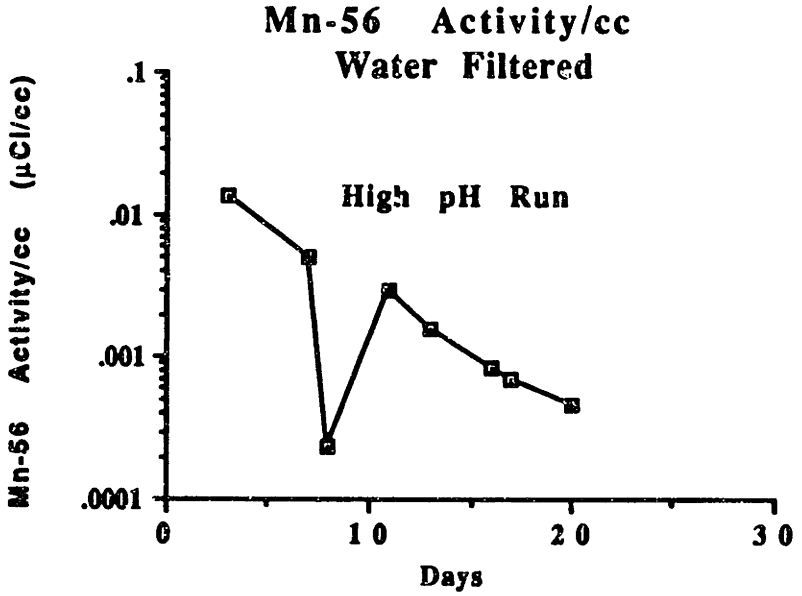

Figure 4.86 Mn-56 Activity Deposited on Filters, High pH Run.

and Y-88 were detected in small quantities.

Zr-97, which is either a fission product or produced as a result of thermal neutron interactions with zirconium metal, was also detected in small quantities and few samples.

Ar-41, Na-24, and W-187 were found, as in the previous runs, in almost every water sample. The Na-24 activity is shown in Fig. 4.91. The irregular activity profile is characterized by a spike occurring 10 days into the run followed by a steady decrease in activity. On the other hand, the W-187 activity profile (Fig. 4.92) shows a downward trend, which also suggests that the release of W-187 into the coolant gradually decreases due to the effect of operating with a positive solubility temperature coefficient.

Mn-56, produced as described in sec. 4.4.7, was found in several water samples. Its downward activity profile confirms the solubility effect already described. The average Mn-56 activity in outlet water samples is an order of magnitude less than those found for the low pH run. Hence it may be a sensitive indicator of deposition related coolant conditions.

Finally, Mn-54 and Co-58, produced as described in sec. 4.2.7, were detected in a small number of samples and in small quantities.

Charging make-up water samples were analyzed using ion chromatograph and an inductively coupled plasma (ICP) technique to determine the input of transition metals into the loop. Table 4.16 shows these results, which are comparable to those obtained for the previous in-pile runs.

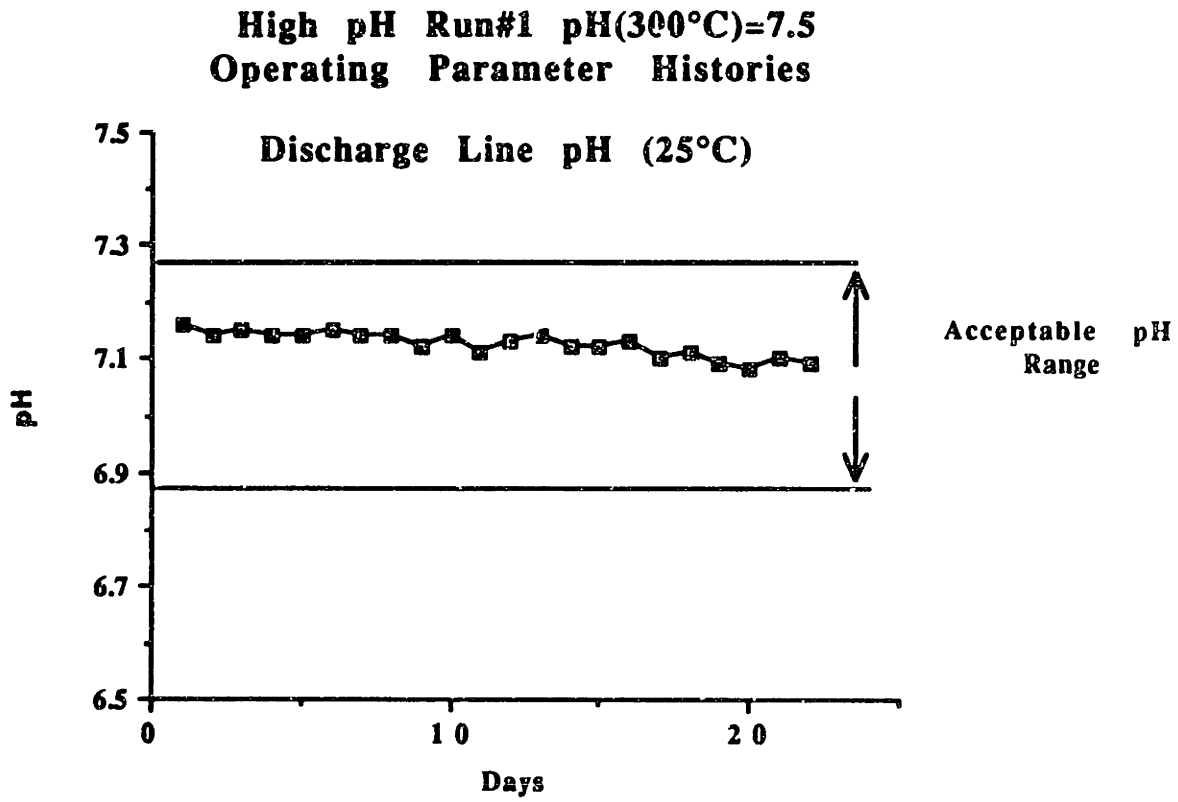

Figure 4.87 Discharge Line pH (25 °C), High pH Run.

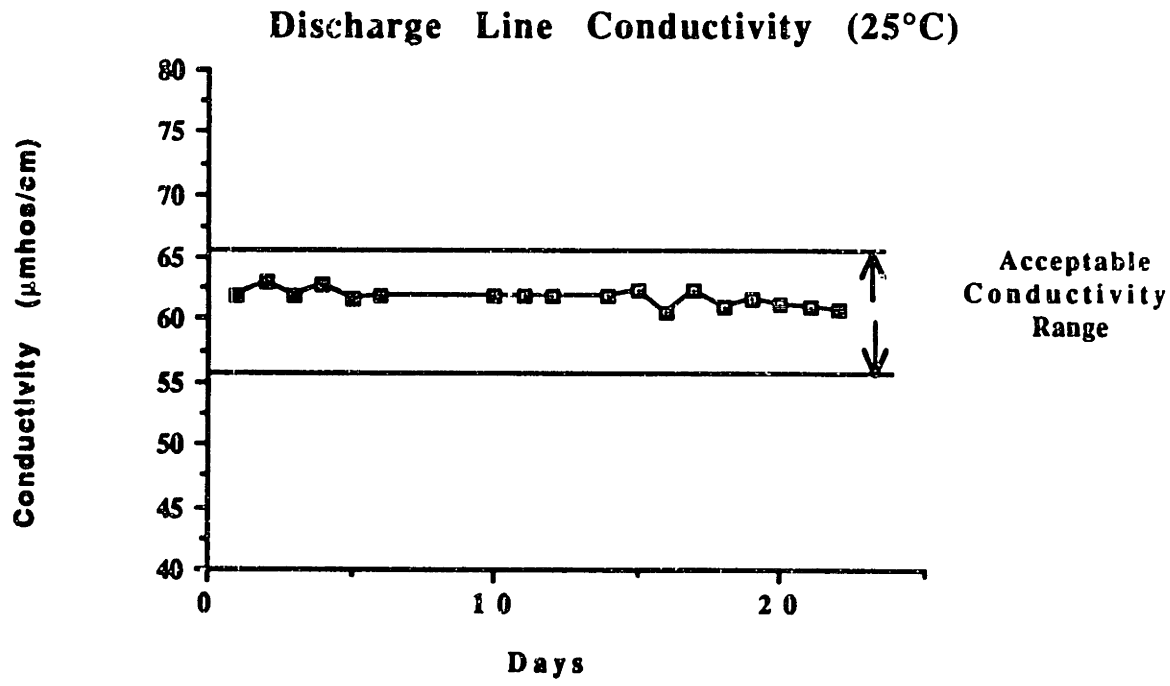

Figure 4.88 Discharge Line Conductivity (25 °C), High pH Run.

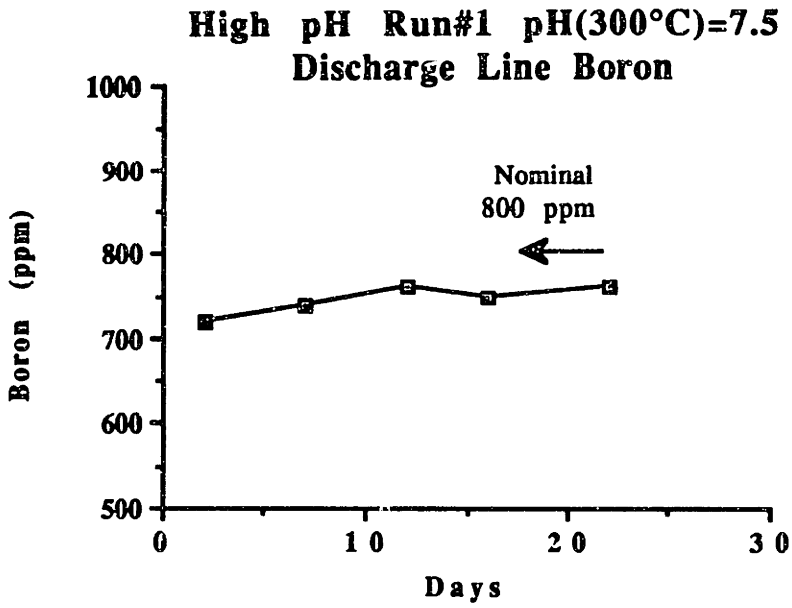

Figure 4.89 Discharge Line Boron, High pH Run.

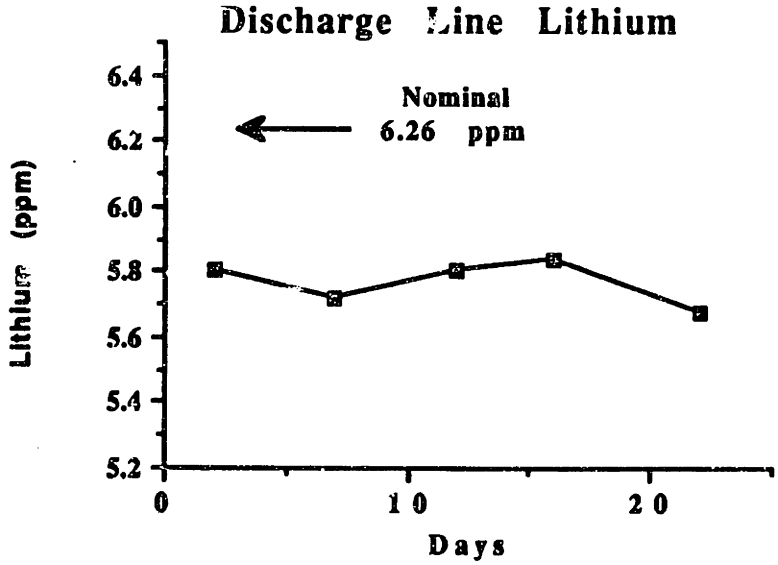

Figure 4.90 Discharge Line Lithium, High pH Run.

4.5.8 Ion Exchange Column

The ion exchange resin was analyzed using, once again, gamma spectroscopy to determine the amount of radioactive contaminants in the let-down water flow. The analysis showed a total Co-58 and Co-60 deposition of 0.4 and 0.02 μCi, respectively with a Co-58/Co-60 ratio of 20. From these results, it is evident that the least deposition of corrosion products on the IX column occurred during this run. Table 4.17 summarizes the total activities of transition metals and other elements. The activity per cm^3 is is inferred from the total amount of coolant that passed through the resin.

4.6 Chapter Summary

In this chapter, the measured deposited activity on loop components for four in-pile runs has been presented, as well as a brief discussion, and some interpretation, of the obtained results. Since the Co-60 deposition activity on the loop components is considered the most important indicator relevant to PWR maintenance dose, table 4.18 summarizes the total Co-60 inventory for the four in-pile runs.

It is clear that operating under high pH coolant chemistry provides a reduction in Co-60 deposition, which will lead to a comparable reduction in the radiation fields on out of core surfaces. Conversely, operation at low pH is exceedingly detrimental.

Table 4.15 Radionuclides in Water Samples, High pH Run.

Radionuclide	Activity/cc (μCi/cc)
Ar-41	3.7E-03 ±1%
Ce-144	7.8E-07 ±77%
Co-58	2.9E-06 ±15%
I-132	7.4E-04 ±3%
I-135	2.6E-04 ±3%
K-85	7.8E-08 ±65%
Mn-54	3.9E-06 ±8%
Na-24	9.5E-04 ±2%
Tc-99	1.8E-07 ±72%
W-187	2.2 E-03 ±1%
Xe-135	2.0E-05 ±22%
Y-88	1.4E-06 ±38%
Zr-97	6.5E-06 ±8%

Table 4.16 Ion Chromatograph Measurements of Make-up Water Trace Elements, High pH Run.

Element	Concentration (ppb)
Zinc	19
Nickel	58 (<10)
Cobalt	4 (<10)
Iron (II)	89 (130)
Manganese	23 (5)
Chromium	(<4)

*Values in parenthesis are Inductively Coupled Plasma (ICP) results, measured by P. Beslu in France.

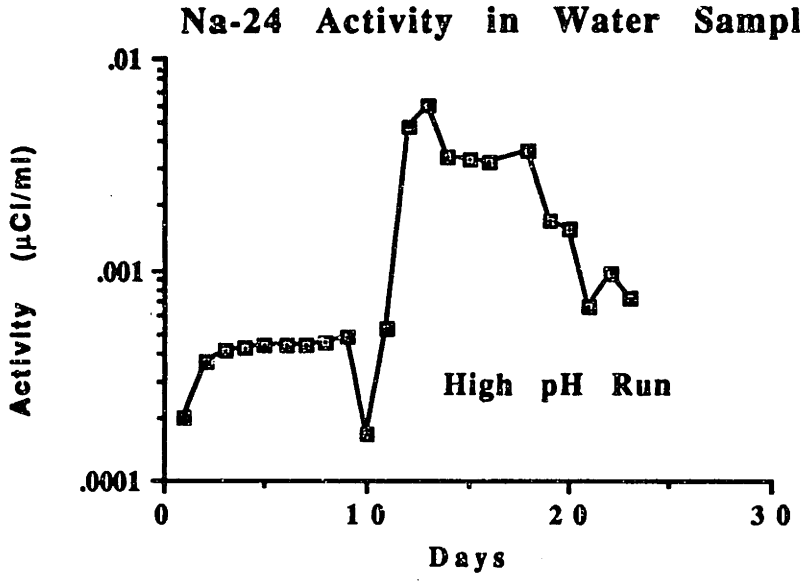

Figure 4.91 Na-24 Activity in Water Samples, High pH Run.

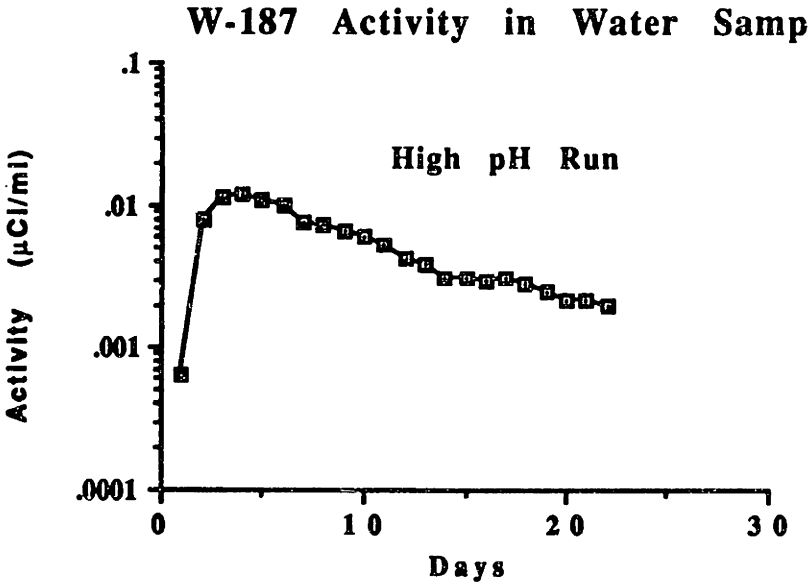

Figure 4.92 W-187 Activity in Water Samples, High pH Run.

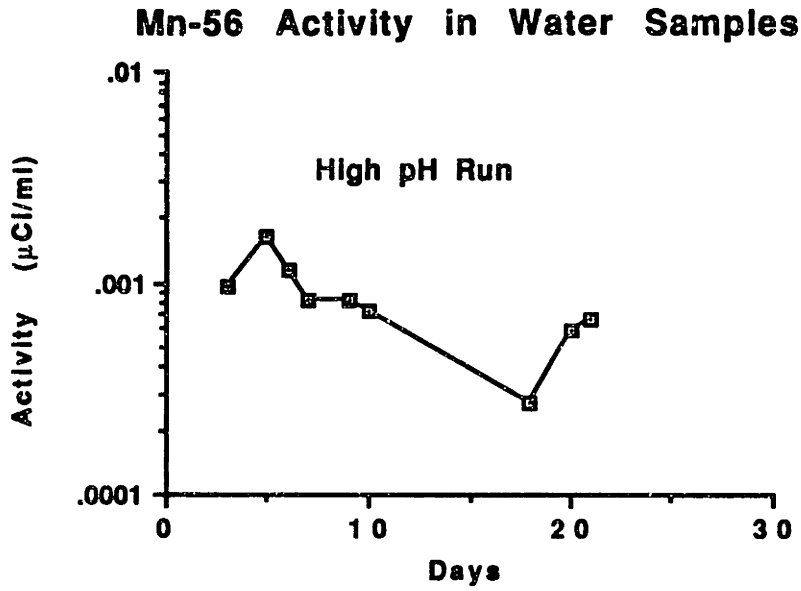

Figure 4.93 Mn-56 Activity in Water Samples, High pH Run.

Table 4.17 Summary of Activity Deposited on IX Column, High pH Run.

Radionuclide	Activity (µCi)	Activity/cc* (µCi/cc)
Ag-110	3.1E-03 ± 15%	2.1E-08
Ba-140	0.08 ± 13%	5.3E-07
Co-57	9.2E-04 ± 21%	6.1E-09
Co-58	0.4 ± 1%	2.6E-06
Co-60	0.02 ± 3%	1.3E-07
Cr-51	0.01 ± 20%	6.6E-08
Fe-59	0.01 ± 17%	6.6E-08
I-131	0.08 ± 7%	5.3E-07
Mn-54	0.15 ± 1%	9.9E-07
Ru-103	0.01 ± 11%	6.6E-08
Sb-124	0.4 ± 1%	2.4E-06
Sn-113	0.001 ± 38%	6.6E-09
Zn-65	0.003 ± 22%	1.9E-10

* Total cc passed through resin = 1.5E05 cc

Table 4.18 Total Co-60 Deposited Inventory on Loop Components.

Run	$pH_{300°C}$	Total Hot Hours	Total MW-hrs	Inconel Tubes (μCi)	Zircaloy Tube (μCi)
PR1	7.0	889.3	2328.3	1.25	7.8
PR2	7.0	536.0	1870.8	0.7	4.5
PL1	6.5	478.0	2115.0	3.1	22.8
PH1	7.5	533.0	2287.9	0.24	2.4

PR1 - First Reference Run, pH_{300}=7.0, (800 ppm B, 1.84 ppm Li).

PR2 - Second Reference Run, pH_{300}=7.0, (800 ppm B, 1.84 ppm Li).

PL1 - Low pH Run, pH_{300}=6.5, (800 ppm B, 0.56 ppm Li).

PH1 - High pH Run, pH_{300}=7.5, (800 ppm B, 6.26 ppm Li).

5 SUMMARY, CONCLUSIONS AND RECOMMENDATIONS

5.1 Introduction

Radiation fields on PWR out-of-core components have been a major cause of personnel exposure during maintenance and operation of PWR nuclear plants. The buildup of these fields is caused by corrosion products which are released into the primary coolant, become activated in the core, and later deposited on out of core surfaces. Solubility studies of transition metals have suggested that the release of corrosion products into the primary coolant can be minimized if the primary system operates at a higher coolant pH. Therefore, changing the current coolant pH to a higher one would result in a decrease of radiation fields on out of core components.

To study the effect of coolant pH, an in-pile loop capable of simulating PWR primary coolant conditions has been constructed and operated. This loop simulates a PWR primary circuit (one unit flow cell: steam generator tube and fuel pin channel, at about 1/3 scale) by matching, as closely as possible, coolant temperatures and temperature differences, heat fluxes, flow velocities, construction materials, surface area ratios, and neutron fluxes. Figure 5.1 shows the main components of the in-pile loop.

Parameters such as film and bulk differential temperatures, which are considered to be important governing factors, are closely reproduced. In addition, the surface area ratios of Zircaloy/Inconel /Stainless Steel exposed to the primary coolant are also matched fairly well. A parametric comparison between a representative PWR plant and the above in-pile loop is presented in table 5.1

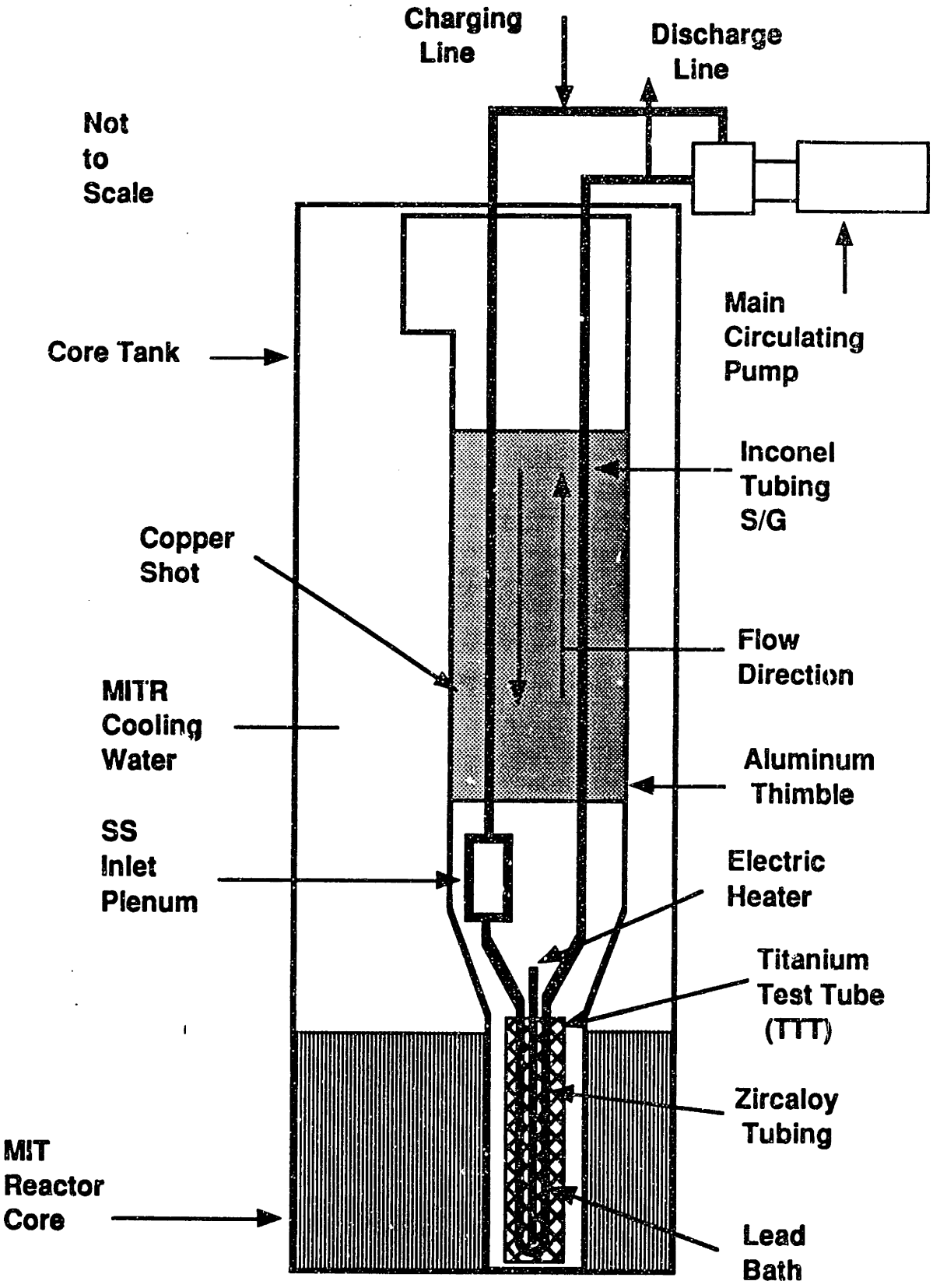

Figure 5.1 Schematic of the In-pile Loop Components.

Table 5.1 Comparison of PWR and MITR-PCCL Design Parameters

Parameter	PWR	MIT PCCL
Core inlet T, °F (°C)	545 (285)	530 (277)
Core outlet T, °F (°C)	608 (320)	600 (316)
Hydraulic dia., in. (cm) Core Steam Gen.	 0.47 (1.2) 0.82 (2.1)	 0.256 (0.65) 0.242 (0.62)
Boundary layer ΔT, °F (°C) Core Steam Gen.	 32.4 (18) 10.26 (5.7)	 35.8 (19.9) 12.8 (7.1)
Coolant Velocity Core (m/sec) Steam Gen. (m/sec)	 4.8 5.9	 2.8 3.0
Core Average, neutron flux, n/cm^2-sec Thermal Fast(>1 Mev)	 2.3E13 9.4E13	 2.6E13 5.0E13
Average Heat flux, (kW/m^2) Core Steam Gen.	 614.6 178.2	 550.0 194.5
Material surface ratios: Total Inconel/Zircaloy Cooled Inconel/heated Zircaloy Total SS/Inconel	 2.73 3.44 0.15	 4.94 2.63 0.24

5.2 Refinements to Loop Design and Operating Procedures

The original conceptual design of the PCCL is recorded in the theses by Burkholder [B-7] and Wicks [W-1]. A substantial part of the present work was concerned with practical implementation of these designs. This involved minor and major changes in many design features.

Table 5.2 lists some of the most important changes implemented during the course of the work carried out by the present author, and table 5.2 lists the major subtasks completed to bring the loop to a state of operational readiness.

A great effort was also placed, once the loop was operational, on adequate control of coolant chemistry parameters to ensure that, for instance, parameters such as coolant pH and conductivity were always within specs.

Table 5.2 List of Major Loop Changes Implemented During the Present Work.

* Heated Autoclave Auxiliary Pressurizer (HAAP).
* Uninterruptible Power Supplies (UPSs).
* Variable Frequency Power Supply for Main Circulating Pump.
* Autoclave Engineering Main Circulating Pump (AE) vs NREC pump.
* Welded Loop components (Inlet Plenum) to replace leak prone fittings.
* Helium feed and bleed lines to reduce humidity in the thimble atmosphere.
* Implementation of the Charging System.
* Titanium Test Tube: design and fabrication of several variations.
* In-pile Heater: change of basic design to a U configuration.
* Loop Handling System: cask, rigging, shielding.
* Hot Cell: design, fabrication and installation of equipment.

Table 5.3 List of Major Subtasks.

* Fabrication of major components such as Coolant Sampling and Let-down System, Systems for pre-conditioning of Loops.

* Out-of-pile testing of loop components such as in-pile heaters, main circulating pumps (NREC and AE), titanium test tube.

* Out-of-pile tests to measure heat rejection under accident scenario conditions.

* In-pile tests to measure gamma heating, and reactivity noise due to boiling conditions in the loop.

* Review by the MIT Safeguards Committee.

5.3 Deposition Measurements

This section summarizes the deposition measurements of the four one month long in-pile runs (table 5.4) that have been completed. Emphasis is given to the Inconel tubes and in-pile Zircaloy tubing deposition data, which represent the major surface areas of the loop.

Prior to the discussion of these results, it is worthwhile to mention that the chemistry control in the four month-long in-pile runs was rigidly controlled. The pH, conductivity, and boron and lithium concentrations of makeup and let-down water were held constant within PWR coolant chemistry guidelines for the four runs. In addition, bulk and film differential temperatures, which are important transport-governing factors, were held at the values specified in table 5.3 throughout the runs.

Deposition measurements on the Inconel tubes for Co-60, Co-58, Fe-59, and Mn-54 for the four runs are shown in Figs. 5.2

through 5.5. From these results, it is evident that operating at low coolant pH is detrimental, since the deposition of activated corrosion products is the highest. On the other hand, operating at a high coolant pH results in less deposited activity on the Inconel tubes, which comfirms transition metal solubility studies that predict this behavior [S-3].

Table 5.4 In-pile Runs Conducted in First Loop Campaign.

Run #	Conditions
1. First Reference Run (PR1)	$pH_{300°C}$ = 7.0, 1.84 ppm Li, 800 ppm B
2. Second Reference Run (PR2)	$pH_{300°C}$ = 7.0, 1.84 ppm Li, 800 ppm B
3. Low pH Run (PL1)	$pH_{300°C}$ = 6.5, 0.56 ppm Li, 800 ppm B
4. High pH Run (PH1)	$pH_{300°C}$ = 7.5, 6.26 ppm Li, 800 ppm B

Another interesting effect is the decrease in deposited activity in the absence of heat flux for the low pH run and the opposite trend for the high pH run, which supports the importance of film differential temperature as a driving force for crud transport and/or oxide film morphology. Further analysis of the nature of oxide film layers in the cooled/isothermal regions is recommended to determine their

differences and the role of the coolant pH in their formation.

Finally, the total Co-60 deposited inventories on the steam generator tubes and in-pile Zircaloy tubing are presented in table 5.3. The Co-60 activities in the two reference runs scale in rough proportion to the total hot hours (ie. time during which transport takes place) and in both runs the ratio of the Zircaloy to Inconel deposition is the same (6.3 ± 0.1), indicating a certain degree of consistency even though these runs were interrupted by operational transients due to component failure or leaks. Again the disadvantages of low pH and the benefits of high pH are evident.

Table 5.3 Total Co-60 Deposited Inventory on Loop Components.

Run	$pH_{300°C}$	Total Hot Hours	Total MW-hrs	Inconel Tubes (μCi)	Zircaloy Tube (μCi)
PR1	7.0	889.3	2328.3	1.25	7.8
PR2	7.0	536.0	1870.8	0.7	4.5
PL1	6.5	478.0	2115.0	3.1	22.8
PH1	7.5	533.0	2287.9	0.24	2.4

PR1 - First Reference Run, pH_{300}=7.0, (800 ppm B, 1.84 ppm Li).

PR2 - Second Reference Run, pH_{300}=7.0, (800 ppm B, 1.84 ppm Li).

PL1 - Low pH Run, pH_{300}=6.5, (800 ppm B, 0.56 ppm Li).

PH1 - High pH Run, pH_{300}=7.5, (800 ppm B, 6.26 ppm Li).

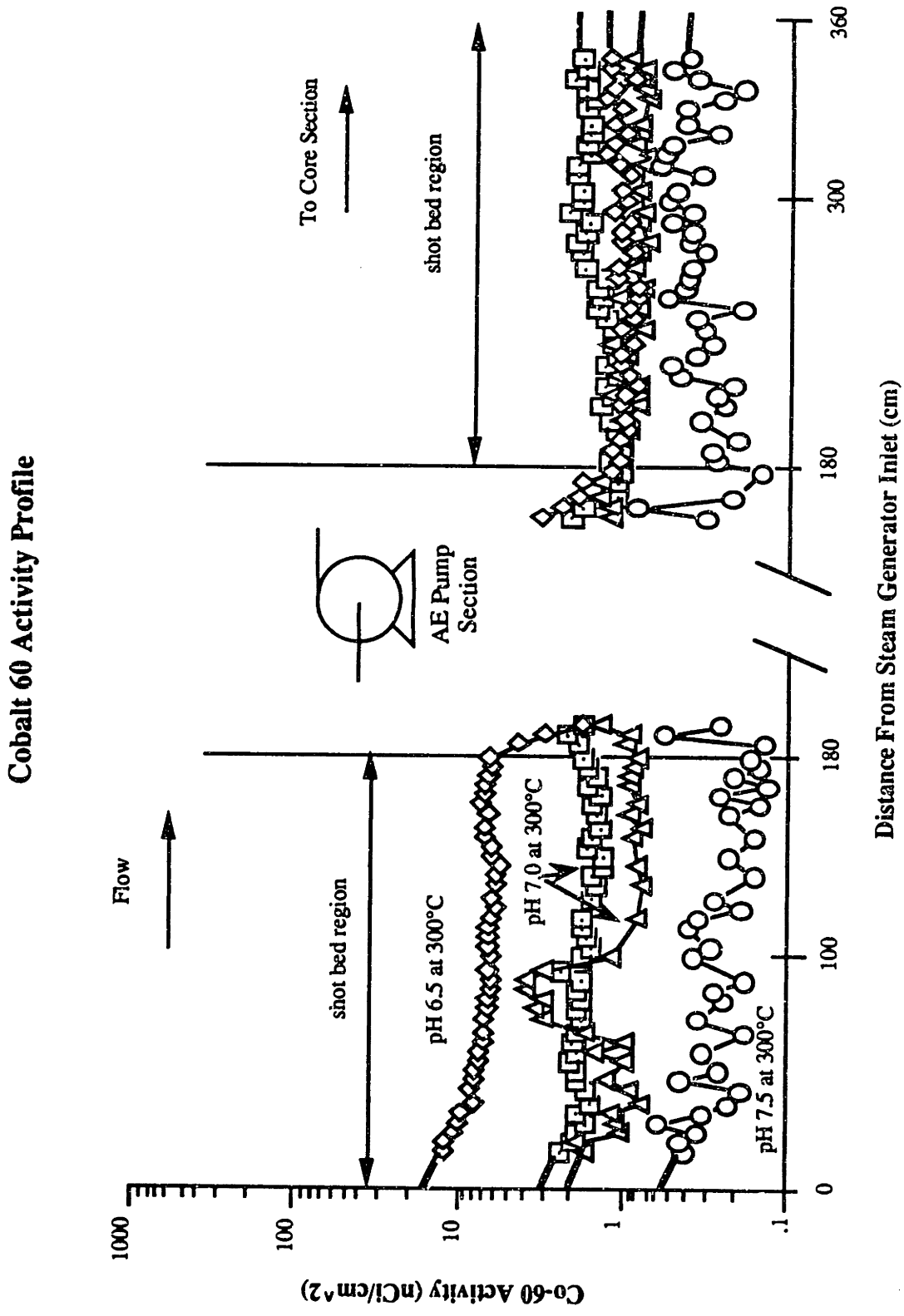

Figure 5.2 Co-60 Activity Deposited on Inconel Tubes for the Four In-pile Runs of the First PCCL Campaign.

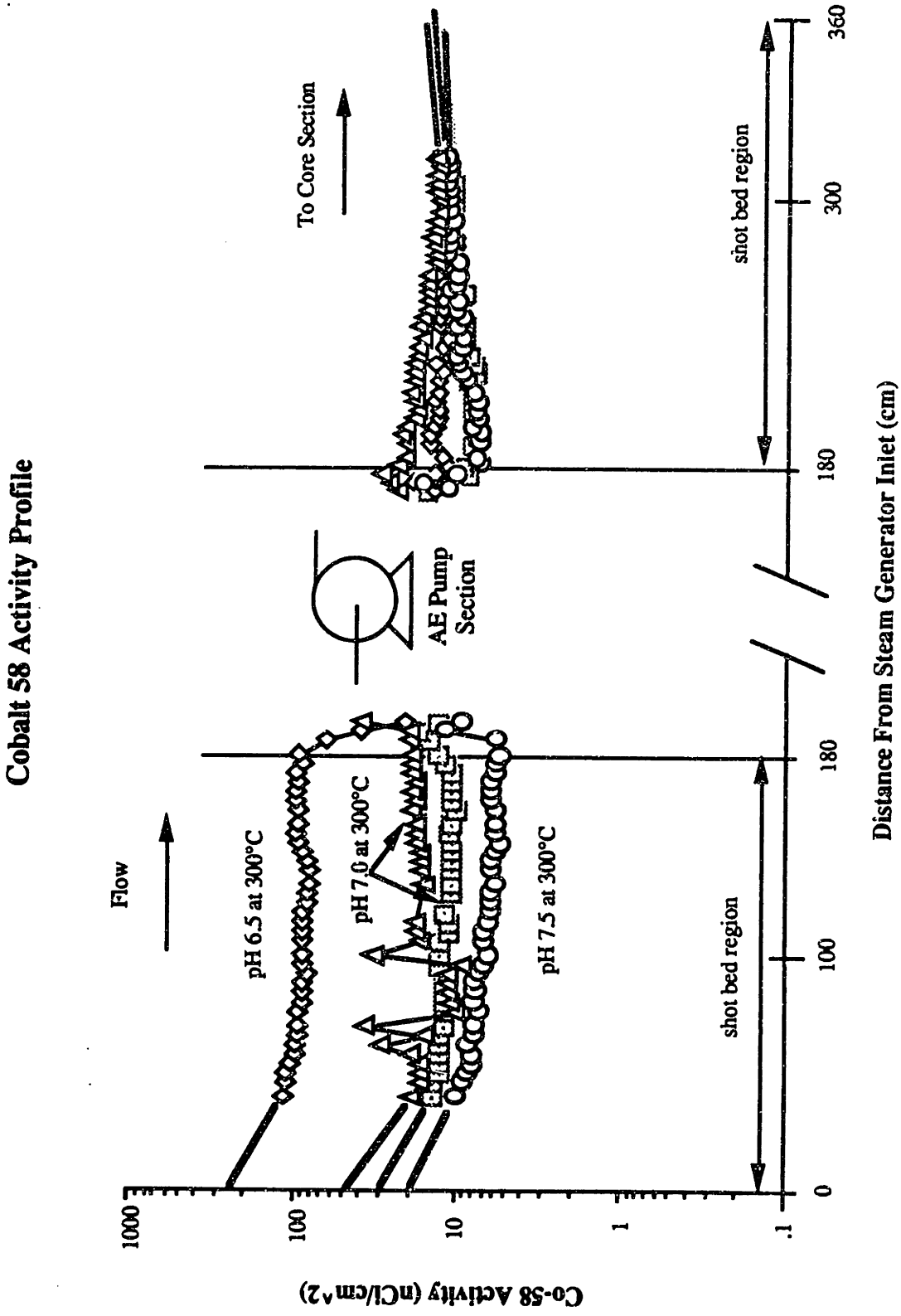

Figure 5.3 Co-58 Activity Deposited on Inconel Tubes for the Four In-pile Runs of the First PCCL Campaign.

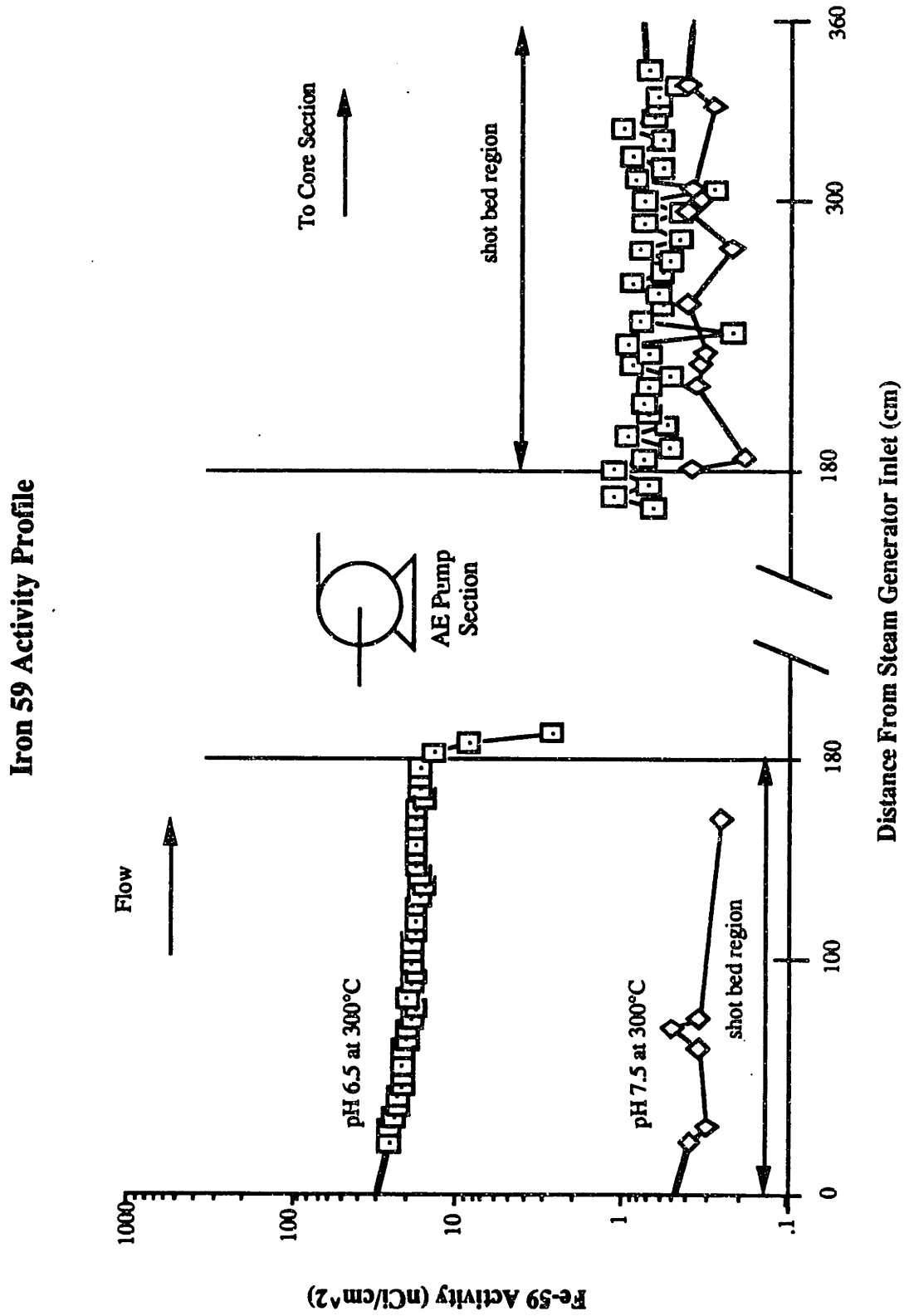

Figure 5.4 Fe-59 Activity Deposited on Inconel Tubes for the High and Low pH In-pile Runs of the First PCCL Campaign.

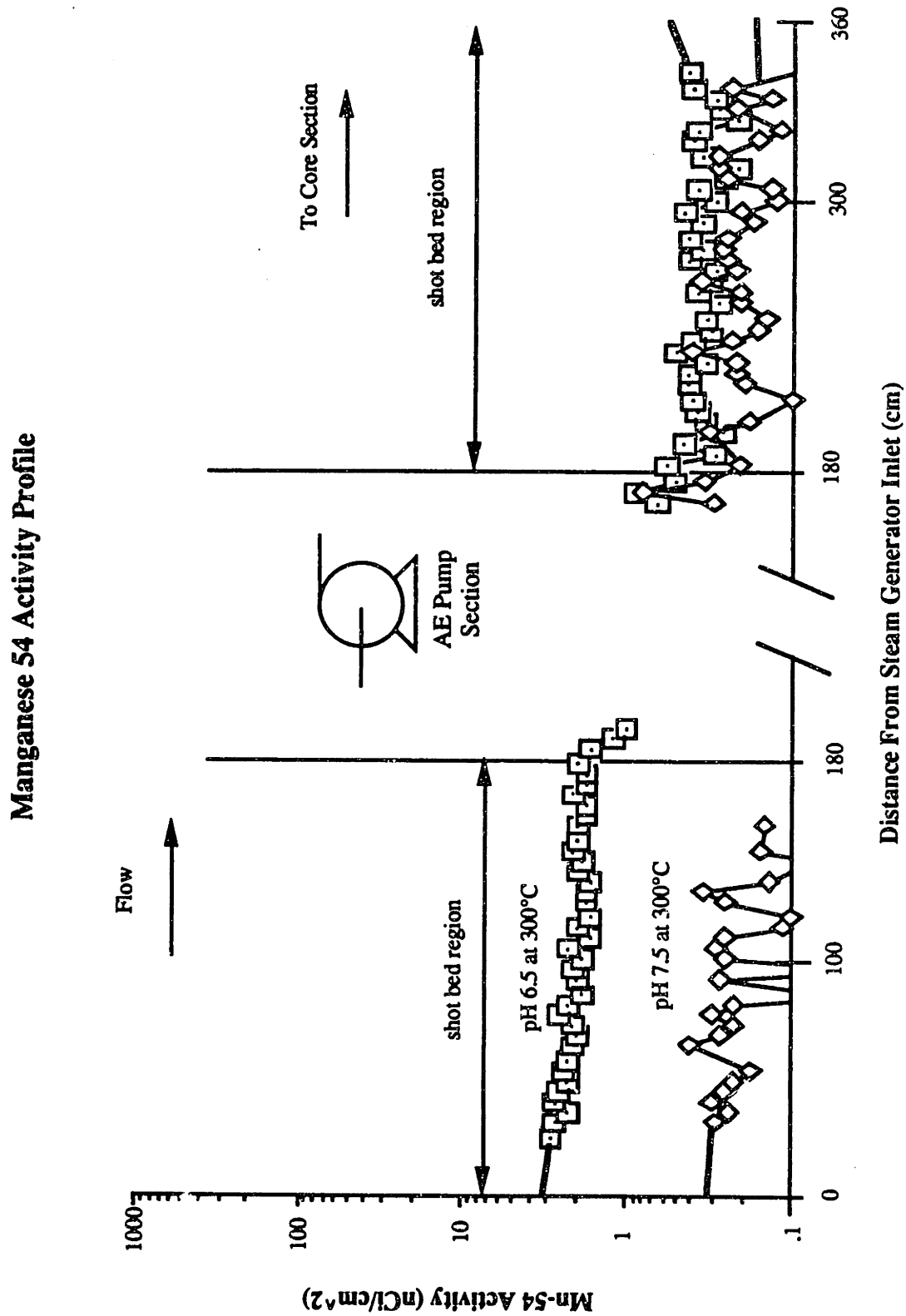

Figure 5.5 Mn-54 Activity Deposited on Inconel Tubes for the High and Low pH In-pile Runs of the First PCCL Campaign.

5.4 Conclusions

An in-pile loop, which closely simulates a PWR primary circuit coolant chemistry environment, has been designed, constructed and operated in the MIT Research Reactor. By itself, this was a major achievement of the present thesis. A series of four in-pile runs have also been carried out to evaluate the effect of coolant pH on the transport and deposition of radionuclides on out-of-core surfaces. Initial results of loop post mortem analyses are summarized in this report.

Activity deposition results, primarily on the simulated steam generator (Inconel) and core (Zircaloy) tubes have shown and confirmed the benefits of operating in the $pH_{300°C}$ = 7.0 to 7.5 range compared to low pH ($pH_{300°C}$=6.5). These results also support a solubility-driven transport mechanism as a dominant factor in corrosion product transport.

5.5 Recommendations for Future Work

The following recommendations address future in-pile runs and their rationale, as well as modifications to the present support systems.

First of all, the work reported here stops at an early stage of the loop data acquisition and interpretation process. Several other theses are in progress which continue this important process, in particular those by Cabello, Borys, and Zhang; and others will follow. Here we will look beyond the scope of such efforts.

Longer in-pile runs should be carried out to confirm the

validity of relatively short time tests of the type carried out here. The Nuclear Power Engineering Test Center (NUPEC) has recently contracted with MIT to carry out three 3000 hour runs, which are otherwise quite similar to the first campaign discussed in this thesis.

Coordinated coolant chemistry in which B (and Li) are reduced as a function of time, at a constant pH, should also be considered for in-pile loop runs to reflect the actual operating conditions in PWR plants. High and zero boron in-pile runs are planned for the second campaign of the current EPRI/ESEERCO program to simulate the beginning and end of fuel cycle in a typical PWR. These runs should indicate whether further investigation is in order.

To further evaluate the effect of the cooled/isothermal zones observed in the low and high pH runs, a section of Inconel tubing (eg 6 cm) in the shot bed region should be thermally isolated (with a tube of insulating material/gas gap). This will remove and restore the thermal boundary layer in the steam generator/insulated tube to facilitate examination of the above effect.

To reduce the input of trace elements into the loop, the stainless steel tubing in the charging system and the Inconel tubing that connects the charging pump to the inlet T connector of the loop should be replaced with corrosion resistant titanium tubing. Alternatively, a ZrO_2 ion exchange column, similar to that used by Lister [L-4] should be installed.

To simulate exactly the bulk differential temperatures of a PWR plant, the in-pile loop should operate at the same inlet and outlet temperatures as a specified class of PWR units for which ex

tensive deposition data is or will become available.

To evaluate the effect of hydrogen, at least one run using a different hydrogen coolant concentration should be carried out. Computer models predict that reducing H_2 by a factor of two will reduce activity deposition by the same factor [B-10] [L-2].

To obtain a more realistic measure of the radioactive and non-radioactive species in the coolant, daily water samples should be taken as closely as possible to the loop, and the line to that point should be trace-heated to maintain the water at its in-loop temperature. Similarly, the deposition monitor (SS filter) should be trace-heated, so that the filter temperature is the same as the bulk temperature in the loop. The filters should be pre-filmed prior to use.

During the weekend mode of operation, when the reactor is shut down, the inlet and outlet loop temperatures should be kept at the same temperature as during weekdays. This will require running the in-pile heater above 20 kW, or derating the heat rejection capability of the shot bed.

In the area of component development, work on several improvements should continue, the most important being in-pile heaters, where greater reliability must be achieved. Successful completion of the development of a small canned rotor pump [E-1] should be pursued. Finally, other versions of the in-pile titanium can should be tested if any further problems with bowing or cracking are experienced.

References

[A-1] T. G. Achorn, "Improving the Reliability of the Pressurized Water Reactor Coolant Chemistry Research Loop (PCCL)", Subject 22.901 Special Project Report, MIT Nuclear Eng. Dept., Aug 1989.

[A-2] R. A. Anduze, "Colorimetric Determination of Titanium in Polyethylene," Analytical Chemistry **29**, pg. 90, 1957.

[B-1] Proceedings of International Conference on Water Chem. Nucl. React. Sys., Bournemouth, BNES, London, 1978.

[B-2] Proceedings of 2nd International Conference on Water Chem. Nucl. React. Sys., Bournemouth, 2BNES, London, 1980.

[B-3] Proceedings of 3rd International Conference on Water Chem. Nucl. React. Sys., Bournemouth, 3BNES, London, 1984.

[B-4] Proceedings of 4th International Conference on Water Chem. Nucl. React. Sys., Bournemouth, 4BNES, London, 1986.

[B-5] Proceedings of 5th International Conference on Water Chem. Nucl. React. Sys., Bournemouth, 5BNES, London, 1989.

[B-6] B. G. Brooks, Occupational Radiation Exposure at Commercial Nuclear Power Reactors, NUREG-0713 5, 1984.

[B-7] K. Burkholder,"An In-Pile Loop for Corrosion Transport Studies in a PWR", S. M. Thesis, Dept. of Nucl. Eng.,

MIT,1985.

[B-8] G. K. Batchelor, et al, "Thermal or Electrical Conduction Through a Granular Material", Proc. R. Soc. London, Vol 355, No. 1682, 13 July 1977.

[B-9] P. Borys, "Acquisition and Interpretation of PWR Coolant Loop Data", Subject 22.901 Special Project Report, MIT Nuclear Eng. Dept., January 1990.

[B-10] P. Borys, et al, "Parametric Studies of the MIT PWR Coolant Chemistry Loop Using the PACTOLE Code", Report No. MITNRL-304, 1989.

[C-1] G. C. W. Comley, "The Significance of Corrosion Products in Water Reactor Coolant Circuits", Progress in Nuclear Energy, Vol. 16, No. 1, pp. 41-72, 1985.

[C-2] E. D. Cabello, "Decontamination Studies of Simulated PWR Primary Coolant System Components", S. M. Thesis, Dept. of Nucl. Eng., MIT,1990.

[D-1] M. Driscoll, "Impurities in PWR Loop Crud and H_20", PCCL Technical Note, Aug 1989.

[E-1] A. Esteves, "Qualification of Miniature Canned Rotor Pumps for In-Pile Loop Service", Nucl. Eng. Thesis, Dept. of Nucl. Eng., MIT,1990.

[F-1] D. G. Franklin, et al., Creep of Zirconium Alloys in Nuclear Reactors, American Society for Testing and Materials Press, 1983.

[H-1] O. K. Harling, M. Driscoll., "Research Proposal on Dose Reduction in Light Water Reactors", MIT, 1986.

[H-2] O. K. Harling, M. J. Driscoll, et al., " Final Report of MIT PWR Loop Pump Task Force", MITNRL-038, 1988.

[H-3] O. K. Harling, et al., "Safety Evaluation Report for the PWR Coolant Chemistry Loop (PCCL)", MITNRL-020, 1987.

[H-4] HACH Co., DR/2000 Spectrophotometer Handbook,1988.

[L-1] J. B. Lumsden, "The Nature of Corrosion Films in Simulated LWR Water", EPRI NP-4061M, 1985.

[L-2] C. B. Lee, "Modeling of Corrosion Product Transport in PWR Primary Coolant", Ph. D. Thesis, Dept. of Nucl. Eng., MIT, 1990.

[L-3] W. T. Lindsay, et al., "The Role of Coolant Chemistry in PWR Radiation-Field Buildup", EPRI NP-4247, 1985.

[L-4] D. Lister, "Corrosion Release - The Primary Process in Activity Transport", Proceedings of the 1988 JAIF International Conference on Water Chemistry in Nuclear. Power Plants, Japan, 1988.

[M-1] A. M. Morillon, "Modelling of Radionuclide Transport in a Simulated PWR Environment", S. M. Thesis, Dept. of Nucl. Eng., MIT, 1987.

[M-2] D. D. Macdonald, et al., "The Growth and Breakdown of Passive Films on Metal Surfaces", EPRI NP-4069M, 1985.

[M-3] MITR-II Technical Specifications for the Massachusetts Institute of Technology Research Reactor, 1975.

[M-4] MATHCAD, "Instruction Manual", 1989.

[P-1] Perkin-Elmer, "Instructions-Model 306 Atomic Absorption Spectrophotometer", May 1971.

[P-2] Perkin-Elmer, "Analytical Methods for Atomic Absorption Spectrophotometry", March 1971.

[R-1] J. C. Rowley, et al., "Steady State Temperature Solution for a Heat-Generating Circular Cylinder Cooled by a Ring of Holes", Journal of Heat Transfer, Trans. ASME, Vol 86 Series No.4, Nov. 1964.

[R-2] R. Riess, et al., "Overview of Activity Built Up in the Later West German PWRs", Proceedings of 5th International Conference on Water Chem. Nucl. React. Sys., Bournemouth, 5BNES, London, 1989.

[R-3] H. Raush, et al., "Reactor Neutron Activation Analysis", Proceedings of a Technical Committee Meeting on Research Reactor Activities in Support of National Nuclear Programmes, Hungary, 1985, IAEA-TECDOC-409.

[S-1] G. R. Solares, "An Automated Computer Controlled Counting System for Radionuclide Analysis of Corrosion Products in LWR Coolant Systems", Nucl. Eng. Thesis, Dept. of Nucl. Eng., MIT, 1988.

[S-2] F. H. Sweeton, and C. F. Baes, Jr., "The Solubility of Magnetite and Hydrolysis of Ferrous Ion in Aqueous Solution at Elevated Temperatures", J. Chem. Thermodynamics, 2, 479 (1970).

[S-3] Y. L. Sandler, and R. H. Kunig, "The Solubility of Nickel Ferrite in Aqueous Boric Acid Solution", Nuclear Science and Engineering, 77, 211 (1981).

[V-1] J. H. Van Sant, "Conduction Heat Transfer Solutions", UCRL-52863 Rev. 1, Aug 1983.

[W-1] J. H. Wicks, "Design, Construction and Testing of an In-Pile Loop for PWR Simulation", S. M. Thesis, Dept. of Nucl. Eng., MIT, 1987.

[W-2] C. J. Wood, "Manual of Recent Techniques for LWR Radiation-Field Control", EPRI NP-4505-SR, 1986.

[W-3] C. J. Wood, "Recent Developments in LWR Radiation Field Control", Progress in Nuclear Energy, Vol. 19, No. 3, pp. 241-266, 1987

[W-4] S. Wirdzek, "Technique for B-10 Concentration Determination by Prompt Gamma Neutron Activation Analysis at the MITR-II Reactor", Internal Report, 1989.

[W-5] C. J. Wood, "PWR Primary Water Chemistry Guidelines: Revision 1", EPRI NP-5960-SR, 1988.

[W-6] Waters company, "Waters Ion Chromatography Methods", Spring 89

[W-7] C. J. Wood, "Sourcebook for Chemical Decontamination of Nuclear Power Plants", EPRI NP-6433, 1989.

Appendices

Appendix A. Chemical Analysis Methods

The main objective of the application of the analytical methods described in this appendix and further documented in reference [B-9] is to verify that the concentrations of anions, cations, and transition metals in charging system and outlet water samples are within acceptable levels. Procedures for preparing the charging water chemistry are also presented.

The techniques used for determining the concentration levels of anions, cations, and transition metals were: Atomic Absorption (AA), Colorimetry, and High Performance Liquid Chromatography (HPLC). These techniques are described in reference [B-9]; nonetheless, a brief description of each technique will be presented in this appendix.

1. Atomic Absorption

Atomic absorption is a phenomenon that occurs when free ground state atoms produced by a high temperature flame absorb light of a characteristic wavelength emitted from a source which is specific for that element. By measuring the amount of light absorbed, quantitative determination of that element can be made. Figure A.1 illustrates the atomic absorption phenomenon.

The atomic absorption instrument used for the analysis of lithium, boron, and calcium in the present work is a Perkin-Elmer model 306. Operating and alignment procedures are well

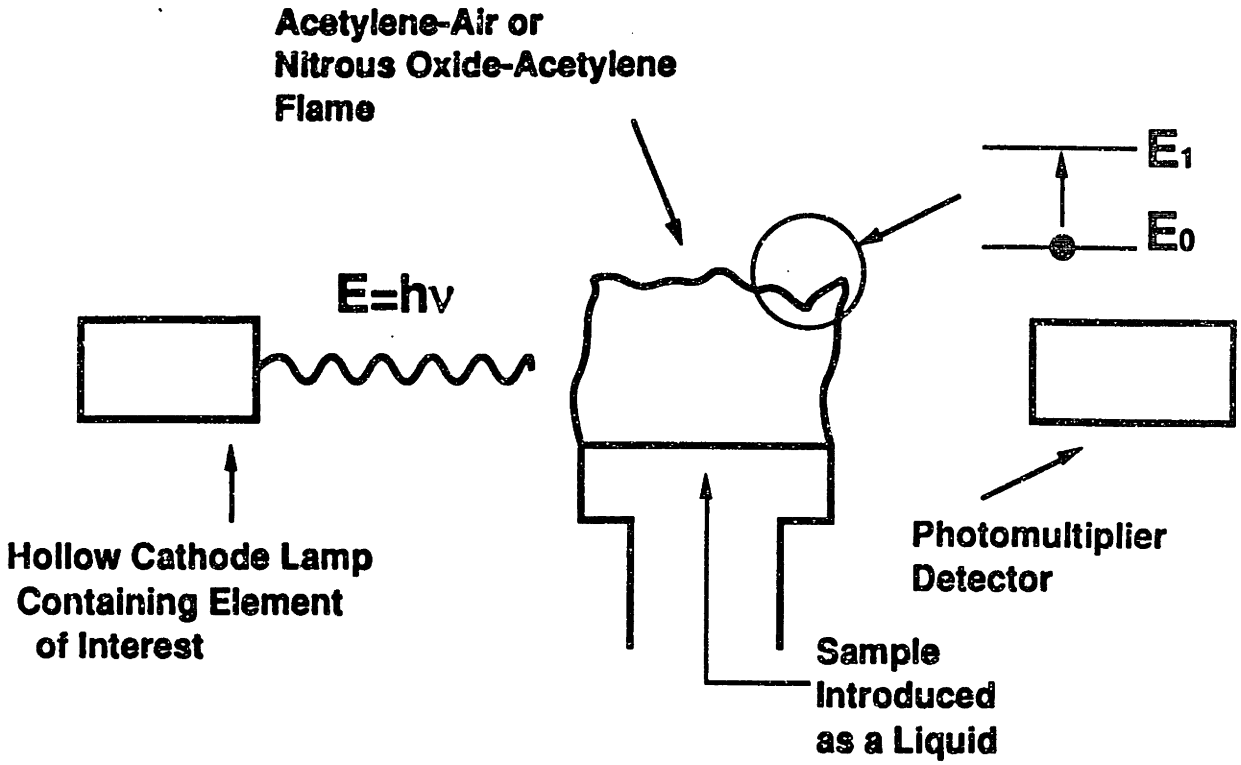

Figure A.1 Principles of Atomic Absorption (AA) Instrument.

documented in references [P-1] and [P-2].

For the analysis of lithium and calcium in the water samples, the AA instrument was operated with an acetylene-air flame and the appropriate hollow cathode lamp. On the other hand, the analysis of boron in water samples required the used of a nitrous oxide-acetylene flame. It should be noted that when operating the nitrous oxide-acetylene flame, gas lines must not be contaminated with oil. Otherwise, there is the possibility of a spontaneous combustion of oil in the presence of nitrous oxide, with explosive results. Experience with these mixture of gases (nitrous oxide and acetylene) has shown that as the nitrous oxide-acetylene flame is either being ignited or extinguished, flashback is most likely to occur if procedures in

reference [P-1] are not properly followed. It is required that the AA operator wear appropriate clothing and safety glasses when operating the AA instrument.

A set of diluted standards were prepared from 1000 ppm standard HACH solutions of lithium, boron, and calcium . From these diluted standards, a linear calibration curve was obtained before starting the analysis of the different elements. The concentration of a particular element was calculated on the basis of the calibration curve, which was checked periodically for linearity and corresponding absorbance.

2. Colorimetry

The instrument used for the colorimetric analysis of water samples is a spectrophotometer model DR/2000 made by the HACH Co. This instrument has been calibrated for more than 120 different colorimetric measurements and has enough memory to store up to 50 more calibrations.

The basic principle of operation for this instrument is very similar to the AA instrument described above. The DR/2000 spectrophotometer (Fig. A2) consists of a tungsten light source which is reflected off a parabolic mirror and dispersed into a double pass high-dispersion prism. The selected wavelength is imaged onto a moving slit, which ensures a more uniform spectral bandwidth. A photodetector measures the amount of light that passes through the sample cell which contains the sample of interest to which selective color-producing reactants have been added. The amount of light

absorbed in the sample cell is directly proportional to the concentration of that element.

The procedures for the analysis of boron, nickel, silica, and iron in water samples are well documented in reference [H-4].

a. Boron

The method used to determine the boron concentration in water samples is based on the reaction of boron with carminic acid in the presence of sulfuric acid. Depending on the concentration of

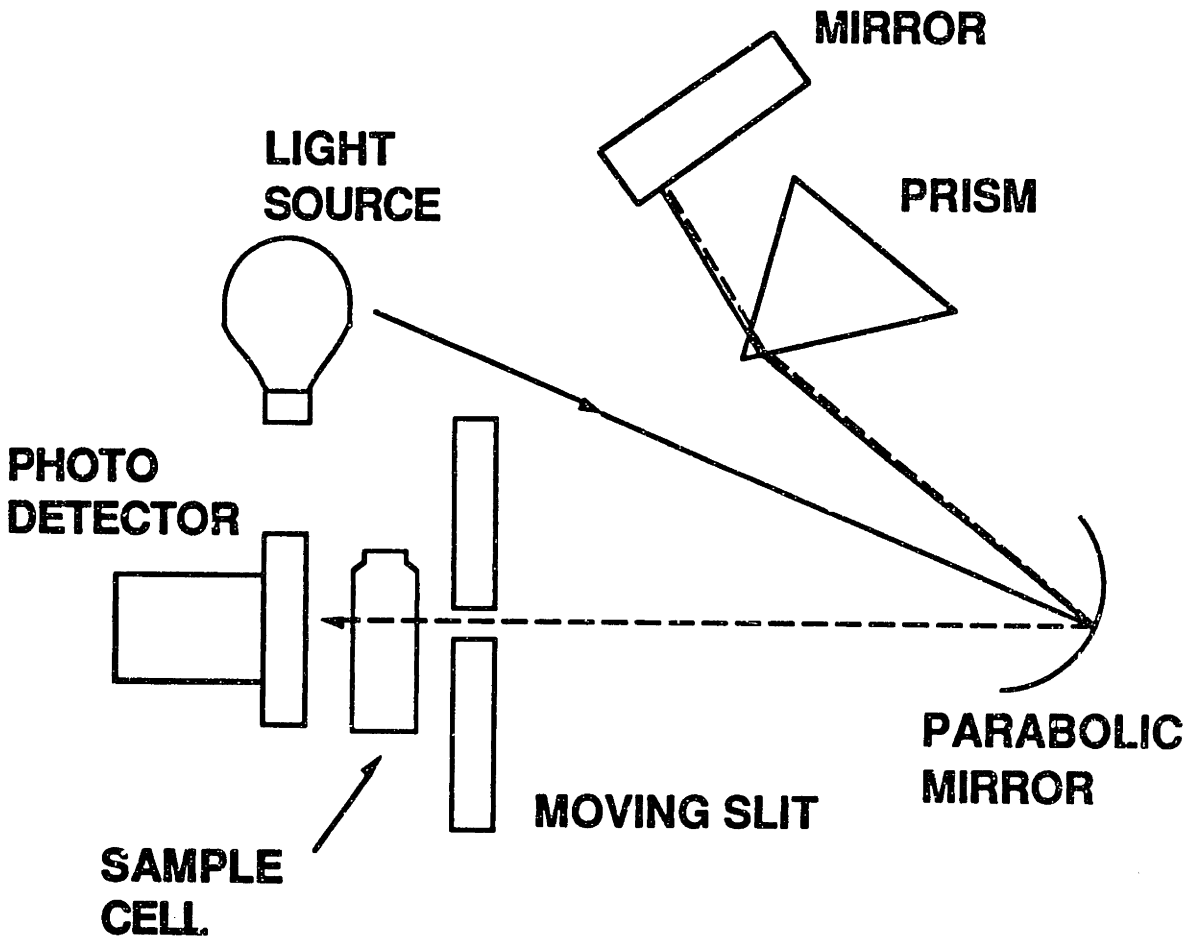

Figure A.2 DR/2000 Colorimeter Optical System.

boron in the sample, the above reaction produces a redish to bluish color. As noted before, the color intensity is directly proportional to the concentration of boron in the sample. This method of boron determination is only useful in the range of 0 to 14 ppm. Because most of the water samples analyzed were on the order of 800 ppm, the samples were diluted by a factor of 100 prior to analysis.

b. Iron

The analysis of iron in water samples was determined by the FerroVer analysis method found in reference [H-4]. FerroVer iron reagent powder was added to the samples to react with all soluble and most insoluble forms of iron, and produce soluble ferrous iron. An orange color was developed when the soluble ferrous iron reacted with the 1, 10 phenanthroline indicator contained in the reagent. The attenuation at 510 nm of the sample is proportional to its iron content. This method was calibrated against a 1 ppm (diluted) HACH standard iron solution, and found to agree within ± 3%. The analyzed samples were kept at a pH between 3 and 5 prior to their analysis. This method is recommended for iron concentrations in the range between 0 and 3 ppm.

c. Nickel

The nickel content in water samples was determined using 1-(2-Pyridylazo)-2-Naphthol (PAN). The samples were kept at a pH between 3 and 8 prior to their analysis. To eliminate the interference of FeIII with the nickel measurement, pyrophosphate was added to

the prepared samples followed by 1-(2-Pyridylazo)-2-Naphthol (PAN) indicator for color development. Finally, EDTA was added to destroy PAN-metal complexes with the exception of cobalt and nickel. Hence, this method can be used for the determination of cobalt and nickel in our water samples. The results showed that the cobalt content was not detectable, which indicated and later confirmed a concentration less than few ppb. This method is recommended for nickel concentrations in the range between 0 and 1 ppm.

d. Silica

The silica content in water samples was determined by the silicomolybdate method. Silica and phosphate react with the molybdate ion under acidic conditions to form a yellow silica complex and a phosphate complex. The addition of citric acid destroys the phosphate complex . Thus, the silica is determined by measuring the absorption by the remaining yellow colored complex. This method is recommended for silica concentrations in the range between 0 and 100 ppm.

3. High Performance Liquid Chromatography (HPLC).

This method of analysis is based on a separation column technique that enables a mixture to be separated into its different solutes. As seen in Fig. A.3, the sample mixture is introduced, over a short time interval, at the top of the column, where it is washed through by the eluting liquid. The separation takes place in the column when a solute is weakly or strongly absorbed, allowing it to

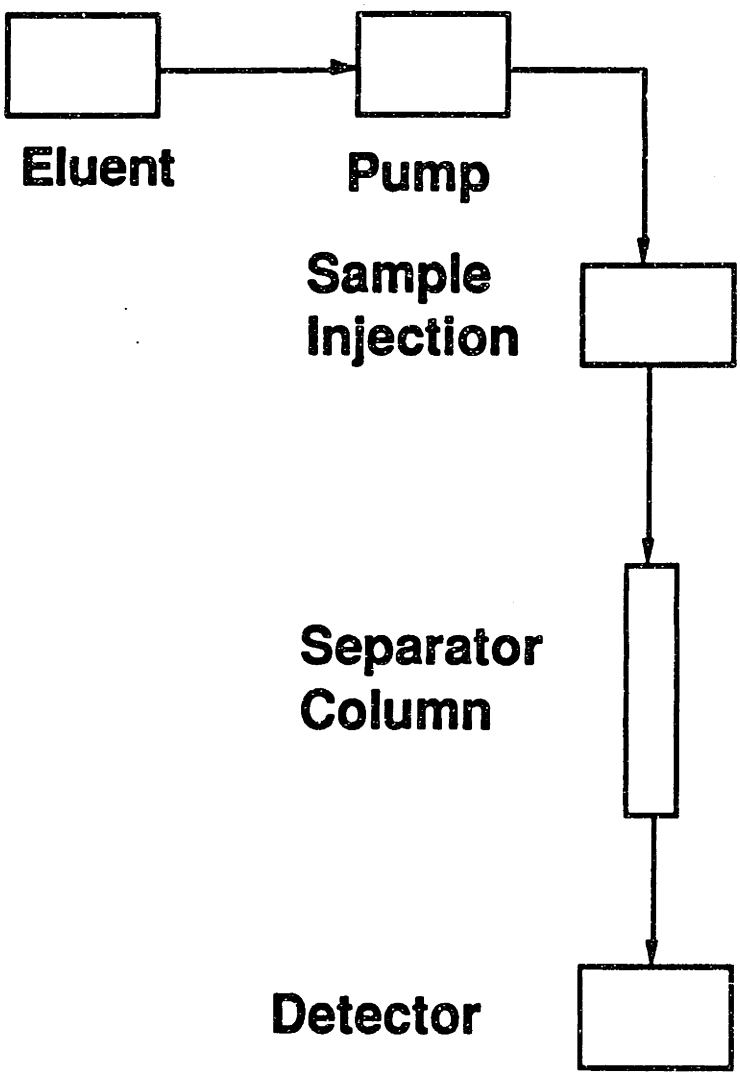

Figure A.3 Schematic of a HPLC System.

travel down the column faster or slower than the other solutes found in the mixture, respectively. Once the solutes have been separated in the separation column, they are sensed in the effluent by an in-line detector to determine their concentration.The time-relationship of the detected solutes provides the separation according to species.

The analysis of the water samples was performed in two types of ion chromatographs. The GE/Dionex HPCL was used only for the

analysis of anions, since the instrument was only equipped with an IC-PAK water anion exchange column. Operating procedures for the GE/Dionex HPCL are described in reference [B-9]. The analysis of the remaining ionic species (cations, transition metals) including again anions, was performed in the second type of HPLC instrument; namely, an ion chromatograph made by Waters. This instrument was equipped with computer software in order to store, and analyze the output data from conductivity or ultraviolet (UV) meters.

For the analysis of anions (such as chloride, nitrite, bromide, nitrate, phosphate, and sulphate ions), the Waters HPCL was used with a Borate/Gluconate eluent. This method (Fig. A.4) is fully described in reference [W-6]. In addition, the HPCL GE/Dionex was also used for the analysis of anions with lithium hydroxide as the eluent. Both of these HPCL instruments were equipped with conductivity meters at the outlet of the separation column.

For the analysis of cations (such as lithium, sodium, ammonium, and potasium), the Waters HPCL was used with an EDTA/Nitric Acid eluent. This method (Fig. A.5) is also described in reference [W-6]. In order to determine the cations, an IC-PAK A HR low capacity cation exchanger was employed.

Finally, transition metals (such as cobalt, copper, lead, zinc, nickel, cadmium, iron II, and manganese) were determined using the Waters HPCL coupled with addition of a reagent at the exit of the Bondapak C18 separation column. The purpose of the reagent is to transform the transition metals into complexes sensitive to light so that they can be detected by an UV detector. Figure A.6 shows the

schematic and the conditions necessary to conduct the transition metal analysis.

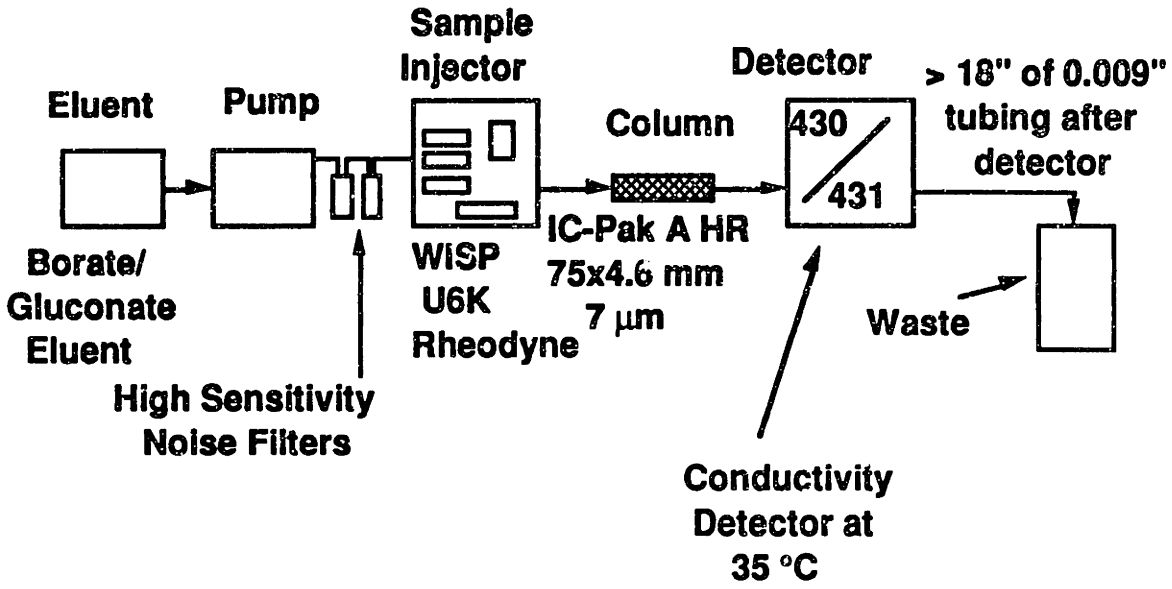

Conditions

Eluent: Borate/Gluconate
Pump: 590 Solvent Delivery Module
Injector: 710B WISP
Column: IC-Pak A HR
Data: 840 Data System
Flow rate: 1.0 ml/hr
Injection: 50 µl of Standard Anion Mix
Detection: 430 Conductivity
Gain: 0.01
Range: 500 µS
Temperature: On
Polarity: +
Background: 274 µS

Figure A.4 Waters HPLC SET UP for Analysis of Anions [W-6].

4. Prompt Gamma Neutron Activation Analysis (PGNAA).

One of the most advantageous and accurate techniques to quantify the amount of boron in water samples is by prompt gamma neutron activation analysis. A PGNAA facility using the MIT nuclear reactor as a thermal neutron source is available for project use [W-4].

It is a well known phenomenon that when thermal neutrons

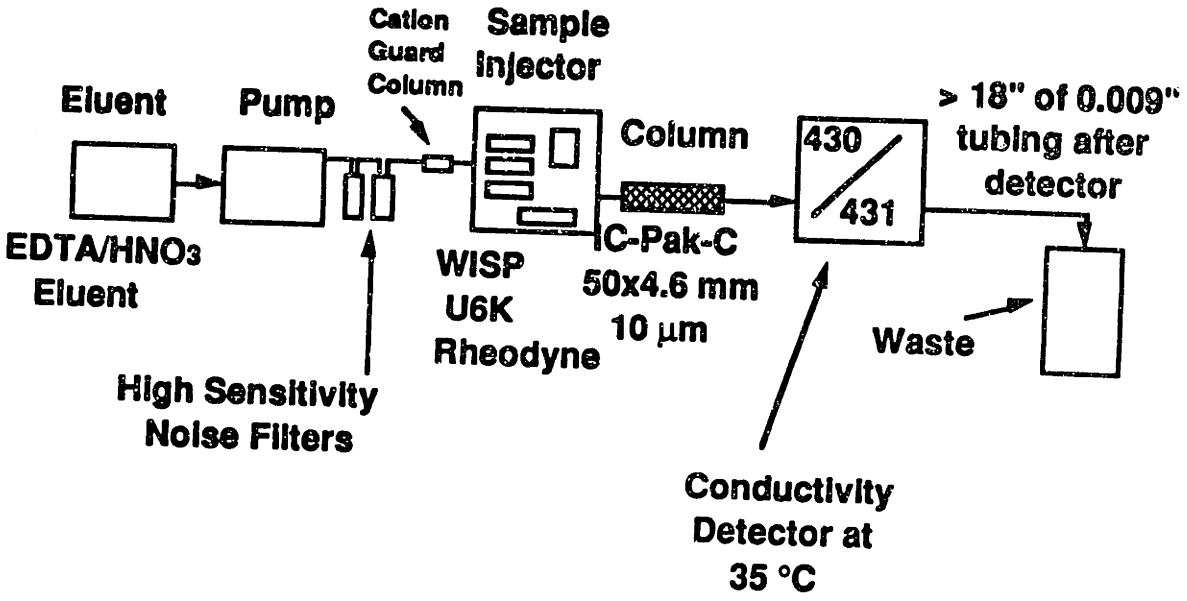

Conditions

Eluent: 0.05 nM EDTA/2 mM HNO3
Pump: 510 Solvent Delivery Module
Injector: 710B WISP
Column: IC-Pak C
Data: 840 Data System
Flow rate: 1.2 ml/hr
Injection: 100 µl of Working Standard

Detection: 430 Conductivity
Gain: 0.01
Range: 500 µS
Temperature: On
Polarity: +
Background: 274 µS

Figure A.5 Water HPLC Set UP for the Analysis of Cations [W-6].

are captured by a target nucleus, the compound nucleus is excited, and in a short period of time deexcites by emitting photons, or photons and alpha particles such as in the case of the B-10(n,α)Li-7* nuclear reaction. Li-7* deexites by emitting photons that give a gamma spectrum which extends over a 13 kev band, due to doppler effects, at an energy of 478 kev. Thus, the counts detected in a multichannel analyzer in this region are directly proportional to the concentration of boron in the sample. Reference [W-4] gives a more

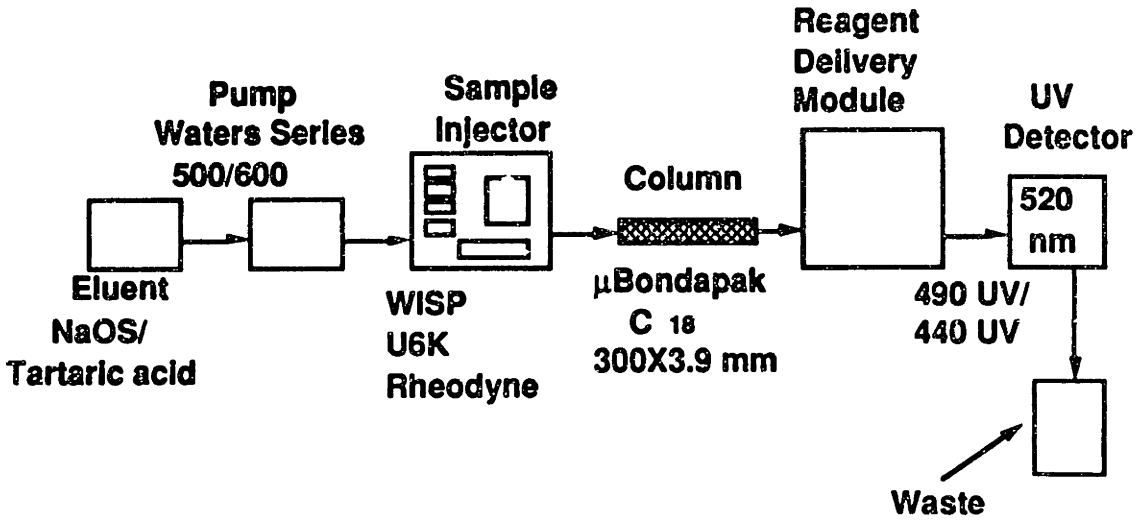

Conditions

Column: µBondapak C18 (30 cmm)
Pump: 590 Solvent Delivery Module
Detection: 490 UV at 520 nm
Injection: 100 µl
Flow rate: 1.0 ml/min
Post-column Reagent: 0.2 mM PAR [4-(2-pyridylazo) resorcinol], 1M Acetic Acid, 3M Ammonium Hydroxide, 0.5 ml/min.

Eluent: 2mM Sodium Octanesulfonate, 50mM Tartaric Acid, 2% Acetonitrile, adjust to pH 3.4 with NaOH
Injector: 712B WISP

Figure A.6 Waters HPLC Set Up for Transition Metals [W-6].

detailed description of the PGNAA facility and its detection system.

Prior to the irradiation of the sample, the instrumentation of the PGNAA facility is set up according to the procedures listed in reference [W-4]. A calibration curve is determined by plotting the ratio of B-10 to Hydrogen count rate peak areas versus the ppm of the standard solutions. The unknown sample is then irradiated in the prompt gamma facility and counted. The count rate area ratio of B-10 to hydrogen peaks (resulting from neutron capture in the light

water of the sample) is evaluated and compared with the calibration curve to determine the amount of B-10. It should be noted that using the ratio of B-10 to H eliminates the geometry effect caused when the sample is placed in a slightly different position and provides a convenient normalization independent of reactor power. Complete procedures to operate the prompt gamma facility are listed in reference [W-4].

5. **Preparation of Water Chemistry.**

As noted before (sec. 4.1, chapter 4), there were four in-pile runs during the first campaign. Two of these runs were at a constant water pH of 7.0 at 300 °C (800 ppm Boron, 1.84 ppm Li), which are considered reference runs. The other two were at a constant pH of 6.5 (800 ppm Boron, 0.56 ppm Lithium) and 7.5 (800 ppm Boron, 6.26 ppm Lithium), respectively.

a. **Reference Run #1 and #2**

The water chemistry for reference runs #1 and #2 contained nominal concentrations of 800 ppm boron and 1.84 ppm lithium, which yielded nominal pH and conductivity values at room temperature (25 °C) of 6.56 pH units and 19.3 μmhos/cm, respectively.

The following steps were carried out to prepare 20 liter water chemistry batches:

First, a 1840 ppm lithium batch solution was prepared by adding 11.12 grams of $LiOH \cdot H_2O$ (containing natural lithium) into one liter of deionized water, followed by thoroughly mixing.

The 20 liter water chemistry (800 ppm B, 1.84 ppm Li) solution was prepared as follows:

1. Pour approximately 4980 ml of deionized water into a 7 liter beaker.

2. Add 91.51 gm of H_3BO_3 to the 7 liter beaker and thoroughly mix using a magnetic stirrer.

3. Add 20 ml of the 1840 ppm lithium batch solution to the 7 liter beaker. Swirl to mix.

4. Pour the 5 liter solution from the 7 liter beaker into a 5 gallon polyethylene container.

5. Add 15 liters of deionized water to the 5 gallon polyethylene container and thoroughly mix.

6. Take a 100 ml sample from the 5 gallon container and measure the pH and conductivity of the solution at room temperature (25 °C).

7. Perform atomic absorption and prompt gamma analysis to determine the concentration of lithium and boron, respectively.

8. Seal the container to prevent excessive contact with air and ambient contaminants prior to use.

b. **Low pH Run #1.**

The water chemistry for this run contained nominal concentrations of 800 ppm of boron and 0.56 ppm lithium, which yielded nominal pH and conductivity values at room temperature of 6.04 pH units and 6.2 μmhos/cm, respectively.

The water chemistry for this run was prepared following the

above procedures. All the previous steps were the same for this run as for reference runs #1 and #2, with the exception of steps #1 and #3. Since the concentration of lithium for this run was lower than reference run #1 and #2, only 6.1 ml of the 1840 ppm lithium solution were added to the 7 liter beaker, which contained 4993.9 ml of deionized water.

c. **High pH Run #1.**

Once again, the water chemistry for the high pH run contained 800 ppm boron. However, the lithium was increased to 6.26 ppm. The high pH solution yielded nominal room temperature pH and conductivity values of 7.01 pH units and 60 μmhos/cm, respectively.

Likewise, all previous steps were the same, with the exception of steps #1 and #3. A total of 68.05 ml of the 1840 ppm lithium solution were added to the 7 liter beaker which contained 4931.95 ml of deionized water.

6. Procedures for Loading Water Chemistry into Charging System.

Once the appropriate water chemistry has been prepared, the following steps are carried out to properly load the water chemistry into the charging system. It is assumed that the charging system water tanks contain a hydrogen overpressure of 5 psig and the water chemistry remaining in charging tank #1 is deoxygenated (<1 ppb).

1. Position container with water chemistry a bit higher than instrument pump.

2. Connect water hose from the spigot of the water chemistry

container to the inlet of the instrument pump (refer to Fig A.7).

3. Place water hose around peristaltic tubing pump head.

4. Open spigot and V-10 valves (refer to Fig. A.7).

5. Position valves V-1 and V-2 in the bypass mode. Make sure that oxygen (Orbisphere) meter is turned off.

6. Position valve V-7 so that neither tank #1 or #2 are selected (middle position).

7. Position valve V-3 so that charging tank #2 is selected.

8. Turn on tubing and instrument pumps. Make sure not to exceed the 50 liter tank capacity.

9. Slightly open venting valve V-12 to avoid overpressurization of charging tanks while loading water chemistry into tank #2.

10. Once the loading of chemistry has been completed, turn off tubing and instrument pumps.

11. Close valve V-10 and position valves V-1, V-2, V-3, and V-7 so that a flow path is established which includes the oxygen flow cell.

12. Switch hydrogen sparging valve V-8 to tank #2.

13. Turn on instrument pump and oxygen meter and make sure that the flow rate through the oxygen cell is between 50 to 250 cc/min.

14. After sparging the water contained in tank #2 for a period of 3 hours, close venting valve V-12.

15. Finally, once oxygen content of water in tank #2 is below 1 ppb, transfer water from tank #2 into tank #1.

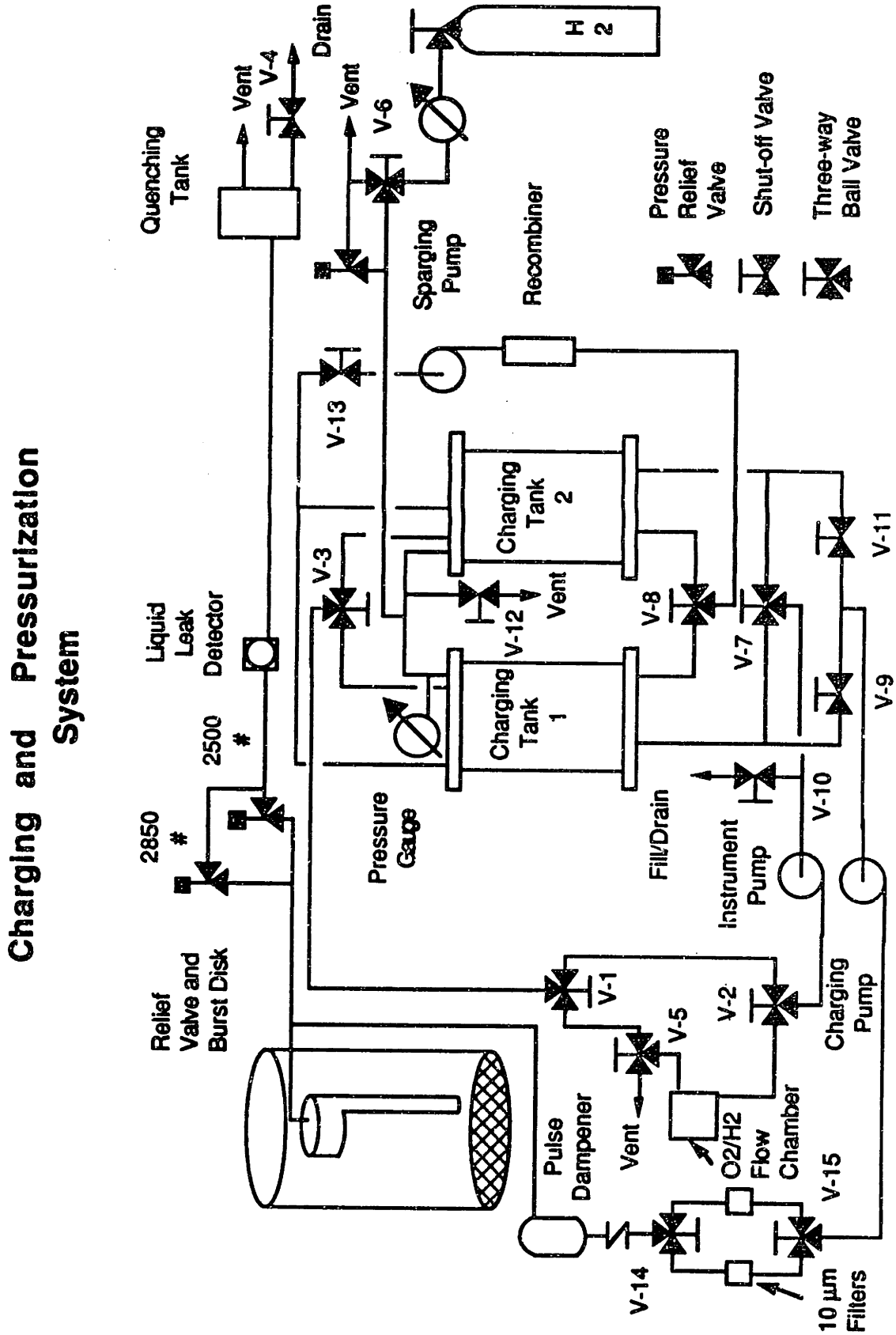

Figure A.7 Charging System.

Appendix B. Loop Characterization Program

A loop characterization computer program was written, with the main objective to calculate the areas, volumes, and ratios of the different construction materials of the loop, as well as heat fluxes and other scaling parameters. The program was written in a Macintosh personal computer using a computational software package known as MATHCAD. A set of instructions on how to use this software is given in the MATHCAD instruction manual, reference [M-4].

The program itself starts with the definition of the unit system followed by three computational parts. Part I computes the construction material areas, volumes, and their ratios, of the loop given a set of dimensions. Part II calculates heat transfer parameters such as: in-core and out-of-core heat fluxes, core and steam generator film differential temperatures, heat transfer coefficients, and several dimensionless parameters. Part III computes the scaling parameter ratios such as: shear stress, erosion rate, particulate transport coefficient, boundary layer thickness, etc, which are discussed in references [M-1], [L-2], [W-1].

Each computational part requires input data that reflects the actual dimensions of the loop or thermohydraulic data that specify flow rates, water density, water dynamic viscosity, etc.. Once the input has been prepared and properly loaded into the program, it takes from 5 to 10 seconds to obtain an output. Tables B.1 and B.2 show the input data required, and output, for the three computational parts, respectively. A listing of the program (table B.3)

is also presented including the input and output, which reflect the actual operating conditions of the first campaign of in-pile runs.

Table B1 Description of Input Variables

Part I

No.	Variable	Description
1	din	Inconel tubing inner diameter (inches)
2	hin	Length of Inconel tubing (inches)
3	ρ	Density of water at 565 °F
4	Dzir	Zircaloy tubing inner diameter (inches)
5	Hzir	Total length of Zircaloy tubing (inches)
6	Hcore	Length of Zircaloy tubing in core region (inches)
7	HcPb	Length of Zircaloy tubing in lead bath
8	SSd	Inner SS tubing diameter (inches)
9	SSh	Length of SS tubing (inches)
10	Avel	Average flow velocity in the loop (ft/sec)
11	Hin	Length of Inconel tubing in S/G cooled region (inches)
12	Ph	Plenum height (inches)
13	Pd	Plenum diameter (inches)
14	PuA	Main circulating pump head area (cm^2)
15	PuV	Main circulating pump head volume (cm^3)

Part II

No.	Variable	Description
16	k	Water thermal conductivity (BTU/hr-ft-°F) at 565 °F

17	Cp	Water heat capacity (BTU/lbm-°F) at 565 °F
18	μ	Dynamic viscocity (lbm/ft-hr) at 565°F
19	Tin	Inlet temperature °F
20	Tout	Outlet temperature °F
21	ΔT	Temperature loss in pump loop (°F)
22	AV	Volumetric flow rate (gal/min)

Part III

No.	Variable	Description
23	ΔTfilmPWRSG	Steam generator film differential temperature in a representative PWR (°F)
24	ΔTfilmPWRcore	Core film differential temperature in the PWR (°F)
24	ΔTbulkPWR	Bulk differential temperature in a representative PWR (°F)
25	ΔTfilmPCCLSG	Steam generator film differential temperature in the PCCL (°F)
26	ΔTfilmPCCLcore	Core film differential temperature in a representative PCCL (°F)
27	ΔTbulkPCCL	Bulk differential temperature in the PCCL (°F)
28	VPWRSG	Steam generator flow velocity in a representative PWR (m/sec)
29	VPWRcore	Core Flow velocity in a representative PWR (m/sec)
30	Dsg	Steam generator tube diameter in a representative PWR (inches)
31	Dcore	Core hydraulic diameter in a representative PWR (inches)
32	SGHFPWR	Steam Generator heat flux in a representative PWR (kW/m^2)
33	CHFPWR	Core heat flux in a representative PWR (kW/m^2)

Table B.2 Description of output

Part I

No.	Dependent Variable	Description
1	ZirA	Total Zircaloy tubing area (cm^2)
2	InA	Total Inconel tubing area (cm^2)
3	PLA	Total Plenum area (cm^2)
4	PLLA	Plenum lateral surface area (cm^2)
5	PLBA	Plenum top and bottom area (cm^2)
6	SStA	Stainless steel tubing area (cm^2)
7	SSTA	Total stainless steel area (cm^2)
8	SGIA	Total Inconel tubing area in S/G region (cm^2)
9	ZirCA	Zircaloy tubing area in core region (cm^2)
10	ZirHA	Zircaloy heated area (cm^2)
11	ZirV	Total Zircaloy volume (cm^3)
12	InV	Total Inconel volume (cm^3)
13	PLV	Total plenum volume (cm^3)
14	SSV	Total SS tubing volume (cm^3)
15	SST	Total SS volume (cm^3)
16	SGIV	Total Inconel tubing volume in S/G region (cm^3)
17	ZirCV	Total in-core Zircaloy volume (cm^3)
18	ZirHV	Total Zircaloy volume in the lead bath (cm^3)

Part I

Area Ratios		
No.	Dependent variable	Description
19	IZA	Area ratio of total Inconel to total Zircaloy
20	IZcA	Area ratio of total Inconel to in-core Zircaloy
21	SSZA	Area ratio of total SS to in-core Zircaloy
22	SSIA	Area ratio of total SS to total Inconel
23	ISGZhA	Area ratio of Inconel (cooled) to Zircaloy (heated)

Volume ratios		
24	IZA	Volume ratio of total Inconel to total Zircaloy
25	IZcV	Volume ratio of total Inconel to in-core Zircaloy
26	SSZV	Volume ratio of total SS to total Zircaloy
27	SSZcV	Volume ratio of total SS to in-core Zircaloy
28	SSIV	Volume ratio of total SS to total Inconel
29	ISGZhV	Volume ratio of Inconel (cooled) to Zircaloy (heated)

Part II

No.	Dependent Variable	Description
30	Re	Reynolds number
31	Pr	Prandtl number
32	Nu	Nusselt number
33	h	Heat transfer coefficient (BTU/hr-ft^{2}-°F)
34	Qcore	Heat generated in core region (kW)
35	Qpu	Heat rejected in pump loop (kW)
36	Qsg	Heat rejected in steam generator (kW)
37	CHF	PCCL Core heat flux (kW/m^2)
38	SGHF	PCCL steam generator heat flux (kW/m^2)

Part III

No.	Dependent Variable	Description
39	AsgPCCL	PCCL steam generator tube cross sectional area (m^2)
40	AcorePCCL	PCCL core Zircaloy tube cross sectional area (m^2)
41	VPCCLSG	PCCL flow velocity in steam generator section (m/sec)
42	VPCCLcore	PCCL flow velocity in steam generator section (m/sec)
43	RatioΔTfilmSG	Ratio of delta T film in S/G between PCCL and a typical PWR

44	RatioΔTfilmcore	Ratio of delta T film in core between PCCL and a typical PWR
45	RatioΔTbulk	Ratio of delta T bulk between PCCL and a typical PWR
46	RatioSSSG	Ratio of shear stress between PCCL and a typical PWR (steam generator section)
47	RatioSScore	Ratio of shear stress between PCCL and a typical PWR (core section)
48	RatioERSG	Ratio of the erosion rate between PCCL and a typical PWR (steam generator section)
49	RatioERcore	Ratio of the erosion rate between PCCL and a typical PWR (core section)
50	RatioPTCSG	Ratio of particulate transport coefficients between PCCL and a typical PWR (S/G)
51	RatioPTCcore	Ratio of particulate transport coefficients between PCCL and a typical PWR (core)
52	RatioBLSG	Ratio of boundary layer thickness between PCCL and a representative PWR (SG)
53	RatioBLcore	Ratio of boundary layer thickness between PCCL and a representative PWR (core)
54	RatioTCSG	Ratio of mass/heat transfer coefficients between PCCL and a typical PWR (S/G)
55	RatioTCcore	Ratio of mass/heat transfer coefficients between PCCL and a typical PWR (core)
56	RatioHFSG	Ratio of heat flux between PCCL and a representative PWR (S/G)
57	RatioHFcore	Ratio of heat flux between PCCL and a representative PWR (S/G)
58	RatioVSG	Ratio of velocities between PCCL and a typical PWR (Steam Generator section)
59	RatioVcore	Ratio of velocities between PCCL and a typical PWR (core section)

Table B.3 Listing of the Loop Characterization Program.

```
UNIT DEFINITIONS                          MKS (SI) unit system

I. Base units

  m ≡ 1L          kg ≡ 1M        sec ≡ 1T   degF ≡ 1

                          9
                 degC ≡ ---·degF
                          5

II. Derived units: Length

   cm ≡ .01·m        km ≡ 1000·m      mm ≡ .001·m
   ft ≡ .3048·m      in ≡ 2.54·cm

III. Derived units: Mass

                -3
      gm ≡ 10   ·kg      lb ≡ 453.59247·gm

IV. Derived units: Time

       min ≡ 60·sec       hr ≡ 3600·sec

V. Derived units: Volume
                     3                        3
    liter ≡ (.1·m)              mL ≡ cm

                                  3
       fl_oz ≡ 29.57353·cm

                          gal ≡ 128·fl_oz
```

VI. Derived units: Force, Energy, Power

$$g \equiv 9.8 \cdot \frac{m}{sec^2}$$

$$newton \equiv kg \cdot \frac{m}{sec^2}$$

$$lbf \equiv g \cdot lb$$

$$dyne \equiv 10^{-5} \cdot newton$$

$$kgf \equiv g \cdot kg$$

$$joule \equiv newton \cdot m$$

$$erg \equiv 10^{-7} \cdot joule$$

$$BTU \equiv 1.05505585262 \cdot 10^{3} \cdot joule$$

$$psi \equiv \frac{lbf}{in^2} \qquad watt \equiv \frac{joule}{sec}$$

$$kW \equiv 1000 \cdot watt$$

Input data (part I)

din	Inner Inconel tubing diameter (inches)
hin	Length of Inconel tubing (inches)
ρ	Density of water at 565 °F
Dzir	Inner Zircaloy tubing diameter (inches)
Hzir	Total length of Zircaloy tubing (inches)
Hcore	Length of Zircaloy tubing in core region (inches)
HcPb	Length of Zircaloy tubing in lead bath
SSd	Inner SS tubing diameter (inches)
SSh	Length of SS tubing (inches)
Avel	Average flow velocity in the loop (ft/sec)
Hin	Length of Inconel tubing in S/G cooled region (inches)
Ph	Plenum height (inches)
Pd	Plenum diameter (inches)
PuA	Main circulating pump head area (cm^2)
PuV	Main circulating pump head volume (cm^3)

$$din := 0.2425 \cdot in \qquad Hin := 389.63 \cdot in$$

$$\rho := 45.67 \cdot \frac{lb}{ft^3} \qquad Dzir := 0.2565 \cdot in$$

$$Hzir := 74.5 \cdot in \qquad Hcore := 50.5 \cdot in$$

$$HcPb := 51.0 \cdot in$$

$$SSd := 0.2425 \cdot in \qquad SSh := 7.5 \cdot in$$

$$Avel := 9.86 \cdot \frac{ft}{sec} \qquad Hin := 141.63 \cdot in$$

$$Ph := 9.625 \cdot in \qquad Pd := 1 \cdot in$$

$$PuA := 225 \cdot cm^2 \qquad PuV := 130 \cdot cm^3$$

Dependent variables to be determined:

ZirA	Total Zircaloy tubing area (cm^2)
InA	Total Inconel tubing area (cm^2)
PLA	Total Plenum surface area (cm^2)
PLLA	Plenum lateral surface area (cm^2)
PLBA	Plenum top and bottom area (cm^2)
SStA	Stainless steel tubing area (cm^2)
SSTA	Total stainless steel area (cm^2)
SGIA	Total Inconel tubing area in S/G region (cm^2)
ZirCA	Zircaloy tubing area in core region (cm^2)
ZirHA	Zircaloy heated area (cm^2)
ZirV	Total Zircaloy volume (cm^3)
InV	Total Inconel volume (cm^3)
PLV	Total plenum volume (cm^3)
SSV	Total SS tubing volume (cm^3)
SST	Total SS volume (cm^3)
SGIV	Total Inconel tubing volume in S/G region (cm^3)
ZirCV	Total in-core Zircaloy volume (cm^3)
ZirHV	Total Zircaloy volume in the lead bath (cm^3)
IZA	Area ratio of total Inconel to total Zircaloy
IZcA	Area ratio of total Inconel to in-core Zircaloy
SSZA	Area ratio of total SS to in-core Zircaloy
SSIA	Area ratio of total SS to total Inconel

ISGZhA	Area ratio of Inconel (cooled) to Zircaloy (heated)
IZA	Volume ratio of total Inconel to total Zircaloy
IZcV	Volume ratio of total Inconel to in-core Zircaloy
SSZV	Volume ratio of total SS to total Zircaloy
SSZcV	Volume ratio of total SS to in-core Zircaloy
SSIV	Volume ratio of total SS to total Inconel
ISGZhV	Volume ratio of Inconel (cooled) to Zircaloy (heated)

Areas and Volume Ratios

Calculation of the areas of Zircaloy and Inconel

$$ZirA := \pi \cdot Dzir \cdot Hzir \qquad InA := \pi \cdot din \cdot hin$$

$$ZirA = 387.312 \cdot cm^2 \qquad InA = 1.915 \cdot 10^3 \cdot cm^2$$

The sources of stainless steel are: the plenum, the main circulating pump, and a seven inch SS tubing segment. The pump head area was calculated from the main circulating pump engineering drawing.

$$PLLA := \pi \cdot Ph \cdot Pd$$

$$PLBA := \pi \cdot \frac{\left[Pd^2 - din^2\right]}{2}$$

$$PLLA = 195.082 \cdot cm^2 \qquad PLBA = 9.538 \cdot cm^2$$

PLA := PLLA + PLBA

$$PLA = 204.621 \cdot cm^2$$

SS tubing area

SStA := π·SSd·SSh

$$SStA = 36.863 \cdot cm^2$$

Total SS area

SSTA := PuA + SStA + PLLA + PLBA

$$SSTA = 466.484 \cdot cm^2$$

Total Inconel area in Steam Generator region (Cooled)

SGIA := π·Hin·din

$$SGIA = 696.12 \cdot cm^2$$

Total Zircaloy area in core region

ZirCA := π·Dzir·Hcore

$$ZirCA = 262.54 \cdot cm^2$$

Total Zircaloy area in the heated bath

$$ZirHA := \pi \cdot Dzir \cdot HcPb$$

$$ZirHA = 265.14 \cdot cm^2$$

Total Zircaloy Volume

$$ZirV := \pi \cdot Dzir \cdot \frac{2\ Hzir}{4}$$

$$ZirV = 63.084 \cdot cm^3$$

Total Inconel Volume

$$InV := \pi \cdot din \cdot \frac{2\ hin}{4}$$

$$InV = 294.895 \cdot cm^3$$

Total SS plenum volume

$$PLV := \pi \cdot \frac{Pd^2}{4} \cdot Ph$$

$$PLV = 123.877 \cdot cm^3$$

SS tubing volume

$$SSV := \pi \cdot \frac{SSd^2}{4} \cdot SSh$$

$$SSV = 5.676 \cdot cm^3$$

Total SS volume

$$SST := SSV + PLV + PuV$$

$$SST = 259.554 \cdot cm^3$$

Inconel Volume in S/G region

$$SGIV := \pi \cdot din^2 \cdot \frac{Hin}{4}$$

$$SGIV = 107.194 \cdot cm^3$$

Total Zircaloy volume in-core

$$ZirCV := \pi \cdot Dzir^2 \cdot \frac{Hcore}{4}$$

$$ZirCV = 42.762 \cdot cm^3$$

Total Zircaloy volume in lead bath

$$ZirHV := \pi \cdot \frac{Dzir^2}{4} \cdot HcPb$$

$$ZirHV = 43.185 \cdot cm^3$$

Areas Ratios

Inconel:Zircaloy(total)

$$IZA := \frac{InA}{ZirA}$$

$$IZA = 4.944$$

Inconel:Zircaloy(in core)

$$IZcA := \frac{InA}{ZirCA}$$

$$IZcA = 7.294$$

SS:Zircaloy(total)

$$SSZA := \frac{SSTA}{ZirA}$$

$$SSZA = 1.204$$

SS:Zircaloy(in core)

$$SSZc := \frac{SSTA}{ZirCA}$$

SSZc = 1.777

SS:Inconel

$$SSIA := \frac{SSTA}{InA}$$

SSIA = 0.244

Inconel(cooled):Zircaloy(heated)

$$ISGZh := \frac{SGIA}{ZirHA}$$

ISGZh = 2.625

Volume Ratios

Inconel:Zircaloy(total)

$$IZV := \frac{InV}{ZirV}$$

IZV = 4.675

Inconel:Zircaloy(in core)

$$IZcV := \frac{InV}{ZirCV}$$

IZcV = 6.896

SS:Zircaloy(total)

$$SSZV := \frac{SST}{ZirV}$$

SSZV = 4.114

SS:Zircaloy(in core)

$$SSZcV := \frac{SST}{ZirCV}$$

SSZcV = 6.07

SS:Inconel

$$SSIV := \frac{SST}{InV}$$

SSIV = 0.88

Inconel(cooled):Zircaloy(heated)

$$ISGZhV := \frac{SGIV}{ZirHV}$$

ISGZhV = 2.482

This section (part II) computes the design thermohydraulic parameters, such as: steam generator and core heat fluxes, film differential temperatures, heat transfer coefficients, and several dimensionless parameters.

Input data (Part II)

k	Thermal conductivity of water (BTU/hr-ft-°F) at 565 °F
Cp	Heat capacity of water (BTU/lbm-°F) at 565 °F
μ	Dynamic viscocity (lbm/ft-hr) at 565°F
Tin	Inlet temperature °F
Tout	Outlet temperature °F
ΔT	Temperature loss in pump loop (°F)
AV	Volumetric flow rate (gal/min)

$$k := 0.3211 \cdot \frac{BTU}{(hr \cdot ft \cdot degF)} \qquad Cp := 1.29375 \cdot \frac{BTU}{(lb \cdot degF}$$

$$\mu := 0.2281 \cdot \frac{lb}{(ft \cdot hr)} \qquad Tin := 530 \cdot degF$$

$$Tout := 600 \cdot degF \qquad AV := 1.5 \cdot \frac{gal}{min}$$

$$\Delta T := 5 \cdot degF$$

Dependent Variables to be determined:

Re	Reynolds number
P_r	Prandtl number
Nu	Nusselt number
h	Heat transfer coefficient (BTU/hr-ft^{2}-°F)
Qcore	Heat generated in core region (kW)
Qpu	Heat rejected in pump loop (kW)
Qsg	Heat rejected in steam generator (kW)
CHF	PCCL Core heat flux (kW/m^{2})
SGHF	PCCL steam generator heat flux (kW/m^{2})

First, let us calculate Reynolds number

S/G section

$$Resg := \rho \cdot Avel \cdot \frac{din}{\mu}$$

$$Resg = 1.436 \cdot 10^{5}$$

Core section

$$Rec := \rho \cdot Avel \cdot \frac{Dzir}{\mu}$$

$$Rec = 1.519 \cdot 10^{5}$$

Average Reynolds number

$$Re := \frac{(Rec + Resg)}{2}$$

$$Re = 1.478 \cdot 10^{5}$$

Prandtl number is given by the following expression:

$$Pr := Cp \cdot \frac{\mu}{k}$$

$$Pr = 0.919$$

Finally, Nusselt number can be obtained by applying the Dittus-Boelter correlation

$$Nu := 0.023 \cdot Re^{0.8} \cdot Pr^{\left[\frac{1}{3}\right]}$$

$$Nu = 305.609$$

An average heat transfer coefficient, h, is calculated by applying the following expression:

$$h := Nu \cdot \frac{k}{din}$$

$$h = 4.856 \cdot 10^{3} \cdot \frac{BTU}{\left[hr \cdot ft^{2} \cdot degF\right]}$$

To calculate the total heat generated in the core section, the following expression is used:

$$Qcore := \rho \cdot AV \cdot Cp \cdot (Tout - Tin)$$

$$Qcore = 14.584 \cdot kW$$

Core Heat flux

$$CHF := \frac{Qcore}{ZirHA} \qquad CHF = 550.032 \cdot \frac{kW}{m^2}$$

The heat rejected in the loop pump section is given by:

$$Qpu := \rho \cdot AV \cdot Cp \cdot \Delta T$$

$$Qpu = 1.042 \cdot kW$$

Heat rejected in steam generator section

$$Qsg := Qcore - Qpu$$

$$Qsg = 13.542 \cdot kW$$

Heat Flux in Steam Generator

$$SGHF := \frac{Qsg}{SGIA} \qquad SGHF = 194.533 \cdot \frac{kW}{m^2}$$

The core and steam generator film differential temperatures are:

Core section

$$\Delta TCore := \frac{CHF}{h}$$

$$\Delta TCore = 19.948 \cdot degC$$

Steam Generator

$$\Delta Tsg := \frac{SGHF}{h}$$

$$\Delta Tsg = 7.055 \cdot degC$$

Finally, part III of this program computes the critical scaling parameters, such as: ΔT film, ΔT bulk, shear stress, etc., ratios.

Input data (Part III):

ΔTfilmPWRSG	Steam generator film differential temperature in a representative PWR (°F)
ΔTfilmPWRcore	Core film differential temperature in a representative PWR (°F)
ΔTbulkPWR	Bulk differential temperature in a representative PWR (°F)

ΔTfilmPCCLSG	Steam generator film differential temperature in the PCCL (°F)
ΔTfilmPCCLcore	Core film differential temperature in the PCCL (°F)
ΔTbulkPCCL	Bulk differential temperature in the PCCL (°F)
VPWRSG	Steam generator flow velocity in a representative PWR (m/sec)
VPWRcore	Core Flow velocity in a representative PWR (m/sec)
Dsg	Steam generator tube diameter in a representative PWR (inches)
Dcore	Core hydraulic diameter in a representative PWR (inches)
SGHFPWR	Steam Generator heat flux in a representative PWR (kW/m^2)
CHFPWR	Core heat flux in a representative PWR (kW/m^2)

$\Delta TfilmPWRSG := 10.26 \cdot degF$ $\Delta TfilmPWRcore := 32.4 \cdot degF$

$\Delta TbulkPWR := 63 \cdot degF$ $\Delta TfilmPCCLSG := 12.699 \cdot degF$

$\Delta TfilmPCCLcore := 35.9 \cdot degF$ $\Delta TbulkPCCL := 70 \cdot degF$

$VPWRSG := 5.87 \cdot \frac{m}{sec}$ $VPWRcore := 4.79 \cdot \frac{m}{sec}$

$Dsg := 0.82 \cdot in$ $Dcore := 0.47 \cdot in$

$$SGHFPWR := 178.2 \cdot \frac{kW}{m^2} \qquad CHFPWR := 614.6 \cdot \frac{kW}{m^2}$$

Scaling parameters to be determined:

AsgPCCL	PCCL steam generator tube cross sectional area (m^2)
AcorePCCL	PCCL core Zircaloy tube cross sectional area (m^2)
VPCCLSG	PCCL flow velocity in steam generator section (m/sec)
VPCCLcore	PCCL flow velocity in steam generator section (m/sec)
RatioΔTfilmSG	Ratio of delta T film in S/G between PCCL and a typical PWR
RatioΔTfilmcore	Ratio of delta T film in core between PCCL and a typical PWR
RatioΔTbulk	Ratio of delta T bulk between PCCL and a typical PWR
RatioSSSG	Ratio of shear stress between PCCL and a typical PWR (steam generator section)
RatioSScore	Ratio of shear stress between PCCL and a typical PWR (core section)
RatioERSG	Ratio of the erosion rate between PCCL and a typical PWR (steam generator section)
RatioERcore	Ratio of the erosion rate between PCCL and a typical PWR (core section)
RatioPTCSG	Ratio of particulate transport coefficients between PCCL and a typical PWR (S/G)
RatioPTCcore	Ratio of particulate transport coefficients between PCCL and a typical PWR (core)
RatioBLSG	Ratio of boundary layer thickness between PCCL and a representative PWR (SG)

RatioBLcore	Ratio of boundary layer thickness between PCCL and a representative PWR (core)
RatioTCSG	Ratio of mass/heat transfer coefficients between PCCL and a typical PWR (S/G)
RatioTCcore	Ratio of mass/heat transfer coefficients between PCCL and a typical PWR (core)
RatioHFSG	Ratio of heat flux between PCCL and a representative PWR (S/G)
RatioHFcore	Ratio of heat flux between PCCL and a representative PWR (S/G)
RatioVSG	Ratio of velocities between PCCL and a typical PWR (Steam Generator section)
RatioVcore	Ratio of velocities between PCCL and a typical PWR (core section)

Calculation of PCCL Inconel and Zircaloy tube cross sectional areas

$$AsgPCCL := \pi \cdot \frac{din^2}{4}$$

$$AsgPCCL = 2.98 \cdot 10^{-5} \cdot m^2$$

$$AcorePCCL := \pi \cdot \frac{Dzir^2}{4}$$

$$AcorePCCL = 3.334 \cdot 10^{-5} \cdot m^2$$

Calculation of PCCL flow velocities in SG and core sections

$$VPCCLSG := \frac{AV}{AsgPCCL}$$

$$VPCCLSG = 3.176 \cdot \frac{m}{sec}$$

$$VPCCLcore := \frac{\Delta V}{AcorePCCL}$$

$$VPCCLcore = 2.839 \cdot \frac{m}{sec}$$

Ratios

ΔT film ratio in steam generator

$$RatioΔTfilmSG := \frac{ΔTfilmPCCLSG}{ΔTfilmPWRSG}$$

$$RatioΔTfilmSG = 1.238$$

ΔT film ratio in core

$$RatioΔTfilmcore := \frac{ΔTfilmPCCLcore}{ΔTfilmPWRcore}$$

$$RatioΔTfilmcore = 1.108$$

ΔT bulk ratio

$$RatioΔTbulk := \frac{ΔTbulkPCCL}{ΔTbulkPWR}$$

$$RatioΔTbulk = 1.111$$

Shear stress ratio (S/G)

$$RatioSSSG := \left[\frac{\left[\left[VPCCLSG^{9} \cdot Dsg\right]\right]}{\left[\left[din \cdot VPWRSG^{9}\right]\right]}\right]^{\left[\frac{1}{5}\right]}$$

$$RatioSSSG = 0.422$$

Shear stress ratio (core)

$$RatioSScore := \left[\frac{\left[\left[VPCCLcore^{9} \cdot Dcore\right]\right]}{\left[\left[Dzir \cdot VPWRcore^{9}\right]\right]}\right]^{\left[\frac{1}{5}\right]}$$

$$RatioSScore = 0.44$$

Erosion rate ratio (SG)

$$RatioERSG := RatioSSSG^{0.83}$$

$$RatioERSG = 0.489$$

Erosion rate ratio (core)

$$RatioERcore := RatioSScore^{0.83}$$

$$RatioERcore = 0.506$$

Particulate transport coefficient ratio (SG)

$$RatioPTCSG := RatioSSSG^{0.5}$$

$$RatioPTCSG = 0.65$$

Particulate transport coefficient ratio (core)

$$RatioPTCcore := RatioSScore^{0.5}$$

$$RatioPTCcore = 0.663$$

Boundary layer thickness ratio (SG)

$$RatioBLSG := \left[\frac{\left[VPWRSG^{4} \cdot din\right]}{\left[Dsg \cdot VPCCLSG^{4}\right]}\right]^{\left[\frac{1}{5}\right]}$$

$$RatioBLSG = 1.281$$

Boundary layer thickness ratio (core)

$$RatioBLcore := \left[\frac{\left[VPWRcore^{4} \cdot Dzir \right]}{\left[Dcore \cdot VPCCLcore^{4} \right]} \right]^{\left[\frac{1}{5}\right]}$$

RatioBLcore = 1.346

Mass/heat transfer coefficient ratio (SG)

$$RatioTCSG := \left[\frac{\left[VPCCLSG^{4} \cdot Dsg \right]}{\left[din \cdot VPWRSG^{4} \right]} \right]^{\left[\frac{1}{5}\right]}$$

RatioTCSG = 0.781

Mass/heat transfer coefficient ratio (core)

$$RatioTCcore := \left[\frac{\left[VPCCLcore^{4} \cdot Dcore \right]}{\left[Dzir \cdot VPWRcore^{4} \right]} \right]^{\left[\frac{1}{5}\right]}$$

RatioTCcore = 0.743

Heat flux ratio (SG)

$$RatioHFSG := \frac{SGHF}{SGHFPWR}$$

$$RatioHFSG = 1.092$$

Heat flux ratio (core)

$$RatioHFcore := \frac{CHF}{CHFPWR}$$

$$RatioHFcore = 0.895$$

Velocity ratio (SG)

$$RatioVSG := \frac{VPCCLSG}{VPWRSG}$$

Velocity ratio (core)

$$RatioVcore := \frac{VPCCLcore}{VPWRcore}$$

$$RatioVcore = 0.593$$

Appendix C. Hot Cell Operating Procedures

The operating procedures for the hot cell can be divided into two major categories; namely, general hot cell, and the "walk in" cell procedures.

The general hot cell procedures establish the limitations and guidelines for the use of both hot cells located on the reactor floor. The following steps are taken when using any of the two hot cells.

1. The use of radioactive material in any of the hot cells must conform to guidelines prescribed by the MITR Technical Specifications, section 6.1.

2. Reactor Operations and MITR Radiation Protection must approve the use of radioactive materials in the hot cell.

3. Prior to using any of the hot cells, the ventilation system must operate properly. Each hot cell should have an air flow of 200 cfm and a differential pressure of at least 0.05" H_2O, as indicated on the front cell manometers. The door in the left cell must be closed and properly sealed with tape. The holes on the top of the cells should be plugged or sealed to obtain a maximum differential pressure in the cells. **It is important to note that improper ventilation exists whenever the upper yellow light in either hot cell is blinking.**

4. Materials inside the hot cell that are extremely radioactive must be separately shielded to reduce radiation levels outside the cell.

5. A permanent log book should be kept to record the date,

time, material description, and radiation level of each of the materials inside the hot cell.

6. Each hot cell filter should be changed when its differential pressure exceeds 3.0" H_2O.

7. In the event of a fire in any of the hot cells, the ventilation system will be automatically cut off and a fire extinguisher will discharge. The ventilation system will be restarted once the fire has been extinguished.

8. Finally, the manipulators must be locked whenever the cell is not in used.

The "walk in" procedures describe the steps that must be followed for entry into the left hot cell. This cell, as described in sec. 2.13, is used to melt the irradiated lead contained in the Titanium Test Tube (TTT). Because some airborne activity is generated whenever the lead is melted, an air sample detector is used to monitor the radiation levels around the hot cell while the melting process is taking place. As expected, during this operation, the cell's interior walls and floor become contaminated.

The following steps are taken to insure that the lowest radiation levels exist prior to entry in the hot cell:

1. The experimenter should notify and obtain approval from the Radiation Protection Officer prior to entry.

2. Highly radioactive materials should be transported to the other cell to reduce radiation levels.

3. After radioactive materials have been transported to the other cell, the cell's interior walls should be decontaminated remotely as well as possible followed by a radiation survey inside the cell to determine the existing radiation levels.

4. Personnel entering the cell should wear appropriate clothing such as coveralls, booties, shoe covers, two pair of gloves, respirator mask, and surgical caps.

5. After exiting the hot cell, personnel should remove protective clothing and survey their hands, feet, body, and any removed equipment.

6. Radioactive signs should be posted at the cell entrance door.

7. Finally, the hot cell door must always be closed and properly sealed.